



**Università
degli Studi
di Palermo**

AREA RICERCA E TRASFERIMENTO TECNOLOGICO
SETTORE DOTTORATI E CONTRATTI PER LA RICERCA
U. O. DOTTORATI DI RICERCA

Dottorato in Scienze Molecolari e Biomolecolari
Dipartimento di Scienze e Tecnologie Biologiche, Chimiche e Farmaceutiche (STEBICEF)
Settore Scientifico Disciplinare: CHIM/08

EXPLORING TRIAZOLE AND THIAZOLE SYSTEMS FOR ANTIVIRAL APPLICATIONS: SYNTHESIS AND BIOLOGICAL EVALUATION

IL DOTTORE
ROBERTA BIVACQUA

IL COORDINATORE
PROF.SSA GIOVANNA PITARRESI

IL TUTOR
PROF.SSA ALESSANDRA MONTALBANO

CO TUTOR
PROF.SSA VIRGINIA SPANÒ

CICLO XXXVI
ANNO CONSEGUIMENTO TITOLO: 2024

Summary

Abbreviations	3
1. Introduction	5
1.1. Triazoles as antiviral agents	6
1.2. Thiazoles as antiviral agents	9
1.3. Coronaviruses	12
1.4. SARS-CoV-2 genome and life cycle	13
1.5. Replication-transcription complex (RTC) proteins as drug targets	18
1.6. SARS-CoV-2 Nsp13	19
1.7. Triazole/thiazole-based compounds targeting Nsp13	22
2. Aim of the project	27
3. Results and discussion	28
3.1. Chemical synthesis of [1,2,3]triazolo[4,5- <i>h</i>][1,6]naphthyridines and [1,2,3]triazolo[4,5- <i>h</i>][1,6]naphthyridine-8-ones	28
3.2. Chemical synthesis of [1,3]thiazolo[5,4- <i>h</i>][1,6]naphthyridines and [1,3]thiazolo[5,4- <i>h</i>][1,6]naphthyridine-8-ones	31
3.3. Biological evaluations of synthesized naphthyridines	34
3.4. Structural modifications: chemical synthesis	39
3.5. Biological evaluations of newly synthesized derivatives	45
3.6. Broad-spectrum screening	47
3.7. Evaluation of drug-like properties	53
4. Conclusions	58
5. Experimental	62
5.1. Chemistry	62
5.2. Biology	92
6. References	95
7. Project in collaboration with the Rega Institute for Medical Research: “Effect of combination therapy of pritelivir or amenamevir with acyclovir or foscarnet on HSV-2 drug resistance evolution”	108
7.1. Introduction	108
7.2. Experimental	112
7.3. Results and Discussion	114
7.4. Conclusions	122

7.5. References	123
8. Project in collaboration with Net4Sciences: “HSV-1 Glycoprotein D and its surface receptors: evaluation of protein-protein interaction and targeting by triazole-based compounds through <i>in silico</i> approaches”	127
8.1. Introduction	127
8.2. Experimental	130
8.3. Results and Discussion	133
8.4. Conclusions	143
8.5. References	144

Abbreviations

3CLpro	3-Chymotrypsin-Like protease
ACN	Acetonitrile
ACVr	Acyclovir-resistant
AMV	Amenamevir
BKV	Human Polyomavirus BK
COPD	Chronic Obstructive Pulmonary Disease
CPE	Cytopathic Effect
DMAP	4-Dimethylaminopyridine
DMEM	Dulbecco's Modified Eagle's Medium
DMF	<i>N,N</i> -dimethylformamide
DMSO	Dimethyl sulfoxide
dsDNA	Double-stranded DNA
dsRNA	Double-stranded RNA
EDC HCl	<i>N</i> -(3-dimethylaminopropyl)- <i>N'</i> -ethylcarbodiimide hydrochloride
EMME	Diethyl ethoxymethylenemalonate
ERGIC	Endoplasmic-Reticulum-Golgi Intermediate Compartment
EV-A71	Enterovirus A71
EVD	Ebola Virus Disease
ExoN	Exonuclease
FBS	Foetal Bovine Serum
HA	Hemagglutinin
HAV	Hepatitis A Virus
HCMV	Human Cytomegalovirus
HCoV	Human Coronavirus
HCV	Hepatitis C Virus
HEL	Human Embryonic Lung fibroblast
Hep2	Human epithelial cells
Hep3B	Hepatocellular carcinoma
HOBt	Hydroxybenzotriazole
HSV	Herpes Simplex Virus

IAV	Influenza A Virus
JCV	Human Polyomavirus JC
MAOS	Microwave-Assisted Organic Synthesis
MCC	Minimum Cytotoxic Concentration
MDCK	Madin-Darby canine kidney
MM-GBSA	Molecular Mechanics Generalized Born Surface Area
MM-PBSA	Molecular Mechanics Poisson-Boltzmann Surface Area
NiRAN	Nidovirus RdRp-associated nucleotidyltransferase
Nsp	Non-structural protein
ORFs	Open Reading Frames
PFA	Foscarnet
PFU	Plaque Forming Units
PLpro	Papain-Like protease
PTV	Pritelivir
RBV	Ribavirin
RdRp	RNA-dependent RNA polymerase
RSV	Respiratory Syncytial Virus
RTC	Replication-Transcription Complex
SA	Sialic Acid
SFV	Semliki Forest Virus
SINV	Sindbis Virus
TEA	Triethylamine
THF	Tetrahydrofuran
TMPRSS2	Transmembrane Serine Protease 2
VZV	Varicella-Zoster Virus
YFV	Yellow Fever Virus
ZBD	Zinc-Binding Domain
ZIKV	Zika Virus

1. Introduction

Viruses have been recognized as the etiological agents responsible for many pathological conditions ranging from asymptomatic infections to serious diseases, even leading to death.

The first virus discovered as pathogen to humans was the Yellow Fever Virus in 1901. Since then, about 270 viruses responsible for human infections have been identified. Some of these viruses have been known for centuries, whereas others have only recently emerged.

Viruses can cause the common cold, influenza and warts or severe diseases such as AIDS, Ebola Virus Disease (EVD) or COVID-19. At least six epidemics have emerged in the last 40 years: Human Immunodeficiency Virus (HIV) in 1981, Severe Acute Respiratory Syndrome Coronavirus (SARS-CoV) in 2002, H1N1 Influenza Virus in 2009, Middle East Respiratory Syndrome Coronavirus (MERS-CoV) in 2012, Ebola Virus in 2013 and the Severe Acute Respiratory Syndrome Coronavirus-2 (SARS-CoV-2) in 2019 [1]. Analysing the chronological order of the latest outbreaks, this is the third time that a virus belonging to the family *Coronaviridae* has caused an epidemic of such a massive scale in the 21st century.

Eradicating diseases caused by viral pathogens on a global scale is not an easy task at all. Indeed, there are only two viruses that have been eradicated in human history by means of vaccines: Smallpox (a human infectious disease caused by the Variola Virus) and Rinderpest Virus (an infectious viral disease affecting cattle and domestic buffalo). Since the introduction of the Smallpox vaccine in 1796, Smallpox was declared eradicated in 1980, thus taking almost two centuries to beat the disease. Rinderpest is the first - and so far the only - animal disease to be eradicated, in 2011.

Despite the progress made in the discovery of new antiviral agents, many viral infections still lack a specific treatment, with drug-resistance issues and the emergence of significant new variants often making the therapeutic approach even more difficult. Therefore, the identification of efficient therapeutic strategies is still an unmet medical need that has yet to be addressed. To overcome these drawbacks, the development of new compounds against potential novel targets could be useful to allow combined therapies aiming at reducing the risk of selection of drug-resistant viral strains.

In this scenario, there is a considerable interest in the identification of new chemical entities able to exert antiviral activity, as proved by the increasing number of publications focused both on repurposing studies and on the synthesis of novel compounds since 2015, with a peak in 2020 due to the COVID-19 pandemic.

1.1 Triazoles as antiviral agents

Nitrogen heterocycles represent a valuable tool in the identification of bioactive molecules, thus making them a precious source of new therapeutic agents in medicinal chemistry. In particular, triazoles have received considerable attention due to their chemical versatility, together with their wide range of biological activities, including anti-cancer [2], anti-inflammatory [3], antitubercular [4], antileishmanial, antitrypanosomal [5], antimalarial [6], antimicrobial [7], antibacterial [8] and antiviral properties [9–12]. Among antiviral drugs on the market, ribavirin (RBV) and taribavirin (a prodrug of ribavirin) are 1,2,4-triazole derivatives clinically used in the treatment of viral infections caused by several RNA viruses [13]. Like other nucleoside-based compounds, they need to be activated inside the cell through subsequent phosphorylation reactions. Unfortunately, as many other nucleoside analogues, they often suffer of several disadvantages, such as low bioavailability, high toxicity and, most notably, the tendency to develop drug resistance [14]. To date, many novel non-nucleoside compounds have been designed trying to solve these problems and to obtain more effective antiviral agents. An overview of the most interesting compounds reported in the literature will be described in this paragraph.

Among triazole-based derivatives, arylsulfonylhydrazide-1,2,3-triazoles **1** and **2** (Figure 1) were identified by Jordão et al. as HSV-1 replication inhibitors in Vero cells, with IC_{50} values of 1.30 and 1.26 μM , respectively. They showed low cytotoxicity ($CC_{50} = 1266$ and $1174 \mu\text{M}$, respectively) and selectivity index (SI) values (**1** = 974; **2** = 932) comparable to that shown by acyclovir used as reference drug ($IC_{50} = 0.99 \mu\text{M}$; $CC_{50} = 860 \mu\text{M}$; SI = 869) [11].

Polyhydroxylated dibenzyl ω -(1*H*-1,2,3-triazol-1-yl)alkylphosphonate derivatives have been synthesized by Glowacka et al. to be evaluated for their activity against a broad variety of DNA and RNA viruses. Among them, the pyrimidinone-triazole derivative **3** exhibited antiviral activity against Influenza A H3N2 subtype ($EC_{50} = 20 \mu\text{M}$) in Madin Darby canine kidney cell cultures (MDCK), while derivative **4** showed an interesting activity against vesicular stomatitis virus and respiratory syncytial virus in HeLa cell cultures with EC_{50} values of 9 and 12 μM , respectively (Figure 1) [15].

The pyrimidinone moiety was also found in a series of 1,2,3-triazoles which have been synthesized as part of a study aiming at identifying novel antiviral agents against Varicella-Zoster virus (VZV). Hybrid derivative **5** (Figure 1) showed an interesting viral growth inhibition,

with an EC₅₀ of 3.6 μM on VZV TK⁺ strain, without measurable cytotoxicity during cell growth (CC₅₀ > 100 μM) [16].

The molecular hybridization approach has also been applied in the design of a class of 4-yl-methylen-heteroaryl decorated molecules. In particular, a set of pyrazine-triazole conjugates with a significant SARS-CoV-2 RdRp activity were identified. Their antiviral and cytotoxic properties and selectivity indexes were evaluated in Vero-E6 cell line. Among all tested derivatives, **6** (Figure 1) was found to be the most active, being endowed with high potency (IC₅₀ = 0.477 μM), low cytotoxicity (CC₅₀ = 4.916 μM) and high selectivity index (SI = 10.3), almost three times higher than the control drug Favipiravir (IC₅₀ = 1.382; CC₅₀ = 5.262 μM; SI = 3.8) [17].

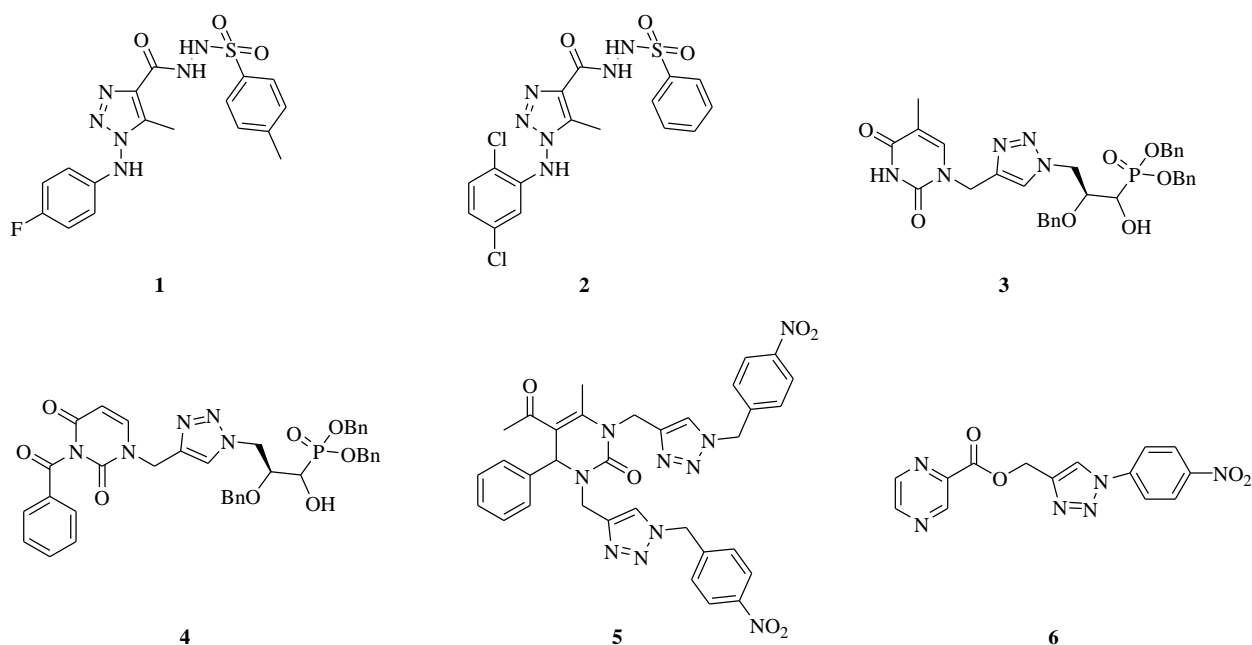


Figure 1. Representative 1,2,3-triazoles with antiviral activity

Condensation of the benzene ring with the triazole core led to some benzotriazole derivatives which have been reported as promising inhibitors of the main protease (3CLpro) of SARS-CoV-2, due to their ability to establish key interactions with the catalytic dyad (Cys145 and His41) of the enzymatic active site. In particular, derivative **7** (Figure 2), emerged as a potent 3CLpro inhibitor, showing an inhibition constant $K_i = 7.5$ nM and an IC₅₀ value of 0.2 μM, without any cytotoxicity at concentration up to 100 μM. *In silico* studies on the mechanism of action showed that compound **7** caused an irreversible inhibition of SARS-CoV 3CLpro via acylation of Cys145 of the catalytic dyad in the active site [18]. As part of a study aimed at identifying new

agents acting with a non-covalent inhibition of 3CLpro, Turlington et al. demonstrated potential antiviral activity of benzotriazoles derivatives **8** and **9** (ML300) (Figure 2), showing IC₅₀ values of 6.2 μM and 4.11 μM, respectively [19]. Replacement of the *N*-methyl pyrrole moiety of derivative **8** with a thiophene ring and introduction of an isopropyl amide (**10**) or cyclobutylamide (**11**) on the acetamide moiety (Figure 2) improved the inhibitory activity with IC₅₀ values of 4.1 and 3.8 μM, respectively [20].

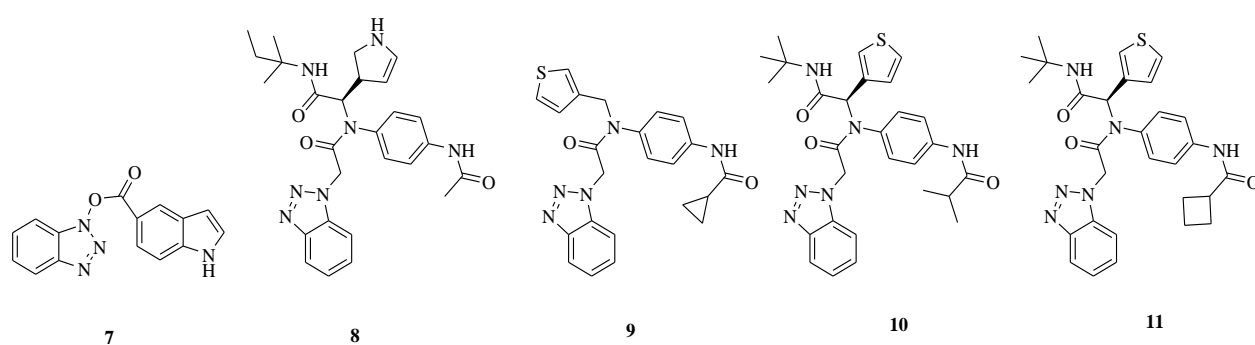


Figure 2. Representative benzotriazoles with antiviral activity

A commonly used strategy in drug development is the condensation with different heterocyclic moieties to enhance the biological effect and drug-like properties of new scaffolds. Thus, the [1,2,4]triazolo[4,3-*a*]pyrimidine derivative **ANA-1** (**12**, Figure 3) showed promising anti-Flu activity in a plaque reduction assay on influenza H1N1 virus, with an EC₅₀ value of 0.55 ± 0.10 μM, while low cytotoxicity (CC₅₀ = 125 ± 18 μM) was found by MTT assay on MDCK cells, with an interesting selectivity index (SI = 227). *In vitro* antiviral activity of **ANA-1** was determined by multi-cycle virus growth assays, showing inhibition of different subtypes of influenza virus in a dose-dependent manner, with most promising antiviral effect against H9N2 virus infection (EC₅₀ = 0.09 ± 0.03 μM). *In vivo* studies were also performed, proving that **ANA-1** could inhibit viral replication on mice. Mechanism of action studies proved that **ANA-1** suppressed viral replication by interfering with polymerase activity [21].

More recently, interesting results have been shown by [1,2,3]triazolo[4,5-*c*]pyridine derivatives **13-17** (Figure 3), which exhibited promising antiviral activity against the human coronavirus 229E (EC₅₀ = 8.90-11.95 μM). No alteration of cell morphology was found for concentrations up to 100 μM, and all compounds showed a good selectivity index (SI > 8). *In silico* studies demonstrated the ability of the triazolo[4,5-*c*]pyridine scaffold to be placed in proximity of the

catalytic dyad of the protease 3CLpro, establishing molecular interactions that determined its inhibition [22].

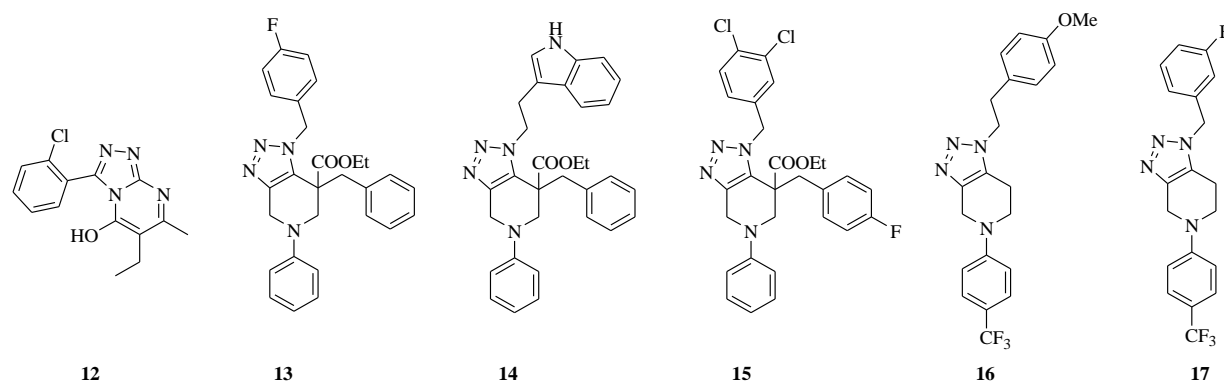


Figure 3. Condensed triazole derivatives with antiviral activity

1.2 Thiazoles as antiviral agents

Among nitrogen-based heterocycles, thiazoles have also demonstrated important applications in medicinal chemistry, thus representing a valuable tool in the identification of bioactive molecules. Thiazoles are five-membered heterocycles containing one nitrogen and one sulphur atom, which have also been found in many marketed synthetic drugs acting as antimicrobial [23], antidepressant [24], antineoplastic [25], antiasthmatic [26], antiulcer [27], anti-inflammatory [28], antifungal [29] and antiviral agents. Among the latter, a relevant example is ritonavir (**18**, Figure 4), an HIV protease inhibitor used in combination with other antivirals in the treatment of HIV infection. In fact, due to its CYP3A inhibition properties, ritonavir is mainly used as a booster of other protease inhibitors to increase their plasmatic concentrations and to improve their pharmacokinetic properties [30]. In 2022, ritonavir was also approved in combination with nirmatrelvir for the treatment of mild-to-moderate coronavirus disease 2019 in adults with high risk to develop severe form of COVID-19. Simeprevir (**19**, Figure 4), another thiazole derivative in the market, is an inhibitor of hepatitis C virus (HCV) NS3/4A protease indicated for the treatment of chronic HCV infection. Simeprevir exhibited a broad-spectrum antiviral activity, and it can also be used in patients with AIDS (acquired immunodeficiency syndrome) and for the treatment of HSV-1 (Herpes simplex type 1), ZIKV (Zika virus) and EV-A71 (Enterovirus A71) virus infections. Recently, simeprevir has also been identified from a virtual screening as a potential candidate for treatment of COVID-19 [31]. Pritelivir (BAY 57–1293) (**20**, Figure 4) is a helicase-primase inhibitor that has been used in clinical trials studying

the prevention of HSV-2 genital herpes and is currently in development for the treatment of acyclovir-resistant (ACVr) Herpes Simplex Virus (HSV) infections. A phase III trial (NCT03073967) evaluating the efficacy and safety of pritelivir tablets for treatment of ACV-resistant mucocutaneous HSV infections in immunocompromised subjects is still ongoing.

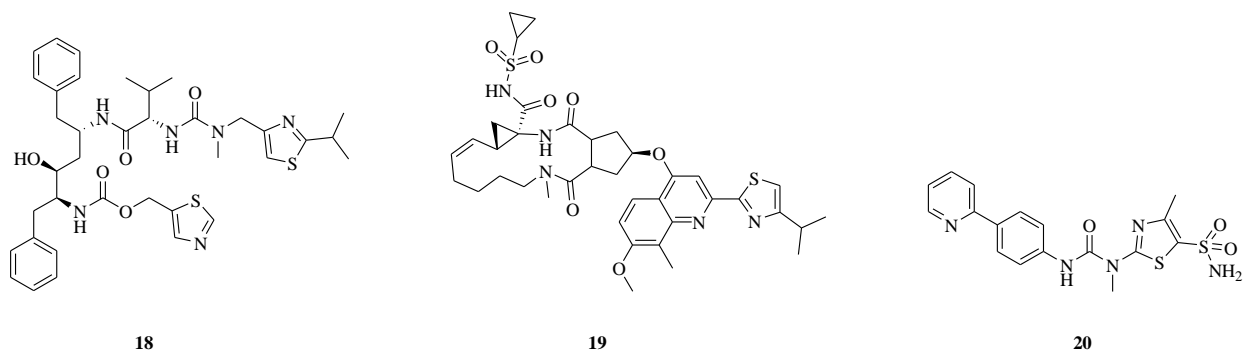


Figure 4. Marketed/approved antiviral drugs containing the thiazole moiety

In addition to approved drugs, to date, several other thiazole-based compounds with different structural features have been reported in the literature for their promising antiviral activity. Among them, focusing on compounds able to inhibit coronaviruses, derivative **21** (Figure 5) has been identified from a structure-based virtual screening as a novel SARS-CoV 3CLpro inhibitor with an IC_{50} value of 3 μ M [32]. Strong inhibition of HCoV-229E replication has been displayed by the spiro-derivative **22** (Figure 5) with an EC_{50} of 5.5 μ M [33].

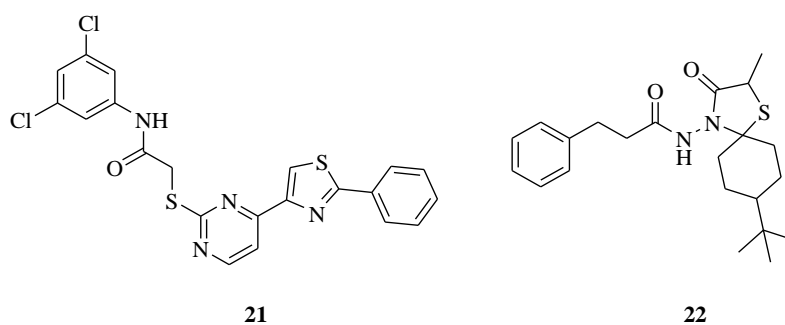


Figure 5. Representative thiazoles with antiviral activity

Condensed ring systems incorporating the thiazole nucleus have been also explored. In particular, benzothiazoles have received notable attention for their potential application as antiviral agents as proved by compound **23** (Figure 6). It emerged as a promising potential

SARS-CoV 3CLpro inhibitor with an IC_{50} value of 4.3 μ M with no detectable inhibition of any of the other tested proteases (HAV 3Cpro, NS3pro, chymotrypsin, and papain) [34].

Condensation of 1,3-thiazole scaffold with the pyridine nucleus led to a novel series of thiazolo[5,4-*c*]pyridines, which were evaluated for their antiviral activity against human polyomaviruses JCV and BKV. Among them, the *N*-(4-((3-(thiazolo[5,4-*c*]pyridin-2-yl)pyridin-2-yl)oxy)-phenyl)acetamide **24** (Figure 6) emerged as the most attractive compound, with a dual inhibitory activity against both JCV and BKV helicases. Derivative **24** was demonstrated to act as an ATP-competitive inhibitor with an IC_{50} value of 0.6 μ M and no marked cytotoxicity in Vero cells [35]. Finally, compound **25** (Figure 6) emerged from a high-throughput screening (HTS), performed on a library of about 6800 compounds with the aim of identifying novel coronaviruses main protease inhibitors. This study led to the identification of derivative **25** as an interesting hit, exhibiting IC_{50} values of about 7.2 μ M and 5.6 μ M against SARS-CoV 3CLpro and HCoV-229E 3CLpro, respectively [36].

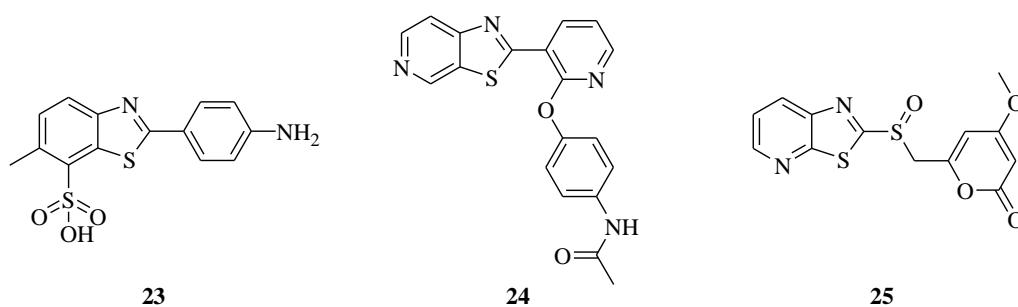


Figure 6. Condensed thiazole derivatives with antiviral activity

From the brief overview on the state of the art concerning triazole- and thiazole-based derivatives reported in the literature, it emerges how the focus of research has turned towards the identification of new antiviral compounds, particularly in response to the COVID-19 pandemic. Besides the efforts to date, the spread of emerging variant strains of SARS-CoV-2 still represents a global concern, pointing out the need for new therapeutic approaches.

Therefore, the aim of my PhD thesis is the synthesis of a small library of triazole- and thiazole-based derivatives to investigate their potential antiviral properties against SARS-CoV-2 and to explore their structure-activity relationships (SARs).

1.3 Coronaviruses

Coronaviruses are enveloped positive-sense single-stranded RNA viruses classified under the order of *Nidovirales* and belonging to the *Coronaviridae* subfamily *Orthocoronavirinae*, in turn divided into four genera: *alphacoronavirus*, *betacoronavirus*, *gammacoronavirus* and *deltacoronavirus* (Figure 7). *Alphacoronaviruses* and *betacoronaviruses* are responsible for infections in mammalian species, while *gammacoronaviruses* and *deltacoronaviruses* are the causative agents of respiratory and enteric diseases in animals. However, animal Coronaviruses can also infect humans, resulting in the spread of the infection through human-to-human transmission [37].

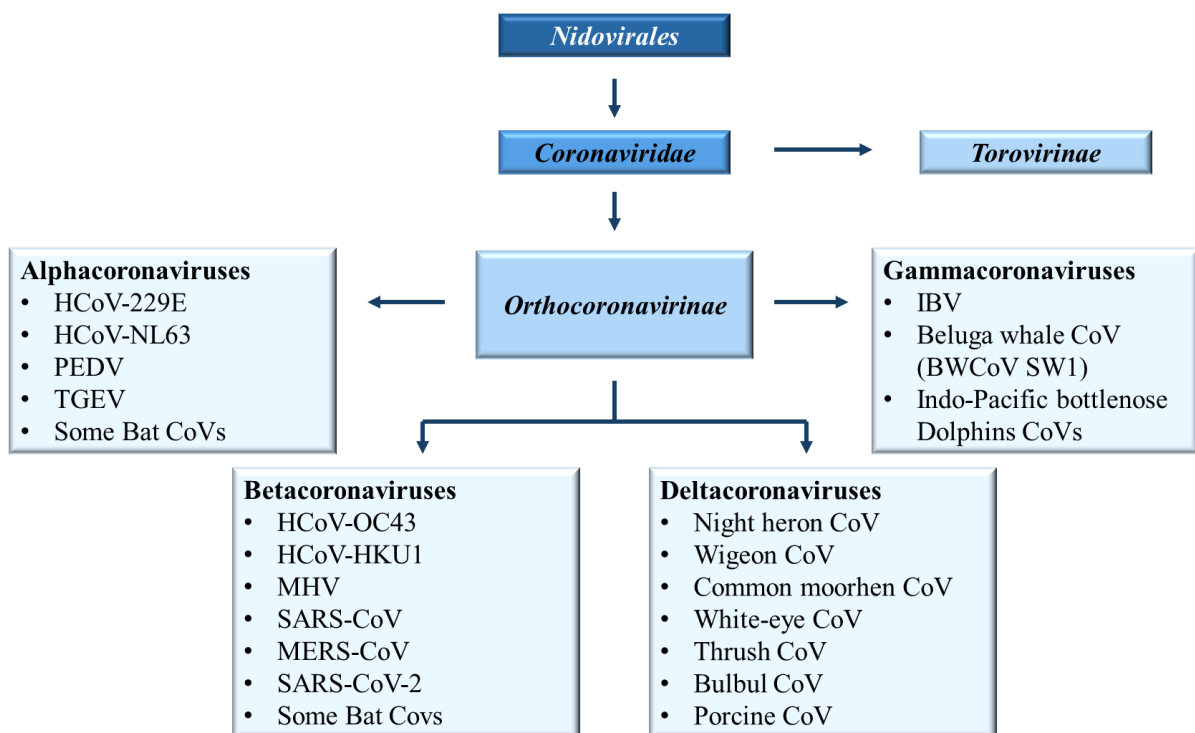


Figure 7. Taxonomy of *Coronaviridae*

To date, seven human coronaviruses (HCoVs) have been discovered. Among them, HCoV-229E, HCoV-NL63, HCoV-OC43 and HCoV-HKU1 cause mild respiratory infections, while Severe Acute Respiratory Syndrome coronavirus (SARS-CoV), Middle East Respiratory Syndrome coronavirus (MERS-CoV) and SARS-CoV-2 are highly infectious agents responsible of severe human respiratory diseases, with potentially high mortality rate [38,39]. SARS-CoV-2, the etiologic agent of the coronavirus disease 2019 (COVID-19) pandemic, resulted in about 676 million infections and more than 6 million deaths worldwide [40]. In order to counteract SARS-

CoV-2 infection and to identify new, more potent inhibitors, several bio-molecular studies have been conducted with the aim of improving the knowledge of the structural features of the virus as well as the mechanisms regulating its replication.

1.4 SARS-CoV-2 genome and life cycle

SARS-CoV-2 is classified as a *betacoronavirus* with a 5'-capped, single-stranded RNA genome of approximately 30 kbs, with a 3' polyadenylated tail of variable length, encoding at least 14 open reading frames (ORFs). Among them, ORF1a and ORF1b occupy two-thirds of the genome and are translated in two polypeptides (pp1a and pp1ab), which are in turn processed by viral proteases 3CL^{pro} (3-chymotrypsin-like protease, Nsp5) and PL^{pro} (papain-like protease, Nsp3) into 4 structural proteins (Spike, Nucleocapsid, Matrix and Envelope), 16 non-structural proteins (Nsp1-16) and 11 accessory proteins (ORF3a, ORF3b, ORF3c, ORF3d, ORF6, ORF7a, ORF7b, ORF8, ORF9b, ORF9c and ORF10) (Figure 8) [41]. Non-structural proteins including primase (Nsp8), RNA-dependent RNA polymerase RdRp (Nsp12) and helicase (Nsp13) are involved in the formation of the replication-transcription complex (RTC), playing an essential role in viral gene replication [42].

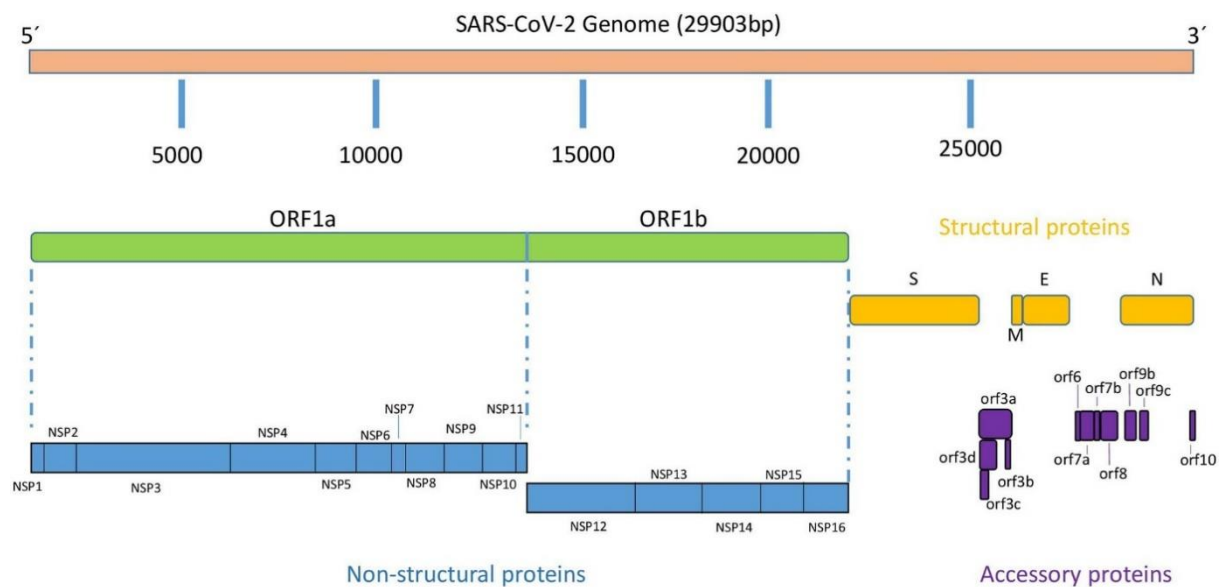


Figure 8. SARS-CoV-2 genome [41]

The entry of SARS-CoV-2 into the host cell starts with the interaction of the receptor binding domain (RBD) of the Spike protein (S-protein) with the cell surface angiotensin-converting

enzyme receptor 2 (ACE2). This process also requires the involvement of the host serine protease TMPRSS2 expressed in the human respiratory tract, which cleaves the viral Spike protein in S1 and S2 subunits, allowing the attachment and the fusion of the virus with the host cell membrane and the endocytosis of the viral particle. Because of the crucial function of the S protein, it is an attractive target for inhibition by neutralizing antibodies (nAbs), and knowledge of its structural features provides valuable information for rational vaccine design [43,44].

After the release of the viral genome into the cytoplasm, the host ribosomal machinery is used for the primary translation of ORF1a and ORF1b from the positive-sense (+ss) genomic RNA to produce the two polyproteins (pp1a and pp1ab) that can be processed by viral proteases (3CLpro and PLpro) to obtain the non-structural proteins (Nsp) necessary for the assembly of the replication-transcription complex (RTC). Due to their essential role in the life cycle of the virus, both viral proteases 3CLpro and PLpro have also been extensively investigated as druggable targets for the development of effective and selective antiviral agents against SARS-CoV-2 [45].

The replication-transcription complex (RTC) is located in convoluted membrane (CM) structures derived from endoplasmic reticulum (ER) and is anchored on site by viral non-structural proteins Nsp3, Nsp4, and Nsp6 [46]. The RdRp complex, which is the key component of the RTC, uses the genome as a template to generate a complementary full-length negative-strand RNA, which in turn functions as a template for synthesis of full-length positive-strand progeny genomes, then packaged into new virions. In addition to genomic replication, the RTC is also responsible for the synthesis of subgenomic (sg RNA) mRNAs, which are translated into structural and accessory proteins. Viral RNA replication and transcription are followed by coating of the viral RNA genome with N protein and translocation of the resulting nucleocapsid into the endoplasmic-reticulum-Golgi intermediate compartment (ERGIC), where structural proteins S, E, and M, translated in the ER from positive-sense subgenomic RNAs, are incorporated into the envelope to generate mature infectious virions. Finally, enveloped virions leave the cell through exocytosis (Figure 9) [38].

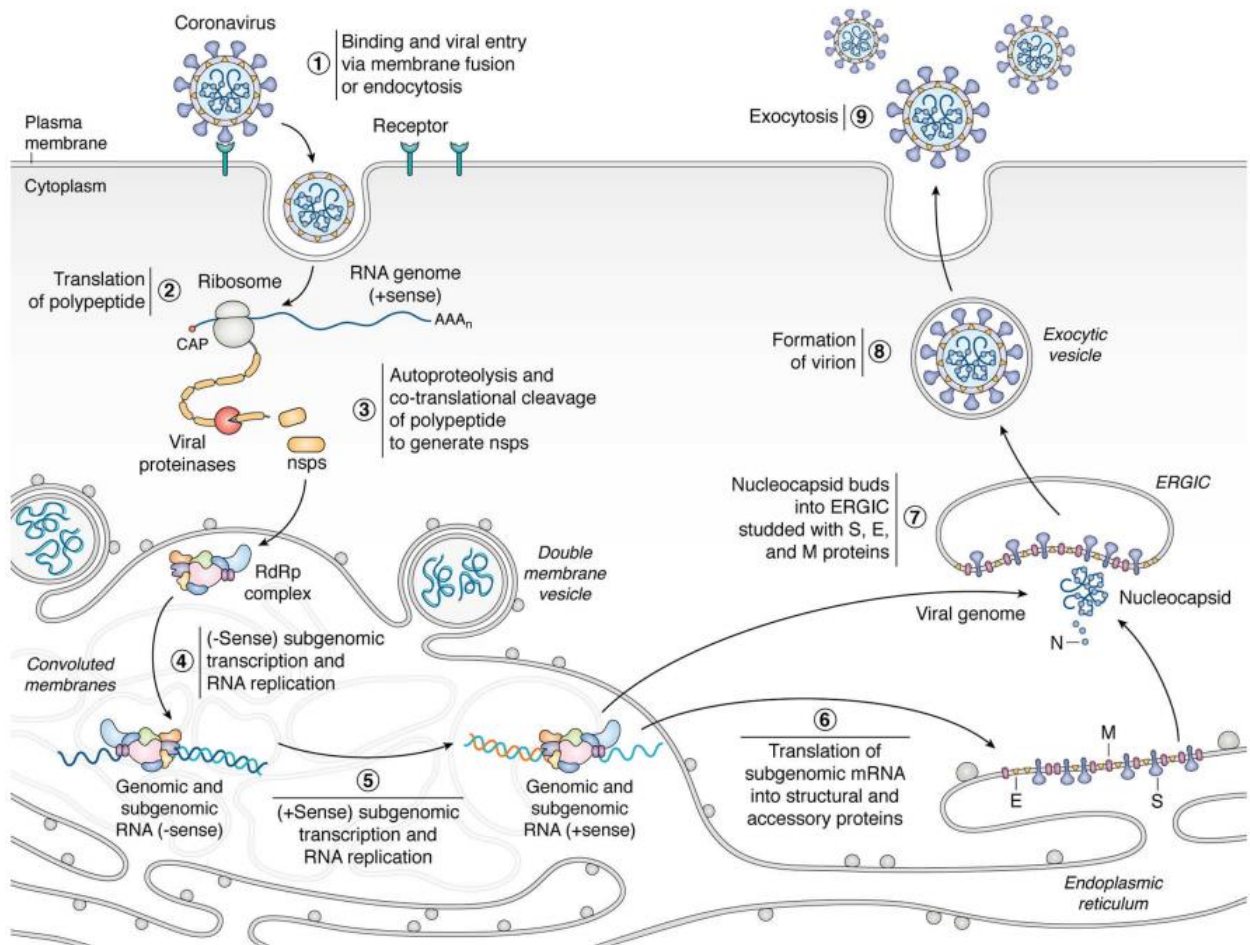


Figure 9. SARS-CoV-2 life cycle [46]

In this complex machinery, it is evident that the assembly of the viral RTC (Figure 10) is a crucial step for virus replication and, due to its structural complexity, it deserves to be described in more detail. RTC involves the activity of several non-structural proteins regulating replication and transcription, unwinding, proofreading and RNA capping functions. The key component of the RTC is the Nsp12 RNA-dependent RNA polymerase (RdRP) catalysing the synthesis of viral RNA. In addition, one Nsp7/Nsp8 heterodimer and a second Nsp8 subunit contribute to the activation of the RdRp complex. Nsp12 shows the typical structure of “right-hand polymerases” [47], with a shape resembling a cupped right hand with “fingers,” “palm,” and “thumb” subdomains, each contributing to the correct arrangement of the substrate and metal ions within the catalytic site of the enzyme [48]. RdRp also have a conserved N-terminal domain with a nucleotidyl transfer activity (NiRAN domain), which is essential for viral replication.

The activity of Nsp12 is Mg^{2+} - and Mn^{2+} -dependent, with the active site located in the palm domain, and the fingers-thumb interaction region containing the binding site for the Nsp7/Nsp8 heterodimer [49]. Nsp7 is a processivity factor for RdRp, while Nsp8 works as a primase also providing a 3'-terminal adenylyltransferase activity, which regulates translation efficiency of the mRNAs and is essential for negative-strand RNA synthesis [50]. Both Nsp7 and Nsp8 were found to stimulate the activity of Nsp12, through stabilisation of the RNA binding regions [47].

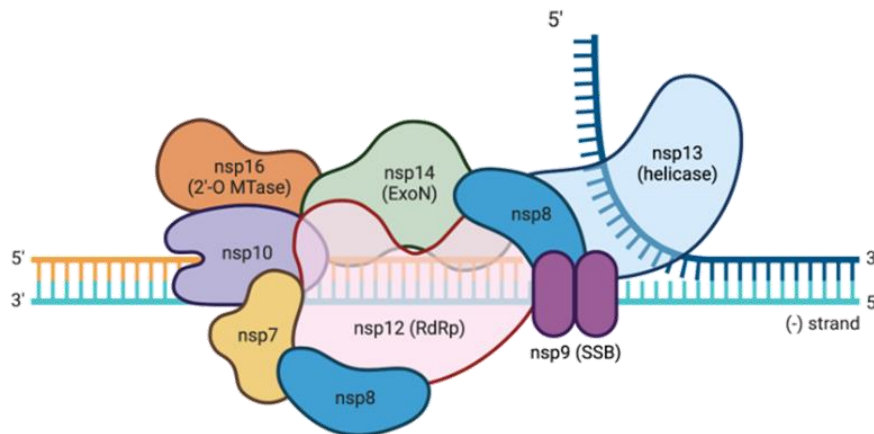


Figure 10. Structures of SARS-CoV-2 replication and transcription complex (created with BioRender.com)

The RTC is also responsible for RNA capping, which normally occurs co-transcriptionally in the nucleus and is essential for viral translation, mRNA protection and escape from host immune system. This process requires the activity of multiple non-structural proteins, which are also assembled in the RTC complex (Figure 10). In this context, another key component of the RTC is the Nsp13, a superfamily 1B (SF1B) $5' \rightarrow 3'$ helicase able to interact with Nsp12 and other components of the RTC, also providing the RNA 5'-triphosphatase activity essential for the formation of the 5' mRNA cap [51]. The coronavirus capping mechanism follows a strictly regulated pathway (Figure 11): it begins with the removal of the γ -phosphate group of the 5'-terminal RNA nucleotide by the RNA 5'-triphosphatase activity of Nsp13, followed by the addition of a cap of guanosine monophosphate (GMP) to the diphosphate RNA by the RdRp-associated nucleotidyl-transferase (NiRAN) domain of Nsp12 with guanylyl-transferase (GTase) activity. The guanosine is then methylated at the N7 position by Nsp14, which possesses a N7-methyltransferase (MTase) activity, using S-adenosylmethionine (SAM) as the methyl donor. Finally, the ribose 2'-O nucleotide is methylated by the capping enzyme Nsp16, providing

the 2'-*O*-methyltransferase activity. This step also requires interactions with the cofactor Nsp10, which is involved in improving substrate and RNA binding of Nsp14 and Nsp16 [46]. The last component of the RTC is the single-strand nucleic acid-binding protein Nsp9 (SSB), which is thought to protect the single-stranded regions of the viral genome from nucleases and regulate the recruitment of Nsp10–Nsp14 or Nsp10–Nsp16 complexes [39,46].

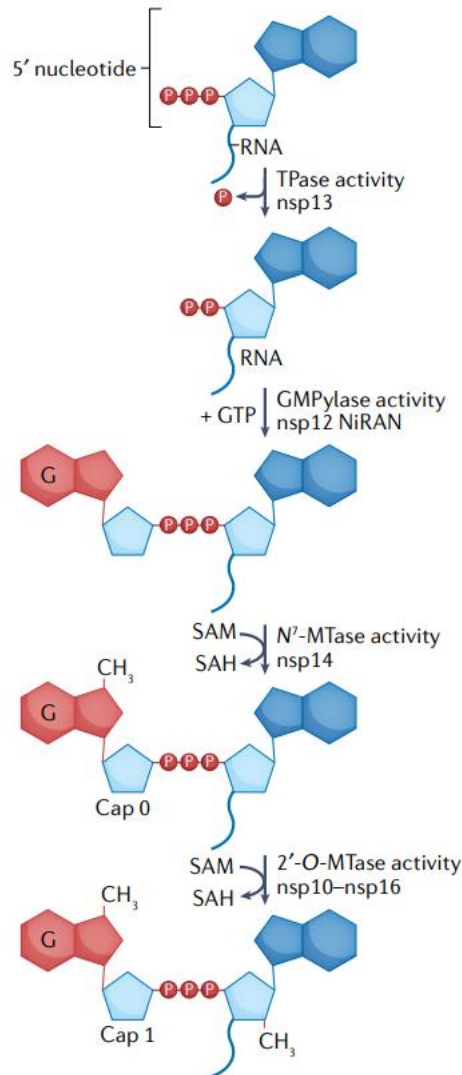


Figure 11. RNA capping pathway of SARS-CoV-2 [52]

Moreover, it has been shown that RTC plays another important role in the error-correcting processes known as proofreading. RNA viruses are typically characterized by high mutation rates due to the lack of RdRp proofreading activity, which increases the genetic diversity and the adaptive potential of the virus. On the other hand, this is also associated with an accumulation of deleterious mutations that can cause a significant reduction of the genome size of most RNA

viruses to ~15 kb [53]. By contrast, Coronaviruses appear to have developed a sophisticated mechanism to prevent the accumulation of such mutations and preserve the integrity of their unusually large genome of ~30 kb. Indeed, they are one of the few RNA viruses that have an exonuclease (ExoN) with a proofreading activity that guarantees low mutation rates and therefore high-fidelity replication [54]. The ExoN resides in the N-terminal domain of Nsp14, which forms an RNA proofreading complex with Nsp10, therefore playing another important role in enhancing the fidelity of genome replication [46].

1.5 Replication-transcription complex (RTC) proteins as drug targets

The assembly of the viral RTC is a crucial step for virus replication, thus representing a promising target for the development of antiviral agents against SARS-CoV-2. Replication and transcription are performed primarily by Nsp12 and Nsp13, while the other RTC components have supporting roles in the RTC and are involved in proofreading, mRNA protection and modulation of host's innate immune responses.

The RNA-dependent RNA polymerase Nsp12 is a proven target for antiviral drugs, as it is essential for the viral life cycle and lacks homologs in the host. Nucleoside analogues targeting RdRp are commonly used as antiviral therapeutics, as reported for remdesivir and molnupiravir. Remdesivir was the first antiviral drug approved by the Food and Drug Administration (FDA) for the treatment of coronavirus disease in hospitalized patients with moderate/severe symptoms. Since remdesivir requires intravenous administration, the oral prodrug molnupiravir has been developed to facilitate administration to non-hospitalized adult patients who have a high risk of developing a severe form of COVID-19.

Molnupiravir has not been approved by FDA but has been authorized in 2021 under an Emergency Use Authorization (EUA) for “the treatment of adults with a current diagnosis of mild-to-moderate coronavirus disease 2019 (COVID-19) who are at high risk for progression to severe COVID-19, including hospitalization or death, and for whom alternative COVID-19 treatment options approved or authorized by FDA are not accessible or clinically appropriate” [55]. On March 2023, the Italian Medicines Agency (AIFA) communicated that the Scientific Technical Commission decided to suspend the use of the molnupiravir following the negative opinion issued by EMA's human medicines committee (CHMP) due to the impossibility to demonstrate the clinical benefit of molnupiravir in term of reduction of mortality and hospitalization risk [56]. The therapeutic efficacy of remdesivir and molnupiravir can be

explained by the unique mechanism of action by which they interfere with the RNA synthesis compared to classical chain terminators. Indeed, once incorporated into the nascent RNA, none of these compounds induces an immediate interruption of RNA synthesis, blocking the chain elongation three nucleotides downstream of their incorporation site. This feature, associated with the high selectivity of the RdRp for remdesivir and molnupiravir over the natural substrate ATP, reduces their recognition by Nsp14 and protects them from ExoN cleavage [57]. An alternative strategy to escape the Nsp14 proofreading activity could be to combine ExoN inhibitors with nucleoside RdRp inhibitors or to develop non-nucleoside *small molecules* able to allosterically inhibit the viral RdRp without susceptibility to the exonuclease activity of ExoN [48,58].

The second key component of the RTC is the Nsp13, a multi-domain protein endowed with NTPase/helicase activity. While the SARS-CoV-2 RNA-dependent RNA polymerase (Nsp12) has been extensively studied as validate drug target, there are no approved drugs for COVID-19 targeting the helicase Nsp13. Although less explored, Nsp13 has recently been identified as one of the most attractive targets for the development of new antiviral agents [59], due to its high degree of genetic conservation among coronavirus species and its essential role in SARS-CoV-2 replication. Consequently, a thorough knowledge of its structural features and the molecular mechanisms regulating its activity may be useful for the identification of novel SARS-CoV-2 therapeutics.

1.6 SARS-CoV-2 Nsp13

SARS-CoV-2 Nsp13 belongs to the helicase superfamily 1B (SF1B) and acts by catalysing the unwinding of dsDNA or RNA in a 5' to 3' direction in a nucleoside triphosphate (NTP) dependent manner. Additionally, it has been shown that Nsp13 is a bifunctional enzyme which also possesses an RNA 5' triphosphatase activity within the same NTPase active site: by removing the γ -phosphate group of the 5'- terminal RNA nucleotide, Nsp13 could play a further essential role during the formation of the 5' mRNA cap, thus contributing to the human immune system evasion and viral diffusion [51]. The Nsp13 helicase is one of the most well-conserved non-structural proteins in the SARS-CoV-2 genome, sharing a 99.8% sequence identity compared to SARS-CoV, from which it differs for only a single amino acid residue (V570 in SARS-CoV-2 Nsp13 instead of I570 in SARS-CoV) [60]. With a triangular pyramidal shape, SARS-CoV-2 Nsp13 contains five conserved domains essential for helicase activity: the N-terminal zinc-binding domain (ZBD) coordinating three zinc ions, the stalk domain and the 1B domain, which

are responsible of protein-protein and/or nucleic acid interactions within the RTC; two “RecA-like” domains 1A and 2A contain the active site for NTP binding and hydrolysis (Figure 12) [51].

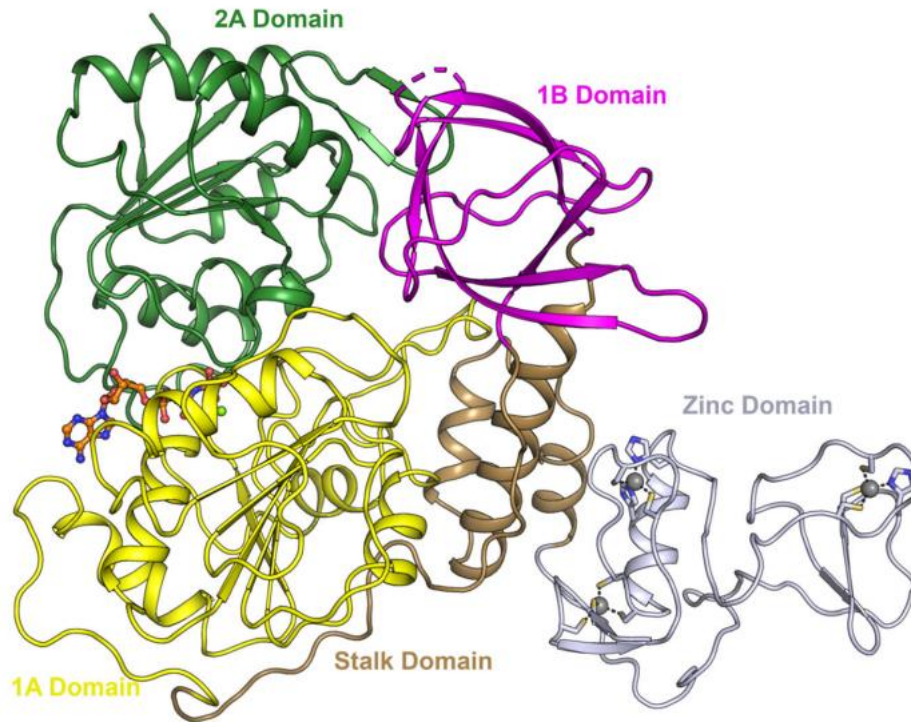


Figure 12. Structure of SARS-CoV-2 Nsp13 [61]

Several studies reported that Nsp13 interacts with other components of the RTC complex (Nsp12/Nsp7/Nsp8), and this interaction seems to significantly enhance the unwinding activity of Nsp13 [62–64]. Structural determination of the Nsp13 containing-RTC (Nsp13₂-RTC, Figure 13) revealed that the replication-transcription complex consists of two copies of Nsp13, interacting with Nsp8 through the N-terminal ZBD. Only one Nsp13 protomer interacts with Nsp12 and is located in proximity to its RNA binding site, while the role of the second Nsp13 molecule is not well understood, although it is supposed to regulate and enhance the enzyme unwinding activity [63,65].

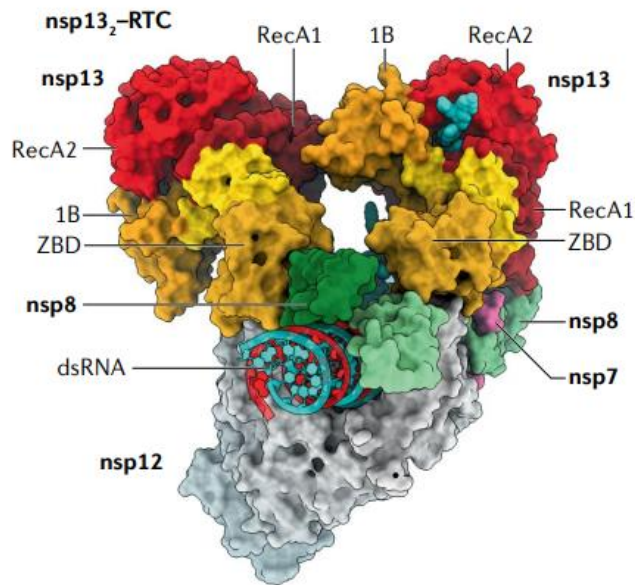


Figure 13. Structure of the SARS-CoV-2 Nsp13 containing-RTC (Nsp13₂-RTC) [52]

The proposed model for the Nsp13 5' → 3' translocation mechanism is based on the transition of the enzyme from a “closed” to an “open” state (Figure 14). The “closed” conformation represents an activated pre-hydrolysis state in which Nsp13 strongly interacts with the 3'-end RNA through its 2A domain. The transition starts with ATP binding, hydrolysis and release of ADP from the nucleotide-binding site, which trigger the conformational changes to the “open” product/APO state characterized by a reduction of the RNA binding affinity for the 2A domain and a strong interaction with the 1A domain. This conformational change causes an “inchworm”-like sliding of the Nsp13 along the single-stranded RNA substrate. The catalytic cycle ends with the binding of a new ATP molecule that induces the conformational changes restoring the “closed” state [61].

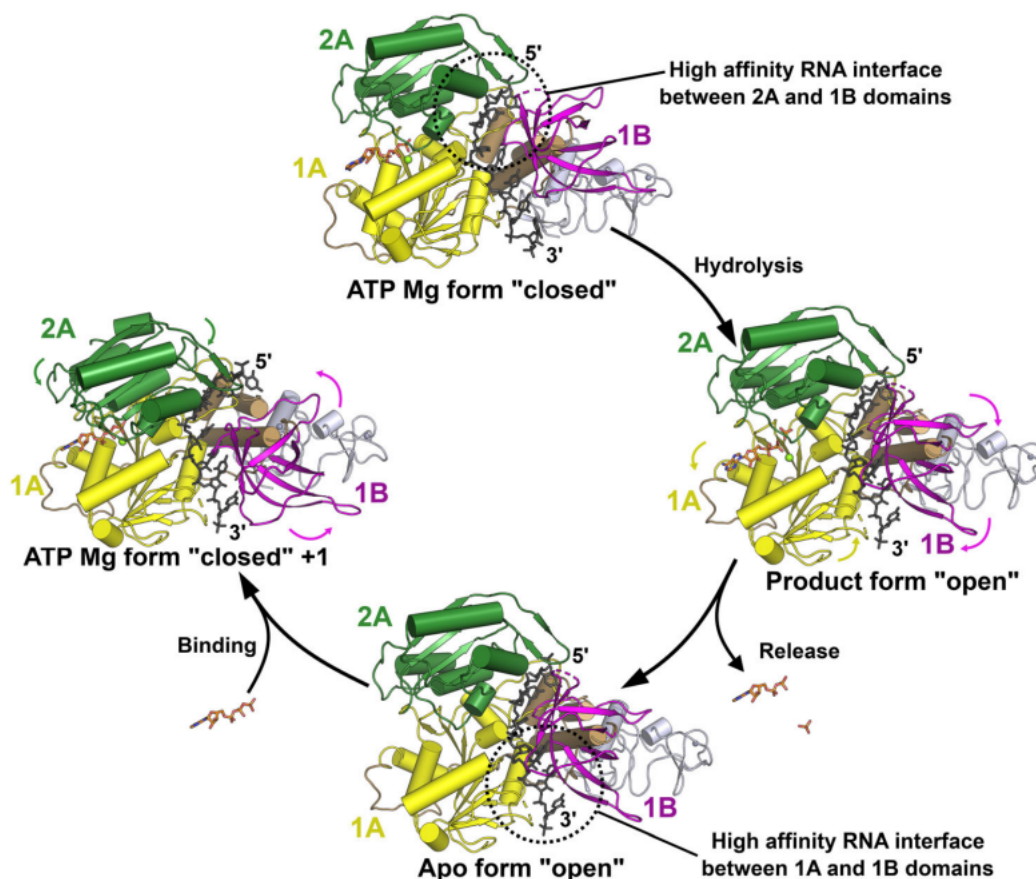


Figure 14. Proposed model for the Nsp13 5' → 3' translocation mechanism [61]

1.7 Triazole/thiazole-based compounds targeting Nsp13

Since the outbreak of the COVID-19 pandemic, many efforts have been made in drug discovery, to identify new effective and safe antiviral agents. Although multiple vaccines have been developed [66] and several clinical trials have been conducted to assess the therapeutic benefit of various drugs approved for other indications (e.g. chloroquine, hydroxychloroquine, ivermectin, corticosteroids dexamethasone and prednisolone, azithromycin, lopinavir/ritonavir, darunavir/cobicistat, low molecular weight heparins, immunomodulators and monoclonal antibodies) [67], to date only three antiviral drugs have been authorized for the treatment of COVID-19.

The paucity of therapeutic options for the treatment of infections caused by SARS-CoV-2, associated with the ongoing spread of this virus and its emerging variants highlight the need for new therapeutic approaches. Therefore, the identification of novel antiviral compounds inhibiting different viral targets, essential for virus replication, is needed.

In this context, structural analysis and experimental fragment screening of the SARS-CoV-2 Nsp13 revealed several druggable conserved pockets that could be relevant for structure-based drug design, highlighting the potentialities of Nsp13 as promising target for the development of broad-spectrum inhibitors that might be effective as pan-coronavirus antiviral agents [61].

Based on drug repurposing approaches, several FDA-approved drugs and other natural or synthetic compounds have been reported to inhibit the coronaviruses helicase activity [59], also including derivatives incorporating triazole or thiazole moieties. The 2,4-dihydro-5-[[[(2-nitrophenyl)thio]methyl]-4-(2-propen-1-yl)-3*H*-1,2,4-triazole-3-thione **SSYA10-001** (26, Figure 15) has been recently identified as a potent inhibitor of SARS-CoV replication ($EC_{50} = 8.95 \mu\text{M}$) with low cytotoxicity ($CC_{50} > 250 \mu\text{M}$) emerged for its ability to block the double-stranded RNA (dsRNA) and DNA (dsDNA) unwinding activities of Nsp13 with IC_{50} values of 5.70 and 5.30 μM , respectively. Inhibition kinetic studies revealed that **SSYA10-001** acts as a noncompetitive inhibitor of Nsp13 with respect to nucleic acid and ATP substrates. Moreover, **SSYA10-001** did not prevent ATP hydrolysis or Nsp13 binding to the nucleic acid substrate, suggesting that it specifically inhibits Nsp13 by inducing conformational changes affecting the catalytic cycle of the enzyme. **SSYA10-001** did not inhibit other viral helicases (HCV NS3h and dengue virus NS3 helicases), as well as bacterial and viral RNA-dependent RNA polymerases, or reverse transcriptase, thus confirming its selectivity for SARS-CoV Nsp13 [68]. However, **SSYA10-001** had no inhibitory effect on the ATPase activity [69]. Furthermore, **SSYA10-001** was recently reported to significantly inhibit the SARS-CoV-2 Nsp13-associated unwinding activity with an IC_{50} value of 1.7 μM , without blocking the ATPase function, as previously reported for SARS-CoV [70]. Finally, molecular docking studies also revealed that **SSYA10-001** possibly interacted with a specific binding site within the MERS-CoV helicase [71], appearing as a good candidate for the development of broad-spectrum inhibitors.

Virtual screenings of the SARS-CoV-2 helicase have been widely used to predict the binding of several clinically approved or investigational drugs to the helicase active site in order to identify possible repurposing candidates with good antiviral properties. **PF-03715455** (27, Figure 15) is a 1,2,4-triazole-containing molecule which has been evaluated in clinical trials for the treatment of asthma, pulmonary disease and Chronic Obstructive Pulmonary Disease (COPD). By using *in silico* repurposing approaches, **PF-03715455** was identified by Romeo et al. as potential helicase inhibitor able to block both the unwinding and NTPase activities of Nsp13 *in vitro* in the low micromolar range, with IC_{50} values of 3.02 μM and 9.26 μM , respectively [72].

From a virtual screening of Food and Drug Administration (FDA) approved antiviral drugs, the Hepatitis C virus (HCV) NS3/4A protease inhibitor simeprevir (**19**, Figure 4) emerged as the best-docked molecule with higher binding affinity to the Nsp13 helicase active site (binding energy = -10.42 kcal/mol) compared to the control inhibitors SSYA10-001 (-7.44 kcal/mol) SSYA10-002 (-8.16 kcal/mol), Myricetin (-6.91 kcal/mol) and Scutellarin (-7.05 kcal/mol). The simeprevir-helicase complex was found to be stabilized by a network of hydrogen bonds and hydrophobic interactions with the key residues of the NTPase binding pocket [73]. Similarly, the Herpes Simplex virus (HSV) helicase-primase inhibitor pritelivir (BAY 57-1293) (**20**, Figure 4) was recently reported for its good theoretical binding affinity to the Nsp13 helicase active site. Pritelivir showed the ability to establish a series of hydrogen bonds with key residues of the binding pocket, maintaining overall stability throughout molecular dynamic simulations (MDs). Thermodynamic studies of pritelivir-Nsp13 complex were also performed by using MM-PBSA and MM-GBSA methodologies, revealing a favourable binding free energy and molecular affinity for Nsp13, thus suggesting the potential use of pritelivir as SARS-CoV-2 helicase inhibitor [74].

Another promising candidate for the treatment of SARS-CoV-2 infection is represented by the N-(4-methyl-3-{[4-(pyridin-3-yl)-1,3-thiazol-2-yl]amino}phenyl)-4-[(4-methylpiperazin-1-yl)methyl]benzamide masitinib (**28**, Figure 15) [75]. It was originally approved for treatment of mast-cell tumors in dogs as tyrosine-kinase inhibitor, but it was also evaluated in phase 2 and 3 clinical trials for the treatment of cancer, asthma, Alzheimer's, multiple sclerosis and amyotrophic lateral sclerosis in humans. In 2020, masitinib was found to strongly inhibit the activity of the SARS-CoV-2 main protease 3CL_{pro} as well as the related viral protease of picornaviruses [76]. One year later, masitinib was also reported to be a potential SARS-CoV-2 helicase inhibitor, due to its ability to block the unwinding function of Nsp13 *in vitro*, with IC₅₀ value of 16.7 μ M.

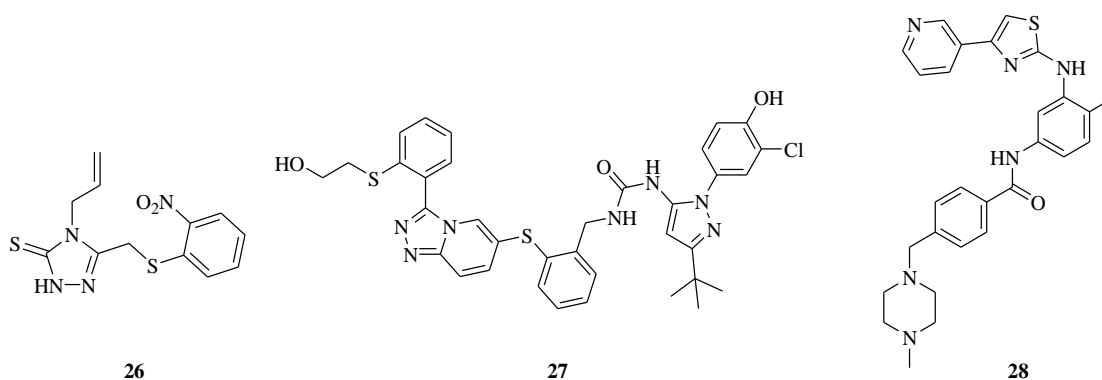
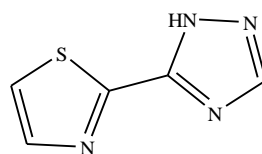


Figure 15. Representative triazole- and thiazole-based derivatives with potential Nsp13 helicase inhibitory activity

Computational approaches represent valuable tools to speed up the drug discovery process, increasing knowledge about biological systems and facilitating the identification of bioactive molecules. As part of a study aiming at evaluating the *druggability* and sequence conservation of SARS-CoV-2 Nsp13, 65 fragment hits have been identified by Newman et al. by performing a crystallographic fragment screening against the most representative pockets of Nsp13 [61]. Although these fragments have not yet been validated as inhibitors in biochemical assays, they represent useful starting points for chemical optimization to obtain potential antiviral agents. A series of PDB entries derived from this study have been deposited in the Protein Data Bank, encouraging the rational drug design and structure-based optimization of novel therapeutic options for COVID-19 treatment. Among them, we put our attention on the crystal structure of the SARS-CoV-2 helicase in complex with the 5-(1,3-thiazol-2-yl)-1*H*-1,2,4-triazole fragment **Z2027049478** (PDB code: 5RLY) [77] (Figure 16).



Z2027049478

Figure 16. Chemical structure of **Z2027049478** fragment

Based on the knowledge about the main features of the biological target and its known ligands and taking into account the recurrence of both triazole and thiazole rings in compounds endowed with antiviral properties, we decided to synthesize a set of condensed triazole- and thiazole-based ligands to obtain novel chemical entities targeting Nsp13. Among the plethora of heterocyclic rings, we focused on naphthyridine systems not only due to the expertise in the synthesis of polycondensed heterocyclic systems of my research group [78–80], but also due to the potential antiviral properties shown by naphthyridines [81–85]. Indeed, pyronaridine (**29**, Figure 17) has recently emerged from a drug repositioning study for its ability to inhibit SARS-CoV-2 replication in A549-ACE2 cells, inhibiting PLpro activity *in vitro* with an IC₅₀ value of 1.8 μM [86]. When tested *in vivo* in a K18-hACE transgenic mouse model of COVID-19, pyronaridine demonstrated significant reduction of viral load in the lungs of SARS-CoV-2-infected mice, as well as a decrease of pro-inflammatory cytokines/chemokine levels and cell infiltration, ultimately resulting in a reduction of lung pathology. In 2022, pyronaridine completed a phase II clinical trial (NCT05633420) evaluating its efficacy and safety in combination with artesunate (Pyramax) in mild to moderate COVID-19 patients.

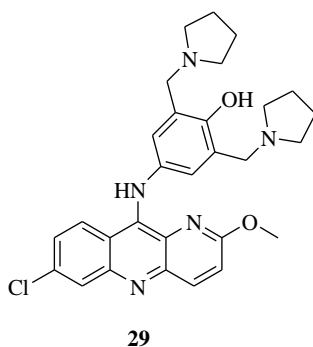


Figure 17. Chemical structure of pyronaridine (**29**)

Considering that both triazole- and thiazole-based compounds as well as naphthyridine derivatives have been reported in the literature for their promising antiviral activity, we synthesized a new series of [1,2,3]triazolo[4,5-*h*][1,6]naphthyridine (**30**) and [1,3]thiazolo[5,4-*h*][1,6]naphthyridine (**31**) derivatives, in order to explore the potentialities of these tricyclic ring systems, and the corresponding [1,2,3]triazolo[4,5-*h*][1,6]naphthyridine-8-ones (**32**) and [1,3]thiazolo[5,4-*h*][1,6]naphthyridine-8-ones (**33**), to extend the structure-activity relationships (SARs) (Figure 18).

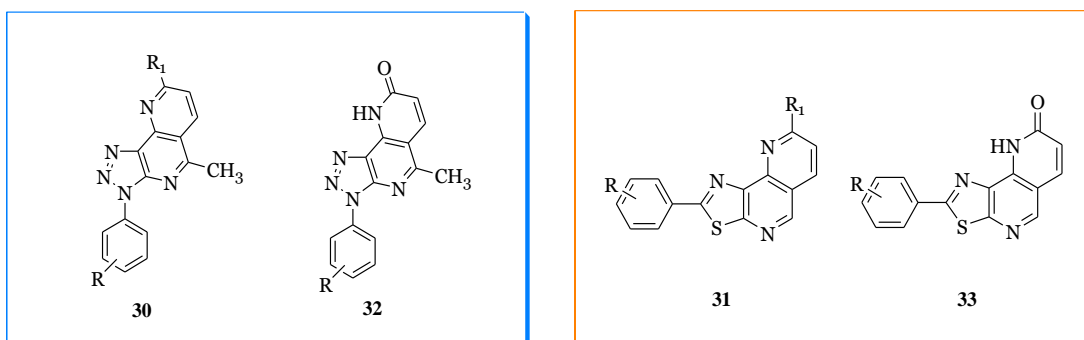


Figure 18. Chemical structure of [1,2,3]triazolo[4,5-*h*][1,6]naphthyridines (**30**) and [1,3]thiazolo[5,4-*h*][1,6]naphthyridines (**31**)

2. Aim of the project

The aim of my PhD thesis was to synthesize a small library of [1,2,3]triazolo[4,5-*h*][1,6]naphthyridines (**30**) and [1,3]thiazolo[5,4-*h*][1,6]naphthyridines (**31**), along with the corresponding [1,2,3]triazolo[4,5-*h*][1,6]naphthyridine-8-ones (**32**) and [1,3]thiazolo[5,4-*h*][1,6]naphthyridine-8-ones (**33**), in order to evaluate them for their antiviral properties and to explore their structure-activity relationships (SARs).

With the aim of searching for novel therapeutic approaches for the treatment of Coronavirus (SARS-CoV-2) infections, all synthesized compounds were evaluated for their ability to inhibit the SARS-CoV-2 Nsp13 helicase, through enzymatic assays performed in collaboration with the University of Cagliari (CA), under the supervision of Prof. Enzo Tramontano. The antiviral activity against SARS-CoV-2 was evaluated on cell cultures in the Laboratory of Virology & Chemotherapy of the Rega Institute for Medical Research, KU Leuven (Belgium), under the supervision of Prof. Graciela Andrei.

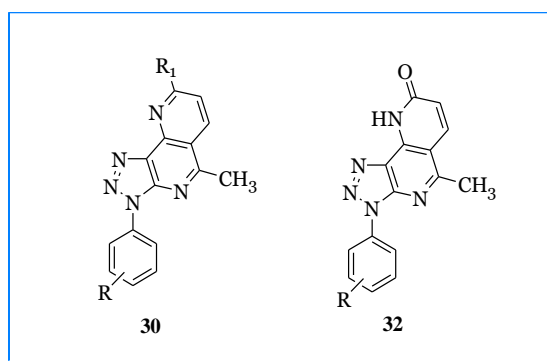
Moreover, with the aim of searching for novel antiviral therapeutics with a broad spectrum of action, according to a protocol applied at the Rega Institute for Medical Research, all the synthesized compounds have also been evaluated for their efficacy in inhibiting the replication of a panel of different viruses (HCoV, Flu, RSV, HSV-1, HSV-2, VZV, HCMV, YFV, ZIKV, SINV and SFV) through cell-based assays.

During my PhD, I spent a research period of 9 months in the Laboratory of Virology & Chemotherapy of the Rega Institute for Medical Research, where I have also been involved in a project aiming at evaluating the effect of combination therapy of helicase-primase inhibitors [pritelivir (PTV) or amenamevir (AMV)] with DNA polymerase inhibitors [acyclovir (ACV) or foscarnet (PFA)] on HSV-2 drug resistance evolution.

In addition, I spent a research period of 6 months at Net4Science, University Magna Graecia of Catanzaro (CZ), under the supervision of Prof. Stefano Alcaro, where computational investigations were performed on the most interesting viral targets, leading to the identification of [1,2,3]triazolo[4,5-*b*]pyridines as potential HSV-1 entry inhibitors due to their good theoretical affinity towards the envelope glycoprotein D (gD) [87].

3. Results and discussion

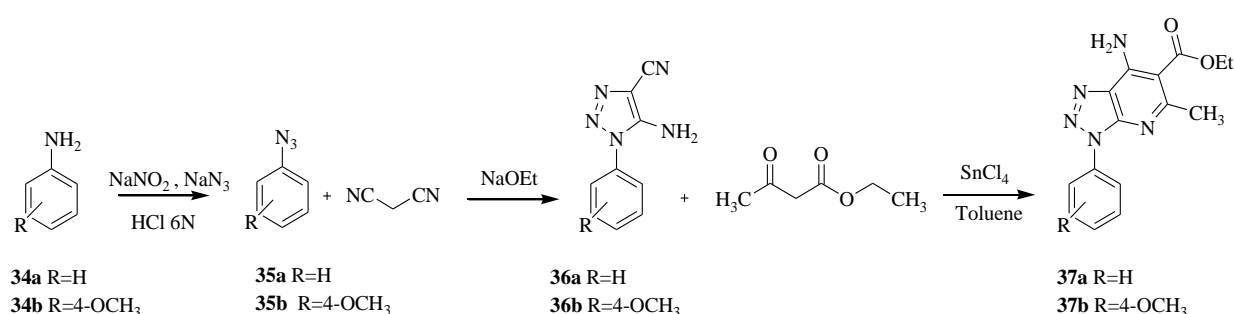
3.1 Chemical synthesis of [1,2,3]triazolo[4,5-*h*][1,6]naphthyridines and [1,2,3]triazolo[4,5-*h*][1,6]naphthyridine-8-ones



The synthetic pathway to obtain [1,2,3]triazolo[4,5-*h*][1,6]naphthyridines (**30**) and [1,2,3]triazolo[4,5-*h*][1,6]naphthyridine-8-ones (**32**) started from the substituted anilines **34a,b** which were reacted with sodium nitrite in hydrochloric acid at a temperature between 0 and -5 °C for 15 minutes. The reaction mixture was stirred for 30 minutes and then a solution of sodium azide in water was added at 0 °C, allowing the isolation of the corresponding 1-azido benzenes

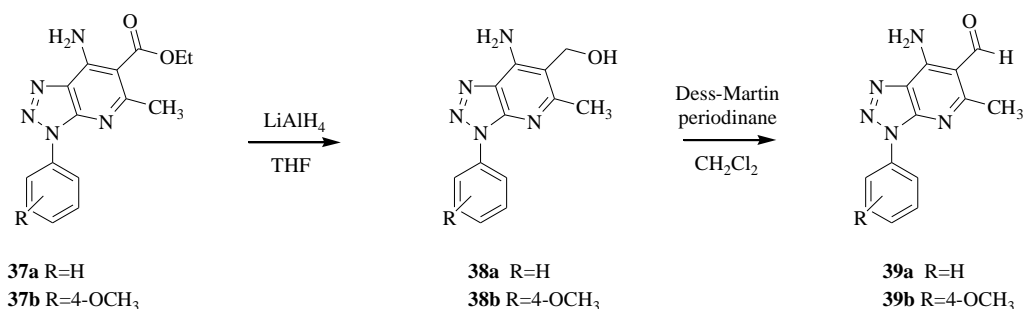
35a,b in good yield (96 – 98%). Subsequent reaction with malononitrile in presence of sodium ethoxide led to the isolation of derivatives **36a,b** in yields ranging from 60% to 70%. 5-Amino-5-methyl-3-phenyl-3*H*[1,2,3]triazolo[4,5-*b*]pyridine-6-carboxylate intermediates **37a,b** were obtained by heating at reflux 5-amino-1-phenyl-1*H*-1,2,3-triazole-4-carbonitrile intermediates **36a,b** with ethyl acetoacetate in toluene, in the presence of stannic chloride as Lewis acid (Scheme 1).

Scheme 1. Synthesis of 5-amino-5-methyl-3-phenyl-3*H*[1,2,3]triazolo[4,5-*b*]pyridine-6-carboxylates **37a,b**.



Subsequent reduction of the carboxyethyl function with LiAlH₄ in anhydrous tetrahydrofuran at room temperature, afforded (7-amino-5-methyl-3-phenyl-3*H*-[1,2,3]triazolo[4,5-*b*]2*H*pyridine-6-yl)methanol derivatives **38a,b**. Finally, oxidation with Dess-Martin periodinane (1,1,1-triacetoxy-1,1-dihydro-1,2-benziodoxol-3(1*H*)-one) in absolute dichloromethane under nitrogen atmosphere at room temperature, led to the isolation of the corresponding key intermediate *o*-aminoaldehydes **39a,b** (Scheme 2).

Scheme 2. Synthesis of 7-amino-5-methyl-3-phenyl-3*H*-[1,2,3]triazolo[4,5-*b*]pyridine-6-carbaldehydes **39a,b**.



Derivatives **39a,b** were versatile intermediates to synthesize both [1,2,3]triazolo[4,5-*h*][1,6]naphthyridines **30a-n** and [1,2,3]triazolo[4,5-*h*][1,6]naphthyridine-8-ones **32a,b** (Scheme 3). To afford the naphthyridine derivatives **30a-n**, the aldehydes **39a,b** were submitted to Friedlander condensation with acetone or suitable acetophenone derivatives, in presence of potassium hydroxide as a base, under nitrogen atmosphere, allowing us to obtain the title compounds **30a-n** (Table 1) from moderate to good yields (30 – 60%). Naphthyridin-8-one derivatives **32a,b** were obtained in good yields (55 – 60%) through a Wittig-Horner reaction by refluxing *o*-aminoaldehydes **39a,b** with triethyl phosphonoacetate in the presence of sodium carbonate as base, in dry ethanol.

Scheme 3. Synthesis of [1,2,3]triazolo[4,5-*h*][1,6]naphthyridines **30a-n** and [1,2,3]triazolo[4,5-*h*][1,6]naphthyridine-8-ones **32a,b**.

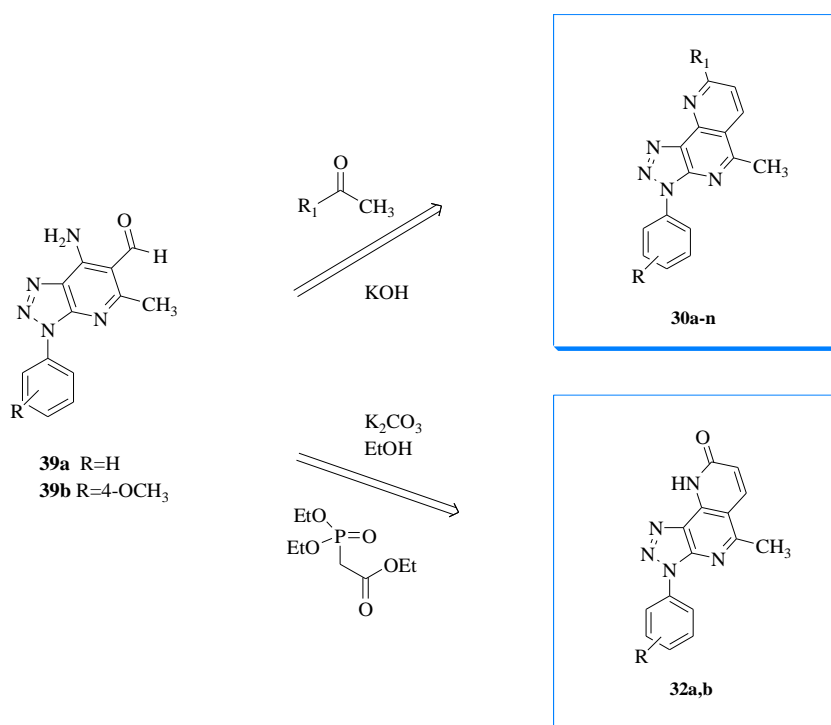
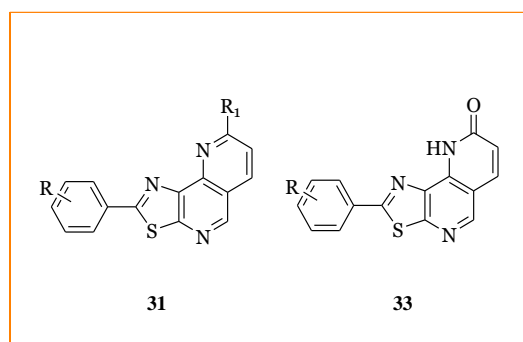


Table 1. [1,2,3]Triazolo[4,5-*h*][1,6]naphthyridines **30a-n** and [1,2,3]triazolo[4,5-*h*][1,6]naphthyridine-8-ones **32a,b**.

Cpd	R	R ₁
30a	H	CH ₃
30b	H	Ph
30c	H	4-OMe-Ph

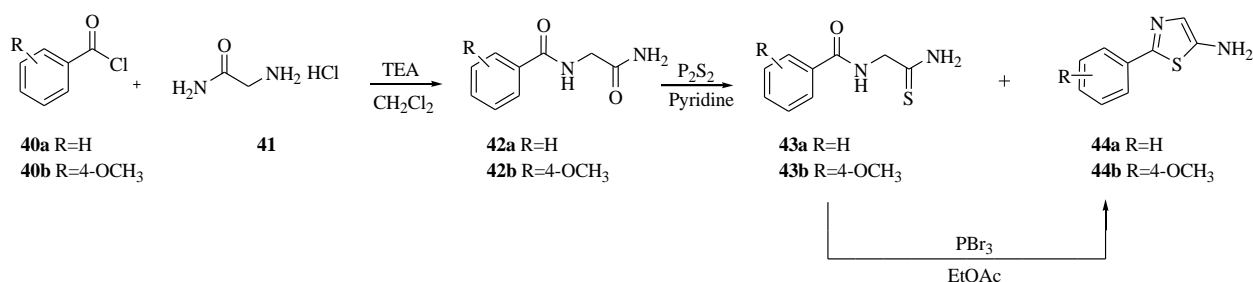
30d	H	2-OMe-Ph
30e	H	2-F-Ph
30f	H	2-CF ₃ -Ph
30g	H	2-Cl-Ph
30h	H	2-NO ₂ -Ph
30i	4-MeO	CH ₃
30j	4-MeO	Ph
30k	4-MeO	4-OMe-Ph
30l	4-MeO	2-OMe-Ph
30m	4-MeO	2-F-Ph
30n	4-MeO	2-CF ₃ -Ph
32a	H	---
32b	4-MeO	---

3.2 Chemical synthesis of [1,3]thiazolo[5,4-*h*][1,6]naphthyridines and [1,3]thiazolo[5,4-*h*][1,6]naphthyridine-8-ones



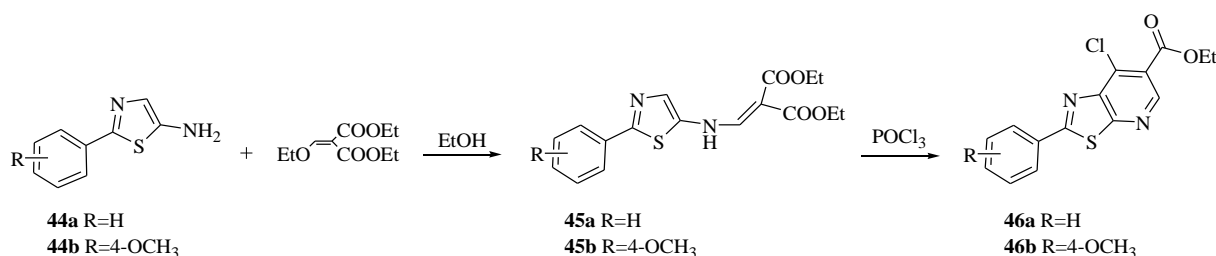
The synthetic pathway to obtain [1,3]thiazolo[5,4-*h*][1,6]naphthyridines (**31**) and [1,3]thiazolo[5,4-*h*][1,6]naphthyridine-8-ones (**33**) started from the synthesis of *N*-(2-amino-2-oxoethyl)benzamide derivatives **42a,b**, in turn obtained by reaction of the suitable benzoyl chlorides (**40a,b**) and glycine hydrochloride (**41**) in anhydrous dichloromethane, in the presence of triethylamine as a base. The obtained *N*-(2-amino-2-oxoethyl)benzamide **42a,b** have been converted into the corresponding primary thioamide **43a,b** using P₂S₅ in anhydrous pyridine. This synthetic approach allowed us not only to afford the thioamide derivatives **43a,b**, but also to isolate, as by-product, small amount of 2-phenyl-1,3-thiazol-5-amino derivative **44a,b**. The latter were obtained from moderate to good yields (30-60%) by cyclization of **43a,b** with phosphorous tribromide in anhydrous ethyl acetate, at room temperature (Scheme 4).

Scheme 4. Synthesis of 2-phenyl-1,3-thiazol-5-amino derivative **44a,b**.



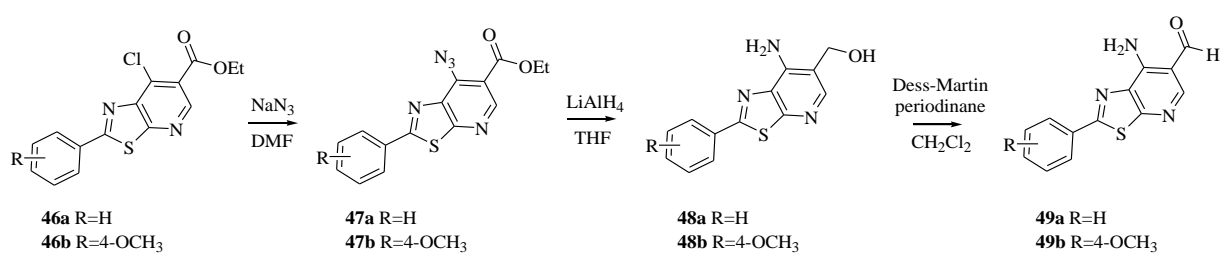
Condensation with diethyl ethoxymethylenemalonate (EMME) in anhydrous ethanol led to the diethyl {[2-(2-phenyl-1,3-thiazol-5-yl)amino]methylidene}propanedioate intermediates **45a,b**, in turn subjected to an oxidative ring closure with phosphoryl chloride, resulting in the 7-chloro intermediates **46a,b** (Scheme 5).

Scheme 5. Synthesis of ethyl 7-chloro-2-phenyl[1,3]thiazolo[5,4-*b*]pyridine-6-carboxylates **46a,b**.



Nucleophilic substitution with sodium azide in *N,N*-dimethylformamide allowed to access the ethyl 7-azido-2-phenyl[1,3]thiazolo[5,4-*b*]pyridine-6-carboxylate derivatives **47a,b**. These latter were subjected to a simultaneous reduction of both azido and ethoxycarbonyl groups with LiAlH₄ in anhydrous tetrahydrofuran, at room temperature, to afford the (7-amino-2-phenyl[1,3]thiazolo[5,4-*b*]pyridine-6-yl)methanol derivatives **48a,b**. Amino-alcohol derivatives **48a,b** represent a versatile synthon for the synthesis of the tricyclic [1,3]thiazolo[5,4-*h*][1,6]naphthyridine system. Indeed, they were subjected to oxidation with Dess-Martin periodinane, thus leading to the corresponding key intermediate *o*-aminoaldehydes **49a,b** (Scheme 6).

Scheme 6. Synthesis of 7-amino-2-phenyl[1,3]thiazolo[5,4-*b*]pyridine-6-carbaldehydes **49a,b**.



[1,3]Thiazolo[5,4-*h*][1,6]naphthyridine derivatives **31a-m** (Table 2) were achieved through Friedlander condensation of derivatives **49a,b** with acetone or properly substituted acetophenones, in basic media. [1,3]Thiazolo[5,4-*h*][1,6]naphthyridine-8-ones **33a,b** (Table 2) were obtained through a Wittig-Horner reaction by refluxing *o*-aminoaldehydes **49a,b** with triethyl phosphonoacetate in anhydrous ethanol, in the presence of sodium carbonate as base (Scheme 7).

Scheme 7. Synthesis of [1,3]thiazolo[5,4-*h*][1,6]naphthyridines **31a-m** and [1,3]thiazolo[5,4-*h*][1,6]naphthyridine-8-ones **33a,b**.

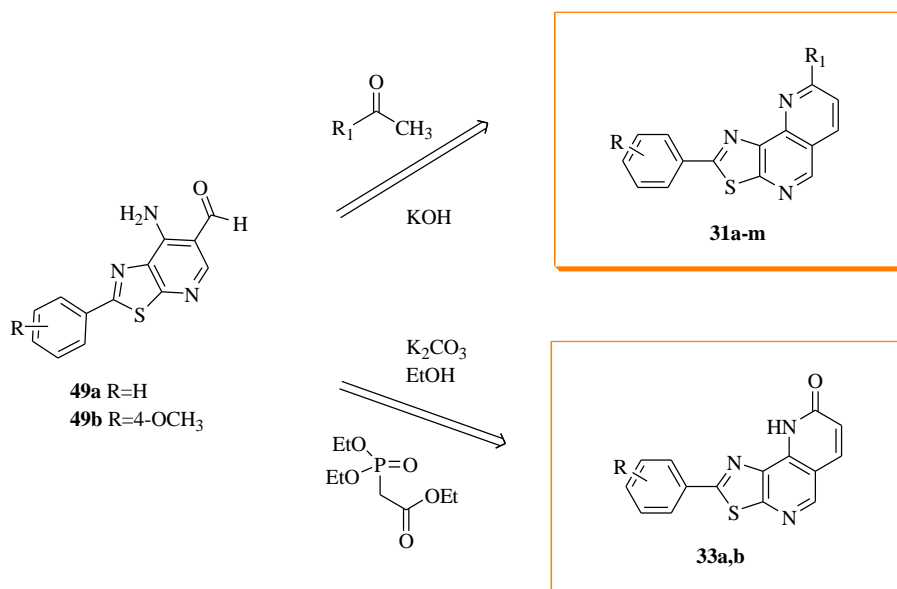


Table 2. [1,3]Thiazolo[5,4-*h*][1,6]naphthyridines **31a-m** and [1,3]thiazolo[5,4-*h*][1,6]naphthyridine-8-ones **33a,b**.

Cpd	R	R ₁
31a	H	CH ₃
31b	H	Ph
31c	H	4-OMe-Ph
31d	H	2-OMe-Ph
31e	H	2-F-Ph
31f	H	2-CF ₃ -Ph
31g	H	2-Cl-Ph
31h	H	2-NO ₂ -Ph
31i	4-MeO	CH ₃
31j	4-MeO	Ph
31k	4-MeO	4-OMe-Ph
31l	4-MeO	2-OMe-Ph
31m	4-MeO	2-F-Ph
33a	H	---
33b	4-MeO	---

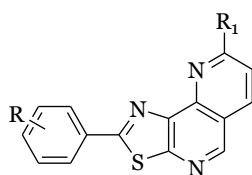
3.3 Biological evaluations of synthesized naphthyridines

Biochemical assays were performed at the University of Cagliari (CA), under the supervision of Prof. Enzo Tramontano, to assess the ability of synthesized compounds to inhibit the non-structural protein 13 (Nsp13).

Both series of compounds were screened for their ability to inhibit the Nsp13-associated enzymatic activities by using two different biochemical assays. The unwinding assay was used to measure the opening of a short double-strand nucleic acid due to the Nsp13 movement along the substrate oligonucleotide, while the ATPase assay was performed to quantify the production of pyrophosphate (Pi) following the ATP hydrolysis [70]. Considering that CoV helicases have been reported to be equally active in unwinding DNA and RNA substrates [88], the Nsp13-associated unwinding activity was measured using a dsDNA as a substrate. The Nsp13-associated ATPase activity was subsequently measured in the absence of any nucleic acid, by quantifying the ATP hydrolysis through a colorimetric assay detecting the release of Pi through the formation of a green complex between the liberated orthophosphate and the Biomol Green Reagent (molybdate/malachite).

Among tested derivatives, [1,3]thiazolo[5,4-*h*][1,6]naphthyridines **31d** (R = H, R₁ = 2-OCH₃-Ph) and **31f** (R = H, R₁ = 2-CF₃-Ph) exhibited inhibition towards the unwinding activity with IC₅₀ values of 19.13 ± 1.5 μM and 16.7 ± 1.2 μM, respectively, without considerably affecting the ATPase function of Nsp13 (Table 3, Figure 19). The most interesting results were obtained for compound **31e** (R = H, R₁ = 2-F-Ph) displaying a dual inhibitory activity towards the enzyme, by interfering both with the unwinding and 5'-triphosphatase activity at micromolar level (Figure 19). In particular, it retained the ability to inhibit the Nsp13-associated unwinding function (IC₅₀ = 26.13 ± 0.76 μM) but it mostly caused ATPase inhibition at IC₅₀ value of 10.15 ± 0.71 μM, comparable to that of the reference drug Licoflavone C (IC₅₀ = 7.6 μM, Table 3). None of the other compounds showed a relevant inhibitory activity against Nsp13 (IC₅₀ > 30 μM, data not shown).

Table 3. Inhibition of SARS-CoV-2 Nsp13-associated enzymatic activities by selected compounds.



31a-m

Compound	R	R ₁	Unwinding IC ₅₀ (μM) ^a	ATPase IC ₅₀ (μM) ^b
31d	H	2-OCH ₃ -Ph	19.13 ± 1.5	> 30 (52%) ^c
31e	H	2-F-Ph	26.13 ± 0.76	10.15 ± 0.71
31f	H	2-CF ₃ -Ph	16.7 ± 1.2	> 30 (61%) ^c
SSYA10-001	---	---	4.7	---
Licoflavone C	---	---	---	7.6

^aCompound concentration required to inhibit the SARS-CoV-2 nsp13-associated unwinding activity by 50%. ^bCompound concentration required to inhibit the SARS-CoV-2 nsp13-associated ATPase activity by 50%. ^cPercentage of control measured in the presence of the highest compound concentration.

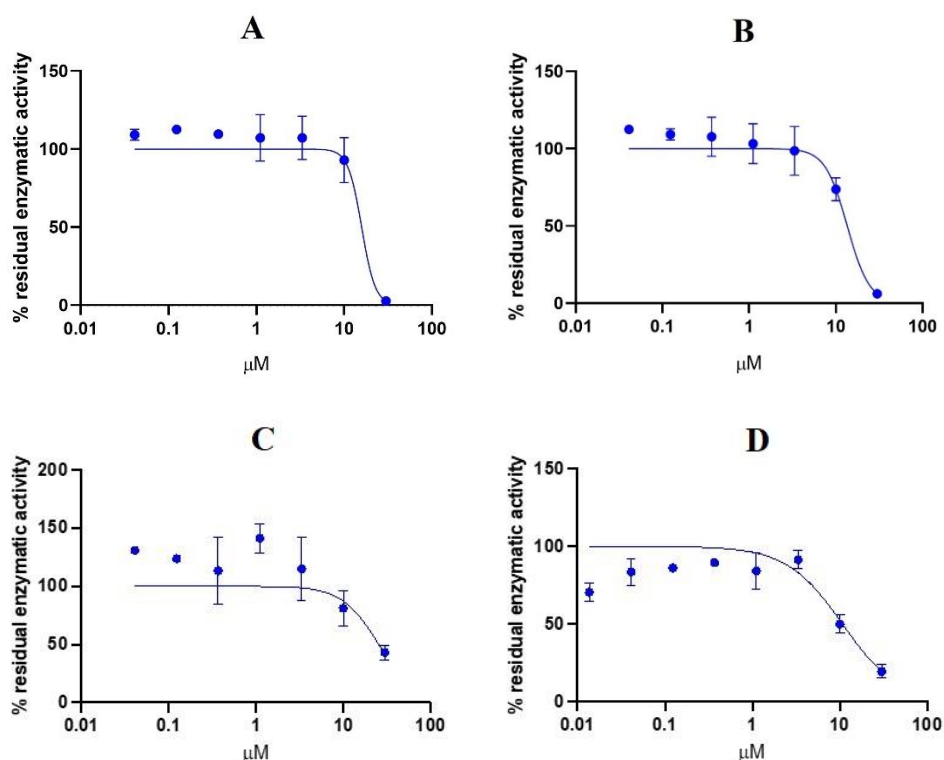


Figure 19. Inhibition of the Nsp13-associated unwinding activity by (A) **31d**, (B) **31f** and (C) **31e**; (D) Inhibition of the Nsp13-associated ATPase activity by **31e**

Both series of naphthyridines along with their synthetic precursors were screened for the antiviral activity at the Rega Institute for Medical Research, KU Leuven (Belgium), through *in vitro* cell-based assays, under the supervision of Prof. Graciela Andrei. The selected compounds were evaluated for their efficacy in inhibiting the replication of two SARS-CoV-2 clinical strains (Wuhan UC-1074 and Omicron BA.1) in Vero cells with remdesivir and molnupiravir as reference compounds. Antiviral activity was expressed as EC_{50} or compound concentration required to reduce viral plaque formation by 50%. In parallel, the cytotoxic effects of compounds were assessed by evaluating the minimum cytotoxic concentration (MCC) or compound concentration that caused a microscopically detectable alteration of cell morphology (Table 4).

Table 4. Cytotoxicity and antiviral activity against SARS-CoV-2 in Vero cells.

Compound	Antiviral activity EC_{50} (μM) ^a		Cytotoxicity (μM)	
	UC-1074 (Wuhan)	BA.1 (Omicron)	Cell morphology (MCC) ^b	Cell growth (CC_{50}) ^c
30a	> 4	> 4	20	ND
30b	> 0.80	> 0.80	4	ND
30c	> 20	> 20	≥ 20	ND

30d	> 100	> 20	≥ 100	ND
30e	> 20	> 20	100	ND
30f	> 0.80	> 0.80	4	ND
30g	> 20	> 20	100	ND
30h	> 20	> 4	≥ 20	ND
30i	> 20	> 20	≥ 20	ND
30j	> 100	> 20	≥ 100	ND
30k	> 20	> 20	≥ 100	ND
30l	> 4	> 4	20	ND
30m	> 20	> 20	100	ND
30n	> 100	> 100	> 100	ND
31a	> 20	> 20	100	ND
31b	> 4	> 4	20	ND
31c	> 4	> 4	20	ND
31d	> 20	> 20	≥ 20	ND
31e	> 0.80	> 0.80	4	ND
31f	> 20	> 4	≥ 20	ND
31g	> 0.80	> 0.80	4	ND
31h	> 4	> 4	≥ 4	ND
31i	> 4	> 4	20	ND
31j	> 4	> 4	20	ND
31k	> 4	> 0.80	≥ 4	ND
31l	> 4	> 4	20	ND
31m	> 0.16	> 0.80	≥ 0.80	ND
32a	> 4	> 4	20	ND
32b	> 4	> 20	≥ 20	ND
33a	> 4	> 4	20	ND
33b	> 20	> 20	≥ 20	ND
37a	> 4	> 4	20	ND
37b	> 20	> 20	100	ND
38a	> 100	> 100	> 100	ND
38b	> 20	> 100	≥ 100	ND
46a	> 100 48.90	63.14 38.07	> 100 > 100	ND ND
46b	> 20	> 100	≥ 100	ND
48a	> 20	> 100	≥ 100	ND
48b	> 20	> 20	100	ND
Remdesivir	3.58 μM 0.82 μM	1.60 μM 0.72 μM	> 40 μM 40 μM	ND ND
Molnupiravir	1.96 μg/mL 1.87 μg/mL	1.10 μg/mL 1.64 μg/mL	20 μg/mL 100 μg/mL	ND ND

^aEffective concentration required to reduce virus plaque formation by 50%. ^bMinimum cytotoxic concentration that causes a microscopically detectable alteration of cell morphology. ^cCytotoxic concentration required to reduce cell growth by 50%. ^dNot determined.

According to the standards of the Rega Institute for Medical Research, cytotoxicity studies revealed an alteration of cell morphology at micromolar concentrations for most of the tested derivatives, thus preventing further investigation of their antiviral activity. Indeed, a basic requirement for studying more deeply the antiviral properties of tested compounds was that the ratio measuring the window between cytotoxicity and antiviral activity (MCC/EC₅₀) was at least > 10.

Antiviral screenings showed that the [1,3]thiazolo[5,4-*b*]pyridine derivative **46a** was the only compound exhibiting some moderate activity against both SARS-CoV-2 clinical strains at micromolar level, without any toxicity for concentrations up to 100 μM. Nevertheless, since the MCC/EC₅₀ ratio was quite low (< 10) and therefore not indicative of a good compound in terms

of antiviral activity, further structural modifications are required to try to improve its antiviral activity.

On the other hand, when tested on SARS-CoV-2 through cell-based assays, unfortunately compounds **31d**, **31e** and **31f**, emerged from biochemical assays, failed to inhibit viral plaque formation, inducing cell morphology alteration at micromolar concentrations.

Based on these results, in the attempt to explore further chemical modifications of the [1,3]thiazolo[5,4-*h*][1,6]naphthyridine scaffold, a structural simplification strategy of the *hit* candidate **31e** has been applied to try to improve its biological properties. Supported by the idea that a scaffold hopping strategy could be beneficial for future pharmacokinetic insights, a series of decorated *N*-(2-phenyl-1,3-thiazol-5-yl)benzamides (**50a-z**, Figure 20) have been synthesized.

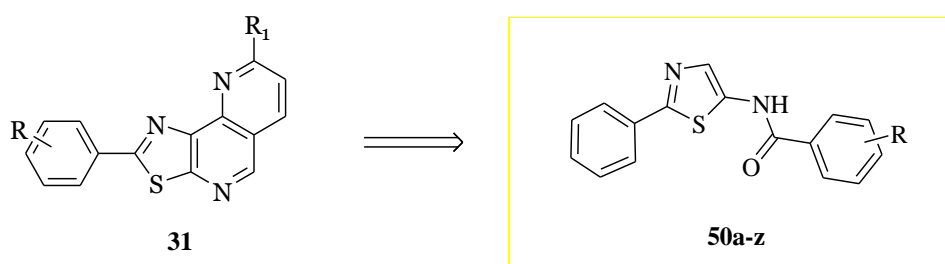


Figure 20. Chemical structure of *N*-(2-phenyl-1,3-thiazol-5-yl)benzamides **50a-z**

In addition, in order to improve the antiviral activity of compound **46a**, we also decided to further explore the potentialities of the bicyclic thiazole-pyridine scaffold by replacing the chlorine atom at position 7 with a bromine (**51**), substituted or unsubstituted amino groups (**52a-c**) or with substituted benzamide groups (**53a-c**). Finally, the effects of replacing the carboxyethyl function of **52a** with substituted benzamide groups (**54a-d**) have also been evaluated (Figure 21).

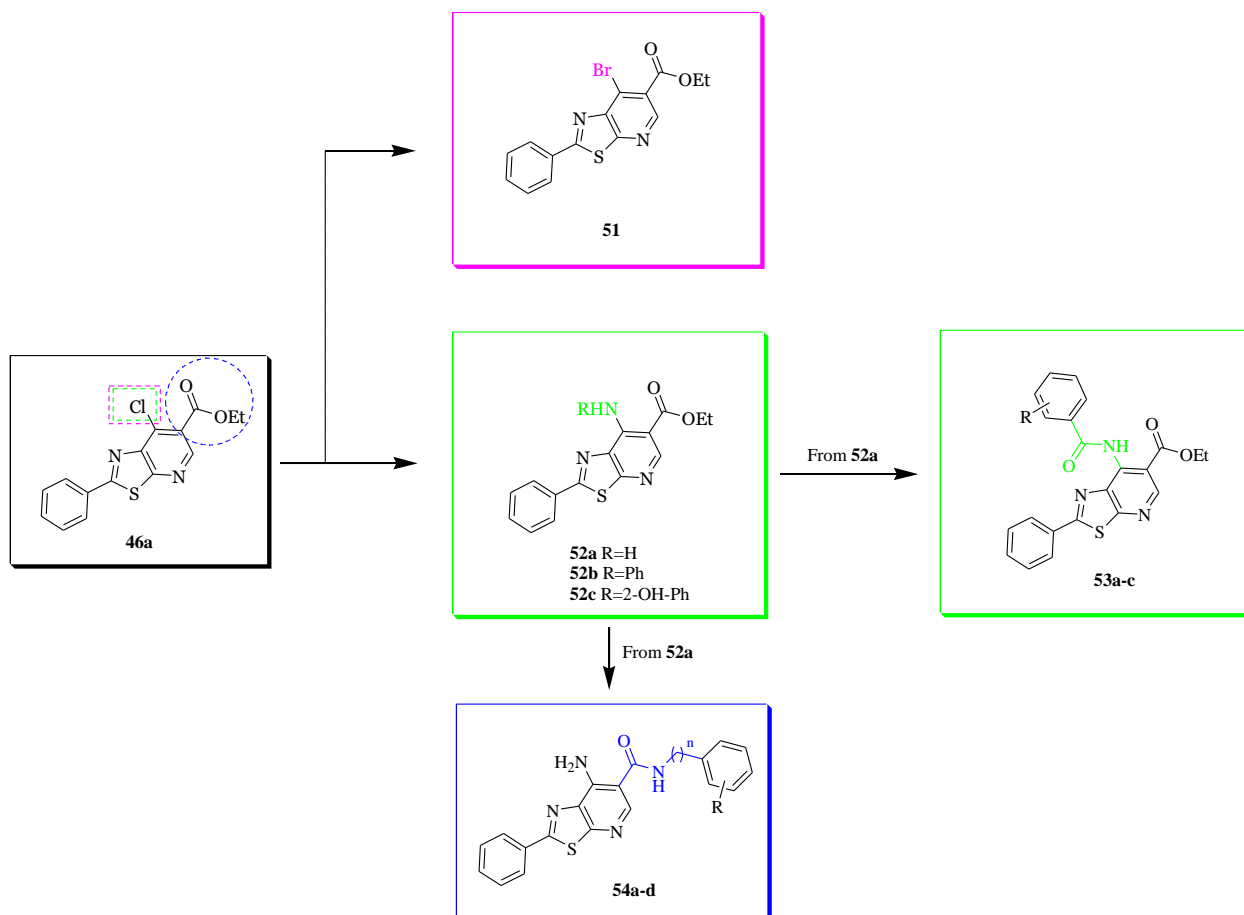
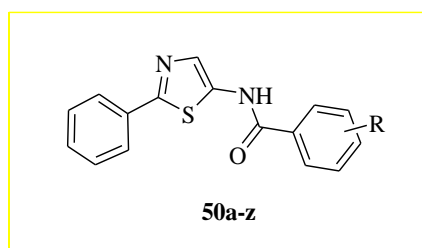


Figure 21. Structural modifications on compound 46a

3.4 Structural modifications: chemical synthesis

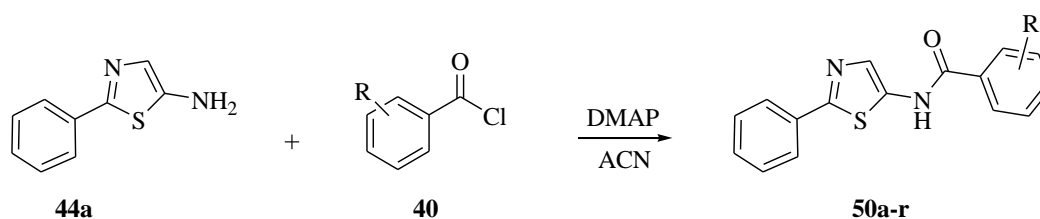
3.4.1 Synthesis of *N*-(2-phenyl-1,3-thiazol-5-yl)benzamides 50a-z



The key intermediate for the synthesis of *N*-(2-phenyl-1,3-thiazol-5-yl)benzamides 50a-z is the 2-phenyl-1,3-thiazol-5-amine derivative 44a, properly obtained by the multistep sequence

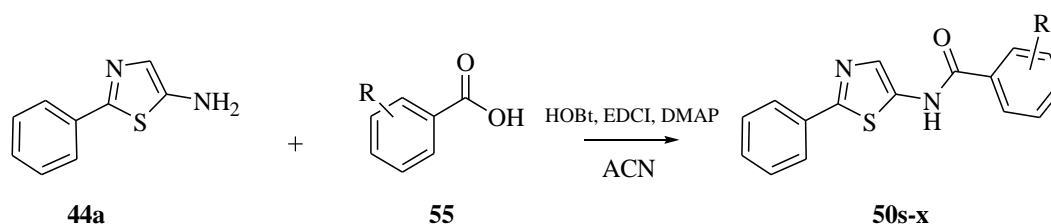
previously described in Scheme 4. Nucleophilic substitution reaction between **44a** and suitable benzoyl chlorides (**40**) in acetonitrile and in the presence of 4-dimethylaminopyridine was achieved through a Microwave-Assisted Organic Synthesis (MAOS technique), by irradiation of the reaction for 40 minutes (2 cycles of 20' each) with a power of 150 W and a temperature of 120 °C, leading to desired *N*-(2-phenyl-1,3-thiazol-5-yl)benzamides **50a-r** (Scheme 8).

Scheme 8. Synthesis of *N*-(2-phenyl-1,3-thiazol-5-yl)benzamides **50a-r**.



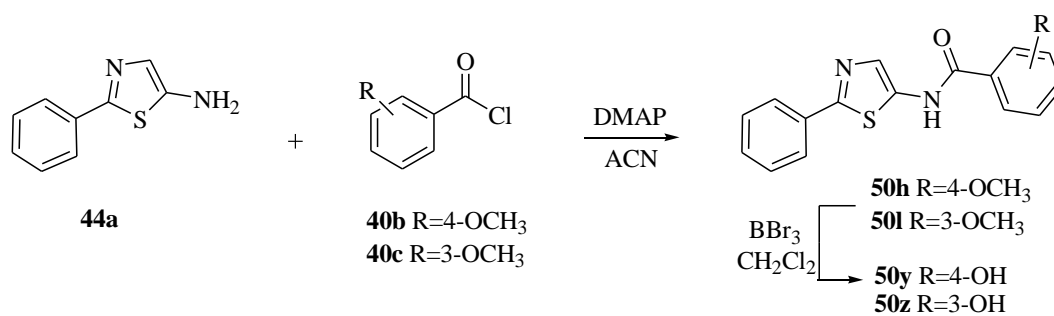
N-(2-phenyl-1,3-thiazol-5-yl)benzamides **50s-x** were obtained through reaction between **44a** and suitable substituted benzoic acids (**55**) in acetonitrile and in the presence of hydroxybenzotriazole (HOBT), *N*-(3-dimethylaminopropyl)-*N'*-ethylcarbodiimide hydrochloride (EDC HCl) and 4-dimethylaminopyridine (DMAP), by irradiating the reaction for 40 minutes (2 cycles of 20' each) with a power of 60 W and a temperature of 50 °C through a Microwave-Assisted Organic Synthesis (Scheme 9).

Scheme 9. Synthesis of *N*-(2-phenyl-1,3-thiazol-5-yl)benzamides **50s-x**.



A two steps procedure was used for derivatives bearing the hydroxyl function at position 4 (**50y**) and 3 (**50z**) of the phenyl ring, starting from reaction of compound **44a** with 4-methoxybenzoyl chloride (**40b**) or 3-methoxybenzoyl chloride (**40c**) to give the corresponding derivatives **50h** or **50l**, respectively, followed by demethylation with boron tribromide, to afford the desired compounds **50y** and **50z** (Scheme 10).

Scheme 10. Synthesis of *N*-(2-phenyl-1,3-thiazol-5-yl)benzamides **50y** and **50z**.

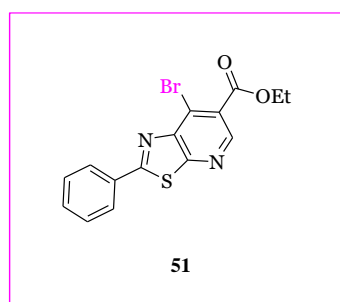


This synthetic pathway allowed us to obtain the title compounds **50a-z** (Table 5) from moderate to good yields (25 - 90%).

Table 5. *N*-(2-phenyl-1,3-thiazol-5-yl)benzamides **50a-z**.

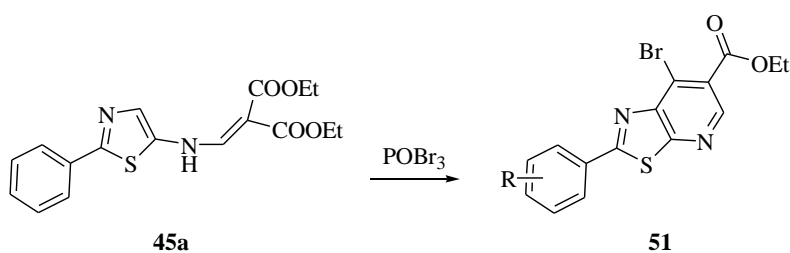
Compound	R	Compound	R
50a	2-Cl	50n	3-CF ₃
50b	2,6-Cl ₂	50o	2-OCF ₃
50c	2-Br	50p	4-CF ₃
50d	2,6-F ₂	50q	3,4-Cl ₂
50e	2-F	50r	3-CN
50f	2-OH	50s	2-OCH ₃
50g	H	50t	4-Cl
50h	4-OCH ₃	50u	2,5-Cl ₂
50i	3-Cl	50v	4-Br
50j	3-Br	50w	4-F
50k	2,4-Cl ₂	50x	2-Br-6-Cl
50l	3-OCH ₃	50y	4-OH
50m	3-F	50z	3-OH

3.4.2 Synthesis of ethyl 7-bromo-2-phenyl[1,3]thiazolo[5,4-*b*]pyridine-6-carboxylate **51**

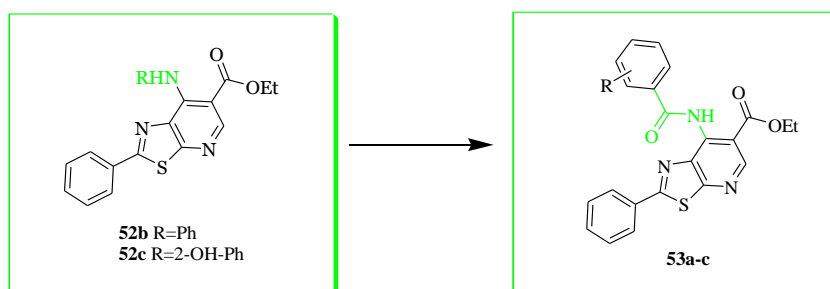


The diethyl {[2-phenyl-1,3-thiazol-5-yl]amino}methylidene}propanedioate intermediate **45a** was subjected to an oxidative ring closure with phosphorus tribromide in absence of solvent, resulting in the desired ethyl 7-bromo-2-phenyl[1,3]thiazolo[5,4-*b*]pyridine-6-carboxylate **51** (Scheme 11).

Scheme 11. Synthesis of ethyl 7-bromo-2-phenyl[1,3]thiazolo[5,4-*b*]pyridine-6-carboxylate **51**.



3.4.3 Synthesis of ethyl 7-anilino-2-phenyl[1,3]thiazolo[5,4-*b*]pyridine-6-carboxylates **52b-c** and ethyl 7-benzamido-2-phenyl[1,3]thiazolo[5,4-*b*]pyridine-6-carboxylates **53a-c**.



To obtain the ethyl 7-anilino-2-phenyl[1,3]thiazolo[5,4-*b*]pyridine-6-carboxylates **52b,c**, the intermediate ethyl 7-chloro-2-phenyl[1,3]thiazolo[5,4-*b*]pyridine-6-carboxylate **46a** was reacted with aniline (for **52b**) or 2-aminophenol (for **52c**) in ethanol and in the presence of small amount of hydrochloric acid, through a Microwave-Assisted Organic Synthesis (MAOS technique), by irradiation of the reaction for 60 minutes (3 cycles of 20' each) with a power of 50 W and a temperature of 60 °C (Scheme 12). Ethyl 7-benzamido-2-phenyl[1,3]thiazolo[5,4-*b*]pyridine-6-carboxylates **53a-c**, were achieved starting from **46a** which was reacted with sodium azide in *N,N*-dimethylformamide allowing the isolation of the corresponding ethyl 7-azido-2-phenyl[1,3]thiazolo[5,4-*b*]pyridine-6-carboxylate derivative **47a**. A selective reduction

of the azido group with sodium dithionite in anhydrous methanol afforded the ethyl 7-amino-2-phenyl[1,3]thiazolo[5,4-*b*]pyridine-6-carboxylate **52a** in excellent yields (90-100%). Finally, the reaction with suitable benzoyl chlorides (**40**) in acetonitrile, in the presence of 4-dimethylaminopyridine, led to the desired ethyl 7-benzamido-2-phenyl[1,3]thiazolo[5,4-*b*]pyridine-6-carboxylates **53a-c**, by irradiating the reaction for 40 minutes (2 cycles of 20' each) with a power of 150 W and a temperature of 120 °C through a Microwave-Assisted Organic Synthesis. Unfortunately, compounds **53a** and **53b** were isolated only in traces, making the spectroscopic characterization difficult. Surprisingly, it was possible to isolate from the same reaction mixture small amount of the corresponding ethyl 7-dibenzoylamino-2-phenyl-thiazolo[5,4-*b*]pyridine-6-carboxylate derivatives **53d-f** (Scheme 12, Table 6).

Scheme 12. Synthesis of ethyl 7-anilino-2-phenyl[1,3]thiazolo[5,4-*b*]pyridine-6-carboxylates **52b,c**, ethyl 7-benzamido-2-phenyl[1,3]thiazolo[5,4-*b*]pyridine-6-carboxylates **53a-c** and ethyl 7-dibenzoylamino-2-phenyl-thiazolo[5,4-*b*]pyridine-6-carboxylates **53d-f**.

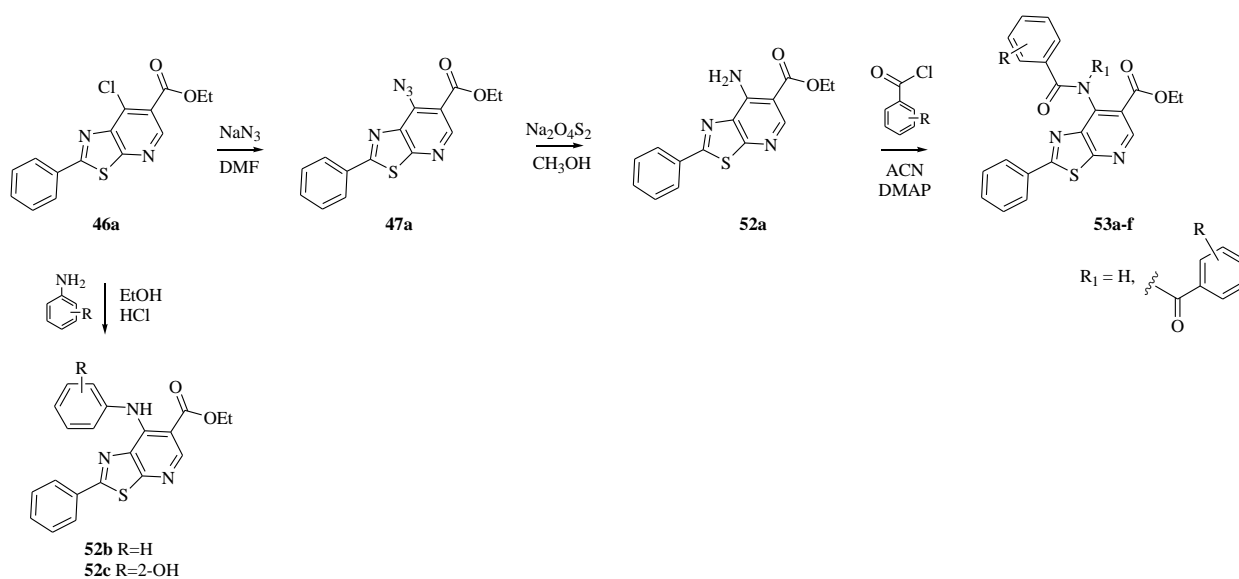
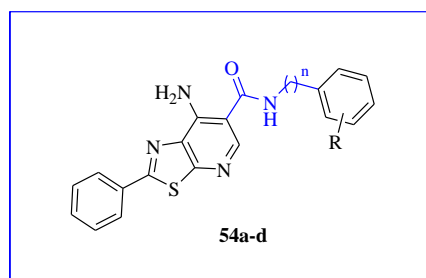


Table 6. Ethyl 7-benzamido-2-phenyl[1,3]thiazolo[5,4-*b*]pyridine-6-carboxylates **53a-c** and ethyl 7-dibenzoylamino-2-phenyl-thiazolo[5,4-*b*]pyridine-6-carboxylates **53d-f**.

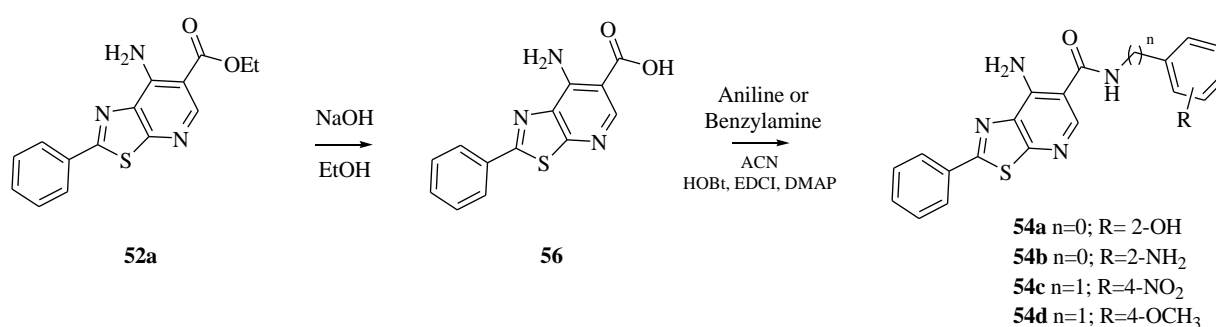
Compound	R	R ₁
53a	2-F	H
53b	H	H
53c	2-Cl	H
53d	2-F	CO-2-F-Ph
53e	H	CO-Ph
53f	2-Cl	CO-2-Cl-Ph

3.4.4 Synthesis of 7-amino-*N*,2-diphenyl[1,3]thiazolo[5,4-*b*]pyridine-6-carboxamides **54a,b** and 7-amino-*N*-benzyl-2-phenyl[1,3]thiazolo[5,4-*b*]pyridine-6-carboxamides **54c,d**.



7-Amino-*N*,2-diphenyl[1,3]thiazolo[5,4-*b*]pyridine-6-carboxamides **54a,b** and 7-amino-*N*-benzyl-2-phenyl[1,3]thiazolo[5,4-*b*]pyridine-6-carboxamides **54c,d** were obtained by heating under reflux the ethyl 7-amino-2-phenyl[1,3]thiazolo[5,4-*b*]pyridine-6-carboxylate derivative **52a** with sodium hydroxide 2N in ethanol to afford the corresponding 7-amino-2-phenyl[1,3]thiazolo[5,4-*b*]pyridine-6-carboxylic acid **56**. Subsequent nucleophilic substitution with the proper aniline (for **54a** and **54b**) or benzylamine (for **54c** and **54d**) in acetonitrile and in the presence of hydroxybenzotriazole (HOBt), *N*-(3-Dimethylaminopropyl)-*N*'-ethylcarbodiimide hydrochloride (EDC HCl) and 4-dimethylaminopyridine (DMAP) led to the desired 7-amino-*N*,2-diphenyl[1,3]thiazolo[5,4-*b*]pyridine-6-carboxamides **54a,b** and 7-amino-*N*-benzyl-2-phenyl[1,3]thiazolo[5,4-*b*]pyridine-6-carboxamides **54c,d**, by irradiating the reaction for 40 minutes (2 cycles of 20' each) with a power of 60 W and a temperature of 50 °C through a Microwave-Assisted Organic Synthesis (Scheme 13).

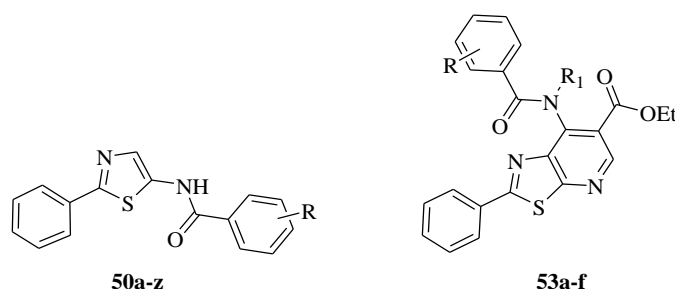
Scheme 13. Synthesis of 7-amino-*N*,2-diphenyl[1,3]thiazolo[5,4-*b*]pyridine-6-carboxamides **54a,b** and 7-amino-*N*-benzyl-2-phenyl[1,3]thiazolo[5,4-*b*]pyridine-6-carboxamides **54c,d**.



3.5 Biological evaluations of newly synthesized derivatives

Biochemical assays were performed to assess the ability of the newly synthesized compounds to inhibit the Nsp13-associated enzymatic activities. Within the *N*-(2-phenyl-1,3-thiazol-5-yl)benzamide series, compounds **50i** (R = 3-Cl) and **50j** (R = 3-Br) exhibited inhibition towards the unwinding activity with IC₅₀ values of 19.8 ± 2.4 μM and 13.3 ± 4.9 μM, respectively, without considerably affecting the ATPase function of Nsp13 (Table 7, Figure 22). Interestingly, derivative **50n** (R = 3-CF₃) retained a moderate dual inhibitory activity towards the enzyme, interfering both with the unwinding and 5'-triphosphatase activity with IC₅₀ values of 24.04 ± 2.21 μM and 17.32 ± 2.39 μM, respectively (Table 7, Figure 22). These results suggested that a halogen substituent at position 3 of the phenyl ring seems to be crucial for the enzymatic activity of *N*-(2-phenyl-1,3-thiazol-5-yl)benzamides, with better results for the 3-trifluoromethyl-substituted derivative **50n**.

Table 7. Inhibition of SARS-CoV-2 Nsp13-associated enzymatic activities by selected compounds.



Compound	R	R ₁	Unwinding IC ₅₀ (μM) ^a	ATPase IC ₅₀ (μM) ^b
50i	3-Cl	---	19.8 ± 2.4	> 30 (54%) ^c
50j	3-Br	---	13.3 ± 4.9	> 30 (55%) ^c
50n	3-CF ₃	---	24.04 ± 2.21	17.32 ± 2.39
53e	H	CO-Ph	> 30 (73%) ^c	21.5 ± 0.6
SSYA10-001	---	---	4.7	---
Licoflavone C	---	---	---	7.6

^aCompound concentration required to inhibit the SARS-CoV-2 nsp13-associated unwinding activity by 50%. ^bCompound concentration required to inhibit the SARS-CoV-2 nsp13-associated ATPase activity by 50%. ^cPercentage of control measured in the presence of the highest compound concentration.

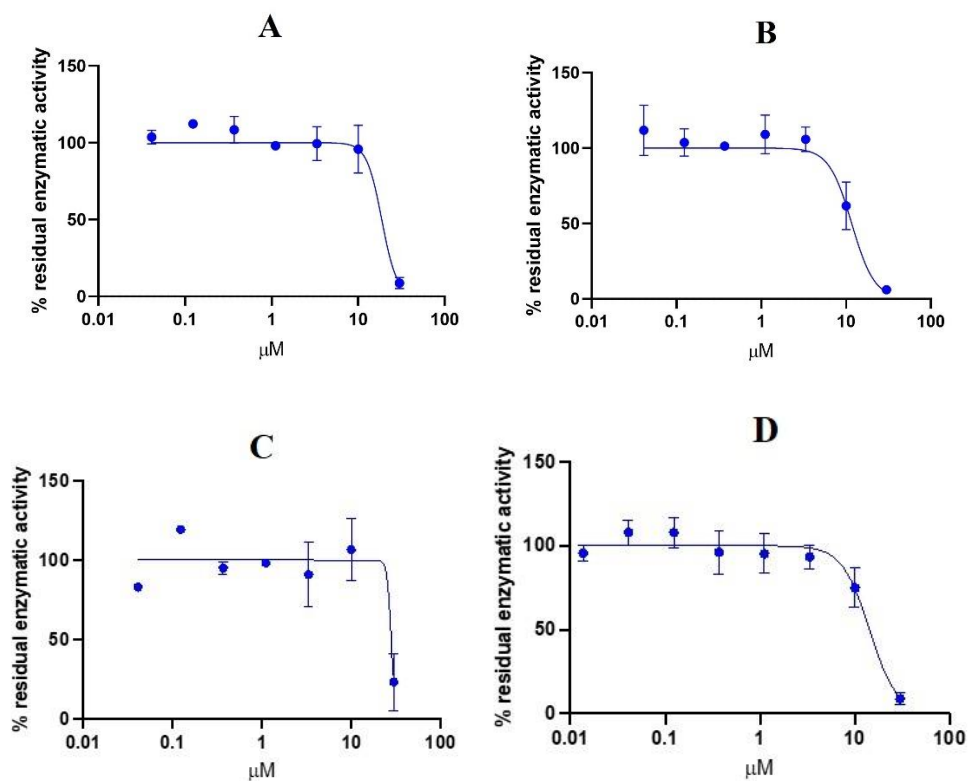


Figure 22. Inhibition of the Nsp13-associated unwinding activity by (A) **50i**, (B) **50j** and (C) **50n**; (D) Inhibition of the Nsp13-associated ATPase activity by **50n**

On the other hand, among tested thiazolo[5,4-*b*]pyridine compounds, **53e** was the only derivative able of weakly inhibiting the ATPase function of Nsp13 with IC₅₀ values of 21.5 ± 0.6 μM, without interfering with the unwinding activity of the enzyme (Table 7, Figure 23).

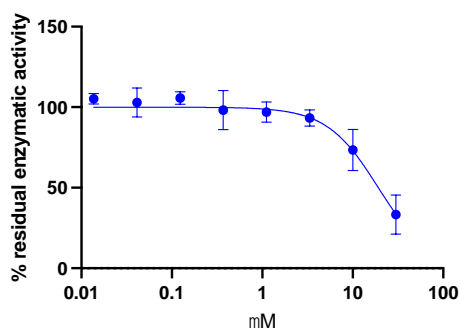


Figure 23. Inhibition of the Nsp13-associated ATPase activity by **53e**

Unfortunately, when tested on SARS-CoV-2 through cell-based assays, all tested derivatives failed to inhibit viral plaque formation, with the intermediate **56** only showing a weak inhibition against SARS-CoV-2 Omicron strain ($EC_{50} = 51.54 \mu\text{M}$), without any toxicity for concentrations up to $100 \mu\text{M}$ (Table 8). The antiviral activity of some of the newly synthesized compounds (**50o-z**, **53a,b** and **54b**) is still under investigation.

Table 8. Cytotoxicity and antiviral activity of newly synthesized compounds against SARS-CoV-2 in Vero cells.

Compound	Antiviral activity EC_{50} (μM) ^a		Cytotoxicity (μM)	
	UC-1074 (Wuhan)	BA.1 (Omicron)	Cell morphology (MCC) ^b	Cell growth (CC_{50}) ^c
50a	> 4	> 4	20	ND
50b	> 4	> 0.80	≥ 4	ND
50c	> 4	> 4	20	ND
50d	> 4	> 4	20	ND
50e	> 20	> 20	100	ND
50f	> 4	> 4	20	ND
50g	> 20	> 20	100	ND
50h	> 20	> 20	100	ND
50i	> 100	> 100	> 100	ND
50j	> 100	> 20	≥ 100	ND
50k	> 20	> 20	≥ 20	ND
50l	> 20	> 4	≥ 20	ND
50m	> 100	> 20	≥ 100	ND
50n	> 20	> 20	≥ 20	ND
51	> 100	> 100	> 100	ND
52a	> 4	> 20	≥ 20	ND
52b	> 100	> 20	≥ 100	ND
52c	> 100	> 100	≥ 100	ND
53c	> 20	> 4	≥ 20	ND
53d	> 100	> 100	≥ 100	ND
53e	> 100	> 100	≥ 100	ND
53f	> 100	> 20	≥ 100	ND
54a	> 100	> 20	≥ 100	ND
54c	> 100	> 20	≥ 100	ND
54d	> 100	> 100	> 100	ND
56	> 100	51.54	> 100	ND
Remdesivir	3.73 μM	2.53 μM	> 40 μM	ND
Molnupiravir	1.96 $\mu\text{g/mL}$	1.79 $\mu\text{g/mL}$	20 $\mu\text{g/mL}$	ND

^aEffective concentration required to reduce virus plaque formation by 50%. ^bMinimum cytotoxic concentration that causes a microscopically detectable alteration of cell morphology. ^cCytotoxic concentration required to reduce cell growth by 50%. ^dNot determined.

3.6 Broad-spectrum screening

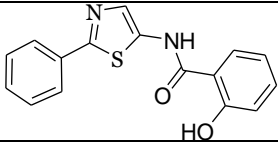
With the aim of searching for novel antiviral therapeutics with a broad spectrum of action, according to a protocol applied at the Rega Institute for Medical Research, KU Leuven (Belgium), all the synthesized compounds have also been evaluated on cell cultures for their efficacy in inhibiting the replication of a panel of different viruses through cell-based assays. In

particular, the antiviral activity was evaluated against human Coronaviruses (HCoV-229E, HCoV-OC43, HCoV-NL63), Influenza virus (A/H1N1, A/H3N2, B), Respiratory Syncytial Virus (RSV), Herpes Simplex Virus 1 (HSV-1 KOS and KOS-ACV⁺) Herpes Simplex Virus 2 (HSV-2 strain G), Varicella-zoster (VZV TK⁺ strain OKA and TK⁻ strain 07-1), Cytomegalovirus (HCMV AD-169 and Davis strains), Yellow Fever Virus (YFV), Zika Virus (ZIK), Sindbis Virus (SINV) and Semliki Forest Virus (SFV). The following cells were used: HEL 299 (HCoV-229E, HCoV-OC43, HSV-1, HSV-2, VZV, HCMV), Hep3B (HCoV-NL63, YFV, ZIK), MDCK (Influenza virus), Hep2 (RSV) and VeroE6 (SINV, SFV). Antiviral activity was expressed as the EC₅₀ and the cytotoxicity was assessed by evaluating the MCC. The cell growth inhibition was calculated as the CC₅₀, or compound concentration required to reduce cell proliferation by 50% compared to the number of cells in the untreated controls and it was only investigated for compounds exhibiting an MCC/EC₅₀ ratio higher than 10.

Biological evaluations are currently ongoing, but on the basis of data available so far, some very interesting results have emerged concerning both pyridine and naphthyridine derivatives as well as the *N*-(2-phenyl-1,3-thiazol-5-yl)benzamide series.

Within the *N*-(2-phenyl-1,3-thiazol-5-yl)benzamide series, interesting results were obtained for compound **50f** (R = 2-OH), exhibiting a dual inhibitory activity toward VZV and HCMV (Table 9). In particular, this derivative displayed a moderate inhibition of both TK⁺ OKA and TK⁻ 07-1 strains of VZV, with EC₅₀ values of 26.15 and 47.58 μM, respectively, coupled with a more significant inhibition of both AD-169 and Davis strains of HCMV, with EC₅₀ values ranging from 8.94 to 12.63 μM, without displaying any cytotoxic effect (CC₅₀ > 100 μM).

Table 9. Antiviral activity of *N*-(2-phenyl-1,3-thiazol-5-yl)benzamide **50f** in human embryonic lung (HEL) cells.

Cpd	Structure	Antiviral activity EC ₅₀ (μM) ^a				Cytotoxicity (μM)	
		TK ⁺ VZV strain OKA	TK ⁻ VZV strain 07-1.	HCMV strain AD-169	HCMV strain Davis	Cell morphology (MCC) ^b	Cell growth (CC ₅₀) ^c
50f		26.15	47.58	---	---	> 100	> 100
		---	---	> 20	12.63	≥ 20	> 100
		---	---	10.31	8.94	100	> 100
		---	---	9.78	8.94	≥ 20	> 100
Acyclovir	---	8.92	30.37	---	---	> 444	> 444
Brivudine	---	0.033	0.014	---	---	> 300.3	> 300.3
Ganciclovir	---	---	---	2.72	2.17	≥ 394	> 394
				7.05	4.89	≥ 394	> 394
				2.36	1.50	≥ 394	> 394

Cidofovir	---	---	---	0.38	0.30	≥ 317	> 317
				1.05	0.51	≥ 317	> 317
				0.35	0.26	≥ 317	> 317

^aEffective concentration required to reduce virus plaque formation by 50%. ^bMinimum cytotoxic concentration that causes a microscopically detectable alteration of cell morphology. ^cCytotoxic concentration required to reduce cell growth by 50%. ^dNot determined.

Among [1,3]thiazolo[5,4-*h*][1,6]naphthyridines, compound **31a** (Table 10) displayed a moderate inhibition of VZV, interfering with the TK⁻ 07-1 strain replication with an EC₅₀ value of 52.53 μ M, but it was found to be cytotoxic for cell cultures (MCC ≥ 20 μ M).

On the other hand, [1,3]thiazolo[5,4-*h*][1,6]naphthyridine derivative **31d** (R = H, R₁ = 2-OCH₃-Ph) showed strong antiviral activity against human coronavirus HCoV-229E on HEL cells, with an EC₅₀ value of 0.85 μ M without any toxicity for concentrations up to 50 μ M. The same viral culture was also found to be inhibited by the [1,3]thiazolo[5,4-*b*]pyridine derivative **51**, albeit with less potency (EC₅₀ = 4.65 μ M) (Table 10).

This is a very interesting result, representing a promising seed in the identification of novel antiviral agents. The exploration of the mechanism of action aimed at identifying their target is currently ongoing and will pave the way for further chemical developments of this class of compounds.

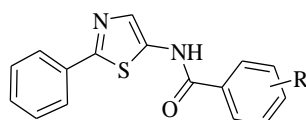
Table 10. Antiviral activity of [1,3]thiazolo[5,4-*h*][1,6]naphthyridines **31a** and **31d** and [1,3]thiazolo[5,4-*b*]pyridine derivative **51** in human embryonic lung (HEL) cells.

Cpd	Structure	Antiviral activity EC ₅₀ (μM) ^a			Cytotoxicity (μM)	
		TK ⁺ VZV strain OKA	TK ⁻ VZV strain 07-1	HCoV 229E	Cell morphology (MCC) ^b	Cell growth (CC ₅₀) ^c
31a		> 20	52.53	ND	≥ 20	ND
31d		> 20	> 4	0.85	≥ 20	> 50
51		> 100	> 100	4.65	> 100	> 50
Acyclovir	---	8.92	43.64	---	> 444	> 444
Brivudine	---	0.19	0.36	---	> 300.3	> 300.3
Remdesivir	---	---	---	0.04	ND	> 10
Ribavirin	---	---	---	141.2	ND	> 250

^aEffective concentration required to reduce virus plaque formation by 50%. ^bMinimum cytotoxic concentration that causes a microscopically detectable alteration of cell morphology. ^cCytotoxic concentration required to reduce cell growth by 50%. ^dNot determined.

However, the most promising results have been shown by derivatives **50b** (R = 2,6-Cl₂) and **50c** (R = 2-Br). In fact, both compounds proved to potently inhibit the replication of different Influenza virus A/H1N1 strains with EC₅₀ values in the submicromolar range (Table 11).

Table 11. Antiviral activity of *N*-(2-phenyl-1,3-thiazol-5-yl)benzamide **50b** and **50c** against Influenza virus in MDCK cells.



50a-z

Cpd	R	Antiviral activity EC ₅₀ (μM) ^a Influenza virus A/H1N1											Cytotoxicity CC ₅₀ (μM) ^b			
		A/FM/1/47			A/Ned/378/05			A/PR/8 RG WT			A/Virginia/ATCC3/09			MDCK		
		Exp.1	Exp.2	Exp.3	Exp.1	Exp.2	Exp.3	Exp.1	Exp.2	Exp.3	Exp.1	Exp.2	Exp.3	Exp.1	Exp.2	Exp.3
50b	2,6-Cl ₂	0.12	0.40	0.31	0.09	0.08	0.10	0.04	0.06	0.09	0.46	0.41	0.33	> 25	11.2	10.1

50c	2-Br	0.54	0.34	0.53	0.40	0.32	0.41	0.37	0.42	1.40	1.70	0.82	1.80	12.8	11.8	11.0
Zanamivir	---	19.2	0.31	-	0.34	0.04	-	0.1	2.1	-	> 25	6.9	-	> 25	> 25	> 25
Ribavirin	---	8.8	15.9	10.6	8.9	6.4	8.0	2.0	14.8	9.2	13.5	8.4	10.9	> 100	> 100	> 100
Rimantadine	---	0.18	0.28	-	> 25	0.07	-	23.0	10.3	-	> 25	> 25	-	> 25	> 25	> 25
Amantadine	---	0.64	0.35	-	6.4	1.6	-	> 25	> 25	-	> 25	> 25	-	> 25	> 25	> 25

^aEffective concentration required to reduce virus plaque formation by 50%. ^bCytotoxic concentration required to reduce cell growth by 50%.

Influenza A virus (IAV) is a highly contagious respiratory pathogen responsible of seasonal and pandemic flu. Notably, the recent outbreak of Influenza A virus H1N1 in 2009 resulted in about 575,000 deaths worldwide [89]. Influenza viruses are characterized by a segmented negative-sense single-strand RNA genome, which provides high genetic variability and development of mutations [90]. Replication of IAV (Figure 24) starts with the binding of viral hemagglutinin (HA) glycoprotein to the *N*-acetylneuraminic acid (sialic acid) terminals of host cell receptors (SA), followed by endocytosis and conformational changes of HA, ultimately resulting in the fusion between viral and host endosomal membranes. After the replication process, new viral particles are assembled in proximity to the cell membrane, where the new virions are still anchored to the sialic acid terminals of the cell surface receptors through their hemagglutinins. Cleavage of these terminal neuraminic acid moieties by viral neuraminidase allows the release of new virions and the spread of the infection [91].

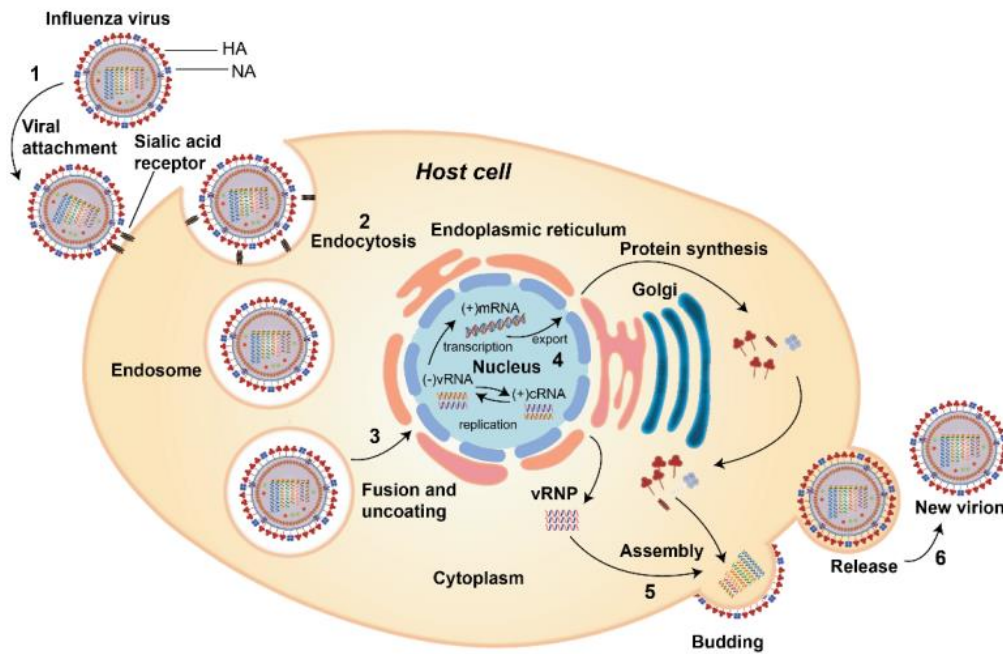


Figure 24. Influenza virus life cycle [92]

Nowadays, several vaccines and antiviral drugs are available for the treatment of Influenza virus. According to the target and the mechanism of action, three classes of antivirals are used in clinical practice. Neuraminidase inhibitors, such as oseltamivir, zanamivir, peramivir and laninamivir, interfere with the release of viral progeny from the host cell [93]. M2 ion channel inhibitors, amantadine and rimantadine, prevent the release of the viral genome into the cytoplasm during early stages of replication [94]. Finally, the cap-dependent endonuclease inhibitor baloxavir marboxil, which acts by blocking the process of viral genome transcription, is the most recent US FDA approved drug for the treatment of influenza A and B viruses [95]. However, the rapid emergence of drug-resistant viral strains and drug toxicity issues point out the need for new therapeutic approaches. The viral envelope hemagglutinin (HA) glycoprotein is one of the most attractive targets for *small molecules* design, due also to the high degree of conservation of the amino acid sequence of its sialic acid binding site. Nevertheless, Arbidol (umifenovir) is the only available antiviral drug targeting the HA glycoprotein. Arbidol is currently licensed in China and Russia for the prophylaxis and treatment of influenza and other respiratory viral infections, and its use as potential agent for the prevention of COVID-19 caused by SARS-CoV-2 infections is under investigation [96]. Arbidol is a broad-spectrum dual-acting direct antiviral/host-targeting agent which demonstrated to be active against several enveloped and non-enveloped DNA and RNA viruses, including influenza A and B viruses. It seems to exert antiviral effects through multiple pathways, including direct interactions with aromatic residues of the viral glycoproteins involved in fusion and cellular recognition. Unfortunately, the use of Arbidol is limited by the high dosages that must be administered to achieve a therapeutic effect [97], highlighting the need for further research to identify more potent and effective HA inhibitors.

With the aim of investigating the mechanism of action of the two active compounds **50b** and **50c** emerged from the cytopathic effect (CPE) reduction assay, the influenza pseudovirus entry assay was performed for H1N1 and H5N1 strains by the research group of Prof. Lieve Naesens from the Rega Institute for Medical Research. The luciferase reporter-based assay was conducted in MDCK cells, with Arbidol included as reference compound. Both derivatives **50b** and **50c** displayed inhibition of HA-mediated viral fusion of H1N1 subtype to the host cellular membrane with EC₅₀ values of 0.47 μM and 4.7 μM, respectively, with compound **50b** also showing an EC₅₀ value of 10 μM against H5N1 subtype (Figure 25).

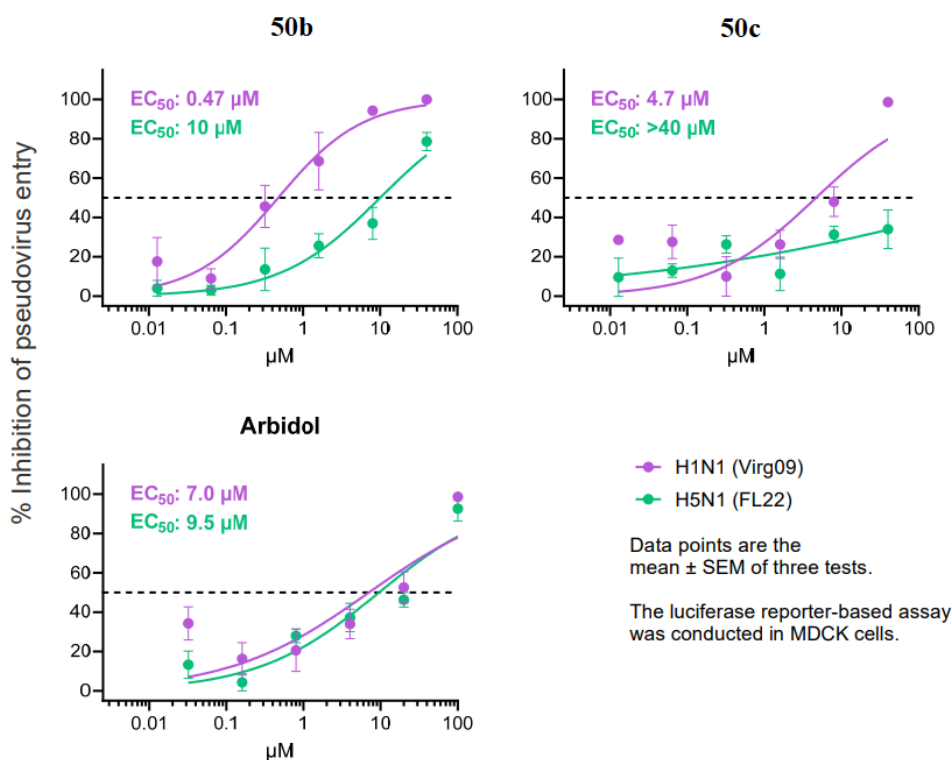


Figure 25. Pseudovirus entry assay of compounds **50b** and **50c** for Influenza virus A/H1N1 and A/H5N1 in MDCK cells

Overall, these results represent a promising basis for further investigation aiming to explore the chemical space of the *N*-(2-phenyl-1,3-thiazol-5-yl)benzamide scaffold, to study the structure-activity relationships of these promising derivatives.

3.7 Evaluation of drug-like properties

In silico ADME (absorption, distribution, metabolism and elimination) properties of the most promising compounds were predicted using the QikProp software [98] and the obtained data are summarized in Tables 12-13. The pharmaceutically relevant properties of each compound were compared with those of 95% of the known drugs. Molecular descriptor values that fall outside the 95% range are expressed as #stars, where a large number of stars suggests that a molecule is less drug-like.

Among the most significant parameters, we evaluated the total solvent accessible surface area (SASA) with its hydrophobic (FOSA) and hydrophilic (FISA) components, showing that all

molecules have a good ability to permeate cell membranes. The majority of our compounds were also found to have a high intestinal absorption capacity by passive diffusion (P_{caco}), a good ability to permeate the blood-brain barrier by passive diffusion (\log_{BB} and P_{MDCK}) but with low neurotoxicity (CNS) and a good oral absorption. The \log_{HERG} values within the limits and a poor ability to bind to human serum albumin ($\log_{K_{ha}}$) also showed a good safety profile of our molecules. With few exceptions, selected compounds complied with Lipinski's rule of five since they have $MW < 500$, $\log P_{o/w} < 5$, $donorHB \leq 5$ and $acceptHB \leq 10$, thus proving to be drug-like molecules.

Table 12. Drug-likeness of selected [1,3]thiazolo[5,4-*b*]pyridines and [1,3]thiazolo[5,4-*h*][1,6]naphthyridines.

Title	#stars	mol MW	SASA	FOSA	FISA	Donor HB	Accept HB	logPo/w	logS	logHERG	Pcaco	logBB	PMDCK	CNS	logKhsa	Human Oral Abs	Rule Of Five
31a	0	277,343	531,833	90,893	46,798	0	3,5	3,65	-4,631	-5,773	3565,421	0,219	3183,234	1	0,271	3	0
31d	2	369,44	671,947	92,691	43,635	0	4,25	5,205	-6,568	-7,243	3820,391	0,076	3429,854	1	0,757	1	1
31e	3	357,404	633,993	0	42,786	0	3,5	5,296	-6,567	-7,1	3891,915	0,252	5593,639	1	0,803	1	1
31f	3	407,412	652,995	0	35,992	0	3,5	5,932	-7,162	-6,857	4514,273	0,46	10000	2	0,988	1	1
46a	0	318,777	576,657	139,928	81,778	0	4,5	3,517	-4,873	-5,678	1661,097	-0,136	2800,142	0	0,14	3	0
51	0	363,228	580,903	139,916	80,376	0	4,5	3,602	-4,976	-5,701	1712,738	-0,112	3094,697	0	0,164	3	0
53e	2	507,563	786,324	140,138	106,721	0	7,5	5,29	-6,547	-7,179	963,535	-0,758	777,465	-1	0,694	1	2
56	0	271,293	485,509	0	179,696	2	4,5	2,089	-3,413	-3,197	49,595	-1,066	39,993	-2	-0,288	3	0

Table 13. Drug-likeness of *N*-(2-phenyl-1,3-thiazol-5-yl)benzamides

Title	#stars	mol MW	SASA	FOSA	FISA	Donor HB	Accept HB	logPo/w	logS	logHERG	Pcaco	logBB	PMDCK	CNS	logKhsa	Human Oral Abs	Rule Of Five
50a	0	314,789	569,914	0	62,113	1	4	4,016	-5,282	-6,355	2552,024	0,055	4237,082	1	0,366	3	0
50b	0	349,234	590,798	0	54,168	1	4	4,519	-5,937	-6,31	3035,449	0,279	10000	1	0,47	3	0
50c	0	359,24	572,771	0	61,956	1	4	4,075	-5,357	-6,353	2560,786	0,066	4467,363	1	0,385	3	0
50d	0	316,325	564,593	0	60,269	1	4	3,992	-5,265	-6,249	2656,884	0,114	5419,708	1	0,334	3	0
50e	0	298,334	557,774	0	63,818	1	4	3,772	-5,018	-6,343	2458,746	-0,009	3122,268	0	0,298	3	0
50f	0	296,343	560,604	0	102,914	1	3,75	3,516	-4,814	-6,33	1047,049	-0,53	822,55	0	0,321	3	0
50g	0	280,344	553,714	0	66,224	1	4	3,593	-4,806	-6,473	2332,891	-0,108	2005,255	0	0,266	3	0
50h	0	310,37	590,554	92,701	66,241	1	4,75	3,686	-5,002	-6,372	2332,052	-0,185	2001,516	0	0,276	3	0
50i	0	314,789	577,769	0	66,212	1	4	4,084	-5,501	-6,398	2333,533	0,052	4945,567	1	0,381	3	0
50j	0	359,24	582,808	0	66,246	1	4	4,161	-5,63	-6,428	2331,806	0,063	5313,826	1	0,405	3	0
50k	0	349,234	593,965	0	62,101	1	4	4,509	-6,029	-6,278	2552,669	0,217	10000	1	0,482	3	0
50l	0	310,37	590,331	91,992	66,33	1	4,75	3,693	-4,996	-6,359	2327,539	-0,186	1983,57	0	0,28	3	0
50m	0	298,334	562,709	0	66,215	1	4	3,827	-5,147	-6,353	2333,352	0,001	3623,881	1	0,308	3	0
50n	0	348,342	606,028	0,692	66,304	1	4	4,577	-6,218	-6,458	2328,83	0,149	8790,648	1	0,525	1	0
50o	0	364,341	619,329	1,829	60,762	1	4	4,804	-6,309	-6,597	2628,39	0,147	10000	1	0,55	1	0
50p	0	348,342	605,794	0,704	66,287	1	4	4,575	-6,214	-6,455	2329,719	0,149	8800,389	1	0,524	1	0
50q	0	349,234	598,184	0	66,253	1	4	4,514	-6,132	-6,316	2331,423	0,185	10000	1	0,488	3	0
50r	0	305,353	591,904	0	138,255	1	5,5	2,843	-5,631	-6,588	483,985	-0,928	366,927	-1	0,103	3	0
50s	0	310,37	597,205	92,442	62,205	1	4,75	3,773	-5,122	-6,503	2546,907	-0,151	2218,605	0	0,294	3	0
50t	0	314,789	577,872	0	66,241	1	4	4,085	-5,504	-6,399	2332,04	0,052	4948,724	1	0,382	3	0

50u	0	349,234	593,92	0	62,096	1	4	4,508	-6,028	-6,278	2552,942	0,217	10000	1	0,482	3	0
50v	0	359,24	582,755	0	66,183	1	4	4,161	-5,629	-6,427	2335,018	0,064	5325,38	1	0,405	3	0
50w	0	298,334	562,739	0	66,213	1	4	3,828	-5,148	-6,353	2333,484	0,001	3629,972	1	0,308	3	0
50x	0	393,685	594,129	0	53,935	1	4	4,585	-6,015	-6,314	3050,975	0,292	10000	1	0,49	3	0
50y	0	296,343	566,255	0	120,943	2	4,75	2,854	-4,522	-6,353	706,317	-0,717	551,154	-1	0,106	3	0
50z	0	296,343	566,022	0	120,795	2	4,75	2,855	-4,518	-6,348	708,6	-0,714	553,284	-1	0,106	3	0

Principal Descriptors. **MW:** molecular weight of the molecule [130.0 – 725.0]. **SASA:** total solvent accessible surface area [300.0 – 1000.0]. **FOSA:** hydrophobic component of the SASA (saturated carbon and attached hydrogen) [0.0 – 750.0]. **FISA:** hydrophilic component of the SASA (N, O, and H on 80 heteroatoms) [7.0 – 330.0]. **HB Donor:** estimated number of hydrogen bonds that would be donated by the solute to water molecules in an aqueous solution [0.0 – 6.0]. **HB Acceptor:** estimated number of hydrogen bonds that would be accepted by the solute from water molecules in an aqueous solution [2.0 – 20.0]. **Properties Predictions.** **LogPo/w:** predicted octanol/water partition coefficient [-2.0 – 6.5]. **LogS:** predicted aqueous solubility [-6.5 – 0.5]. **LogHERG:** predicted IC50 value for blockage of HERG K⁺ channels [concern below -5]. **Pcaco:** predicted apparent Caco-2 cell permeability in nm/sec; Caco-2 cells are a model for the gut-blood barrier. Predictions are for non-active transport [500 great]. **LogBB:** predicted brain/blood partition coefficient [-3.0 – 1.2]. **PMDCK:** predicted apparent MDCK cell permeability in nm/sec. MDCK cells are considered to be a good mimic for the blood-brain barrier. Predictions are for non-active transport [<25 poor, >500 great]. **CNS:** predicted central nervous system activity on a -2 (inactive) to +2 (active) scale. **LogKhsa:** prediction of binding to human serum albumin [-1.5 – 1.5]. **Human Oral Absorption:** predicted qualitative human oral absorption: 1, low; 2, medium; 3, high. **Lipinski Rule or Rule of Five:** number of violations of Lipinski's rule of five. The four rules are: mol_MW < 500, cLogPo/w < 5, HB donor ≤ 5, HB acceptor ≤ 10. Compounds that satisfy these rules are considered drug-like [max 4]. **#Stars:** number of property or descriptor values that are outside the 95% range of similar values for known drugs. A large number of stars suggests that a molecule is less drug-like than molecules with few stars [0 – 5]

4. Conclusions

In conclusion, the synthesis of a small library of [1,2,3]thiazolo[4,5-*h*][1,6]naphthyridines and [1,3]thiazolo[5,4-*h*][1,6]naphthyridines has been reported and their antiviral properties have been investigated. In particular, with the aim of searching for novel therapeutic approaches for the treatment of SARS-CoV-2 infections, all synthesized compounds were evaluated for their ability to inhibit the SARS-CoV-2 Nsp13 helicase. Among tested derivatives, [1,3]thiazolo[5,4-*h*][1,6]naphthyridines **31d** and **31f** exhibited inhibition towards the unwinding activity of Nsp13 with IC₅₀ values of 19.13 ± 1.5 μM and 16.7 ± 1.2 μM, respectively. The most interesting results were obtained for compound **31e**, displaying a dual inhibitory activity towards the enzyme, by interfering both with the unwinding (IC₅₀ = 26.13 ± 0.76 μM) and 5'-triphosphatase (IC₅₀ = 10.15 ± 0.71 μM) activities at micromolar level. Unfortunately, when tested on SARS-CoV-2 through cell-based assays, none of these compounds showed the ability to inhibit viral plaque formation, inducing cell morphology alteration at micromolar concentrations.

A structural simplification strategy of the *hit* candidate **31e** has been applied to try to improve its biological properties, leading to a new series of decorated *N*-(2-phenyl-1,3-thiazol-5-yl)benzamides.

On the other hand, the thiazolo[5,4-*b*]pyridine derivative **46a** exhibited some moderate activity against SARS-CoV-2 at micromolar level, without any toxicity for concentrations up to 100 μM. Therefore, the potentialities of the bicyclic thiazole-pyridine system have been further investigated through the synthesis of a series of [1,3]thiazolo[5,4-*b*]pyridine derivatives. Biochemical assays on Nsp13 revealed some interesting results concerning both the *N*-(2-phenyl-1,3-thiazol-5-yl)benzamide and the [1,3]thiazolo[5,4-*b*]pyridine series, even though the antiviral activity of some of the newly synthesized compounds is still under investigation.

Finally, with the aim of searching for novel antiviral therapeutics with a broad spectrum of action, all synthesized compounds have also been evaluated for their efficacy in inhibiting the replication of a panel of different viruses (HCoV, Flu, RSV, HSV-1, HSV-2, VZV, HCMV, YFV, ZIKV, SINV and SFV) through cell-based assays. These screenings led to some relevant results, that will pave the way for further chemical developments of this class of compounds. In particular, the [1,3]thiazolo[5,4-*h*][1,6]naphthyridine derivative **31d**, showed strong antiviral activity against human coronavirus HCoV-229E (EC₅₀ = 0.85 μM).

The most promising results have been obtained with the *N*-(2-phenyl-1,3-thiazol-5-yl)benzamide compounds **50b** and **50c**, which potently inhibited influenza virus (IAV) A/H1N1

replication, with EC₅₀ values in the submicromolar range. In order to investigate their mechanism of action, an A/H1N1 pseudovirus entry assay has been performed, thus confirming strong inhibition of the HA-mediated entry process, with EC₅₀ values of 0.47 μM (**50b**) and 4.7 μM (**50c**), respectively.

Overall, results obtained so far confirmed the value of [1,3]thiazolo[5,4-*h*][1,6]naphthyridine and *N*-(2-phenyl-1,3-thiazol-5-yl)benzamide systems as promising scaffold for the development of novel antiviral agents. Exploration of the chemical space around the hit compounds identified as a result of my PhD project will be performed, with the aim of improving the MedChem properties of our class of thiazole-based systems.

Furthermore, several scientific publications have been produced during my PhD course:

- Renda M., Barreca M., Borrelli A., Spanò V., Montalbano A., Raimondi M.V., **Bivacqua R.**, Musante I., Scudieri P., Guidone D., Buccirosi M., Genovese M., Venturini A., Bandiera T., Barraja P., Galietta L.J.V. Novel tricyclic pyrrolo-quinolines as pharmacological correctors of the mutant CFTR chloride channel. *Scientific Reports* (2023), 13(1), 7604, doi: 10.1038/s41598-023-34440-0.
- **Bivacqua R.**, Romeo I., Barreca M., Barraja P., Alcaro S., Montalbano A. HSV-1 Glycoprotein D and its surface receptors: evaluation of protein-protein interaction and targeting by triazole-based compounds through *in silico* approaches. *International Journal of Molecular Sciences* (2023), 24(8), 7092, doi: [10.3390/ijms24087092](https://doi.org/10.3390/ijms24087092).
- Barreca M., Spanò V., Rocca R., **Bivacqua R.**, Gualtieri G., Raimondi M.V., Gaudio E., Bortolozzi R., Manfreda L., Bai R., Montalbano A., Alcaro S., Hamel E., Bertoni F., Viola G., Barraja P. Identification of pyrrolo[3',4':3,4]cyclohepta[1,2-*d*][1,2]oxazoles as promising new candidates for the treatment of lymphomas. *European Journal of Medicinal Chemistry* (2023), 254, 115372, doi: 10.1016/j.ejmech.2023.115372.
- **Bivacqua R.**, Barreca M., Spanò V., Raimondi M.V., Romeo I., Alcaro S., Andrei G., Barraja P., Montalbano A. Insight into non-nucleoside triazole-based systems as viral polymerases inhibitors. *European Journal of Medicinal Chemistry* 249 (2023) 115136, doi: 10.1016/j.ejmech.2023.115136.
- Barreca M., Spanò V., Rocca R., **Bivacqua R.**, Abel A.C., Maruca A., Montalbano A., Raimondi M.V., Tarantelli C., Gaudio E., Cascione L., Rinaldi A., Bai R., Steinmetz M.O.,

Prota A.E., Alcaro S., Hamel E., Bertoni F., Barraja P. Development of [1,2]oxazoloisindoles tubulin polymerization inhibitors: Further chemical modifications and potential therapeutic effects against lymphomas. *European Journal of Medicinal Chemistry* (2022), 243, 114744, doi: 10.1016/j.ejmech.2022.114744.

- Barreca M., Spanò V., Raimondi M.V., **Bivacqua R.**, Giuffrida S., Montalbano A., Cavalli A., Bertoni F., Barraja P. GPCR Inhibition in Treating Lymphoma. *ACS Medicinal Chemistry Letters* (2022), 13(3), 358-364, doi: 10.1021/acsmchemlett.1c00600.

Finally, several conference contributions have been presented:

Oral communications:

- **In silico approaches for the identification of HSV-1 Glycoprotein D inhibitors.** **Bivacqua R.**, Romeo I., Barreca M., Spanò V., Alcaro S., Barraja P., Snoeck R., Andrei G. and Montalbano A. XI Paul Ehrlich Euro-PhD Network Meeting, Barcelona, 14-16 July 2022.
- **Search for novel anti SARS-CoV-2 agents targeting Nsp13: computational studies and biological evaluations.** **Bivacqua R.**, Romeo I., Barreca M., Spanò V., Alcaro S., Barraja P., Snoeck R., Andrei G., Montalbano A. Autumn Meeting for Young Chemists in Biomedical Sciences (AMYC BIOMED 2022), Naples, 17-19 October 2022.
- **Antiviral activity of novel thiazole-based compounds targeting SARS-CoV-2 Nsp13.** **Bivacqua R.**, Romeo I., Emmolo R., Barreca M., Spanò V., Alcaro S., Corona A., Barraja P., Snoeck R., Tramontano E., Andrei G. and Montalbano A. XII Paul Ehrlich Euro-PhD Network, Thessaloniki, 16-18 July 2023.

Posters:

- **A systematic approach to small molecules in the treatment of viral infections.** **Bivacqua R.**, Barreca M., Spanò V., Andrei G., Alcaro S., Barraja P., Montalbano A. Paul Ehrlich Euro-PhD Network Virtual Meeting 2021, 26-28 July 2021.
- **Synthesis and biological evaluation of novel thiazole-based compounds as potential anti SARS-CoV-2 agents.** **Bivacqua R.**, Romeo I., Barreca M., Spanò V., Raimondi M.V.,

Alcaro S., Barraja P., Snoeck R., Andrei G., Montalbano A. Innovative Approaches for Identification of Antiviral Agents Summer School (6th IAAASS), Pula (CA), 26-30 September 2022.

- **Transcriptome and computational analysis assess the anti-tubulin activity of [1,2]oxazole derivatives in lymphoma.** Barreca M., Spanò V., Rocca R., **Bivacqua R.**, Maruca A., Montalbano A., Raimondi M.V., Tarantelli C., Gaudio E., Cascione L., Rinaldi A., Bai R., Prota A., Abel A.C., Steinmetz M., Alcaro S., Hamel E., Bertoni F., Barraja P. 34th EORTC-NCI-AACR Symposium, 27 October 2022. *European Journal of Cancer*, 2022, 174, pp. S65–S66.
- **Triazole-based compounds as potential anti SARS-CoV-2 agents targeting Nsp13.** **Bivacqua R.**, Romeo I., Barreca M., Spanò V., Raimondi M.V., Alcaro S., Barraja P., Snoeck R., Andrei G., Montalbano A. First STeBiCeF Young Researcher Workshop, Palermo, 12 January 2023.
- **Functional rescue of F508del-CFTR using small nitrogen heterocycles.** Barreca M., **Bivacqua R.**, Renda M., Borrelli A., Venturini A., Guidone D., Genovese M., Musante I., Scudieri P., Raimondi M. V., Spanò V., Montalbano A., Alcaro S., Galiotta L.J.V., Barraja P. First STeBiCeF Young Researcher Workshop, Palermo, 12 January 2023.
- **Identification of new small molecules for the treatment of lymphoma.** Giuffrida S., Barreca M., Spanò V., **Bivacqua R.**, Montalbano A., Raimondi M.V., Tarantelli C., Gaudio E., Cascione L., Rinaldi A., Bertoni F., Barraja P. First STeBiCeF Young Researcher Workshop, Palermo, 12 January 2023.
- **New pharmacological modulators for the rescue of mutant CFTR protein.** Barreca, M.; Spanò, V.; Raimondi, M.V.; Montalbano, A.; Barraja, P.; Renda, M.; Borrelli, A.; Venturini, A.; **Bivacqua R.**; Buccirosi, M.; Guidone, D.; Genovese, M.; Galiotta, L. J. V. 21st Convention of investigators in Cystic Fibrosis, Verona, 23-25 November 2023.
- **New Small Chemical Entities Targeting Olfactory Receptors for the Treatment of Lymphoma.** Giuffrida, S.; Barreca, M.; Sartori, G.; Ghiringhelli, A.; Sgrignani, J.; **Bivacqua, R.**; Raimondi, M.V.; Spanò, V.; Montalbano, A.; Cavalli, A.; Bertoni, F.; Barraja, P. Convegno Congiunto delle Sezioni Sicilia e Calabria della Società Chimica Italiana, Palermo, 11-12 December 2023.

- **Nitrogen-based heterocyclic systems as potential inhibitors of FLT3.** Titone, G.M.; Giuffrida, S.; **Bivacqua, R.**; Barreca, M.; Raimondi, M.V.; Spanò, V.; Montalbano, A.; Barraja, P. Convegno Congiunto delle Sezioni Sicilia e Calabria della Società Chimica Italiana, Palermo, 11-12 December 2023.

5. Experimental

5.1 Chemistry

All melting points were taken on a Büchi melting point M-560 apparatus. IR spectra were determined in bromoform with a Shimadzu FT/IR 8400S spectrophotometer. ¹H and ¹³C NMR spectra were measured at 200 and 50.0 MHz, respectively, in DMSO-*d*₆ or CDCl₃ solution using a Bruker Avance II series 200 MHz spectrometer. Column chromatography was performed with Merck silica gel (230–400 mesh ASTM) or a Büchi Sepacor chromatography module (prepacked cartridge system). Elemental analyses (C, H, N) were within ±0.4% of theoretical values and were performed with a VARIO EL III elemental analyzer. The purity of all the tested compounds was >95%, determined by HPLC (Agilent 1100 series).

General procedure for the synthesis of azidobenzenes 35a,b

Azidobenzene derivatives **35a,b** were synthesized according to the procedure reported in the literature [99,100]. To a stirred solution of the suitable anilines **34a,b** (10 mmol) in hydrochloric acid 6N (10 mL), a solution of sodium nitrite (15 mmol) in water (25 mL) was slowly added at -5 °C. After 30 minutes, a solution of sodium azide (40 mmol) in water (50 mL) was added dropwise. The reaction mixture was stirred for 12 hours and extracted with ethyl acetate. The organic layer was dried over sodium sulphate and the solvent was evaporated under reduced pressure, to give a solid which was used in the next step without further purifications.

Phenyl azide 35a: The spectroscopic data are in agreement with the literature [99,100].

1-Azido-4-methoxybenzene 35b: The spectroscopic data are in agreement with the literature [99,100].

General procedure for the synthesis of 5-amino-1-phenyl-1H-1,2,3-triazole-4-carbonitriles 36a,b

To a solution of metallic sodium (4.30 mmol) in anhydrous ethanol (10 mL), malononitrile (4.08 mmol) was added at room temperature. After 15 minutes, the reaction mixture was cooled at 0 °C and a solution of the properly substituted azido derivatives **35a,b** (3.40 mmol) in anhydrous ethanol (10 mL) was added dropwise. The reaction mixture was stirred for 12 hours at room temperature and then the solvent was evaporated under reduced pressure, giving a solid which was purified by silica gel chromatography, using dichloromethane: ethyl acetate (95:5) as eluent.

5-Amino-1-phenyl-1H-1,2,3-triazole-4-carbonitrile 36a: This compound was obtained by reaction of **35a**. Mp: 125.5-126.6 °C; yield: 60%; IR cm^{-1} : 3380-3330 (NH_2), 2249 (CN); ^1H NMR CDCl_3 (ppm): 5.02 (2H, bs, NH_2), 7.50-7.63 (5H, m, Ar). ^{13}C NMR CDCl_3 (ppm): 103.9, 112.4, 124.4 (2 x C), 130.4 (2 x C), 130.5, 136.7, 146.6. Anal. Calcd for $\text{C}_9\text{H}_7\text{N}_5$: C, 58.37; H, 3.81; N, 37.82. Found: C, 58.15; H, 3.92; N, 37.74.

5-Amino-1-(4-methoxyphenyl)-1H-1,2,3-triazole-4-carbonitrile 36b: This compound was obtained by reaction of **35b**. Mp: 189.5-190.0 °C; yield: 70%; IR cm^{-1} : 3347-3290 (NH_2), 2234 (CN); ^1H NMR DMSO-d_6 (ppm): 3.84 (3H, s, CH_3O), 7.02 (2H, bs, NH_2), 7.14 (2H, d, $J = 10.0$ Hz, H_2' and H_6'), 7.23 (2H, d, $J = 10.0$ Hz, H_3' and H_5'). ^{13}C NMR DMSO-d_6 (ppm): 55.6, 100.9, 113.5, 114.9 (2 x C), 126.6, 126.8 (2 x C), 148.0, 160.0. Anal. Calcd for $\text{C}_{10}\text{H}_9\text{N}_5\text{O}$: C, 55.81; H, 4.22; N, 32.54. Found: C, 55.93; H, 4.03; N, 32.67.

General procedure for the synthesis of ethyl 7-amino-5-methyl-3-phenyl-3H-[1,2,3]triazolo [4,5-b]pyridine-6-carboxylates 37a,b

To a mixture of 5-amino-1-phenyl-1H-1,2,3-triazole-4-carbonitriles **36a,b** (1.27 mmol) and ethyl acetoacetate (1.54 mmol) in anhydrous toluene (50 mL), stannic chloride (1.54 mmol) was slowly added at 0 °C. The mixture was stirred at room temperature for 1 hour and then refluxed for 5 and a half hours using a Dean-Stark apparatus. Then, the reaction mixture was cooled, neutralized to pH=10 with a 5M sodium hydroxide solution and extracted with ethyl acetate. The organic layer was dried over sodium sulphate and the solvent was evaporated under reduced pressure. The solid was purified by silica gel chromatography, using dichloromethane: ethyl acetate (9:1) as eluent.

Ethyl 7-amino-5-methyl-3-phenyl-3H-[1,2,3]triazolo[4,5-b]pyridine-6-carboxylate 37a: This compound was obtained by reaction of **36a**. Mp: 164.8-165.1 °C; yield: 45%; IR cm^{-1} : 3496-3359 (NH_2), 1680 (CO); ^1H NMR CDCl_3 (ppm): 1.44 (3H, t, $J = 8.0$ Hz, CH_3), 2.84 (3H, s, CH_3), 4.43 (2H, q, $J = 8.0$ Hz, CH_2), 7.32 (2H, s, NH_2), 7.43 (1H, t, $J = 7.2$ Hz, H-4'), 7.57 (t, 2H, $J = 7.2$ Hz, $\text{H}_{3'}$ and $\text{H}_{5'}$), 8.28 (d, 2H, $J = 7.2$ Hz, $\text{H}_{2'}$ and $\text{H}_{6'}$). ^{13}C NMR CDCl_3 (ppm): 14.3, 28.5, 61.1, 102.8, 121.4 (2 x C), 128.0, 128.1, 129.4 (2 x C), 136.6, 145.2, 149.5, 164.3, 168.6. Anal. Calcd for $\text{C}_{15}\text{H}_{15}\text{N}_5\text{O}_2$: C, 60.60; H, 5.09; N, 23.56. Found: C, 60.71; H, 4.89; N, 23.42.

Ethyl 7-amino-3-(4-methoxyphenyl)-5-methyl-3H-[1,2,3]triazolo[4,5-b]pyridine-6-carboxylate 37b: This compound was obtained by reaction of **36b**. Mp: 179.1-180.0 °C; yield: 62%; IR cm^{-1} : 3448-3333 (NH_2), 1688 (CO); ^1H NMR CDCl_3 (ppm): 1.44 (3H, t, $J = 8.0$ Hz, CH_3), 2.83 (3H, s, CH_3), 3.88 (3H, s, CH_3O), 4.46 (2H, q, $J = 8.0$ Hz, CH_2), 7.08 (2H, d, $J = 8.0$ Hz, $\text{H}_{2'}$ and $\text{H}_{6'}$), 7.28 (2H, bs, NH_2), 8.12 (2H, d, $J = 8.0$ Hz, $\text{H}_{3'}$ and $\text{H}_{5'}$). ^{13}C NMR CDCl_3 (ppm): 14.3, 28.5, 55.6, 61.0, 102.7, 114.6 (2 x C), 123.2 (2 x C), 127.8, 129.7, 145.0, 149.4, 159.3, 164.2, 168.7. Anal. Calcd for $\text{C}_{16}\text{H}_{17}\text{N}_5\text{O}_3$: C, 58.71; H, 5.23; N, 21.39. Found: C, 58.54; H, 5.30; N, 21.48.

General procedure for the synthesis of (7-amino-5-methyl-3-phenyl-3H-[1,2,3]triazolo[4,5-b]pyridin-6-yl)methanol 38a,b

To a suspension of lithium aluminium hydride (3.14 mmol) in anhydrous tetrahydrofuran (5 mL), the suitable ethyl 7-amino-5-methyl-3-phenyl-3H-[1,2,3]triazolo[4,5-b]pyridine-6-carboxylates **37a,b** (1.04 mmol) was gradually added at 0 °C and the suspension was stirred for 12 hours at room temperature. Then, the reaction mixture was poured onto crushed ice. The formed solid was filtered off, collected and recrystallized from diethyl ether.

(7-Amino-5-methyl-3-phenyl-3H-[1,2,3]triazolo[4,5-b]pyridin-6-yl)methanol 38a: This compound was obtained by reaction of **37a**. Mp: >350 °C; yield: 92%; IR cm^{-1} : 3460 (OH), 3421-3335 (NH_2); ^1H NMR DMSO-d_6 (ppm): 2.58 (3H, s, CH_3), 4.61 (2H, d, $J = 5.2$ Hz, CH_2), 4.84 (1H, t, $J = 5.2$ Hz, OH), 7.12 (2H, s, NH_2), 7.48 (1H, t, $J = 7.3$ Hz, H-4'), 7.65 (2H, t, $J = 7.3$ Hz, $\text{H}_{3'}$ and $\text{H}_{5'}$), 8.26 (2H, d, $J = 7.3$ Hz, $\text{H}_{2'}$ and $\text{H}_{6'}$). ^{13}C NMR DMSO-d_6 (ppm): 23.4, 55.5, 111.8, 120.8 (2 x C), 127.6, 127.9 (2 x C), 129.5, 136.6, 144.6, 145.8, 160.1. Anal. Calcd for $\text{C}_{13}\text{H}_{13}\text{N}_5\text{O}$: C, 61.17; H, 5.13; N, 27.43. Found: C, 61.23; H, 5.01; N, 27.54.

(7-Amino-3-(4-methoxyphenyl)-5-methyl-3H-[1,2,3]triazolo[4,5-b]pyridin-6-yl)methanol

38b: This compound was obtained by reaction of **37b**. Mp: >350 °C; yield: 58%; IR cm⁻¹: 3439 (OH), 3347-3238 (NH₂); ¹H NMR DMSO-d₆ (ppm): 2.56 (3H, s, CH₃), 3.85 (3H, s, CH₃O), 4.60 (2H, d, J = 5.1 Hz, CH₂), 4.82 (1H, t, J = 5.1 Hz, OH), 7.07 (2H, s, NH₂), 7.19 (2H, d, J = 7.1 Hz, H_{2'} and H_{6'}), 8.09 (2H, d, J = 7.1 Hz, H_{3'} and H_{5'}). ¹³C NMR DMSO-d₆ (ppm): 23.4, 55.4, 55.5, 111.6, 114.5 (2 x C), 122.7 (2 x C), 127.8, 129.6, 144.4, 145.7, 158.5, 159.9. Anal. Calcd for C₁₄H₁₅N₅O₂: C, 58.94; H, 5.30; N, 24.55. Found: C, 58.83; H, 5.42; N, 24.63.

General procedure for the synthesis of 7-amino-5-methyl-3-phenyl-3H-[1,2,3]triazolo[4,5-b]pyridine-6-carbaldehyde 39a,b

To a solution of (7-amino-5-methyl-3-phenyl-3H-[1,2,3]triazolo[4,5-b]pyridin-6-yl)methanol derivatives **38a,b** (1.16 mmol) in anhydrous dichloromethane (20 mL), Dess-Martin periodinane (1.39 mmol) was added under nitrogen atmosphere and at room temperature. The reaction mixture was stirred for 48 hours and then diethyl ether (20 mL) was added. The organic phase was washed with a 5% aqueous solution of sodium thiosulfate (20 mL) and a sodium bicarbonate saturated aqueous solution (20 mL). The reaction mixture was extracted with ethyl acetate, the organic phase was dried over sodium sulphate and the solvent was evaporated under reduced pressure. The obtained solid was used in the next step without further purifications.

General procedure for the synthesis of 5-methyl-2-phenyl[1,3]triazolo[5,4-h][1,6]naphthyridines 30a-n

To a suspension of 7-amino-5-methyl-2-phenyl[1,3]triazolo[5,4-b]pyridine-6-carbaldehyde derivatives **39a,b** (0.5 mmol) and potassium hydroxide (0.6 mmol) in anhydrous ethanol (20 mL), the proper substituted acetophenone (0.6 mmol) was added. To obtain derivatives **30a** and **30i**, *o*-aminoaldehydes **39a,b** (0.5 mmol) were added to a solution of potassium hydroxide (0.6 mmol) in acetone (20 mL). The reaction mixture was refluxed under nitrogen atmosphere for 12 hours. After cooling, the solvent was removed under reduced pressure and the residue was purified by silica gel chromatography, using dichloromethane: ethyl acetate (98:2) as eluent.

5,8-Dimethyl-3-phenyl-3H-[1,2,3]triazolo[4,5-h][1,6]naphthyridine 30a: This compound was obtained from reaction of **39a** with acetone. Mp: 190.0-190.5 °C; yield: 56%; ¹H NMR CDCl₃ (ppm): 2.94 (3H, s, CH₃), 3.08 (3H, s, CH₃), 7.50-7.67 (4H, m, ArH), 8.33-8.48 (3H, m, ArH).

^{13}C NMR CDCl_3 (ppm): 23.0, 28.2, 119.0, 122.1 (2 x C), 122.8, 128.4, 129.4 (2 x C), 133.1, 135.1, 136.6, 143.7, 143.8, 162.2, 165.4. Anal. Calcd for $\text{C}_{16}\text{H}_{13}\text{N}_5$: C, 69.80; H, 4.76; N, 25.44. Found: C, 69.64; H, 4.93; N, 25.52.

5-Methyl-3,8-diphenyl-3H-[1,2,3]triazolo[4,5-h][1,6]naphthyridine 30b: This compound was obtained by reaction of **39a** with acetophenone. Mp: 262.8-263.0 °C; yield: 45%; ^1H NMR CDCl_3 (ppm): 3.06 (3H, s, CH_3), 7.48-7.65 (6H, m, ArH), 8.05 (1H, d, $J = 8.8$ Hz, H_7), 8.31-8.40 (4H, m, ArH), 8.54 (1H, d, $J = 8.8$ Hz, H_6). ^{13}C NMR CDCl_3 (ppm): 23.1, 119.2, 119.5, 122.2 (2 x C), 128.2 (2 x C), 128.4, 128.9 (2 x C), 129.5 (2 x C), 130.7, 133.3, 135.9, 136.5, 137.9, 143.9, 144.1, 161.7, 162.2. Anal. Calcd for $\text{C}_{21}\text{H}_{15}\text{N}_5$: C, 74.76; H, 4.48; N, 20.76. Found: C, 74.83; H, 4.32; N, 20.65.

8-(4-Methoxyphenyl)-5-methyl-3-phenyl-3H-[1,2,3]triazolo[4,5-h][1,6]naphthyridine 30c: This compound was obtained by reaction of **39a** with 4-methoxy-acetophenone. Mp: 227.8-228.0 °C; yield: 53%; ^1H NMR CDCl_3 (ppm): 3.04 (3H, s, CH_3), 3.91 (3H, s, CH_3O), 7.06 (2H, d, $J = 6.9$ Hz, ArH), 7.45-7.66 (3H, m, ArH), 7.98 (1H, d, $J = 8.9$ Hz, H_7), 7.32-8.38 (4H, m, ArH), 8.48 (1H, d, $J = 8.9$ Hz, H_6). ^{13}C NMR CDCl_3 (ppm): 23.0, 55.5, 114.3 (2 x C), 118.5, 119.1, 122.2 (2 x C), 128.4, 129.4 (2 x C), 129.8 (2 x C), 130.4, 133.4, 135.6, 136.6, 144.0, 144.2, 161.2, 161.9, 162.1. Anal. Calcd for $\text{C}_{22}\text{H}_{17}\text{N}_5\text{O}$: C, 71.92; H, 4.66; N, 19.06. Found: C, 72.02; H, 4.54; N, 18.94.

8-(2-Methoxyphenyl)-5-methyl-3-phenyl-3H-[1,2,3]triazolo[4,5-h][1,6]naphthyridine 30d: This compound was obtained from reaction of **39a** with 2-methoxy-acetophenone. Mp: 247.7-248.0 °C; yield: 42%; ^1H NMR CDCl_3 (ppm): 3.11 (3H, s, CH_3), 3.93 (3H, s, CH_3O), 7.07 (1H, d, $J = 8.8$ Hz, H_7), 7.19 (1H, t, $J = 7.5$ Hz, ArH), 7.45-7.54 (2H, m, ArH), 7.59-7.67 (2H, m, ArH), 8.27-8.38 (4H, m, ArH), 8.54 (1H, d, $J = 8.8$ Hz, H_6). ^{13}C NMR CDCl_3 (ppm): 23.1, 55.7, 111.4, 119.3, 121.5, 122.2 (2 x C), 124.2, 128.0, 128.4, 129.4 (2 x C), 131.6, 132.7, 133.5, 134.3, 136.6, 143.8, 144.1, 157.6, 161.7, 162.1. Anal. Calcd for $\text{C}_{22}\text{H}_{17}\text{N}_5\text{O}$: C, 71.92; H, 4.66; N, 19.06. Found: C, 71.84; H, 4.82; N, 19.19.

8-(2-Fluorophenyl)-5-methyl-3-phenyl-3H-[1,2,3]triazolo[4,5-h][1,6]naphthyridine 30e: This compound was obtained from reaction of **39a** with 2-fluoro-acetophenone. Mp: 225.7-226.2 °C; yield: 43%; ^1H NMR CDCl_3 (ppm): 3.10 (3H, s, CH_3), 7.19-7.28 (1H, m, ArH), 7.36-7.41 (1H, m, ArH), 7.47- 7.54 (2H, m, ArH), 7.63 (2H, t, $J = 7.8$ Hz, ArH), 8.17 (1H, d, $J = 8.0, 2.0$ Hz, ArH), 8.34 (2H, d, $J = 7.4$ Hz, ArH), 8.51-8.59 (2H, m, ArH). The poor solubility of compound

30e prevented ^{13}C NMR spectra from being recorded. Anal. Calcd for $\text{C}_{21}\text{H}_{14}\text{FN}_5$: C, 70.98; H, 3.97; N, 19.71. Found: C, 70.85; H, 4.12; N, 19.86.

8-(2-Trifluoromethyl-phenyl)-5-methyl-3-phenyl-3H-[1,2,3]triazolo[4,5-

h][1,6]naphthyridine 30f: This compound was obtained from reaction of **39a** with 2-trifluoromethyl-acetophenone. Mp: 197.6-198.4 °C; yield: 45%; ^1H NMR CDCl_3 (ppm): 3.15 (3H, s, CH_3), 7.50 (1H, t, $J = 7.3$ Hz, ArH), 7.60-7.84 (7H, m, ArH), 8.34 (2H, d, $J = 7.9$ Hz, ArH), 8.64 (1H, d, $J = 8.6$ Hz, H_6). ^{13}C NMR CDCl_3 (ppm): 25.2, 119.8, 122.2 (2 x C), 123.1, 124.0, 125.0, 126.7, 126.7, 128.1, 128.4, 128.6, 129.5 (2 x C), 132.8, 135.0 (d, $J_{\text{CF}_3} = 246.0$ Hz) 246, 137.4, 148.0, 149.3, 160.7, 164.4. Anal. Calcd for $\text{C}_{22}\text{H}_{14}\text{F}_3\text{N}_5$: C, 65.18; H, 3.48; N, 17.28. Found: C, 65.01; H, 3.52; N, 17.43.

8-(2-Chlorophenyl)-5-methyl-3-phenyl-3H-[1,2,3]triazolo[4,5-h][1,6]naphthyridine 30g:

This compound was obtained from reaction of **39a** with 2-chloro-acetophenone. Mp: 269.4-270.2 °C; yield: 42%; ^1H NMR CDCl_3 (ppm): 3.16 (3H, s, CH_3), 7.36-7.84 (6H, m, ArH), 7.89-8.23 (2H, m, ArH), 8.36 (2H, d, $J = 6.8$ Hz, ArH), 8.65 (1H, d, $J = 7.7$ Hz, ArH). ^{13}C NMR CDCl_3 (ppm): 25.2, 119.4, 123.1 (2 x C), 124.1, 125.0, 127.0, 128.4, 129.1, 129.7 (2 x C), 130.2, 130.8, 131.9, 134.0, 137.1, 137.4, 149.3, 149.8, 160.7, 164.3. Anal. Calcd for $\text{C}_{21}\text{H}_{14}\text{ClN}_5$: C, 67.83; H, 3.80; N, 18.84. Found: C, 67.97; H, 3.62; N, 18.97.

5-Methyl-8-(2-nitrophenyl)-3-phenyl-3H-[1,2,3]triazolo[4,5-h][1,6]naphthyridine 30h:

This compound was obtained from reaction of **39a** with 2-nitro-acetophenone. Mp: 267.6-268.4 °C; yield: 47%; ^1H NMR DMSO-d_6 (ppm): 3.13 (3H, s, CH_3); 7.63 (1H, s, ArH); 7.75 (2H, s, ArH); 7.86 (1H, s, ArH); 7.98 (2H, s, ArH); 8.19-8.24 (4H, m, ArH); 9.06 (1H, d, $J = 8.6$ Hz, H_6). ^{13}C NMR DMSO-d_6 (ppm): 25.2, 121.7, 121.8, 123.1 (2 x C), 125.0, 126.1, 126.6, 128.4, 129.1, 129.3 (2 x C), 130.7, 132.1, 133.4, 137.4, 146.3, 149.3, 150.5, 160.7, 164.2. Anal. Calcd for $\text{C}_{21}\text{H}_{14}\text{N}_6\text{O}_2$: C, 65.96; H, 3.69; N, 21.98. Found: C, 65.70; H, 3.82; N, 21.80.

3-(4-Methoxyphenyl)-5,8-dimethyl-3H-[1,2,3]triazolo[4,5-h][1,6]naphthyridine 30i:

This compound was obtained from reaction of **39b** with acetone. Mp: 228.0-229.1 °C; yield: 44%; ^1H NMR CDCl_3 (ppm): 2.91 (3H, s, CH_3), 3.03 (3H, s, CH_3), 3.90 (3H, s, CH_3O), 7.11 (2H, d, $J = 9.0$ Hz, H_2' and H_6'), 7.48 (1H, d, $J = 8.6$ Hz, H_7), 8.18 (2H, d, $J = 9.0$ Hz, H_3' and H_5'), 8.40 (1H, d, $J = 8.6$ Hz, H_6). ^{13}C NMR CDCl_3 (ppm): 23.0, 25.7, 55.6, 114.5 (2 x C), 118.9, 122.7, 123.7 (2 x C), 129.7, 132.8, 135.0, 143.5, 143.7, 159.6, 161.9, 165.2. Anal. Calcd for $\text{C}_{17}\text{H}_{15}\text{N}_5\text{O}$: C, 66.87; H, 4.95; N, 22.94. Found: C, 66.79; H, 5.03; N, 23.11.

3-(4-Methoxyphenyl)-5-methyl-8-phenyl-3H-[1,2,3]triazolo[4,5-h][1,6]naphthyridine 30j:

This compound was obtained through reaction of **39b** with acetophenone. Mp: 276.0-277.4 °C; yield: 65%; ¹H NMR CDCl₃ (ppm): 3.09 (3H, s, CH₃), 3.92 (3H, s, CH₃O), 7.13 (2H, d, J=9.0 Hz, H₂' and H₆'), 7.55-7.58 (3H, m, ArH), 8.09-8.21 (3H, m, ArH), 8.38-8.43 (2H, m, ArH), 8.60 (1H, d, J = 8.8 Hz, H₆). ¹³C NMR CDCl₃ (ppm): 23.1, 55.6, 114.6 (2 x C), 119.2, 119.6, 124.0 (2 x C), 128.2 (2 x C), 129.0 (2 x C), 129.6, 130.7, 133.2, 135.9, 137.9, 144.3, 159.7, 161.8, 162.0 (2 x C). Anal. Calcd for C₂₂H₁₇N₅O: C, 71.92; H, 4.66; N, 19.06. Found: C, 71.98; H, 4.54; N, 19.18.

3,8-bis(4-Methoxyphenyl)-5-methyl-3H-[1,2,3]triazolo[4,5-h][1,6]naphthyridine 30k:

This compound was obtained from reaction of **39b** with 4-methoxy-acetophenone. Mp: 238.9-239.6 °C; yield: 60%; ¹H NMR CDCl₃ (ppm): 3.06 (3H, s, CH₃), 3.91 (3H, s, CH₃O), 3.92 (3H, s, CH₃O), 7.06-7.15 (4H, m, ArH), 8.04 (1H, d, J = 8.8 Hz, H₇), 8.18 (2H, d, J = 9.0 Hz, ArH), 8.40 (2H, d, J = 9.0 Hz, ArH), 8.53 (1H, d, J = 8.8 Hz, H₆). ¹³C NMR CDCl₃ (ppm): 23.1, 55.5, 55.6, 114.3 (2 x C), 114.6 (2 x C), 118.5, 119.2, 123.9 (2 x C), 129.7, 129.8 (2 x C), 130.5, 133.2, 135.7, 143.9, 144.3, 159.6, 161.2, 161.9. Anal. Calcd for C₂₃H₁₉N₅O₂: C, 69.51; H, 4.82; N, 17.62. Found: C, 69.45; H, 4.93; N, 17.78.

8-(2-Methoxyphenyl)-3-(4-methoxyphenyl)-5-methyl-3H-[1,2,3]triazolo[4,5-

h][1,6]naphthyridine 30l: This compound was obtained from reaction of **39b** with 2-methoxy-acetophenone. Mp: 215.1-215.4 °C; yield: 55%; ¹H NMR CDCl₃ (ppm): 3.09 (3H, s, CH₃), 3.91 (3H, s, CH₃O), 3.93 (3H, s, CH₃O), 7.04-7.23 (4H, m, ArH), 7.44-7.53 (1H, m, ArH), 8.17-8.31 (4H, m, ArH), 8.53 (1H, d, J = 8.8 Hz, H₆). ¹³C NMR CDCl₃ (ppm): 23.1, 55.6, 55.7, 111.4, 114.6 (2 x C), 119.3, 121.4, 123.9 (2 x C), 124.2, 128.0, 129.7, 131.5, 132.7, 133.2, 134.3, 143.7, 144.1, 157.6, 159.6, 161.6, 161.9. Anal. Calcd for C₂₃H₁₉N₅O₂: C, 69.51; H, 4.82; N, 17.62. Found: C, 69.62; H, 4.74; N, 17.43.

8-(2-Fluorophenyl)-3-(4-methoxyphenyl)-5-methyl-3H-[1,2,3]triazolo[4,5-

h][1,6]naphthyridine 30m: This compound was obtained from reaction of **39b** with 2-fluoro-acetophenone. Mp: 226.8-227.6 °C; yield: 61 %; ¹H NMR CDCl₃ (ppm): 3.12 (3H, s, CH₃), 3.94 (3H, s, CH₃O), 7.16 (2H, d, J = 9.0 Hz, ArH), 7.20-7.27 (1H, m, ArH), 7.41 (1H, t, J = 7.1 Hz, ArH), 7.49-7.57 (1H, m, ArH), 8.18-8.25 (3H, m, ArH), 8.51-8.67 (2H, m, ArH). The poor solubility of compound **30m** prevented ¹³C NMR spectra from being recorded. Anal. Calcd for C₂₂H₁₆FN₅O: C, 68.56; H, 4.18; N, 18.17. Found: C, 68.68; N, 4.07; N, 18.01.

8-(2-Trifluoromethyl-phenyl)-3-(4-methoxyphenyl)-5-methyl-3H-[1,2,3]triazolo[4,5-

h][1,6]naphthyridine 30n: This compound was obtained from reaction of **39b** with 2-trifluoromethyl-acetophenone. Mp: 238.2-239.0 °C; yield: 30%; ¹H NMR CDCl₃ (ppm): 3.13 (3H, s, CH₃), 3.92 (3H, s, CH₃O), 7.19-7.09 (2H, m, ArH), 7.90-7.57 (5H, m, ArH), 8.19 (2H, d, J = 9.0 Hz, ArH), 8.63 (1H, d, J = 8.5 Hz, H₆). The poor solubility of compound **30n** prevented ¹³C NMR spectra from being recorded. Anal. Calcd for C₂₃H₁₆F₃N₅O: C, 63.45; H, 3.70; N, 16.08. Found: C, 63.61; H, 3.57; N, 15.96.

General procedure for the synthesis of 5-methyl-3-phenyl-3,9-dihydro-8H-[1,2,3]triazolo[4,5-h][1,6]naphthyridin-8-one 32a,b

To a suspension of 7-amino-5-methyl-2-phenyl[1,3]triazolo[5,4-*b*]pyridine-6-carbaldehyde derivatives **39a,b** (0.35 mmol) and potassium carbonate (1.05 mmol) in anhydrous ethanol (10 mL), triethyl phosphonoacetate (1.05 mmol) was added under nitrogen atmosphere and at room temperature. The reaction mixture was refluxed for 12 hours. After cooling, the solvent was removed under reduced pressure and the solid was poured into water and ice. The suspension was filtered off and the precipitate was purified by silica gel chromatography, using dichloromethane: ethyl acetate (8:2) as eluent. The poor solubility of compounds **32a,b** prevented ¹³C NMR spectra from being recorded.

5-Methyl-3-phenyl-3,9-dihydro-8H-[1,2,3]triazolo[4,5-h][1,6]naphthyridin-8-one 32a: This compound was obtained by reaction of **39a**. Mp: 304.5-305.2 °C; yield: 60%; IR cm⁻¹: 3610 (NH), 1675 (CO); ¹H NMR DMSO-*d*₆ (ppm): 2.87 (3H, s, CH₃), 6.65 (1H, d, J = 10.0 Hz, H₇), 7.57-7.74 (3H, m, ArH and H₆), 8.18-8.32 (3H, m, ArH), 13.26 (1H, s, NH). Anal. Calcd for C₁₅H₁₁N₅O: C, 64.97; H, 4.00; N, 25.26. Found: C, 64.77; H, 4.15; N, 25.38.

3-(4-Methoxyphenyl)-5-methyl-3,9-dihydro-8H-[1,2,3]triazolo[4,5-h][1,6]naphthyridin-8-one 32b: This compound was obtained by reaction of **39b**. Mp: 279.1-280.0 °C; yield: 55%; IR cm⁻¹: 3421 (NH), 1669 (CO); ¹H NMR DMSO-*d*₆ (ppm): 2.80 (3H, s, CH₃), 3.87 (3H, s, CH₃O), 6.53 (1H, d, J = 10.0 Hz, H₇), 7.23 (2H, d, J = 8.0 Hz, H_{2'} and H_{6'}), 8.06 (3H, m, H_{3'}, H_{5'} and H₆), 13.24 (1H, s, NH). Anal. Calcd for C₁₆H₁₃N₅O₂: C, 62.53; H, 4.26; N, 22.79. Found: C, 62.65; H, 4.21; N, 22.65.

General procedure for the synthesis of *N*-(2-amino-2-oxoethyl)benzamides 42a,b

To a stirred solution of glycine hydrochloride (7.96 mmol) in anhydrous dichloromethane (30 mL), triethylamine (4.4 mL, 31.50 mmol) was added dropwise at 0 °C. The reaction mixture was stirred for 15 minutes at 0 °C and then a solution of the proper benzoyl chloride (8.76 mmol) in anhydrous dichloromethane (10 mL) was added at room temperature. After complete depletion of the starting material, the reaction mixture was washed with NaHCO₃ saturated aqueous solution and extracted with ethyl acetate. The organic layer was dried over sodium sulphate and the solvent was removed under reduced pressure to afford a solid which was recrystallized from dichloromethane.

***N*-(2-Amino-2-oxoethyl)benzamide 42a:** This compound was obtained by reaction with benzoyl chloride. Mp 185.1-186.3 °C; yield: 88%; IR cm⁻¹: 4144 (NH), 1730 (CO), 1680 (CO); ¹H NMR DMSO-*d*₆ (ppm): 3.83 (2H, d, J= 5.8 Hz, CH₂), 7.06 (1H, s, NH), 7.39 (1H, s, OH), 7.43-7.58 (3H, m, H₃, H₄ and H₅), 7.90 (2H, dd, J=7.8, 1.5 Hz, H₂ and H₆), 8.68 (1H, t, J= 5.8 Hz, NH). ¹³C NMR DMSO-*d*₆ (ppm): 42.4, 127.3 (2 x C), 128.2 (2 x C), 131.2, 134.1, 166.4, 171.0. Anal. Calcd for C₉H₁₀N₂O₂: C, 60.66; H, 5.66; N, 15.72. Found: C, 60.91; H, 5.84; N, 15.57.

***N*-(2-Amino-2-oxoethyl)-4-methoxybenzamide 42b:** This compound was obtained by reaction with 4-methoxy-benzoyl chloride. Mp 205.3 - 206.0 °C; yield: 82%; IR cm⁻¹: 3310 (NH), 3156 (NH), 1695 (CO), 1639 (CO); ¹H NMR DMSO-*d*₆ (ppm): 3.79-3.82 (5H, m, CH₂ and CH₃O), 6.98 - 7.03 (3H, m, H₃ and H₅, NH), 7.38 (1H, s, OH), 7.87 (2H, d, J=8.9 Hz, H₂ and H₆), 8.57 (1H, t, J=5.8 Hz, NH). ¹³C NMR DMSO-*d*₆ (ppm): 45.2, 55.3, 113.4 (2 x C), 126.3, 129.2 (2 x C), 161.5, 165.8, 171.2. Anal. Calcd for C₁₀H₁₂N₂O₃: C, 57.68; H, 5.81; N, 13.45. Found: C, 57.38; H, 5.93; N, 13.58.

General procedure for the synthesis of 2-phenyl-1,3-thiazol-5-amines 44a,b

To a solution of *N*-(2-amino-2-oxoethyl)benzamide derivatives **42a,b** (2.90 mmol) in anhydrous pyridine (10 mL) phosphorus pentasulfide (2.90 mmol) was added under nitrogen atmosphere at room temperature. The reaction mixture was heated under reflux for 6 hours. After cooling, NaHCO₃ saturated aqueous solution was added and the mixture was extracted with ethyl acetate. The organic layer was dried over sodium sulphate and the solvent was removed under reduced pressure. The residue was purified by silica gel chromatography using dichloromethane/ethyl

acetate (7:3) as eluent, allowing the isolation of 2-phenyl-1,3-thiazol-5-amine derivatives **44a,b** as well as the corresponding thioamides **43a,b**.

***N*-(2-Amino-2-thioxyethyl)benzamide 43a**: This compound was obtained by reaction of **42a**. Mp 112.6 - 113.0 °C; yield: 31%; IR cm^{-1} : 2255 (NH), 1297 (CS); ^1H NMR CDCl_3 (ppm): 4.49 (2H, d, $J=5.2$ Hz, CH_2), 7.43-7.60 (5H, m, H_3 , H_4 , H_5 , 2xNH), 7.85 (2H, dd, $J=8.1$, 1.5 Hz, H_2 and H_6), 8.39 (1H, bs, SH). The poor solubility of compound **43a** prevented ^{13}C NMR spectra from being recorded. Anal. Calcd for $\text{C}_9\text{H}_{10}\text{N}_2\text{OS}$: C, 55.65; H, 5.19; N, 14.42. Found: C, 55.87; H, 5.3; N, 14.19.

***N*-(2-Amino-2-thioxyethyl)-4-methoxybenzamide 43b**: This compound was obtained by reaction of **42b**. Mp 167.8-168.1 °C; yield: 31%; IR cm^{-1} : 2255 (NH), 1148 (CS); ^1H NMR CDCl_3 (ppm): 3.75 (2H, d, $J=6.0$ Hz, CH_2), 3.86 (3H, s, CH_3O), 6.95 (2H, d, $J=8.0$ Hz, H_3 and H_5), 7.17 (1H, s, NH), 7.71 (1H, s, NH), 7.82 (2H, d, $J=8.0$ Hz, H_2 and H_6), 8.25 (1H, s, SH). The poor solubility of compound **43b** prevented ^{13}C NMR spectra from being recorded. Anal. Calcd for $\text{C}_{10}\text{H}_{12}\text{N}_2\text{O}_2\text{S}$: C, 53.55; H, 5.39; N, 12.49. Found: C, 53.61; H, 5.51; N, 12.38.

2-Phenyl-1,3-thiazol-5-amines 44a: This compound was obtained by reaction of **42a**. Oil; yield: 30%; IR cm^{-1} : 3352 (NH_2); ^1H NMR CDCl_3 (ppm): 3.81 (2H, s, NH_2), 7.09 (1H, s, H_4), 7.29-7.44 (3H, m, H_3 , H_4 and H_5), 7.75-7.81 (2H, m, H_2 and H_6). ^{13}C NMR CDCl_3 (ppm): 125.5 (2 x C), 126.7, 128.8 (2 x C), 128.9, 134.1, 146.6, 156.3. Anal. Calcd for $\text{C}_9\text{H}_8\text{N}_2\text{S}$: C, 61.34; H, 4.58; N, 15.90. Found: C, 61.44; H, 4.67; N, 15.97.

2-(4-Methoxyphenyl)-1,3-thiazol-5-amine 44b: This compound was obtained by reaction of **42b**. Mp 89.5 - 89.8 °C; yield: 38%; IR cm^{-1} : 3346 (NH_2); ^1H NMR CDCl_3 (ppm): 3.76 (2H, s, NH_2), 3.83 (3H, s, CH_3O), 6.89 (2H, d, $J=8.8$, H_3 and H_5), 7.04 (1H, s, H_4), 7.71 (2H, d, $J=8.8$, H_2 and H_6). ^{13}C NMR CDCl_3 (ppm): 55.4, 114.2, 126.7, 127.0, 127.2, 145.7, 156.7, 160.4. Anal. Calcd for $\text{C}_{10}\text{H}_{10}\text{N}_2\text{OS}$: C, 58.23; H, 4.89; N, 13.58. Found: C, 58.13; H, 5.06; N, 13.28.

General procedure for the synthesis of 2-phenyl-1,3-thiazol-5-amines 44a,b from thioamides 43a,b

To a solution of *N*-(2-amino-2-thioxyethyl)benzamide derivatives **43a,b** (2.47 mmol) in anhydrous ethyl acetate (12 mL), phosphorous tribromide (1.97 mmol) was added under nitrogen atmosphere and the reaction mixture was stirred at room temperature for 20 minutes. Phosphorous tribromide (0.5 mmol) has been further added and the reaction mixture was stirred

for 48 hours. Ethyl acetate (50 mL) was added and the mixture was washed with NaHCO₃ saturated aqueous solution (25 mL) and extracted with ethyl acetate. The organic layer was dried over anhydrous sodium sulphate and the solvent was removed under reduced pressure. The crude was purified using silica gel chromatography with dichloromethane/ethyl acetate (9:1) as eluent.

2-Phenyl-1,3-thiazol-5-amines 44a: This product was also prepared according to this procedure in 67% yield.

2-(4-Methoxyphenyl)-1,3-thiazol-5-amine 44b: This product was also prepared according to this procedure in 55% yield.

General procedure for the synthesis of diethyl {(2-phenyl-1,3-thiazol-5-yl)amino}methylidene}propanedioates 45a,b

To a solution of the suitable 2-phenylthiazol-5-amine **44a,b** (1.12 mmol) in anhydrous ethanol (10 mL), diethylethoxymethylenemalonate (1.12 mmol) was added and the reaction mixture was refluxed for 12 hours. After cooling, the solvent was removed under reduced pressure and the residue was recrystallized from ethanol.

Diethyl {(2-phenyl-1,3-thiazol-5-yl)amino}methylidene}propanedioate 45a: This compound was obtained by reaction of **44a**. Mp 122.7 - 123.4 °C; yield: 50%; IR cm⁻¹: 3390 (NH), 1720 (CO); ¹H NMR CDCl₃ (ppm): 1.32 (3H, t, J=5.2 Hz, CH₃), 1.39 (3H, t, J=5.2 Hz, CH₃), 4.29 (4H, m, 2 x CH₂), 7.43-7.45 (3H, m, H_{3'}, H_{4'} and H_{5'}), 7.49 (1H, s, H₄), 7.84-7.88 (2H, m, H_{2'} and H_{6'}), 8.17 (1H, d, J=12.9 Hz, CH), 11.13 (1H, d, J=12.9 Hz, NH). ¹³C NMR CDCl₃ (ppm): 14.2, 14.4, 60.4, 60.8, 95.4, 126.0 (2 x C), 129.1 (2 x C), 130.2, 130.9, 133.2, 140.2, 154.5, 161.1, 164.9, 168.9. Anal. Calcd for C₁₇H₁₈N₂O₄S: C, 58.94; H, 5.24; N, 8.09. Found: C, 58.85; H, 5.15; N, 8.15.

Diethyl {(2-(4-methoxyphenyl)-1,3-thiazol-5-yl)amino}methylidene}propanedioate 45b: This compound was obtained by reaction of **44b**. Mp 101.3 - 101.8 °C; yield: 59%; IR cm⁻¹: 3392 (NH), 1610 (CO); ¹H NMR CDCl₃ (ppm): 1.32 (3H, t, J=7.0 Hz, CH₃), 1.38 (3H, t, J=7.0, CH₃), 3.85 (3H, s, CH₃O), 4.18- 4.39 (4H, m, 2 x CH₂), 6.94 (2H, d, J=8.8 Hz, H_{3'} and H_{5'}), 7.43 (1H, s, H₄), 7.78 (2H, d, J=8.8 Hz, H_{2'} and H_{6'}), 8.15 (1H, d, J=12.8 Hz, CH), 11.07 (1H, d, J=12.8 Hz, NH). ¹³C NMR CDCl₃ (ppm): 14.3, 14.4, 55.4, 60.3, 60.8, 95.2, 114.4 (2 x C), 126.1, 127.6 (2 x C), 130.8 (2 x C), 139.2, 154.7, 161.3, 164.9, 169.1. Anal. Calcd for C₁₈H₂₀N₂O₅S: C, 57.43; H, 5.36; N, 7.44. Found: C, 57.13; H, 5.23; N, 7.19.

General procedure for the synthesis of ethyl 7-chloro-2-phenyl[1,3]thiazolo[5,4- b]pyridine-6-carboxylates 46a,b

The proper diethyl {[2-phenyl-1,3-thiazol-5-yl]amino}methylidene}propanedioate **45a,b** (0.89 mmol) was dissolved in phosphorous oxychloride (48 mmol) and the reaction mixture was refluxed for 12 hours. After cooling, the excess of phosphoryl chloride was removed under reduced pressure. The residue was poured in water and ice and neutralized with NaHCO₃ saturated aqueous solution. The suspension was filtered off and the precipitate was dried to afford the title compounds **46a,b**.

Ethyl 7-chloro-2-phenyl[1,3]thiazolo[5,4-b]pyridine-6-carboxylate 46a: This compound was obtained by reaction of **45a**. Mp 131.2-131.6 °C; yield: 55%; IR cm⁻¹: 1727 (CO); ¹H NMR CDCl₃ (ppm): 1.47 (3H, t, J=7.3 Hz, CH₃), 4.50 (2H, q, J=7.3 Hz, CH₂), 7.61-7.48 (3H, bs, H_{3'}, H_{4'} and H_{5'}), 8.15 (2H, bs, H_{2'} and H_{6'}), 8.98 (1H, s, H₅). ¹³C NMR CDCl₃ (ppm): 14.3, 62.2, 124.0, 127.9 (2 x C), 129.3 (2 x C), 132.3, 132.8, 137.6, 145.5, 148.7, 161.2, 164.1, 170.2. Anal. Calcd for C₁₅H₁₁ClN₂O₂S: C, 56.52; H, 3.48; N, 8.79. Found: C, 56.73; H, 3.59; N, 8.68.

Ethyl 7-chloro-2-(4-methoxyphenyl)[1,3]thiazolo[5,4-b]pyridine-6-carboxylate 46b: This compound was obtained by reaction of **45b**. Mp 138.7 - 138.9 °C; yield : 77%; IR cm⁻¹: 1726 (CO); ¹H NMR CDCl₃ (ppm): 1.46 (3H, t, J=7.2 Hz, CH₃), 3.90 (3H, s, CH₃O), 4.49 (2H, q, J=7.2 Hz, CH₂), 7.00 (2H, d, J=8.8 Hz, H_{3'} and H_{5'}), 8.08 (2H, d, J=8.8 Hz, H_{2'} and H_{6'}), 8.93 (1H, s, H₅). ¹³C NMR CDCl₃ (ppm): 14.3, 55.6, 62.1, 114.6 (2 x C), 123.9, 125.6, 129.7 (2 x C), 130.9, 145.6, 148.2, 161.3, 163.0, 164.2, 169.9. Anal. Calcd for C₁₆H₁₃ClN₂O₃S: C, 55.09; H, 3.76; N, 8.03. Found: C, 55.21; H, 3.64; N, 8.24.

General procedure for the synthesis of ethyl 7-azido-2-phenyl[1,3]thiazolo[5,4-b]pyridine-6-carboxylates 47a,b

A suspension of the suitable ethyl 7-chloro-2-phenyl[1,3]thiazolo[5,4-b]pyridine-6-carboxylate **46a,b** (0.69 mmol) in N,N-dimethylformamide (1.5 mL) and sodium azide (0.69 mmol) was added at room temperature under nitrogen atmosphere. The reaction mixture was stirred overnight and was subsequently poured in water and ice. The suspension was filtered off and the precipitate was dried to afford the desired products.

Ethyl 7-azido-2-phenyl[1,3]thiazolo[5,4-b]pyridine-6-carboxylate 47a: This compound was obtained by reaction of **46a**. Mp 159.3 -160.5 °C; yield : 52%; IR cm⁻¹: 2120 (N₃), 1630 (CO);

¹H NMR CDCl₃ (ppm): 1.44 (3H, t, J=7.2 Hz, CH₃), 4.44 (2H, q, J=7.2 Hz, CH₂), 7.58-7.42 (3H, m, H_{3'}, H_{4'} and H_{5'}), 8.03 - 8.07 (2H, m, H_{2'} and H_{6'}), 8.90 (1H, s, H₅). ¹³C NMR CDCl₃ (ppm): 14.3, 61.7, 115.0, 127.5 (2 x C), 129.3 (2 x C), 132.0, 132.7, 140.6, 141.4, 149.7, 161.9, 164.0, 167.5. Anal. Calcd for C₁₅H₁₁N₅O₂S: C, 55.38; H, 3.41; N, 21.53. Found: C, 55.47; H, 3.52; N, 21.40.

Ethyl 7-azido-2-(4-methoxyphenyl)[1,3]thiazolo[5,4-b]pyridine-6-carboxylate 47b: This compound was obtained by reaction of **46b**. Mp 111.8 - 112.7 °C; yield: 63%; IR cm⁻¹: 2117 (N₃), 1604 (CO); ¹H NMR CDCl₃ (ppm): 1.44 (3H, t, J=7.2 Hz, CH₃), 3.90 (3H, s, CH₃O), 4.43 (2H, q, J=7.2 Hz, CH₂), 7.03 (2H, d, J=8.8 Hz, H_{3'} and H_{5'}), 7.99 (2H, d, J=8.8 Hz, H_{2'} and H_{6'}), 8.86 (1H, s, H₅). ¹³C NMR CDCl₃ (ppm): 14.3, 55.6, 66.7, 114.6 (2 x C), 115.1, 125.6, 129.7 (2 x C), 140.7, 140.8, 149.1, 161.9, 162.8, 164.1, 167.3. Anal. Calcd for C₁₆H₁₃N₅O₃S: C, 54.08; H, 3.69; N, 19.71. Found: C, 54.37; H, 3.59; N, 20.01.

General procedure for the synthesis of (7-amino-2-phenyl[1,3]thiazolo[5,4-b]pyridin-6-yl)methanols 48a,b

To a suspension of lithium aluminium hydride (2.11 mmol) in tetrahydrofuran (10 mL), the suitable ethyl 7-azido-2-phenyl[1,3]thiazolo[5,4-b]pyridine-6-carboxylate **47a,b** (0.64 mmol) was added at 0 °C and the suspension was stirred overnight at room temperature. The reaction mixture was poured in water and ice and the suspension thus obtained was filtered off. The solid was recrystallized from diethyl ether.

[7-Amino-2-phenyl[1,3]thiazolo[5,4-b]pyridin-6-yl)methanol 48a: This compound was obtained by reaction of **47a**. Mp 180.8-180.9 °C; yield: 52%; IR cm⁻¹: 3590 (OH), 3450, 3358 (NH₂); ¹H NMR CDCl₃ (ppm): 4.56 (2H, d, J=5.2 Hz, CH₂), 5.17 (1H, t, J=5.2 Hz, OH), 6.58 (2H, bs, NH₂), 7.53-7.63 (3H, m, H_{3'}, H_{4'} and H_{5'}), 8.04-8.15 (3H, m, H₅, H_{2'} and H_{6'}). ¹³C NMR CDCl₃ (ppm): 61.5, 104.5, 127.1 (2 x C), 129.1 (2 x C), 130.9, 132.2, 132.4, 146.9, 149.5, 158.0, 167.8. Anal. Calcd for C₁₃H₁₁N₃OS: C, 60.68; H, 4.31; N, 16.33. Found: C, 60.84; H, 4.47; N, 16.45.

[7-Amino-2-(4-methoxyphenyl)[1,3]thiazolo[5,4-b]pyridin-6-yl)methanol 48b: This compound was obtained by reaction of **47b**. Mp 179.9 - 180.1 °C; yield: 63%; IR cm⁻¹: 3480 (OH), 3320, 3240 (NH₂); ¹H NMR DMSO-*d*₆ (ppm): 3.85 (CH₃O), 4.55 (2H, bs, CH₂), 5.14 (1H, bs, OH), 6.46 (2H, d, J=8.0 Hz, NH₂), 7.12 (2H, d, J=8.0 Hz, H_{3'} and H_{5'}), 8.03 (3H, s, H_{2'}

and H₆, H₅). ¹³C NMR DMSO-*d*₆ (ppm): 55.5, 58.3, 114.6 (2 x C), 117.0, 126.0, 128.4 (2 x C), 134.4, 146.0, 146.8, 156.4, 161.5, 161.6. Anal. Calcd for C₁₄H₁₃N₃O₂S: C, 58.52; H, 4.56; N, 14.62. Found: C, 58.32; H, 4.70; N, 14.50.

General procedure for the synthesis of 7-amino-2-phenyl[1,3]thiazolo[5,4-*b*]pyridine-6-carbaldehydes 49a,b

To a solution of (7-amino-2-phenyl[1,3]thiazolo[5,4-*b*]pyridin-6-yl)methanol derivative **48a,b** (1.74 mmol) in anhydrous dichloromethane (20 mL), Dess-Martin periodinane (2.44 mmol) was added under nitrogen atmosphere and at room temperature. The reaction mixture was stirred for 48 hours and then diethyl ether (20 mL) was added. The organic phase was washed with a 5% solution of sodium thiosulfate (20 mL) and a NaHCO₃ saturated aqueous solution (20 mL). The reaction mixture was extracted with ethyl acetate and the organic phase was dried over sodium sulphate and evaporated in vacuo. The obtained solid was used for the next step without further purifications.

General procedure for the synthesis of 2-phenyl[1,3]thiazolo[5,4-*h*][1,6]naphthyridines 31a-*m*

To the suspension of 7-amino-2-phenylthiazolo[5,4-*b*]pyridine-6-carbaldehyde derivative **49a-b** (0.5 mmol) and potassium hydroxide (0.6 mmol) in anhydrous ethanol (20 mL), the proper substituted acetophenone (0.5 mmol) was added. To obtain derivatives **31a** and **31i**, *o*-aminoaldehydes **49a-b** (0.5 mmol) were added to a solution of potassium hydroxide (0.6 mmol) in acetone (20 mL) under nitrogen atmosphere. The reaction mixture was heated for 12 hours. After cooling, the solvent was removed under reduced pressure and the residue was purified by silica gel chromatography using dichloromethane: ethyl acetate as eluant or by crystallization.

8-Methyl-2-phenyl[1,3]thiazolo[5,4-*h*][1,6]naphthyridine 31a: This compound was obtained through reaction of **49a** with acetone and it was purified by silica gel chromatography using dichloromethane: ethyl acetate (95:5) as eluant. Mp 181.3 - 182.5 °C; yield: 22%; ¹H NMR CDCl₃ (ppm): 2.96 (3H, s, CH₃), 7.57-7.48 (4H, m, ArH), 8.36- 8.24 (3H, m, ArH), 9.12 (1H, s, H₅). ¹³C NMR CDCl₃ (ppm): 26.3, 120.7, 123.4, 127.9 (2 x C), 128.9 (2 x C), 131.2, 133.4, 136.3, 142.3, 144.8, 150.0, 155.6, 165.3, 168.2. Anal. Calcd for C₁₆H₁₁N₃S: C, 69.29; H, 4.00; N, 15.15. Found: C, 69.40; H, 4.15; N, 14.83.

2,8-Diphenyl[1,3]thiazolo[5,4-h][1,6]naphthyridine 31b: This compound was obtained through reaction of **49a** with acetophenone and was crystallized with ethanol and diethyl ether. Mp 194.8 -195.1 °C; yield: 44%; ¹H NMR CDCl₃ (ppm): 7.48- 7.61 (6H, m, ArH), 8.11 (1H, d, J=8.0 Hz, H₇), 8.24-8.33 (2H, m, ArH), 8.34-8.41 (2H, m, ArH), 8.47 (1H, d, J=8.0 Hz, H₆), 9.15 (1H, s, H₅). ¹³C NMR CDCl₃ (ppm): 120.0, 121.8, 127.8 (2 x C), 128.3 (2 x C), 128.9 (2 x C), 129.0 (2 x C), 130.6, 131.3, 133.6, 137.1, 138.5, 142.7, 145.1, 149.9, 155.9, 161.9, 168.1. Anal. Calcd for C₂₁H₁₃N₃S: C, 74.31; H, 3.86; N, 12.38. Found: C, 74.01; H, 4.00; N, 12.65.

8-(4-Methoxyphenyl)-2-phenyl[1,3]thiazolo[5,4-h][1,6]naphthyridine 31c: This compound was obtained through reaction of **49a** with 4-methoxy acetophenone and was crystallized with diethyl ether. Mp >350 °C; yield: 45%; ¹H NMR CDCl₃ (ppm): 3.93 (3H, s, CH₃O), 7.10 (2H, d, J=8.0 Hz, ArH), 7.50-7.58 (3H, m, ArH), 8.08 (1H, d, J= 8.0 Hz, H₇), 8.25 - 8.34 (2H, m, ArH), 8.38 (2H, d, J=10.0 Hz, ArH), 8.44 (1H, d, J=8.0 Hz, H₆), 9.13 (1H, s, H₅). ¹³C NMR CDCl₃ (ppm): 55.5, 114.3 (2 x C), 119.4, 121.0, 127.8 (2 x C), 129.0 (2 x C), 129.9 (2 x C), 131.0, 131.3, 133.6, 136.9, 145.2, 149.9, 155.9, 161.3, 161.9 (2 x C), 167.9. Anal. Calcd for C₂₂H₁₅N₃OS: C, 71.52; H, 4.09; N, 11.37. Found: C, 71.55; H, 4.02; N, 11.25.

8-(2-Methoxyphenyl)-2-phenyl[1,3]thiazolo[5,4-h][1,6]naphthyridine 31d: This compound was obtained through reaction of **49a** with 2-methoxy acetophenone and was crystallized with diethyl ether. Mp 158.3 -159.6 °C; yield: 20%; ¹H NMR CDCl₃ (ppm): 3.91 (3H, s, CH₃O), 7.05 (1H, d, J=8.0 Hz, ArH), 7.2 (1H, t, J=8.0 Hz, ArH), 7.50 - 7.52 (4H, m, ArH), 8.30 - 8.41 (4H, m, ArH), 8.39 (1H, d, J=8.0 Hz, H₆), 9.16 (1H, s, H₅). ¹³C NMR CDCl₃ (ppm): 55.7, 111.4, 121.0, 121.4, 124.9, 127.8 (2 x C), 128.7, 128.9 (2 x C), 131.2, 131.4, 132.6, 133.6, 135.2, 142.8, 145.1, 149.9, 155.5, 158.0, 161.8, 167.9. Anal. Calcd for C₂₂H₁₅N₃OS: C, 71.52; H, 4.09; N, 11.37. Found: C, 71.47; H, 3.96; N, 11.52.

8-(2-Fluorophenyl)-2-phenyl[1,3]thiazolo[5,4-h][1,6]naphthyridine 31e: This compound was obtained through reaction of **49a** with 2-fluoro acetophenone and it was purified by silica gel chromatography using dichloromethane: ethyl acetate (95:5) as eluent. Mp 200.2-201.0 °C; yield: 43%; ¹H NMR CDCl₃ (ppm): 7.17-7.30 (1H, m, ArH), 7.39 (1H, t, J = 7.5 Hz, ArH), 7.46-7.58 (4H, m, ArH), 8.16 (1H, dd, J = 8.6, 2.1 Hz, ArH), 8.24-8.33 (2H, m, ArH), 8.42-8.48 (2H, m, ArH), 9.18 (1H, s, H₅). ¹³C NMR CDCl₃ (ppm): 116.3 (d, J_{C3''-F} = 22.5 Hz), 121.12, 123.8 (d, J_{C6''-F} = 10.1 Hz), 124.9, 127.0 (d, J_{C1''-F} = 12.1 Hz), 127.8 (2 x C), 129.0 (2 x C), 131.3, 132.0 (d, J_{C4''-F} = 9.0 Hz), 132.5, 133.56, 136.45, 142.67, 145.0, 150.0, 157.2 (d, J_{C2''-F} = 289.9

Hz), 159.89, 168.23. Anal. Calcd for C₂₁H₁₂FN₃S: C, 70.57; H, 3.38; N, 11.76. Found: C, 70.45; H, 3.52; N, 11.91.

2-Phenyl-8-[2-(trifluoromethyl)phenyl][1,3]thiazolo[5,4-h][1,6]naphthyridine 31f: This compound was obtained through reaction of **49a** with 2-trifluoromethyl acetophenone and it was purified by silica gel chromatography using dichloromethane: ethyl acetate (9:1) as eluent. Mp 213.2-214.4 °C; yield: 38%; ¹H NMR CDCl₃ (ppm): 7.46-7.54 (3H, m, ArH), 7.64 (1H, t, J = 7.7 Hz, ArH), 7.72 (1H, t, J = 7.5, ArH), 7.80-7.83 (3H, m, ArH), 8.22-8.30 (2H, m, ArH), 8.50 (1H, d, J = 8.5 Hz, H₆), 9.24 (1H, s, H₅). The poor solubility of compound **31f** prevented ¹³C NMR spectra from being recorded. Anal. Calcd for C₂₂H₁₂F₃N₃S: C, 64.86; H, 2.97; N, 10.31. Found: C, 64.99; H, 2.73; N, 10.19.

8-(2-Chlorophenyl)-2-phenyl[1,3]thiazolo[5,4-h][1,6]naphthyridine 31g: This compound was obtained through reaction of **49a** with 2-chloro acetophenone and it was purified by silica gel chromatography using dichloromethane: ethyl acetate (93:7) as eluant. Mp 219.4-220.2 °C; yield: 51%; ¹H NMR CDCl₃ (ppm): 7.41-7.57 (6H, m, ArH), 7.93-7.99 (1H, m, ArH), 8.06 (1H, d, J = 8.5 Hz, H₇), 8.24-8.31 (2H, m, ArH), 8.49 (1H, d, J = 8.5, H₆), 9.23 (1H, s, H₅). The poor solubility of compound **31g** prevented ¹³C NMR spectra from being recorded. Anal. Calcd for C₂₁H₁₂ClN₃S: C, 67.47; H, 3.24; N, 11.24. Found: C, 67.65; H, 3.07; N, 11.51.

8-(2-Nitrophenyl)-2-phenyl[1,3]thiazolo[5,4-h][1,6]naphthyridine 31h: This compound was obtained through reaction of **49a** with 2-nitro acetophenone and it was purified by silica gel chromatography using dichloromethane: ethyl acetate (9:1) as eluant. Mp 269.0-270.2 °C; yield: 62%; ¹H NMR DMSO-*d*₆ (ppm): 7.59-7.66 (3H, m, ArH), 7.83-7.86 (1H, m, ArH), 7.92-7.98 (2H, m, ArH), 8.10-8.19 (4H, m, ArH), 8.92 (1H, d, J = 8.0 Hz, H₆), 9.47 (1H, s, H₅). The poor solubility of compound **31h** prevented ¹³C NMR spectra from being recorded. Anal. Calcd for C₂₁H₁₂N₄O₂S: C, 65.61; H, 3.15; N, 14.57. Found: C, 65.78; H, 3.01; N, 14.74.

2-(4-Methoxyphenyl)-8-methyl[1,3]thiazolo[5,4-h][1,6]naphthyridine 31i: This compound was obtained by reaction of **49b** with acetone and it was purified by silica gel chromatography using dichloromethane: ethyl acetate (95:5) as eluant. Mp 191.0-191.7 °C; yield: 25%; ¹H NMR CDCl₃ (ppm): 2.95 (3H, s, CH₃), 3.90 (3H, s, CH₃O), 7.02 (2H, d, J=7.4 Hz, H_{3'} and H_{5'}), 7.51 (1H, d, J=10.0 Hz, H₇), 8.22 (2H, d, J=7.4 Hz, H_{2'} and H_{6'}), 8.30 (1H, d, J=10.0 Hz, H₆), 9.07 (1H, s, H₅). ¹³C NMR CDCl₃ (ppm): 26.3, 55.7, 114.2 (2 x C), 120.6, 123.2, 126.3, 129.5 (2 x C), 136.2, 142.2, 144.5, 149.4, 155.4, 162.2, 165.0, 168.1. Anal. Calcd for C₁₇H₁₃N₃OS: C, 66.43; H, 4.26; N, 13.67. Found: C, 66.57; H, 4.12; N, 16.79.

2-(4-Methoxyphenyl)-8-phenyl[1,3]thiazolo[5,4-h][1,6]naphthyridine 31j: This compound was obtained by reaction of **49b** with acetophenone and it was purified by silica gel chromatography using dichloromethane: ethyl acetate (95:5) as eluant. Mp 185.5 -186.3 °C; yield: 21%; ¹H NMR CDCl₃ (ppm): 3.90 (3H, s, CH₃O), 7.04 (2H, d, J=7.9 Hz, ArH), 7.52-7.61 (3H, m, ArH), 8.10 (1H, d, J=8.0 Hz, H₇), 8.24 (2H, d, J=7.9 Hz, ArH), 8.37 (2H, dd, J=7.9, 2.0 Hz, ArH), 8.46 (1H, d, J=8.0 Hz, H₆), 9.11 (1H, s, H₅). ¹³C NMR CDCl₃ (ppm): 55.5, 114.3 (2 x C), 119.9, 121.2, 126.4, 128.3 (2 x C), 128.9 (2 x C), 129.4 (2 x C), 130.5, 137.1, 138.5, 142.8, 144.8, 149.4, 155.7, 161.7, 162.2, 168.0. Anal. Calcd for C₂₂H₁₅N₃OS: C, 71.52; H, 4.09; N, 11.37. Found: C, 71.34; H, 4.28; N, 11.21.

2,8-bis(4-Methoxyphenyl)[1,3]thiazolo[5,4-h][1,6]naphthyridine 31k: This compound was obtained by reaction of **49b** with 4-methoxy acetophenone and it was crystallized from ethanol. Mp 227.7 - 228.3 °C; yield: 40%; ¹H NMR CDCl₃ (ppm): 3.90 (3H, s, CH₃O), 3.92 (3H, s, CH₃O), 6.99 - 7.14 (4H, m, ArH), 8.06 (1H, d, J=8.0 Hz, H₇), 8.25 (2H, d, J=10.0 Hz, ArH), 8.32 - 8.46 (3H, m, ArH), 9.09 (1H, s, H₅). ¹³C NMR CDCl₃ (ppm): 55.5, 55.6, 114.2 (2 x C), 114.3 (2 x C), 119.3, 120.9, 126.5, 129.4 (2 x C), 129.8 (2 x C), 131.0, 136.8, 142.7, 144.8, 149.3, 155.7, 161.2, 161.8, 162.2, 167.8. Anal. Calcd for C₂₃H₁₇N₃O₂S: C, 69.15; H, 4.29; N, 10.52. Found: C, 69.30; H, 4.32; N, 10.61.

8-(2-Methoxyphenyl)-2-(4-methoxyphenyl)[1,3]thiazolo[5,4-h][1,6]naphthyridine 31l: This compound was obtained by reaction of **49b** with 2-methoxy acetophenone and it was purified by silica gel chromatography using dichloromethane: ethyl acetate (95:5) as eluant. Mp 161.5 - 162.3 °C; yield: 33%; ¹H NMR CDCl₃ (ppm): 3.89 (3H, s, CH₃O), 3.90 (3H, s, CH₃O), 7.08-6.69 (3H, m, ArH), 7.19 (1H, d, J= 8.0 Hz, H₇), 7.48 (1H, dd, J= 6.0, 2.0 Hz, ArH), 8.20 (2H, d, J=8.0 Hz, ArH), 8.22 (2H, d, J=8.0 Hz, ArH), 8.37 (1H, d, J=8.0 Hz, H₆), 9.12 (1H, s, H₅). ¹³C NMR CDCl₃ (ppm): 55.5, 55.7, 111.4, 114.3 (2 x C), 121.0, 121.0, 124.8, 126.5, 128.8, 129.4 (2 x C), 131.5, 132.5, 135.1, 142.9, 144.9, 149.4, 155.3, 157.6, 161.7, 162.2, 167.8. Anal. Calcd for C₂₃H₁₇N₃O₂S: C, 69.15; H, 4.29; N, 10.52. Found: C, 68.98; H, 4.13; N, 10.65.

8-(2-Fluorophenyl)-2-(4-methoxyphenyl)[1,3]thiazolo[5,4-h][1,6]naphthyridine 31m: This compound was obtained by reaction of **49b** with 2-fluoro acetophenone and it was purified by silica gel chromatography using dichloromethane: ethyl acetate (95:5) as eluant. Mp 198.2-199.0 °C; yield: 28%; ¹H NMR CDCl₃ (ppm): 3.92 (3H, s, CH₃O), 7.04 (2H, d, J = 8.4 Hz, ArH), 7.21-7.25 (1H, m, ArH), 7.40 (1H, t, J = 7.5 Hz, ArH), 7.49-7.56 (1H, m, ArH), 8.17 (1H, d, J = 8.6 Hz, ArH), 8.24 (2H, d, J = 8.4 Hz, ArH), 8.42-8.50 (2H, m, ArH), 9.17 (1H, s, H₅). ¹³C NMR

CDCl₃ (ppm): 55.5, 114.3 (2 x C), 116.2 (d, J_{C3''-F} = 22.5 Hz), 121.2, 123.7 (d, J_{C6''-F} = 9.8 Hz), 124.9 (d, J_{C5''-F} = 3.0 Hz), 126.5, 127.1 (d, J_{C1''-F} = 14.3 Hz), 129.5 (2 x C), 131.9 (d, J_{C4''-F} = 8.2 Hz), 132.5, 136.4, 142.8, 144.9, 149.4, 155.6, 160.4 (d, J_{C2''-F} = 273.8 Hz), 160.6, 162.8, 168.2. Anal. Calcd for C₂₂H₁₄FN₃OS: C, 68.20; H, 3.64; N, 10.85. Found: C, 68.32; H, 3.46; N, 10.70.

General procedure for the synthesis of 2-phenyl[1,3]thiazolo[5,4-h][1,6]naphthyridin-8(9H)-ones 33a,b

To a suspension of the proper 7-amino-2-phenyl[1,3]thiazolo[5,4-*b*]pyridine-6-carbaldehyde derivative **49a,b** (0.42 mmol) and potassium carbonate (0.84 mmol) in anhydrous ethanol (10 mL), triethyl phosphonoacetate (1.26 mmol) was added at room temperature, under nitrogen atmosphere. The reaction mixture was heated under reflux for 12 hours. After cooling, the solvent was removed under reduced pressure and the solid was poured into water and ice. The suspension was filtered off, dried and purified by silica gel chromatography using dichloromethane: ethyl acetate (8:2) as eluent.

2-Phenyl[1,3]thiazolo[5,4-h][1,6]naphthyridin-8(9H)-one 33a: This compound was obtained by reaction of **49a**. Mp 291.0 - 292.3 °C; yield: 30%; IR cm⁻¹: 1670 (CO); ¹H NMR CDCl₃ (ppm): 6.78 (1H, d, J=9.8 Hz, H₆), 7.60-7.48 (3H, m, H₃, H₄ and H₅), 7.93 (1H, d, J=9.8 Hz, H₇), 8.16-8.03 (2H, m, H₂ and H_{6'}), 8.72 (1H, s, H₅), 9.95 (1H, s, NH). ¹³C NMR CDCl₃ (ppm): 113.4, 123.1, 127.5 (2 x C), 129.3 (2 x C), 131.9, 133.0, 133.6, 137.0, 138.7, 146.9, 157.7, 161.7, 168.6. Anal. Calcd for C₁₅H₉N₃OS: C, 64.50; H, 3.25; N, 15.04. Found: C, 64.66; H, 3.35; N, 15.21.

2-(4-Methoxyphenyl)[1,3]thiazolo[5,4-h][1,6]naphthyridin-8(9H)-one 33b: This compound was obtained by reaction of **49b**. Mp >350 °C; yield: 46%; IR cm⁻¹: 1689 (CO); ¹H NMR CDCl₃ (ppm): 3.91 (3H, s, CH₃O), 6.76 (1H, d, J=10.0 Hz, H₆), 7.04 (2H, d, J=8.0 Hz, H₃ and H₅), 7.92 (1H, d, J=10.0 Hz, H₇), 8.03 (2H, d, J=8.0 Hz, H₂ and H_{6'}), 8.67 (1H, s, H₅). ¹³C NMR CDCl₃ (ppm): 55.6, 113.4, 114.6 (2 x C), 122.9, 125.7, 129.1 (2 x C), 133.6, 136.6, 138.7, 146.4, 157.5, 162.6, 168.4. Anal. Calcd for C₁₆H₁₁N₃O₂S: C, 62.12; H, 3.58; N, 13.58. Found: C, 62.24; H, 3.63; N, 13.20.

General procedure for the synthesis of *N*-(2-phenyl-1,3-thiazol-5-yl)benzamides 50a-r

To a solution of 2-phenyl-1,3-thiazol-5-amine **44a** (0.57 mmol) in acetonitrile (4 mL), the proper benzoyl chloride (1.14 mmol) and 4-dimethylaminopyridine (0.57 mmol) were added and the desired product was obtained through a Microwave-Assisted Organic Synthesis (MAOS technique), irradiating the reaction for 40 minutes (2 cycles of 20') with a power of 150 W and a temperature of 120 °C. After cooling, the reaction mixture was poured onto crushed ice and extracted with ethyl acetate. The organic layer was dried over sodium sulphate and the solvent was removed under reduced pressure. The crude product was purified by silica gel chromatography or crystallized with dichloromethane.

2-Chloro-*N*-(2-phenyl-1,3-thiazol-5-yl)benzamide 50a: This compound was obtained by reaction of **44a** with 2-chlorobenzoyl chloride and it was purified by silica gel chromatography using dichloromethane as eluent. Mp: 135.6-136.4 °C; yield: 67%; IR cm^{-1} : 3240 (NH), 1665 (CO); ^1H NMR DMSO- d_6 (ppm): 7.40-7.51 (4H, m, ArH), 7.53-7.63 (2H, m, ArH), 7.66 (1H, dd, $J = 7.5, 1.7$ Hz, ArH), 7.69 (1H, s, ArH), 7.90-7.93 (2H, m, ArH), 12.06 (1H, s, NH). ^{13}C NMR DMSO- d_6 (ppm): 126.0 (2 x C), 127.8, 129.6 (2 x C), 129.8, 129.9, 130.0, 130.4, 130.8, 132.3, 134.1, 135.3, 135.7, 158.9, 163.6. Anal. Calcd for $\text{C}_{16}\text{H}_{11}\text{ClN}_2\text{OS}$: C, 61.05; H, 3.52; N, 8.90. Found: C, 60.89; H, 3.69; N, 9.05.

2,6-Dichloro-*N*-(2-phenyl-1,3-thiazol-5-yl)benzamide 50b: This compound was obtained by reaction of **44a** with 2,6-dichlorobenzoyl chloride and it was purified by silica gel chromatography using dichloromethane: ethyl acetate (95:5) as eluent. Mp: 254.4-255.2 °C; yield: 75%; IR cm^{-1} : 3235 (NH), 1658 (CO); ^1H NMR DMSO- d_6 (ppm): 7.41-7.52 (3H, m, ArH), 7.54-7.58 (1H, m, ArH), 7.60-7.65 (2H, m, ArH), 7.68 (1H, s, ArH), 7.92 (2H, dd, $J = 8.0, 1.2$ Hz, ArH), 12.34 (1H, s, NH). ^{13}C NMR DMSO- d_6 (ppm): 126.1 (2 x C), 128.9 (2 x C), 129.7 (2 x C), 130.1, 130.2, 131.9 (2 x C), 132.6, 133.9, 135.2, 146.8, 159.4, 161.1. Calcd for $\text{C}_{16}\text{H}_{10}\text{Cl}_2\text{N}_2\text{OS}$: C, 55.03; H, 2.89; N, 8.02. Found: C, 55.16; H, 2.71; N, 7.87.

2-Bromo-*N*-(2-phenyl-1,3-thiazol-5-yl)benzamide 50c: This compound was obtained by reaction of **44a** with 2-bromobenzoyl chloride and it was purified by silica gel chromatography using dichloromethane: ethyl acetate (9:1) as eluent. Mp: 165.2-166.0 °C; yield: 17%; IR cm^{-1} : 3220 (NH), 1653 (CO); ^1H NMR CDCl_3 (ppm): 7.28-7.39 (2H, m, ArH), 7.39-7.47 (3H, m, ArH), 7.60 (2H, d, $J = 4.0$ Hz, ArH), 7.64 (1H, s, ArH), 7.81-7.94 (2H, m, ArH), 9.35 (1H, s, NH). ^{13}C NMR CDCl_3 (ppm): 119.6, 126.0 (2 x C), 127.8, 129.0 (2 x C), 129.6, 129.7, 130.3,

132.4, 133.2, 133.7, 134.3, 135.4, 161.5, 163.9. Anal. Calcd for C₁₆H₁₁BrN₂OS: C, 53.49; H, 3.09; N, 7.80. Found: C, 53.65; H, 3.11; N, 7.68.

2,6-Difluoro-N-(2-phenyl-1,3-thiazol-5-yl)benzamide 50d: This compound was obtained by reaction of **44a** with 2,6-difluorobenzoyl chloride and it was purified by silica gel chromatography using dichloromethane: ethyl acetate (9:1) as eluent. Mp 189.4-190.2 °C; yield: 21%; IR cm⁻¹: 3222 (NH), 1656 (CO); ¹H NMR DMSO-*d*₆ (ppm): 7.30 (2H, t, J = 8.2 Hz, ArH), 7.52 - 7.41 (3H, m, ArH), 7.68 - 7.61 (1H, m, ArH), 7.71 (1H, s, ArH), 7.94 - 7.89 (2H, m, ArH), 12.38 (1H, s, NH). The poor solubility of compound **50d** prevented ¹³C NMR spectra from being recorded. Anal. Calcd for C₁₆H₁₀F₂N₂OS: C, 60.75; H, 3.19; N, 8.86. Found: C, 60.89; H, 3.03; N, 8.77.

2-Fluoro-N-(2-phenyl-1,3-thiazol-5-yl)benzamide 50e: This compound was obtained by reaction of **44a** with 2-fluorobenzoyl chloride and it was purified by silica gel chromatography using dichloromethane as eluent. Mp: 150.2-151.0 °C; yield: 29%; IR cm⁻¹: 3230 (NH), 1661 (CO); ¹H NMR DMSO-*d*₆ (ppm): 7.33-7.54 (5H, m, ArH), 7.61-7.67 (1H, m, ArH), 7.71-7.81 (2H, m, ArH), 7.91 (2H, d, J = 7.2 Hz, ArH), 11.95 (1H, s, NH). ¹³C NMR DMSO-*d*₆ (ppm): 114.4, 116.9 (d, J_{C3'-F} = 22.2 Hz), 123.0 (d, J_{C6'-F} = 12.1 Hz), 125.2, 125.9 (2 x C), 129.7 (2 x C), 129.9, 130.1 (d, J_{C1'-F} = 24.2 Hz), 130.7, 134.0, (d, J_{C4'-F} = 9.1 Hz), 135.8, 158.8, 159.6 (d, J_{C2'-F} = 251.5 Hz), 161.4. Anal. Calcd for C₁₆H₁₁FN₂OS: C, 64.41; H, 3.72; N, 9.39. Found: C, 64.52; H, 3.53; N, 9.26.

2-Hydroxy-N-(2-phenyl-1,3-thiazol-5-yl)benzamide 50f: This compound was obtained by reaction of **44a** with *O*-acetylsalicyloyl chloride and it was purified by silica gel chromatography using petroleum ether: ethyl acetate (7:3) as eluent. Mp: 263.6-264.4 °C; yield: 15%; IR cm⁻¹: 3229 (NH), 3082 (OH), 1655 (CO); ¹H NMR CDCl₃ (ppm): 6.98 (1H, t, J = 7.6 Hz, ArH), 7.08 (1H, d, J = 8.4 Hz, ArH), 7.54 - 7.41 (4H, m, ArH), 7.59 (1H, dd, J = 8.0, 1.5 Hz, ArH), 7.74 (1H, s, H₅), 7.98 - 7.94 (2H, m, ArH), 8.74 (1H, s, NH), 9.81 (1H, s, OH). The poor solubility of compound **50f** prevented ¹³C NMR spectra from being recorded. Anal. Calcd for C₁₆H₁₂N₂O₂S: C, 64.85; H, 4.08; N, 9.45. Found: C, 64.97; H, 3.96; N, 9.33.

N-(2-Phenyl-1,3-thiazol-5-yl)benzamide 50g: This compound was obtained by reaction of **44a** with benzoyl chloride and it was crystallized with dichloromethane. Mp: 221.2-222.0 °C; yield: 24%; IR cm⁻¹: 3124 (NH), 1664 (CO); ¹H NMR DMSO-*d*₆ (ppm): 7.40-7.50 (3H, m, ArH), 7.57 (2H, t, J = 7.4 Hz, ArH), 7.64 (1H, t, J = 7.3 Hz, ArH), 7.90-7.92 (3H, m, ArH), 8.05-8.14 (2H, m, ArH), 12.11 (1H, s, NH). ¹³C NMR DMSO-*d*₆ (ppm): 110.9, 125.9 (2 x C), 128.4 (2 x C),

129.1 (2 x C), 129.7 (2 x C), 129.9, 132.8, 134.0, 136.5, 158.6, 164.0, 170.2. Anal. Calcd for C₁₆H₁₂N₂OS: C, 68.55; H, 4.31; N, 9.99. Found: C, 68.42; H, 4.56; N, 10.66.

4-Methoxy-N-(2-phenyl-1,3-thiazol-5-yl)benzamide 50h: This compound was obtained by reaction of **44a** with 4-methoxybenzoyl chloride and it was purified by silica gel chromatography using dichloromethane: ethyl acetate (95:5) as eluent. Mp: 216.6-217.4 °C; yield: 76%; IR cm⁻¹: 3155 (NH), 1668 (CO); ¹H NMR DMSO-*d*₆ (ppm): 3.85 (3H, s, CH₃O), 7.11 (2H, d, J = 8.8 Hz, H-3'' and H-5''), 7.39-7.49 (3H, m, ArH), 7.79 (1H, s, ArH), 7.90 (2H, d, J = 7.2 Hz, ArH), 8.02 (2H, d, J = 8.8 Hz, H-2'' and H-6''), 11.68 (1H, s, NH). ¹³C NMR DMSO-*d*₆ (ppm): 56.0, 99.9, 114.4 (2 x C), 125.0, 125.8 (2 x C), 129.6 (2 x C), 130.3 (2 x C), 134.3, 136.7, 158.4, 163.0, 163.4, 167.3. Anal. Calcd for C₁₇H₁₄N₂O₂S: C, 65.79; H, 4.55; N, 9.03. Found: C, 65.65; H, 4.69; N, 9.14.

3-Chloro-N-(2-phenyl-1,3-thiazol-5-yl)benzamide 50i: This compound was obtained by reaction of **44a** with 3-chlorobenzoyl chloride and it was crystallized with dichloromethane. Mp: 194.2-195.0 °C; yield: 59%; IR cm⁻¹: 3147 (NH), 1662 (CO); ¹H NMR DMSO-*d*₆ (ppm): 7.40-7.50 (3H, m, ArH), 7.61 (1H, t, J = 7.9 Hz, ArH), 7.67-7.74 (1H, m, ArH), 7.81 (1H, s, ArH), 7.87-7.93 (2H, m, ArH), 7.98 (1H, d, J = 7.8 Hz, ArH), 8.05-8.10 (1H, m, ArH), 11.95 (1H, s, NH). ¹³C NMR DMSO-*d*₆ (ppm): 125.9 (2 x C), 127.1, 127.9, 129.7 (2 x C), 129.9, 130.3, 131.2, 132.6, 134.0, 133.9, 134.9, 136.1, 158.9, 162.6. Anal. Calcd for C₁₆H₁₁ClN₂OS: C, 61.05; H, 3.52; N, 8.90. Found: C, 61.22; H, 3.35; N, 9.08.

3-Bromo-N-(2-phenyl-1,3-thiazol-5-yl)benzamide 50j: This compound was obtained by reaction of **44a** with 3-bromobenzoyl chloride and it was crystallized with dichloromethane. Mp: 189.2-190.0 °C; yield: 58%; IR cm⁻¹: 3164 (NH), 1659 (CO); ¹H NMR DMSO-*d*₆ (ppm): 7.36-7.61 (4H, m, ArH), 7.79-7.87 (2H, m, ArH), 7.88-7.94 (2H, m, ArH), 8.02 (1H, d, J = 7.9 Hz, ArH), 8.21 (1H, s, ArH), 11.95 (1H, s, NH). ¹³C NMR DMSO-*d*₆ (ppm): 122.4, 125.9 (2 x C), 127.5, 129.7 (2 x C), 129.9, 130.3, 130.7, 131.4, 134.1, 135.1, 135.5, 136.1, 158.9, 162.5. Anal. Calcd for C₁₆H₁₁BrN₂OS: C, 53.49; H, 3.09; N, 7.80. Found: C, 53.36; H, 3.21; N, 7.99.

2,4-Dichloro-N-(2-phenyl-1,3-thiazol-5-yl)benzamide 50k: This compound was obtained by reaction of **44a** with 2,4-dichlorobenzoyl chloride and it was purified by silica gel chromatography using dichloromethane: ethyl acetate (9:1) as eluent. Mp: 197.8-198.6 °C; yield: 65%; IR cm⁻¹: 3157 (NH), 1663 (CO); ¹H NMR DMSO-*d*₆ (ppm): 7.40-7.52 (3H, m, ArH), 7.60 (1H, dd, J = 8.3, 1.8 Hz, ArH), 7.68-7.75 (2H, m, ArH), 7.81 (1H, d, J = 1.8 Hz, ArH), 7.91 (2H, d, J = 7.0 Hz, ArH), 12.12 (1H, s, NH). ¹³C NMR DMSO-*d*₆ (ppm): 126.0 (2 x C), 128.1,

129.7 (2 x C), 130.0 (2 x C), 130.1, 131.3, 132.1, 134.0, 134.1, 135.6, 136.2, 159.1, 162.8. Anal. Calcd for C₁₆H₁₀Cl₂N₂OS: C, 55.03; H, 2.89; N, 8.02. Found: C, 54.86; H, 3.01; N, 8.14.

3-Methoxy-N-(2-phenyl-1,3-thiazol-5-yl)benzamide 50l: This compound was obtained by reaction of **44a** with 3-methoxybenzoyl chloride and it was crystallized with dichloromethane. Mp: 138.6-139.4 °C; yield: 77%; IR cm⁻¹: 3167 (NH), 1668 (CO); ¹H NMR DMSO-*d*₆ (ppm): 3.85 (3H, s, CH₃O), 7.21 (1H, dd, J = 8.1, 2.1 Hz, ArH), 7.39-7.53 (4H, m, ArH), 7.56-7.72 (2H, m, ArH), 7.82 (1H, s, ArH), 7.88-7.93 (2H, m, ArH), 11.83 (1H, s, NH). ¹³C NMR DMSO-*d*₆ (ppm): 55.9, 113.5, 118.6, 120.4, 125.9 (2 x C), 129.7 (2 x C), 129.8, 130.1, 130.3, 134.2, 134.3, 136.4, 158.7, 159.8, 163.7. Anal. Calcd for C₁₇H₁₄N₂O₂S: C, 65.79; H, 4.55; N, 9.03. Found: C, 65.67; H, 4.66; N, 9.16.

3-Fluoro-N-(2-phenyl-1,3-thiazol-5-yl)benzamide 50m: This compound was obtained by reaction of **44a** with 3-fluorobenzoyl chloride and it was crystallized with dichloromethane. Mp: 211.6-212.4 °C; yield: 83%; IR cm⁻¹: 3145 (NH), 1658 (CO); ¹H NMR DMSO-*d*₆ (ppm): 7.39-7.54 (4H, m, ArH), 7.61-7.67 (1H, m, ArH), 7.79-7.94 (5H, m, ArH), 11.92 (1H, s, NH). ¹³C NMR DMSO-*d*₆ (ppm): 115.1 (d, J_{C²-F} = 23.2 Hz), 119.8 (d, J_{C⁴-F} = 21.2 Hz), 124.5, 125.9 (2 x C), 129.7 (2 x C), 129.9, 130.3, 131.4 (d, J_{C⁵-F} = 8.1 Hz), 134.1, 135.2 (d, J_{C¹-F} = 7.1 Hz), 136.2, 137.4, 157.6, 160.1 (d, J_{C³-F} = 237.4 Hz), 162.7. Anal. Calcd for C₁₆H₁₁FN₂OS: C, 64.41; H, 3.72; N, 9.39. Found: C, 64.59; H, 3.60; N, 9.26.

N-(2-Phenyl-1,3-thiazol-5-yl)-3-(trifluoromethyl)benzamide 50n: This compound was obtained by reaction of **44a** with 3-trifluoromethylbenzoyl chloride and it was crystallized from dichloromethane. Mp: 200.4-201.2 °C; yield: 93%; IR cm⁻¹: 3155 (NH), 1660 (CO); ¹H NMR DMSO-*d*₆ (ppm): 7.37-7.53 (3H, m, ArH), 7.77-8.06 (2H, m, ArH), 7.87-7.96 (2H, m, ArH), 8.02 (1H, d, J = 7.8 Hz, ArH), 8.32 (1H, d, J = 7.8 Hz, ArH), 12.07 (1H, s, NH). ¹³C NMR DMSO-*d*₆ (ppm): 124.7, 124.80, 125.9 (2 x C), 129.4, 129.7 (2 x C), 130.0, 130.4, 130.5, 131.2 (d, J_{CF₃} = 255.5 Hz), 133.9, 134.0, 136.1, 159.0 162.6. Anal. Calcd for C₁₇H₁₁F₃N₂OS: C, 58.62; H, 3.18; N, 8.04. Found: C, 58.79; H, 3.05; N, 8.19.

N-(2-Phenyl-1,3-thiazol-5-yl)-2-(trifluoromethoxy)benzamide 50o: This compound was obtained by reaction of **44a** with 2-trifluoromethoxybenzoyl chloride and it was crystallized from dichloromethane. Mp: 179.8-180.6 °C; yield: 83%; IR cm⁻¹: 3152 (NH), 1665 (CO); ¹H NMR DMSO-*d*₆ (ppm): 7.52-7.39 (3H, m, ArH), 7.61-7.52 (2H, m, ArH), 7.75-7.66 (2H, m, ArH), 7.80 (1H, dd, J = 7.6, 1.7 Hz, ArH), 7.95-7.88 (2H, m, ArH), 12.05 (1H, s, NH). The poor

solubility of compound **50o** prevented ^{13}C NMR spectra from being recorded. Anal. Calcd for $\text{C}_{17}\text{H}_{11}\text{F}_3\text{N}_2\text{O}_2\text{S}$: C, 56.04; H, 3.04; N, 7.69. Found: C, 55.92; H, 3.20; N, 7.81.

***N*-(2-Phenyl-1,3-thiazol-5-yl)-4-(trifluoromethyl)benzamide 50p**: This compound was obtained by reaction of **44a** with 4-trifluoromethylbenzoyl chloride and it was purified by silica gel chromatography using dichloromethane: ethyl acetate (98:2) as eluent. Mp: 258.6-259.4 °C; yield: 33%; IR cm^{-1} : 3148 (NH), 1656 (CO); ^1H NMR DMSO- d_6 (ppm): 7.41-7.50 (3H, m, ArH), 7.77-8.06 (5H, m, ArH), 8.22 (2H, d, $J = 8.0$ Hz, ArH), 12.09 (1H, s, NH). ^{13}C NMR DMSO- d_6 (ppm): 125.9 (2 x C), 126.2, 129.2 (2 x C), 129.7 (2 x C), 129.9, 130.2, 130.5 (2 x C), 132.3, 135.4 (d, $J_{\text{CF}_3} = 269.7$ Hz), 136.1, 150.7, 159.0, 162.8. Anal. Calcd for $\text{C}_{17}\text{H}_{11}\text{F}_3\text{N}_2\text{OS}$: C, 58.62; H, 3.18; N, 8.04. Found: C, 58.77; H, 3.05; N, 7.91.

***3,4-Dichloro-N*-(2-phenyl-1,3-thiazol-5-yl)benzamide 50q**: This compound was obtained by reaction of **44a** with 3,4-dichlorobenzoyl chloride and it was crystallized from dichloromethane. Mp: 215.2-216.0 °C; yield: 100%; IR cm^{-1} : 3157 (NH), 1666 (CO); ^1H NMR DMSO- d_6 (ppm): 7.40-7.47 (3H, m, ArH), 7.73-7.93 (4H, m, ArH), 7.96-8.07 (1H, m, ArH), 8.27 (1H, d, $J = 1.9$ Hz, ArH), 12.05 (1H, s, NH). ^{13}C NMR DMSO- d_6 (ppm): 125.9 (2 x C), 128.6, 129.6 (2 x C), 129.9, 130.1, 130.4, 131.5, 132.0, 133.2, 134.0, 135.6, 136.0, 159.0, 161.7. Anal. Calcd for $\text{C}_{16}\text{H}_{10}\text{Cl}_2\text{N}_2\text{OS}$: C, 55.03; H, 2.89; N, 8.02. Found: C, 54.19; H, 3.02; N, 8.18.

***3-Cyano-N*-(2-phenyl-1,3-thiazol-5-yl)benzamide 50r**: This compound was obtained by reaction of **44a** with 3-cyanobenzoyl chloride and it was crystallized with dichloromethane. Mp: 234.6-235.4 °C; yield: 82%; IR cm^{-1} : 3201 (NH), 2256 (CN), 1661 (CO); ^1H NMR DMSO- d_6 (ppm): 7.32-7.55 (3H, m, ArH), 7.73-7.99 (4H, m, ArH), 8.11 (1H, d, $J = 7.7$ Hz, ArH), 8.30 (1H, d, $J = 7.7$ Hz, ArH), 8.45 (1H, s, ArH), 12.04 (1H, s, NH). ^{13}C NMR DMSO- d_6 (ppm): 104.2, 112.3, 118.6, 125.9 (2 x C), 129.7 (2 x C), 130.0, 130.4, 130.6, 131.9, 133.1, 134.0, 136.0, 136.1, 159.0, 162.2. Anal. Calcd for $\text{C}_{17}\text{H}_{11}\text{N}_3\text{OS}$: C, 66.87; H, 3.63; N, 13.76. Found: C, 66.99; H, 3.75; N, 13.61.

General procedure for the synthesis of *N*-(2-phenyl-1,3-thiazol-5-yl)benzamides 50s-x

To a solution of 2-phenyl-1,3-thiazol-5-amine **44a** (0.57 mmol) in anhydrous acetonitrile (4 mL), the proper substituted benzoic acid (0.86 mmol), hydroxybenzotriazole (HOBt, 0.114 mmol), *N*-(3-Dimethylaminopropyl)-*N'*-ethylcarbodiimide hydrochloride (EDC HCl, 1.14 mmol) and 4-dimethylaminopyridine (DMAP, 0.86 mmol) were added and the desired product was obtained

through a Microwave-Assisted Organic Synthesis (MAOS technique), irradiating the reaction for 40 minutes (2 cycles of 20') with a power of 60 W and a temperature of 50 °C. After cooling, the reaction mixture was poured into crushed ice and the formed solid was filtered off. The solid was dried and crystallized or purified by silica gel chromatography.

2-Methoxy-N-(2-phenyl-1,3-thiazol-5-yl)benzamide 50s: This compound was obtained by reaction of **44a** with 2-methoxybenzoic acid and it was purified by silica gel chromatography using dichloromethane: ethyl acetate (98:2) as eluent. Mp: 182.2-183.0 °C; yield: 91%; IR cm^{-1} : 3222 (NH), 1664 (CO); ^1H NMR DMSO- d_6 (ppm): 3.90 (3H, s, CH_3O), 7.06-7.09 (1H, m, ArH), 7.19-7.21 (1H, m, ArH), 7.38-7.43 (1H, m, ArH), 7.44-7.47 (2H, m, ArH), 7.52-7.56 (1H, m, ArH), 7.68 (1H, dd, $J = 7.6, 1.7$ Hz, ArH), 7.76 (1H, s, ArH), 7.87-7.89 (2H, m, ArH), 11.44 (1H, s, NH). ^{13}C NMR DMSO- d_6 (ppm): 56.4, 112.5, 121.0, 123.0, 125.8 (2 x C), 129.6 (2 x C), 129.8, 129.8, 130.5, 133.4, 134.2, 135.8, 157.2, 158.4, 163.2. Anal. Calcd for $\text{C}_{17}\text{H}_{14}\text{N}_2\text{O}_2\text{S}$: C, 65.79; H, 4.55; N, 9.03. Found: C, 65.96; H, 4.43; N, 8.89.

4-Chloro-N-(2-phenyl-1,3-thiazol-5-yl)benzamide 50t: This compound was obtained by reaction of **44a** with 4-chlorobenzoic acid and it was purified by silica gel chromatography using dichloromethane: ethyl acetate (98:2) as eluent. Mp: 239.8-240.6 °C; yield: 66%; IR cm^{-1} : 3218 (NH), 1667 (CO); ^1H NMR DMSO- d_6 (ppm): 7.49-7.37 (3H, m, H-3', H-4' and H-5'), 7.65 (2H, d, $J = 8.5$ Hz, H-3'' and H-5''), 7.80 (1H, s, H-5), 7.89 (2H, d, $J = 7.2$ Hz, H-2' and H-6'), 8.04 (2H, d, $J = 8.5$ Hz, H-2'' and H-6''), 11.91 (1H, s, NH). ^{13}C NMR DMSO- d_6 (ppm): 125.8 (2 x C), 129.2 (2 x C), 129.6 (2 x C), 129.8, 130.2 (2 x C), 131.6, 134.1, 136.2, 137.7, 158.8, 162.9. Anal. Calcd for $\text{C}_{16}\text{H}_{11}\text{ClN}_2\text{OS}$: C, 61.05; H, 3.52; N, 8.90. Found: C, 61.18; H, 3.39; N, 9.02.

2,5-Dichloro-N-(2-phenyl-1,3-thiazol-5-yl)benzamide 50u: This compound was obtained by reaction of **44a** with 2,5-dichlorobenzoic acid and it was crystallized from dichloromethane. Mp: 170.2-171.0 °C; yield: 30%; IR cm^{-1} : 3215 (NH), 1662 (CO); ^1H NMR DMSO- d_6 (ppm): 7.42-7.47 (3H, m, ArH), 7.83 (1H, s, ArH), 7.63 (2H, s, ArH), 7.68 (1H, s, ArH), 7.90 (2H, d, $J = 6.8$ Hz, ArH), 12.15 (1H, s, NH). ^{13}C NMR DMSO- d_6 (ppm): 125.9 (2 x C), 129.6, 129.6 (2 x C), 130.0, 130.2, 132.1, 132.4, 133.9, 135.4, 135.5, 136.6, 159.1, 162.2. Anal. Calcd for $\text{C}_{16}\text{H}_{10}\text{Cl}_2\text{N}_2\text{OS}$: C, 55.03; H, 2.89; N, 8.02. Found: C, 54.17; H, 3.04; N, 7.88.

4-Bromo-N-(2-phenyl-1,3-thiazol-5-yl)benzamide 50v: This compound was obtained by reaction of **44a** with 4-bromobenzoic acid and it was crystallized with diethyl ether. Mp: 248.6-249.4 °C; yield: 53%; IR cm^{-1} : 3216 (NH), 1661 (CO); ^1H NMR DMSO- d_6 (ppm): 7.38-7.50 (3H, m, ArH), 7.76-7.82 (3H, m, ArH), 7.89-7.90 (2H, m, ArH), 7.93-7.99 (2H, m, ArH), 11.92

(1H, s, NH). ¹³C NMR DMSO-*d*₆ (ppm): 125.8 (2 x C), 126.7, 129.6 (2 x C), 129.8, 130.2, 130.3 (2 x C), 132.0, 132.2 (2 x C), 134.1, 136.2, 158.8, 163.0. Anal. Calcd for C₁₆H₁₁BrN₂OS: C, 53.49; H, 3.09; N, 7.80. Found: C, 53.33; H, 3.27; N, 7.96.

4-Fluoro-N-(2-phenyl-1,3-thiazol-5-yl)benzamide 50w: This compound was obtained by reaction of **44a** with 4-fluorobenzoic acid and it was crystallized with diethyl ether. Mp: 236.2-237.0 °C; yield: 81%; IR cm⁻¹: 3228 (NH), 1667 (CO); ¹H NMR DMSO-*d*₆ (ppm): 7.30-7.58 (5H, m, ArH), 7.80 (1H, s, H-5), 7.88-7.91 (2H, m, ArH), 8.01-8.18 (2H, m, ArH), 11.87 (1H, s, NH). ¹³C NMR DMSO-*d*₆ (ppm): 116.2 (2x d, J_{C3'-F} = 22.2 Hz), 125.9 (2 x C), 129.6, 129.6 (2 x C), 129.83, 130.05, 131.1 (2x d, J_{C2'-F} = 9.1 Hz), 134.1, 136.3, 158.7, 162.9, 165.0 (d, J_{C4'-F} = 250.5 Hz). Anal. Calcd for C₁₆H₁₁FN₂OS: C, 64.41; H, 3.72; N, 9.39. Found: C, 64.26; H, 3.63; N, 9.51.

2-Bromo-6-chloro-N-(2-phenyl-1,3-thiazol-5-yl)benzamide 50x: This compound was obtained by reaction of **44a** with 2-bromo-6-chlorobenzoic acid and it was purified by silica gel chromatography using dichloromethane: ethyl acetate (9:1) as eluent. Mp 245.6-246.4 °C; yield: 21%; IR cm⁻¹: 3232 (NH), 1655 (CO); ¹H NMR CDCl₃ (ppm): 7.29 (1H, d, J = 8.1 Hz, ArH), 7.41-7.46 (4H, m, ArH), 7.56 (1H, dd, H = 8.1, 0.9 Hz, ArH), 7.67 (1H, s, H-5), 7.94 (2H, dd, J = 8.0, 1.5 Hz, ArH), 8.28 (1H, s, NH). The poor solubility of compound **50x** prevented ¹³C NMR spectra from being recorded. Anal. Calcd for C₁₆H₁₀BrClN₂OS: C, 48.81; H, 2.56; N, 7.12. Found: C, 48.69; H, 2.68; N, 7.01.

General procedure for the synthesis of N-(2-phenyl-1,3-thiazol-5-yl)benzamides 50y and 50z

To a suspension of the suitable *N*-(2-phenyl-1,3-thiazol-5-yl)benzamide **50h** (for **50y**) or **50l** (for **50z**) (22 mmol) in anhydrous dichloromethane (1 mL), BBr₃ (1.13 mmol) was added dropwise at 0 °C. The reaction mixture was stirred overnight and then was poured onto crushed ice and the formed solid was filtered off. The solid was dried and crystallized or purified by silica gel chromatography.

4-Hydroxy-N-(2-phenyl-1,3-thiazol-5-yl)benzamide 50y: This compound was obtained by reaction of **50h** and it was purified by silica gel chromatography using dichloromethane: ethyl acetate (8:2) as eluent. Mp: 274.6-275.4 °C; yield: 82%; IR cm⁻¹: 3223 (NH), 3078 (OH), 1657 (CO); ¹H NMR DMSO-*d*₆ (ppm): 6.93-6.88 (2H, m, ArH), 7.50-7.38 (3H, m, ArH), 7.76 (1H, s, ArH), 7.94-7.86 (4H, m, ArH), 10.26 (1H, s, OH), 11.57 (1H, s, NH). The poor solubility of

compound **50y** prevented ^{13}C NMR spectra from being recorded. Anal. Calcd for $\text{C}_{16}\text{H}_{12}\text{N}_2\text{O}_2\text{S}$: C, 64.85; H, 4.08; N, 9.45. Found: C, 64.73; H, 4.18; N, 9.56.

3-Hydroxy-N-(2-phenyl-1,3-thiazol-5-yl)benzamide 50z: This compound was obtained by reaction of **50l** and it was crystallized with diethyl ether. Mp: 284.8-285.6 °C; yield: 88%; IR cm^{-1} : 3235 (NH), 3094 (OH), 1659 (CO); ^1H NMR DMSO- d_6 (ppm): 7.01-7.03 (1H, m, ArH), 7.33-7.51 (6H, m, ArH), 7.80 (1H, s, ArH), 7.88-7.92 (2H, m, ArH), 9.82 (1H, s, OH), 11.74 (1H, s, NH). The poor solubility of compound **50z** prevented ^{13}C NMR spectra from being recorded. Anal. Calcd for $\text{C}_{16}\text{H}_{12}\text{N}_2\text{O}_2\text{S}$: C, 64.85; H, 4.08; N, 9.45. Found: C, 64.99; H, 3.92; N, 9.31.

General procedure for the synthesis of ethyl 7-bromo-2-phenyl[1,3]thiazolo[5,4- b]pyridine-6-carboxylate 51

A mixture of diethyl {[2-phenyl-1,3-thiazol-5-yl]amino}methylidene}propanedioate **45a** (0.3 mmol) and POBr_3 (0.9 mmol) was heated at 100 °C for 2 hours. After cooling, the excess of the reagent was removed under reduced pressure, the residue was neutralized with a NH_4OH (25% aqueous solution) and extracted with dichloromethane. The organic phase was dried over Na_2SO_4 and the solvent was removed under reduced pressure. The crude was purified by silica gel chromatography using dichloromethane as eluent [101]. Mp: 136.4-137.2 °C; yield: 31%; IR cm^{-1} : 1724 (CO); ^1H NMR CDCl_3 (ppm): 1.48 (3H, t, $J=7.1$ Hz, CH_3), 4.51 (2H, q, $J=7.1$ Hz, CH_2), 7.62-7.50 (3H, m, $\text{H}_{3'}$, $\text{H}_{4'}$ and $\text{H}_{5'}$), 8.18-8.11 (2H, m, $\text{H}_{2'}$ and $\text{H}_{6'}$), 8.88 (1H, s, H_5). ^{13}C NMR CDCl_3 (ppm): 14.2, 62.2, 126.5, 127.3, 127.9 (2 x C), 129.2 (2 x C), 132.2, 132.8, 147.0, 148.2, 148.8, 164.6, 170.0. Anal. Calcd for $\text{C}_{15}\text{H}_{11}\text{BrN}_2\text{O}_2\text{S}$: C, 49.60; H, 3.05; N, 7.71. Found: C, 49.48; H, 3.22; N, 7.89.

General procedure for the synthesis of ethyl 7-amino-2-phenyl[1,3]thiazolo[5,4-b]pyridine-6-carboxylate 52a

To a solution of ethyl 7-azido-2-phenyl[1,3]thiazolo[5,4-b]pyridine-6-carboxylate **47a** (0.3 mmol) in anhydrous methanol (10 mL), sodium dithionite (0.3 mmol) was added at room temperature and the reaction mixture was heated at 80 °C for an hour and half. Sodium dithionite (0.3 mmol) was further added and the reaction mixture has been heated under reflux for an hour and half. After cooling, the mixture was poured into ice and the suspension was filtered off, dried

and recrystallized from ethanol [102]. Mp: 183.2-184.0 °C; yield: 98%; IR cm^{-1} : 3332, 3247 (NH₂), 1625 (CO); ¹H NMR CDCl₃ (ppm): 1.43 (3H, t, J = 7.1 Hz, CH₃), 4.40 (2H, q, J = 7.1 Hz, CH₂), 6.34 (2H, s, NH₂), 7.40-7.56 (3H, m, H₃, H₄ and H₅), 8.01-8.03 (2H, m, H₂ and H₆), 8.85 (1H, s, H₅). ¹³C NMR CDCl₃ (ppm): 14.3, 60.8, 104.5, 127.1 (2 x C), 129.0 (2 x C), 131.1, 133.4, 135.3, 149.4, 150.6, 160.0, 165.0, 167.7. Anal. Calcd for C₁₅H₁₃N₃O₂S: C, 60.18; H, 4.38; N, 14.04. Found: C, 60.29; H, 4.22; N, 13.89.

General procedure for the synthesis of ethyl 7-anilino-2-phenyl[1,3]thiazolo[5,4-b]pyridine-6-carboxylates 52b,c

To a solution of ethyl 7-chloro-2-phenyl[1,3]thiazolo[5,4-b]pyridine-6-carboxylate **46a** (0.30 mmol) in ethanol (5 mL), the proper aniline (0.45 mmol) and HCl (2-3 drops) were added and the desired product was obtained through a Microwave-Assisted Organic Synthesis (MAOS technique), irradiating the reaction for 60 minutes (3 cycles of 20') with a power of 50 W and a temperature of 60 °C. After cooling, the solvent was removed under reduced pressure and the residue was washed with NaHCO₃ saturated aqueous solution. The formed solid was filtered off, dried and purified by silica gel chromatography using dichloromethane as eluent (for derivative **52b**) or crystallized with diethyl ether (for derivative **52c**).

Ethyl 7-anilino-2-phenyl[1,3]thiazolo[5,4-b]pyridine-6-carboxylate 52b: This compound was obtained by reaction of **46a** with aniline. Mp: 241.6-242.4 °C; yield: 15%; IR cm^{-1} : 3218 (NH), 1667 (CO); ¹H NMR CDCl₃ (ppm): 1.46 (3H, t, J = 7.1 Hz, CH₃), 4.44 (2H, q, J = 7.1 Hz, CH₂), 7.24- 7.45 (8H, m, ArH), 7.54-7.61 (2H, m, ArH), 8.98 (1H, s, ArH), 10.41 (1H, s, NH). The poor solubility of compound **52b** prevented ¹³C NMR spectra from being recorded. Anal. Calcd for C₂₁H₁₇N₃O₂S: C, 67.18; H, 4.56; N, 11.19. Found: C, 67.34; H, 4.32; N, 11.27.

Ethyl 7-(2-hydroxyanilino)-2-phenyl[1,3]thiazolo[5,4-b]pyridine-6-carboxylate 52c: This compound was obtained by reaction of **46a** with 2-aminophenol. Mp: 254.4-255.2 °C; yield: 89%; IR cm^{-1} : 3244 (NH), 3084 (OH), 1669 (CO); ¹H NMR DMSO-*d*₆ (ppm): 1.36 (3H, t, J = 7.1 Hz, CH₃), 4.37 (2H, q, J = 7.1 Hz, CH₂), 6.77-6.98 (2H, m, ArH), 7.09-7.27 (2H, m, ArH), 7.35-7.53 (3H, m, ArH), 7.56-7.65 (2H, m, ArH), 8.83 (1H, s, ArH), 9.68 (1H, s, OH), 10.04 (1H, s, NH). ¹³C NMR DMSO-*d*₆ (ppm): 14.6, 61.5, 98.2, 106.5, 113.3, 115.9, 118.8, 126.8 (2 x C), 127.2, 128.0, 129.6 (2 x C), 131.7, 133.2, 134.5, 150.3, 152.2, 161.6, 162.6, 168.1. Anal. Calcd for C₂₁H₁₇N₃O₃S: C, 64.43; H, 4.38; N, 10.73. Found: C, 64.26; H, 4.52; N, 10.59.

General procedure for the synthesis of ethyl 7-benzamido-2-phenyl[1,3]thiazolo[5,4-*b*]pyridine-6-carboxylates 53a-c and ethyl 7-dibenzoylamino-2-phenyl-thiazolo[5,4-*b*]pyridine-6-carboxylates 53d-f

To a solution of ethyl 7-amino-2-phenyl[1,3]thiazolo[5,4-*b*]pyridine-6-carboxylate **52a** (0.33 mmol) in acetonitrile (4 mL), the proper benzoyl chloride (0.66 mmol) and 4-dimethylaminopyridine (0.33 mmol) were added and the desired product was obtained through a Microwave-Assisted Organic Synthesis (MAOS technique), irradiating the reaction for 40 minutes (2 cycles of 20') with a power of 150 W and a temperature of 120 °C. After cooling, the reaction mixture was poured onto crushed ice and extracted with ethyl acetate. The organic layer was dried over sodium sulphate and the solvent was removed under reduced pressure. The solid obtained was crystallized with dichloromethane or purified by silica gel chromatography. From purification, it was possible to obtain both mono- (**53a-c**) and di-substituted (**53d-f**) derivatives. Unfortunately, compounds **53a** and **53b** were isolated only in traces, making their spectroscopic characterization difficult.

Ethyl 7-(2-chlorobenzamido)-2-phenyl[1,3]thiazolo[5,4-*b*]pyridine-6-carboxylate 53c: This compound was obtained by reaction of **52a** with 2-chlorobenzoyl chloride and it was purified by silica gel chromatography using dichloromethane: ethyl acetate (9:1) as eluent. Mp: 189.2-190.0 °C; yield: 16%; IR cm^{-1} : 1726 (CO), 1683 (CO); ^1H NMR CDCl_3 (ppm): 1.42 (3H, t, $J = 7.1$ Hz, CH_3), 4.45 (2H, q, $J = 7.1$ Hz, CH_2), 7.41-7.59 (6H, m, ArH), 7.89-7.95 (1H, m, ArH), 8.06-8.12 (2H, m, ArH), 9.00 (1H, s, ArH), 9.98 (1H, s, NH). The poor solubility of compound **53c** prevented ^{13}C NMR spectra from being recorded. Anal. Calcd for $\text{C}_{22}\text{H}_{16}\text{ClN}_3\text{O}_3\text{S}$: C, 60.34; H, 3.68; N, 9.60. Found: C, 60.17; H, 3.83; N, 9.76.

7-[Bis-(2-fluoro-benzoyl)-amino]-2-phenyl-thiazolo[5,4-*b*]pyridine-6-carboxylic acid ethyl ester 53d: This compound was obtained by reaction of **52a** with 2-fluorobenzoyl chloride and it was crystallized with dichloromethane. Mp: 236.6-237.4 °C; yield: 25%; IR cm^{-1} : 1726 (CO), 1724 (CO), 1689 (CO); ^1H NMR CDCl_3 (ppm): 1.39 (3H, t, $J = 7.1$ Hz, CH_3), 4.44 (2H, q, $J = 7.1$ Hz, CH_2), 6.95 (2H, t, $J = 9.2$ Hz, ArH), 7.11 (2H, t, $J = 7.4$ Hz, ArH), 7.37 (2H, s, ArH), 7.46-7.56 (3H, m, ArH), 7.89 (2H, t, $J = 6.4$ Hz, ArH), 8.06 (2H, d, $J = 7.1$ Hz, ArH), 9.19 (1H, s, ArH). The poor solubility of compound **53d** prevented ^{13}C NMR spectra from being recorded. Anal. Calcd for $\text{C}_{29}\text{H}_{19}\text{F}_2\text{N}_3\text{O}_4\text{S}$: C, 64.08; H, 3.52; N, 7.73. Found: C, 64.27; H, 3.35; N, 7.59.

7-Dibenzoylamino-2-phenyl-thiazolo[5,4-*b*]pyridine-6-carboxylic acid ethyl ester 53e: This compound was obtained by reaction of **52a** with benzoyl chloride and it was crystallized with

dichloromethane. Mp: 259.8-260.6 °C; yield: 15%; IR cm^{-1} : 1728 (CO), 1725 (CO), 1686 (CO); ^1H NMR CDCl_3 (ppm): 1.36 (3H, t, $J = 7.1$ Hz, CH_3), 4.40 (2H, q, $J = 7.1$ Hz, CH_2), 7.29-7.32 (4H, m, ArH), 7.37-7.48 (4H, m, ArH), 7.49-7.54 (1H, m, ArH), 7.85-7.92 (4H, m, ArH), 7.93-8.00 (2H, m, ArH), 9.18 (1H, s, ArH). The poor solubility of compound **53e** prevented ^{13}C NMR spectra from being recorded. Anal. Calcd for $\text{C}_{29}\text{H}_{21}\text{N}_3\text{O}_4\text{S}$: C, 68.62; H, 4.17; N, 8.28. Found: C, 68.46; H, 4.29; N, 8.44.

7-[Bis-(2-chloro-benzoyl)-amino]-2-phenyl-thiazolo[5,4-b]pyridine-6-carboxylic acid ethyl ester 53f: compound was obtained by reaction of **52a** with 2-chlorobenzoyl chloride and it was purified by silica gel chromatography using dichloromethane: ethyl acetate (9:1) as eluent. Mp: 219.8-220.6 °C; yield: 15%; IR cm^{-1} : 1722 (CO), 1719 (CO), 1685 (CO); ^1H NMR CDCl_3 (ppm): 1.45 (3H, t, $J = 7.1$ Hz, CH_3), 4.47 (2H, q, $J = 7.1$ Hz, CH_2), 7.14-7.23 (4H, m, ArH), 7.31 (2H, t, $J = 7.4$ Hz, ArH), 7.45-7.57 (3H, m, ArH), 8.01-8.06 (2H, m, ArH), 8.23 (2H, d, $J = 6.3$ Hz, ArH), 9.27 (1H, s, ArH). The poor solubility of compound **53f** prevented ^{13}C NMR spectra from being recorded. Anal. Calcd for $\text{C}_{29}\text{H}_{19}\text{Cl}_2\text{N}_3\text{O}_4\text{S}$: C, 60.42; H, 3.32; N, 7.29. Found: C, 60.56; H, 3.17; N, 7.15.

General procedure for the synthesis of 7-amino-2-phenyl[1,3]thiazolo[5,4-b]pyridine-6-carboxylic acid 56

To a solution of ethyl 7-amino-2-phenyl[1,3]thiazolo[5,4-b]pyridine-6-carboxylate **52a** (0.18 mmol) in ethanol (10 mL), 2N NaOH (0.24 mL) was added and the mixture was heated under reflux for 2 hours. After cooling, the solvent was removed under reduced pressure, cold water was added and the solution was acidified to pH=5 with acetic acid. The suspension thus obtained was filtered off, allowing the isolation of the desired pure product. Mp: 272.8-273.6 °C; yield: 92%; IR cm^{-1} : 3331, 3250 (NH_2), 3127 (OH), 1631 (CO); ^1H NMR $\text{DMSO-}d_6$ (ppm): 4.09 (1H, s, OH), 6.39 (2H, s, NH_2), 7.56 -7.57 (3H, m, H_3' , H_4' and H_5'), 8.07-8.09 (2H, m, H_2' and H_6'), 8.70 (1H, s, H_5). ^{13}C NMR $\text{DMSO-}d_6$ (ppm): 104.3, 127.3 (2 x C), 129.8 (2 x C), 131.7, 133.4, 135.2, 149.9, 151.4, 159.4, 163.0, 169.8. Anal. Calcd for $\text{C}_{13}\text{H}_9\text{N}_3\text{O}_2\text{S}$: C, 57.55; H, 3.34; N, 15.49. Found: C, 57.48; H, 3.41; N, 15.57.

General procedure for the synthesis of 7-amino-N,2-diphenyl[1,3]thiazolo[5,4-b]pyridine-6-carboxamides 54a,b and 7-amino-N-benzyl-2-phenyl[1,3]thiazolo[5,4-b]pyridine-6-carboxamides 54c,d

To a solution of 7-amino-2-phenyl[1,3]thiazolo[5,4-b]pyridine-6-carboxylic acid **56** (0.37 mmol) in acetonitrile (4 mL), the proper aniline (for **54a,b**) (0.56 mmol) or benzylamine (for **54c,d**), hydroxybenzotriazole (HOBt, 0.074 mmol), *N*-(3-Dimethylaminopropyl)-*N*-ethylcarbodiimide hydrochloride (EDC HCl, 0.74 mmol) and 4-dimethylaminopyridine (DMAP, 0.74 mmol) were added and the desired product was obtained through a Microwave-Assisted Organic Synthesis (MAOS technique), irradiating the reaction for 40 minutes (2 cycles of 20') with a power of 60 W and a temperature of 50 °C. After cooling, the reaction mixture was poured onto crushed ice and the formed solid was filtered off. The solid was dried and crystallized or purified by silica gel chromatography.

7-Amino-N-(2-hydroxyphenyl)-2-phenyl[1,3]thiazolo[5,4-b]pyridine-6-carboxamide 54a:

This compound was obtained by reaction of **56** with 2-aminophenol and it was purified by silica gel chromatography using dichloromethane: ethyl acetate (95:5) as eluent. Mp: 311.2-312.0 °C; yield: 15%; IR cm^{-1} : 3331, 3250 (NH_2), 3390 (NH), 3127 (OH), 1631 (CO); ^1H NMR CDCl_3 (ppm): 3.77 (2H, s, NH_2), 6.49 (1H, s, OH), 6.83-6.90 (2H, m, ArH), 7.13 (2H, d, $J = 7.6$ Hz, ArH), 7.52 (3H, s, ArH), 7.92 (1H, s, NH), 8.07 (2H, d, $J = 3.6$ Hz, ArH), 9.13 (1H, s, H_5). The poor solubility of compound **54a** prevented ^{13}C NMR spectra from being recorded. Anal. Calcd for $\text{C}_{19}\text{H}_{14}\text{N}_4\text{O}_2\text{S}$: C, 62.97; H, 3.89; N, 15.46. Found: C, 62.79; H, 4.07; N, 15.31.

7-Amino-N-(2-aminophenyl)-2-phenyl[1,3]thiazolo[5,4-b]pyridine-6-carboxamide 54b:

This compound was obtained by reaction of **56** with *O*-phenylenediamine and it was crystallized with diethyl ether. Mp: 319.6-320.4 °C; yield: 40%; IR cm^{-1} : 3334, 3253 (NH_2), 3387 (NH), 1642 (CO); ^1H NMR $\text{DMSO-}d_6$ (ppm): 6.59 (2H, t, $J = 7.0$ Hz, ArH), 6.78 (2H, d, $J = 8.0$ Hz, ArH), 6.94 - 7.01 (1H m, ArH), 7.16 (2H, d, $J = 7.7$ Hz, ArH), 7.56 - 7.60 (4H, m, ArH and NH_2), 7.76 (2H, s, NH_2), 8.09 - 8.11 (3H, m, ArH), 8.82 (1H, s, NH), 9.67 (1H, s, H_5). The poor solubility of compound **54b** prevented ^{13}C NMR spectra from being recorded. Anal. Calcd for $\text{C}_{19}\text{H}_{15}\text{N}_5\text{OS}$: C, 63.14; H, 4.18; N, 19.38. Found: C, 63.33; H, 3.98; N, 19.26.

7-Amino-N-[(4-nitrophenyl)methyl]-2-phenyl[1,3]thiazolo[5,4-b]pyridine-6-carboxamide

54c: This compound was obtained by reaction of **56** with 4-nitrobenzylamine hydrochloride and it was crystallized with dichloromethane. Mp: 259.2-260.0 °C; yield: 71%; IR cm^{-1} : 3466 (NH_2), 3344 (NH), 2298 (NO_2) 1664 (CO); ^1H NMR $\text{DMSO-}d_6$ (ppm): 4.61 (2H, d, $J = 5.8$ Hz, CH_2),

7.49-7.67 (5H, m, ArH), 7.84 (2H, s, NH₂), 8.04-8.14 (2H, m, ArH), 8.21 (2H, d, J = 8.7 Hz, ArH), 8.71 (1H, s, ArH), 9.27 (1H, t, J = 5.8 Hz, NH). ¹³C NMR DMSO-*d*₆ (ppm): 42.5, 107.9, 124.0 (2 x C), 127.4 (2 x C), 128.7 (2 x C), 129.8 (2 x C), 131.8, 133.3, 135.4, 146.9, 148.1, 149.3, 158.9, 163.4, 168.2. Anal. Calcd for C₂₀H₁₅N₅O₃S: C, 59.25; H, 3.73; N, 17.27. Found: C, 59.40; H, 3.58; N, 17.13.

7-Amino-N-[(4-methoxyphenyl)methyl]-2-phenyl[1,3]thiazolo[5,4-b]pyridine-6-carboxamide

54d: This compound was obtained by reaction of **56** with 4-methoxybenzylamine and it was crystallized with dichloromethane. Mp: 243.0-243.8 °C; yield: 75%; IR cm⁻¹: 3460 (NH₂), 3348 (NH), 1659 (CO); ¹H NMR DMSO-*d*₆ (ppm): 3.72 (3H, s, CH₃O), 4.42 (2H, d, J = 5.0 Hz, CH₂), 6.90 (2H, d, J = 8.3 Hz, H-3'' and H-5''), 7.28 (2H, d, J = 8.3 Hz, H-2'' and H-6''), 7.56 (3H, s, H-3', H-4' and H-5'), 7.84 (2H, s, NH₂), 8.08 (2H, s, H-2' and H-6'), 8.65 (1H, s, H-5), 9.06 (1H, t, J = 5.0 Hz, NH). ¹³C NMR DMSO-*d*₆ (ppm): 42.3, 55.5, 108.3, 114.2 (2 x C), 127.3 (2 x C), 129.2 (2 x C), 129.8 (2 x C), 131.8, 131.9, 133.4, 135.4, 148.0, 149.2, 158.7, 158.8, 163.3, 167.8. Anal. Calcd for C₂₁H₁₈N₄O₂S: C, 64.60; H, 4.65; N, 14.35. Found: C, 64.47; H, 4.81; N, 14.52.

5.2 Biology

5.2.1 Cells and viruses

All synthesized compounds were investigated against the following viruses: Coronaviruses [SARS-CoV-2 "UC-1074" (Wuhan) and "BA.1" (Omicron) strains isolated from clinical samples in the early SARS-CoV-2 waves, HCoV-229E, HCoV-OC43, HCoV-NL63], Influenza virus (A/H1N1, A/H3N2, B), Respiratory Syncytial Virus (RSV), Herpes Simplex Virus 1 (HSV-1 KOS and KOS-ACV⁺) Herpes Simplex Virus 2 (HSV-2 strain G), Varicella-zoster (VZV TK⁺ strain OKA and TK⁻ strain 07-1), Human Cytomegalovirus (HCMV AD-169 and Davis strains), Yellow Fever Virus (YFV), Zika Virus (ZIK), Sindbis Virus (SINV) and Semliki Forest Virus (SFV).

Cell lines used: human embryonic lung fibroblasts (HEL 299), hepatocellular carcinoma (Hep3B), Madin-Darby canine kidney (MDCK), human epithelial (Hep2) and African green monkey kidney (VeroE6) cells. Human embryonic lung fibroblasts (HEL 299) and African green monkey kidney (Vero) cells were cultured in Dulbecco's Modified Eagle's Medium (DMEM) supplemented with 8% foetal bovine serum (FBS), 0.1 mM non-essential amino acids, 10 mM

HEPES, 1 mM sodium pyruvate and 2 mM Penicillin-Streptomycin-Glutamine (100x), at 37 °C in a 5% CO₂ humidified atmosphere. Madin-Darby canine kidney (MDCK) cells were cultured in DMEM supplemented with 10% foetal bovine serum (FBS), 1 mM sodium pyruvate, and 0.075% sodium bicarbonate. All experiments were performed with confluent cells.

5.2.2 Antiviral assays

All synthesized compounds were dissolved in dimethyl sulfoxide (DMSO) to obtain a stock concentration of 20 or 25 mM and were stored frozen at 4 °C.

5.2.2.1 SARS-CoV-2

For the antiviral assays, Vero cells were seeded in 96-well plates with a density/concentration of 50.000 living cells/mL. After 24 hours growth, the cell culture medium was removed and confluent cells were treated with different compound concentrations in DMEM 2% FBS and inoculated with 100 CCID₅₀ of virus (1 CCID₅₀ = virus dose infecting 50% of the cell cultures). After 5 days of incubation at 37 °C, viral CPE was recorded microscopically and the EC₅₀ (compound concentration required to reduce viral plaque formation by 50%) was calculated for each compound and the reference drugs (remdesivir and molnupiravir).

5.2.2.2 Other viruses

The antiviral assays investigated the inhibition of virus-induced cytopathic effect or viral plaque formation. Confluent cell cultures in microtiter 96-well plates were inoculated with 100 CCID₅₀ of virus or with 20 plaque forming units (PFU). After 2 hours adsorption, the viral inoculum was removed, and the cell cultures were treated with fresh medium containing varying concentrations of compounds starting at 50 or 100 µM (solution in DMSO). Viral cytopathic effect or plaque formation was recorded as soon as it reached completion in the control virus-infected cell cultures that were not treated with the tested compounds. Antiviral activity was expressed as the EC₅₀ for each compound and the reference drugs. The following control compounds were included: acyclovir (HSV-1, HSV-2, VZV), brivudine (HSV-1, HSV-2, VZV), ganciclovir (HSV-1, HCMV), cidofovir (HSV-1, HCMV), remdesivir (HCoV-229E, HCoV-OC43, HCoV-NL63, RSV, YFV, ZIK), ribavirin (HCoV-229E, HCoV-OC43, HCoV-NL63, RSV, YFV, ZIK, Influenza

viruses A/H1N1, A/H3N2, B), zanamivir (Influenza viruses A/H1N1, A/H3N2, B), rimantadine (Influenza viruses A/H1N1, A/H3N2, B) and DS-10,000 (HSV-1, HSV-2, RSV, SINV, SFV).

5.2.3 *Cytostatic activity assays*

The cytotoxicity of all synthesized compounds was assessed by evaluating the minimum cytotoxic concentration (MCC) or compound concentration that causes a microscopically detectable alteration of cell morphology. Alternatively, the cytostatic activity of active compounds was measured based on inhibition of cell growth. Cells were seeded at a rate of 5×10^3 living cells/well into 96-well plates and, after 24 hours growth, fresh medium containing different concentrations of compounds was added. After 3 days of incubation at 37 °C, the cell number was determined with a Beckman Coulter counter. The cytostatic concentration was expressed as CC_{50} , or the compound concentration required to reduce cell proliferation by 50% compared to the number of cells in the untreated controls. CC_{50} values were estimated from graphic plots of the number of cells (percentage of control) as a function of the tested compounds concentration.

5.2.4 *Biochemical assays*

5.2.4.1 *SARS-CoV-2 Nsp13 expression and purification*

SARS-CoV-2 Nsp13 was expressed from pNIC-ZB vector in Rosetta cells, using TB medium for culture, according to Newman et al. [61]. For the first step of purification, a HisTrap column was used, and eluted fractions were further purified on a HiTrap SP column. After overnight digestion with TEV protease, sample was loaded onto a HiLoad 16/600 Superdex pg column. The final yield of purification was around 3 mg of pure protein from 4 L of culture [70].

5.2.4.2 *Determination of SARS-CoV-2 Nsp13 unwinding-associated activity*

The SARS-CoV-2 Nsp13 unwinding-associated activity was measured in black 384-well plates (PerkinElmer), in 40 μ L of reaction volume containing 20 mM Tris-HCl, pH 7.2, 50 mM NaCl, 2 μ M Hel Capture oligo (5'-TGG TGC TCG AAC AGT GAC-3') from Biomers, 5 mM $MgCl_2$, 5% DMSO (or compound), and 1 nM purified Nsp13. The reaction mixture containing the

enzyme was preincubated for 10 min with compound at room temperature. The reaction was started by adding 1 mM ATP and 750 nM annealed DNA substrate (5'-AGT CTT CTC CTG GTG CTC GAA CAG TGA C-Cy3-3', 5'-BHQ-2-GTC ACT GTT CGA GCA CCA CCT CTT CTG A-3') from Biomers. After 15 min of incubation at 37 °C, products were measured with Victor Nivo (Perkin) at 530/580 nm [70].

5.2.4.3 Determination of SARS-CoV-2 Nsp13 ATPase-associated activity

The SARS-CoV-2 Nsp13 ATPase-associated activity was measured in a transparent 96-well plate (PerkinElmer), 25 µL of reaction volume containing 20 mM Tris-HCl, pH 7.2, 50 mM NaCl, 2 mM MgCl₂, 5% DMSO (or compound), and 25 nM purified Nsp13, with 10 µg/mL of BSA and 180 µM TCEP. The reaction was started by adding 400 µM ATP. After 30 min of incubation at 37 °C, 50 µL of Biomol Green Reagent (Prod. No. BML-AK111, Enzo Lifescience) was added, and the reaction was incubated for 10 min at room temperature, protected from the light. Products were measured with Victor Nivo (Perkin) at 650 nm [70].

6. References

- [1] S. Roychoudhury, A. Das, P. Sengupta, S. Dutta, S. Roychoudhury, A.P. Choudhury, A.B. Fuzayel Ahmed, S. Bhattacharjee, P. Slama, Viral pandemics of the last four decades: Pathophysiology, health impacts and perspectives, *Int. J. Environ. Res. Public Health*. 17 (2020) 9411. <https://doi.org/10.3390/ijerph17249411>.
- [2] K. Arul, A. Anton Smith, In-Silico design, synthesis and in vitro antitubercular activity of novel 1,2,4-Triazole derivatives, *Int. J. Pharm. Pharm. Sci.* 6 (2014) 213–217.
- [3] D. Sarigol, A. Uzgoren-Baran, B.C. Tel, E.I. Somuncuoglu, I. Kazkayasi, K. Ozadali-Sari, O. Unsal-Tan, G. Okay, M. Ertan, B. Tozkoparan, Novel thiazolo[3,2-b]-1,2,4-triazoles derived from naproxen with analgesic/anti-inflammatory properties: Synthesis, biological evaluation and molecular modeling studies, *Bioorganic Med. Chem.* 23 (2015) 2518–2528. <https://doi.org/10.1016/j.bmc.2015.03.049>.
- [4] M. Shaikh, D. Subhedar, L. Nawale, D. Sarkar, F.A. Kalam Khan, J.N. Sangshetti, B.B. Shingate, 1,2,3-Triazole Derivatives as Antitubercular Agents: Synthesis, Biological

- Evaluation and Molecular Docking Study, *Medchemcomm.* 6 (2015) 1104–1116.
<https://doi.org/https://doi.org/10.1039/C5MD00057B>.
- [5] R. Adam, P. Bilbao-Ramos, B. Abarca, R. Ballesteros, M.E. González-Rosende, M.A. Dea-Ayuela, F. Estevan, G. Alzuet-Pina, Triazolopyridopyrimidines: an emerging family of effective DNA photocleavers. DNA binding. Antileishmanial activity, *Org. Biomol. Chem.* 13 (2015) 4903–4917. <https://doi.org/10.1515/ci.2004.26.6.31>.
- [6] R. Chopra, K. Chibale, K. Singh, Pyrimidine-chloroquinoline hybrids: Synthesis and antiplasmodial activity, *Eur. J. Med. Chem.* 148 (2018) 39–53. <https://doi.org/10.1016/j.ejmech.2018.02.021>.
- [7] P. Nagender, G. Malla Reddy, R. Naresh Kumar, Y. Poornachandra, C. Ganesh Kumar, B. Narsaiah, Synthesis, cytotoxicity, antimicrobial and anti-biofilm activities of novel pyrazolo[3,4-b]pyridine and pyrimidine functionalized 1,2,3-triazole derivatives, *Bioorganic Med. Chem. Lett.* 24 (2014) 2905–2908. <https://doi.org/10.1016/j.bmcl.2014.04.084>.
- [8] S. Nagarajan, P. Shanmugavelan, M. Sathishkumar, An eco-friendly water mediated synthesis of 1,2,3-triazolyl-2-aminopyrimidine hybrids as highly potent anti-bacterial agents, *Chinese Chem. Lett.* 25 (2014) 419–422. <https://doi.org/http://dx.doi.org/10.1016/j.ccllet.2013.12.017>.
- [9] K. Bozorov, J. Zhao, H.A. Aisa, 1,2,3-Triazole-containing hybrids as leads in medicinal chemistry: A recent overview, *Bioorganic Med. Chem.* 27 (2019) 5311–5351. <https://doi.org/https://doi.org/10.1016/j.bmc.2019.07.005>.
- [10] D. Dheer, V. Singh, R. Shankar, Medicinal attributes of 1,2,3-triazoles: Current developments, *Bioorg. Chem.* 71 (2017) 30–54. <https://doi.org/10.1016/j.bioorg.2017.01.010>.
- [11] A.K. Jordão, V.F. Ferreira, T.M.L. Souza, G.G. De Souza Faria, V. MacHado, J.L. Abrantes, M.C.B.V. De Souza, A.C. Cunha, Synthesis and anti-HSV-1 activity of new 1,2,3-triazole derivatives, *Bioorganic Med. Chem.* 19 (2011) 1860–1865. <https://doi.org/10.1016/j.bmc.2011.02.007>.
- [12] M. Negi, P.A. Chawla, A. Faruk, V. Chawla, Role of heterocyclic compounds in SARS and SARS CoV-2 pandemic, *Bioorg. Chem.* 104 (2020) 104315.

<https://doi.org/https://doi.org/10.1016/j.bioorg.2020.104315>.

- [13] R. Kharb, M. Shahar Yar, P. Chander Sharma, Recent Advances and Future Perspectives of Triazole Analogs as Promising Antiviral Agents, *Mini-Reviews Med. Chem.* 11 (2011) 84–96. <https://doi.org/10.2174/138955711793564051>.
- [14] S.L. Deev, M. V. Yasko, I.L. Karpenko, A.N. Korovina, A.L. Khandazhinskaya, V.L. Andronova, G.A. Galegov, T.S. Shestakova, E.N. Ulomskii, V.L. Rusinov, O.N. Chupakhin, M.K. Kukhanova, 1,2,4-Triazoloazine derivatives as a new type of herpes simplex virus inhibitors, *Bioorg. Chem.* 38 (2010) 265–270. <https://doi.org/10.1016/j.bioorg.2010.09.002>.
- [15] I.E. Głowacka, J. Balzarini, G. Andrei, R. Snoeck, D. Schols, D.G. Piotrowska, Design, synthesis, antiviral and cytostatic activity of ω -(1H-1,2,3-triazol-1-yl)(polyhydroxy)alkylphosphonates as acyclic nucleotide analogues, *Bioorganic Med. Chem.* 22 (2014) 3629–3641. <https://doi.org/http://dx.doi.org/10.1016/j.bmc.2014.05.020>.
- [16] H. Kaoukabi, Y. Kabri, C. Curti, M. Taourirte, J.C. Rodriguez-Ubis, R. Snoeck, G. Andrei, P. Vanelle, H.B. Lazrek, Dihydropyrimidinone/1,2,3-triazole hybrid molecules: Synthesis and anti-varicella-zoster virus (VZV) evaluation, *Eur. J. Med. Chem.* 155 (2018) 772–781. <https://doi.org/10.1016/j.ejmech.2018.06.028>.
- [17] I.A. Seliem, A.S. Girgis, Y. Moatasim, A. Kandeil, A. Mostafa, M.A. Ali, M.S. Bekheit, S.S. Panda, New Pyrazine Conjugates: Synthesis, Computational Studies, and Antiviral Properties against SARS-CoV-2, *ChemMedChem.* 16 (2021) 3418–3427. <https://doi.org/10.1002/cmdc.202100476>.
- [18] C.Y. Wu, K.Y. King, C.J. Kuo, J.M. Fang, Y.T. Wu, M.Y. Ho, C.L. Liao, J.J. Shie, P.H. Liang, C.H. Wong, Stable Benzotriazole Esters as Mechanism-Based Inactivators of the Severe Acute Respiratory Syndrome 3CL Protease, *Chem. Biol.* 13 (2006) 261–268. <https://doi.org/10.1016/j.chembiol.2005.12.008>.
- [19] M. Turlington, A. Chun, S. Tomar, A. Eggler, V. Grum-tokars, Discovery of N-(benzo[1,2,3]triazol-1-yl)-N-(benzyl)acetamido)phenyl) carboxamides as severe acute respiratory syndrome coronavirus (SARS-CoV) 3CLpro inhibitors: Identification of ML300 and noncovalent nanomolar inhibitors with an induced-fit binding, *Bioorganic Med. Chem. Lett.* 23 (2013) 6172–6177. <https://doi.org/http://dx.doi.org/10.1016/j.bmcl.2013.08.112>.

- [20] J. Jacobs, V. Tokars, Y. Zhou, M. Turlington, A. Saldanha, P. Chase, A. Eggler, E. Dawson, Y.M. Baez-Santos, S. Tomar, A.M. Mielech, S.C. Baker, C.W. Lindsley, P. Hodder, A.D. Mesecar, S.R. Stauffer, Discovery, synthesis, and structure-based optimization of a series of N-(tert-butyl)-2-(N-arylamido)-2-(pyridin-3-yl) acetamides (ML188) as potent non-covalent small molecule inhibitors of the severe acute respiratory syndrome coronavirus (SARS-CoV) 3CL p, *J. Med. Chem.* 56 (2013) 534–546. <https://doi.org/10.1021/jm301580n.Discovery>.
- [21] S. Yuan, H. Chu, H. Zhao, K. Zhang, K. Singh, B.K.C. Chow, R.Y.T. Kao, J. Zhou, B.J. Zheng, Identification of a small-molecule inhibitor of influenza virus via disrupting the subunits interaction of the viral polymerase, *Antiviral Res.* 125 (2016) 34–42. <https://doi.org/10.1016/j.antiviral.2015.11.005>.
- [22] K. Karypidou, S.R. Ribone, M.A. Quevedo, L. Persoons, C. Pannecouque, C. Helsen, F. Claessens, W. Dehaen, Synthesis, biological evaluation and molecular modeling of a novel series of fused 1,2,3-triazoles as potential anti-coronavirus agents, *Bioorganic Med. Chem. Lett.* 28 (2018) 3472–3476. <https://doi.org/https://doi.org/10.1016/j.bmcl.2018.09.019> Received.
- [23] V.E. Borisenko, A. Koll, E.E. Kolmakov, A.G. Rjasnyi, Hydrogen bonds of 2-aminothiazoles in intermolecular complexes (1:1 and 1:2) with proton acceptors in solutions, *J. Mol. Struct.* 783 (2006) 101–115. <https://doi.org/10.1016/j.molstruc.2005.08.006>.
- [24] J. Maj, Z. Rogó z, G. Skuza, K. Ko łodziejczyk, Antidepressant effects of pramipexole, a novel dopamine receptor agonist, *J. Neural Transm.* 104 (1997) 525–533. <https://doi.org/10.1007/BF01277669>.
- [25] G.W.A. Milne, *Ashgate Handbook of Antineoplastic Agents* (1st ed.), Gower; Ashgate, Ed., London, UK, 2020. <https://doi.org/https://doi.org/10.4324/9781315192376>.
- [26] M. Britschgi, S. Greyerz, C. Burkhardt, W. Pichler, Molecular Aspects of Drug Recognition by Specific T Cells, *Curr. Drug Targets.* 4 (2003) 1–11. <https://doi.org/10.2174/1389450033347082>.
- [27] M.P. Knadler, R.F. Bergstrom, J.T. Callaghan, A. Rubin, Nizatidine, an H₂-blocker. Its metabolism and disposition in man, *Drug Metab. Dispos.* 14 (1986) 175–182.
- [28] M. Zia-ur-Rehman, J.A. Choudary, S. Ahmad, An efficient synthesis of 2-alkyl-4-hydroxy-

- 2H-1,2-benzothiazine-3- carboxamide-1,1-dioxides, *Bull. Korean Chem. Soc.* 26 (2005) 1771–1775. <https://doi.org/10.5012/bkcs.2005.26.11.1771>.
- [29] P. Beuchet, M. Varache-Lembège, A. Neveu, J.M. Léger, J. Vercauteren, S. Larrouture, G. Deffieux, A. Nuhrich, New 2-sulfonamidothiazoles substituted at C-4: Synthesis of polyoxygenated aryl derivatives and in vitro evaluation of antifungal activity, *Eur. J. Med. Chem.* 34 (1999) 773–779. [https://doi.org/10.1016/S0223-5234\(99\)00215-9](https://doi.org/10.1016/S0223-5234(99)00215-9).
- [30] M.W. Hull, J.S.G. Montaner, Ritonavir-boosted protease inhibitors in HIV therapy, *Ann. Med.* 43 (2011) 375–388. <https://doi.org/10.3109/07853890.2011.572905>.
- [31] F.S. Hosseini, M. Amanlou, Anti-HCV and anti-malaria agent, potential candidates to repurpose for coronavirus infection: Virtual screening, molecular docking, and molecular dynamics simulation study, *Life Sci.* 258 (2020) 118205. <https://doi.org/10.1016/j.lfs.2020.118205>.
- [32] K.C. Tsai, S.Y. Chen, P.H. Liang, I.L. Lu, N. Mahindroo, H.P. Hsieh, Y.S. Chao, L. Liu, D. Liu, W. Lien, T.H. Lin, S.Y. Wu, Discovery of a novel family of SARS-CoV protease inhibitors by virtual screening and 3D-QSAR studies, *J. Med. Chem.* 49 (2006) 3485–3495. <https://doi.org/10.1021/jm050852f>.
- [33] Ç.B. Apaydın, N. Cesur, A. Stevaert, L. Naesens, Z. Cesur, Synthesis and anti-coronavirus activity of a series of 1-thia-4-azaspiro[4.5]decan-3-one derivatives, *Arch. Pharm. (Weinheim)*. 352 (2019) 1800330. <https://doi.org/10.1002/ardp.201800330>.
- [34] J. Blanchard, N.H. Elowe, C. Huitema, P.D. Fortin, J.D. Cechetto, L.D. Eltis, E.D. Brown, High-Throughput Screening Identifies Inhibitors of the SARS Coronavirus Main Proteinase, *Chem. Biol.* 11 (2004) 1445–1453. <https://doi.org/10.1016/j>.
- [35] D. Bonafoux, S. Nanthakumar, U.K. Bandarage, C. Memmott, D. Lowe, A.M. Aronov, G.R. Bhisetti, K.C. Bonanno, J. Coll, J. Leeman, C.A. Lepre, F. Lu, E. Perola, R. Rijnbrand, W.P. Taylor, D. Wilson, Y. Zhou, J. Zwahlen, E. Ter Haar, Fragment-Based Discovery of Dual JC Virus and BK Virus Helicase Inhibitors, *J. Med. Chem.* 59 (2016) 7138–7151. <https://doi.org/10.1021/acs.jmedchem.6b00486>.
- [36] C.J. Kuo, H.G. Liu, Y.K. Lo, C.M. Seong, K.I. Lee, Y.S. Jung, P.H. Liang, Individual and common inhibitors of coronavirus and picornavirus main proteases, *FEBS Lett.* 583 (2009) 549–555. <https://doi.org/10.1016/j.febslet.2008.12.059>.

- [37] J. Cui, F. Li, Z.L. Shi, Origin and evolution of pathogenic coronaviruses, *Nat. Rev. Microbiol.* 17 (2019) 181–192. <https://doi.org/10.1038/s41579-018-0118-9>.
- [38] P. V'kovski, A. Kratzel, S. Steiner, H. Stalder, V. Thiel, Coronavirus biology and replication: implications for SARS-CoV-2, *Nat. Rev. Microbiol.* 19 (2021) 155–170. <https://doi.org/10.1038/s41579-020-00468-6>.
- [39] H. Yang, Z. Rao, Structural biology of SARS-CoV-2 and implications for therapeutic development, *Nat. Rev. Microbiol.* 19 (2021) 685–700. <https://doi.org/10.1038/s41579-021-00630-8>.
- [40] COVID-19 Map - Johns Hopkins Coronavirus Resource Center (jhu.edu), (n.d.). <https://coronavirus.jhu.edu/map.html>.
- [41] N. Redondo, S. Zaldívar-López, J.J. Garrido, M. Montoya, SARS-CoV-2 Accessory Proteins in Viral Pathogenesis: Knowns and Unknowns, *Front. Immunol.* 12 (2021) 708264. <https://doi.org/10.3389/fimmu.2021.708264>.
- [42] L. Alanagreh, F. Alzoughool, M. Atoum, The Human Coronavirus Disease COVID-19: Its Origin, Characteristics, and Insights into Potential Drugs and Its Mechanisms, *Pathogens.* 9 (2020) 331. <https://doi.org/10.3390/pathogens9050331>.
- [43] A.N. Spratt, F. Gallazzi, T.P. Quinn, C.L. Lorson, A. Sönnnerborg, K. Singh, Coronavirus helicases: attractive and unique targets of antiviral drug-development and therapeutic patents, *Expert Opin. Ther. Pat.* 31 (2021) 339–350. <https://doi.org/10.1080/13543776.2021.1884224>.
- [44] R. Yapasert, P. Khaw-On, R. Banjerdpongchai, Coronavirus infection-associated cell death signaling and potential therapeutic targets, *Molecules.* 26 (2021) 7459. <https://doi.org/10.3390/molecules26247459>.
- [45] A. Citarella, A. Dimasi, D. Moi, D. Passarella, A. Scala, A. Piperno, N. Micale, Recent Advances in SARS-CoV-2 Main Protease Inhibitors: From Nirmatrelvir to Future Perspectives, *Biomolecules.* 13 (2023) 1339. <https://doi.org/10.3390/biom13091339>.
- [46] E. Hartenian, D. Nandakumar, A. Lari, M. Ly, J.M. Tucker, B.A. Glaunsinger, The molecular virology of coronaviruses, *J. Biol. Chem.* 295 (2020) 12910–12934. <https://doi.org/10.1074/jbc.REV120.013930>.
- [47] Q. Peng, R. Peng, B. Yuan, J. Zhao, M. Wang, X. Wang, Q. Wang, Y. Sun, Z. Fan, J. Qi,

- G.F. Gao, Y. Shi, Structural and Biochemical Characterization of the nsp12-nsp7-nsp8 Core Polymerase Complex from SARS-CoV-2, *Cell Rep.* 31 (2020) 107774. <https://doi.org/10.1016/j.celrep.2020.107774>.
- [48] R. Bivacqua, M. Barreca, V. Spanò, M.V. Raimondi, I. Romeo, S. Alcaro, G. Andrei, P. Barraja, A. Montalbano, Insight into non-nucleoside triazole-based systems as viral polymerases inhibitors, *Eur. J. Med. Chem.* 249 (2023) 115136. <https://doi.org/10.1016/j.ejmech.2023.115136>.
- [49] R.N. Kirchdoerfer, A.B. Ward, Structure of the SARS-CoV nsp12 polymerase bound to nsp7 and nsp8 co-factors, *Nat. Commun.* 10 (2019) 2342. <https://doi.org/10.1038/s41467-019-10280-3>.
- [50] J. Tvarogavá, R. Madhugiri, G. Bylapudi, L.J. Ferguson, N. Karl, J. Ziebuhr, Identification and Characterization of a Human Coronavirus 229E Nonstructural Protein 8-Associated RNA 3'-Terminal Adenylyltransferase Activity, *J. Virol.* 93 (2019) e00291. <https://doi.org/https://doi.org/10.1128/JVI.00291-19>.
- [51] A.K. Yazdi, P. Pakarian, S. Perveen, T. Hajian, V. Santhakumar, A. Bolotokova, F. Li, M. Vedadi, Kinetic Characterization of SARS-CoV-2 nsp13 ATPase Activity and Discovery of Small-Molecule Inhibitors, *ACS Infect. Dis.* 8 (2022) 1533–1542. <https://doi.org/10.1021/acsinfecdis.2c00165>.
- [52] B. Malone, N. Urakova, E.J. Snijder, E.A. Campbell, Structures and functions of coronavirus replication–transcription complexes and their relevance for SARS-CoV-2 drug design, *Nat. Rev. Mol. Cell Biol.* 23 (2022) 21–39. <https://doi.org/10.1038/s41580-021-00432-z>.
- [53] E.C. Smith, N.R. Sexton, M.R. Denison, Thinking outside the triangle: Replication fidelity of the largest RNA viruses, *Annu. Rev. Virol.* 1 (2014) 111–132. <https://doi.org/10.1146/annurev-virology-031413-085507>.
- [54] E. Minskaia, T. Hertzog, A.E. Gorbalenya, V. Campanacci, C. Cambillau, B. Canard, J. Ziebuhr, Discovery of an RNA virus 3'→5' exoribonuclease that is critically involved in coronavirus RNA synthesis, *Proc. Natl. Acad. Sci. U. S. A.* 103 (2006) 5108–5113. <https://doi.org/10.1073/pnas.0508200103>.
- [55] U.S. FOOD & DRUG ADMINISTRATION, (n.d.). <https://www.fda.gov/news->

events/press-announcements/coronavirus-covid-19-update-fda-authorizes-additional-oral-antiviral-treatment-covid-19-certain.

- [56] EUROPEAN MEDICINES AGENCY - “Refusal of the marketing authorisation for Lagevrio (molnupiravir),” (n.d.). https://www.aifa.gov.it/documents/20142/1616529/Questions_answers_lagevrio-molnupiravir_en.pdf.
- [57] C.J. Gordon, E.P. Tchesnokov, E. Woolner, J.K. Perry, J.Y. Feng, D.P. Porter, M. Götte, Remdesivir is a direct-acting antiviral that inhibits RNA-dependent RNA polymerase from severe acute respiratory syndrome coronavirus 2 with high potency, *J. Biol. Chem.* 295 (2020) 6785–6797. <https://doi.org/10.1074/jbc.RA120.013679>.
- [58] M.L. Agostini, A.J. Pruijssers, J.D. Chappell, J. Gribble, X. Lu, E.L. Andres, G.R. Bluemling, M.A. Lockwood, T.P. Sheahan, A.C. Sims, M.G. Natchus, M. Saindane, A.A. Kolykhalov, G.R. Painter, R.S. Baric, R. Denison, Small-Molecule Antiviral β -D-N4-Hydroxycytidine Inhibits a Proofreading-Intact Coronavirus with a High Genetic Barrier to Resistance, *J. Virol.* 93 (2019) e01348. <https://doi.org/https://doi.org/10.1128/JVI.01348-19>.
- [59] M.T.J. Halma, M.J.A. Wever, S. Abeln, D. Roche, G.J.L. Wuite, Therapeutic potential of compounds targeting SARS-CoV-2 helicase, *Front. Chem.* 10 (2022) 1062352. <https://doi.org/10.3389/fchem.2022.1062352>.
- [60] F.K. Yoshimoto, The Proteins of Severe Acute Respiratory Syndrome Coronavirus-2 (SARS CoV-2 or n-COV19), the Cause of COVID-19, *Protein J.* 39 (2020) 198–216. <https://doi.org/10.1007/s10930-020-09901-4>.
- [61] J.A. Newman, A. Douangamath, S. Yadzani, Y. Yosaatmadja, A. Aimon, J. Brandão-Neto, L. Dunnett, T. Gorrie-stone, R. Skyner, D. Fearon, M. Schapira, F. von Delft, O. Gileadi, Structure, mechanism and crystallographic fragment screening of the SARS-CoV-2 NSP13 helicase, *Nat. Commun.* 12 (2021) 4848. <https://doi.org/10.1038/s41467-021-25166-6>.
- [62] Z. Jia, L. Yan, Z. Ren, L. Wu, J. Wang, J. Guo, L. Zheng, Z. Ming, L. Zhang, Z. Lou, Z. Rao, Delicate structural coordination of the Severe Acute Respiratory Syndrome coronavirus Nsp13 upon ATP hydrolysis, *Nucleic Acids Res.* 47 (2019) 6538–6550. <https://doi.org/10.1093/nar/gkz409>.

- [63] J. Chen, B. Malone, E. Llewellyn, M. Grasso, P.M.M. Shelton, P.D.B. Olinares, K. Maruthi, E.T. Eng, H. Vatandaslar, B.T. Chait, T.M. Kapoor, S.A. Darst, E.A. Campbell, Structural Basis for Helicase-Polymerase Coupling in the SARS-CoV-2 Replication-Transcription Complex, *Cell*. 182 (2020) 1560–1573. <https://doi.org/10.1016/j.cell.2020.07.033>.
- [64] K.J. Mickolajczyk, P.M.M. Shelton, M. Grasso, X. Cao, S.E. Warrington, A. Aher, S. Liu, T.M. Kapoor, Force-dependent stimulation of RNA unwinding by SARS-CoV-2 nsp13 helicase, *Biophys. J.* 120 (2021) 1020–1030. <https://doi.org/10.1016/j.bpj.2020.11.2276>.
- [65] L. Yan, Y. Zhang, J. Ge, L. Zheng, Y. Gao, T. Wang, Z. Jia, H. Wang, Y. Huang, M. Li, Q. Wang, Z. Rao, Z. Lou, Architecture of a SARS-CoV-2 mini replication and transcription complex, *Nat. Commun.* 11 (2020) 5874. <https://doi.org/10.1038/s41467-020-19770-1>.
- [66] U.S. FOOD & DRUG ADMINISTRATION, (n.d.). <https://www.fda.gov/emergency-preparedness-and-response/coronavirus-disease-2019-covid-19/covid-19-vaccines>.
- [67] S.A. Khan, K. Al-Balushi, Combating COVID-19: The role of drug repurposing and medicinal plants, *J. Infect. Public Health.* 14 (2021) 495–503. <https://doi.org/10.1016/j.jiph.2020.10.012>.
- [68] A.O. Adedeji, K. Singh, N.E. Calcaterra, M.L. DeDiego, L. Enjuanes, S. Weiss, S.G. Sarafianos, Severe acute respiratory syndrome coronavirus replication inhibitor that interferes with the nucleic acid unwinding of the viral helicase, *Antimicrob. Agents Chemother.* 56 (2012) 4718–4728. <https://doi.org/10.1128/AAC.00957-12>.
- [69] A.O. Adedeji, W. Severson, C. Jonsson, K. Singh, S.R. Weiss, S.G. Sarafianos, Novel Inhibitors of Severe Acute Respiratory Syndrome Coronavirus Entry That Act by Three Distinct Mechanisms, *J. Virol.* 87 (2013) 8017–8028. <https://doi.org/10.1128/jvi.00998-13>.
- [70] A. Corona, K. Wycisk, C. Talarico, C. Manelfi, J. Milia, R. Cannalire, F. Esposito, P. Gribbon, A. Zaliani, D. Iaconis, A.R. Beccari, V. Summa, M. Nowotny, E. Tramontano, Natural Compounds Inhibit SARS-CoV-2 nsp13 Unwinding and ATPase Enzyme Activities, *ACS Pharmacol. Transl. Sci.* 5 (2022) 226–239. <https://doi.org/10.1021/acspsci.1c00253>.
- [71] A.O. Adedeji, K. Singh, A. Kassim, C.M. Coleman, R. Elliott, S.R. Weiss, M.B. Frieman, S.G. Sarafianos, Evaluation of SSYA10-001 as a replication inhibitor of severe acute respiratory syndrome, mouse hepatitis, and Middle East respiratory syndrome

- coronaviruses, *Antimicrob. Agents Chemother.* 58 (2014) 4894–4898. <https://doi.org/10.1128/AAC.02994-14>.
- [72] I. Romeo, F.A. Ambrosio, G. Costa, A. Corona, M. Alkhatib, R. Salpini, S. Lemme, D. Vergni, V. Svicher, M.M. Santoro, E. Tramontano, F. Ceccherini-Silberstein, A. Artese, S. Alcaro, Targeting SARS-CoV-2 nsp13 Helicase and Assessment of Druggability Pockets: Identification of Two Potent Inhibitors by a Multi-Site In Silico Drug Repurposing Approach, *Molecules*. 27 (2022) 7522. <https://doi.org/10.3390/molecules27217522>.
- [73] A.B. Gurung, In silico structure modelling of SARS-CoV-2 Nsp13 helicase and Nsp14 and repurposing of FDA approved antiviral drugs as dual inhibitors, *Gene Reports*. 2 (2020) 100860. <https://doi.org/https://doi.org/10.1016/j.genrep.2020.100860>.
- [74] R. Nandi, D. Bhowmik, R. Srivastava, A. Prakash, D. Kumar, Discovering potential inhibitors against SARS-CoV-2 by targeting Nsp13 Helicase, *J. Biomol. Struct. Dyn.* 40 (2022) 12062–12074. <https://doi.org/10.1080/07391102.2021.1970024>.
- [75] N. Mehyar, A. Mashhour, I. Islam, H.A. Alhadrami, A.M. Tolah, B. Alghanem, S. Alkhaldi, B.A. Somaie, M. Al Ghobain, Y. Alobaida, A.S. Alaskar, M. Boudjelal, Discovery of Zafirlukast as a novel SARS-CoV-2 helicase inhibitor using in silico modelling and a FRET-based assay, *SAR QSAR Environ. Res.* 32 (2021) 963–983. <https://doi.org/10.1080/1062936X.2021.1993995>.
- [76] N. Drayman, K.A. Jones, S.-A. Azizi, H.M. Froggatt, K. Tan, N.I. Maltseva, S. Chen, V. Nicolaescu, S. Dvorkin, K. Furlong, R.S. Kathayat, M.R. Firpo, V. Mastrodomenico, E.A. Bruce, M.M. Schmidt, R. Jedrzejczak, M.Á. Muñoz-Alía, B. Schuster, V. Nair, J.W. Botten, C.B. Brooke, S.C. Baker, B.C. Mounce, N.S. Heaton, B.C. Dickinson, A. Jaochimiak, G. Randall, S. Tay, Drug repurposing screen identifies masitinib as a 3CLpro inhibitor that blocks replication of SARS-CoV-2 in vitro., *BioRxiv Prepr. Serv. Biol.* (2020) 1–32. <https://doi.org/10.1101/2020.08.31.274639>.
- [77] PROTEIN DATA BANK, (n.d.). https://www.wwpdb.org/pdb?id=pdb_00005rly.
- [78] M. Renda, M. Barreca, A. Borrelli, V. Spanò, A. Montalbano, M.V. Raimondi, R. Bivacqua, I. Musante, P. Scudieri, D. Guidone, M. Buccirosi, M. Genovese, A. Venturini, T. Bandiera, P. Barraja, L.J.V. Galiotta, Novel tricyclic pyrrolo-quinolines as pharmacological correctors of the mutant CFTR chloride channel, *Sci. Rep.* 13 (2023) 7604. <https://doi.org/10.1038/s41598-023-34440-0>.

- [79] M. Barreca, A.M. Ingarra, M.V. Raimondi, V. Spanò, A.P. Piccionello, M. De Franco, L. Menilli, V. Gandin, G. Miolo, P. Barraja, A. Montalbano, New tricyclic systems as photosensitizers towards triple negative breast cancer cells, *Arch. Pharm. Res.* 45 (2022) 806–821. <https://doi.org/10.1007/s12272-022-01414-1>.
- [80] I. Frasson, V. Spanò, S. Di Martino, M. Nadai, F. Doria, B. Parrino, A. Carbone, S.M. Cascioferro, P. Diana, G. Cirrincione, M. Freccero, P. Barraja, S.N. Richter, A. Montalbano, Synthesis and photocytotoxic activity of [1,2,3]triazolo[4,5-h][1,6]naphthyridines and [1,3]oxazolo[5,4-h][1,6]naphthyridines, *Eur. J. Med. Chem.* 162 (2019) 176–193. <https://doi.org/10.1016/j.ejmech.2018.10.071>.
- [81] L. Chan, H. Jin, T. Stefanac, J.F. Lavallée, G. Falardeau, W. Wang, J. Bédard, S. May, L. Yuen, Discovery of 1,6-Naphthyridines as a Human Cytomegalovirus Inhibitors, *J. Med. Chem.* 42 (1999) 3023–3025. <https://doi.org/10.1021/jm9902483>.
- [82] L. Chan, T. Stefanac, J.F. Lavallée, H. Jin, J. Bédard, S. May, G. Falardeau, Design and synthesis of new potent human cytomegalovirus (HCMV) inhibitors based on internally hydrogen-bonded 1,6-naphthyridines, *Bioorganic Med. Chem. Lett.* 11 (2001) 103–105. [https://doi.org/10.1016/S0960-894X\(00\)00607-7](https://doi.org/10.1016/S0960-894X(00)00607-7).
- [83] G. Falardeau, H. Lachance, A. St-Pierre, C.G. Yannopoulos, M. Drouin, J. Bédard, L. Chan, Design and synthesis of a potent macrocyclic 1,6-naphthyridine anti-human cytomegalovirus (HCMV) inhibitors, *Bioorganic Med. Chem. Lett.* 15 (2005) 1693–1695. <https://doi.org/10.1016/j.bmcl.2005.01.050>.
- [84] L. Zhuang, J.S. Wai, M.W. Embrey, T.E. Fisher, M.S. Egbertson, L.S. Payne, J.P. Guare, J.P. Vacca, D.J. Hazuda, P.J. Felock, A.L. Wolfe, K.A. Stillmock, M. V Witmer, G. Moyer, W.A. Schleif, L.J. Gabryelski, Y.M. Leonard, J.J. Lynch, S.R. Michelson, Design and Synthesis of 8-Hydroxy-[1,6]Naphthyridines as Novel Inhibitors of HIV-1 Integrase in Vitro and in Infected Cells, *J. Med. Chem.* 46 (2003) 453–456. <https://doi.org/10.1021/jm025553u>.
- [85] M.W. Embrey, J.S. Wai, T.W. Funk, C.F. Homnick, D.S. Perlow, S.D. Young, J.P. Vacca, D.J. Hazuda, P.J. Felock, K.A. Stillmock, M. V. Witmer, G. Moyer, W.A. Schleif, L.J. Gabryelski, L. Jin, I.W. Chen, J.D. Ellis, B.K. Wong, J.H. Lin, Y.M. Leonard, N.N. Tsou, L. Zhuang, A series of 5-(5,6)-dihydrouracil substituted 8-hydroxy-[1,6]naphthyridine- 7-carboxylic acid 4-fluorobenzylamide inhibitors of HIV-1 integrase and viral replication in

cells, *Bioorganic Med. Chem. Lett.* 15 (2005) 4550–4554. <https://doi.org/10.1016/j.bmcl.2005.06.105>.

- [86] A.C. Puhl, G.F. Gomes, S. Damasceno, A.S. Godoy, G.D. Noske, A.M. Nakamura, V.O. Gawriljuk, R.S. Fernandes, N. Monakhova, O. Riabova, T.R. Lane, V. Makarov, F.P. Veras, S.S. Batah, A.T. Fabro, G. Oliva, F.Q. Cunha, J.C. Alves-Filho, T.M. Cunha, S. Ekins, Pyronaridine Protects against SARS-CoV-2 Infection in Mouse, *ACS Infect. Dis.* 8 (2022) 1147–1160. <https://doi.org/10.1021/acsinfecdis.2c00091>.
- [87] R. Bivacqua, I. Romeo, M. Barreca, P. Barraja, S. Alcaro, A. Montalbano, HSV-1 Glycoprotein D and Its Surface Receptors: Evaluation of Protein–Protein Interaction and Targeting by Triazole-Based Compounds through In Silico Approaches, *Int. J. Mol. Sci.* 24 (2023) 7092. <https://doi.org/10.3390/ijms24087092>.
- [88] A.O. Adedeji, B. Marchand, A.J.W. Te Velthuis, E.J. Snijder, S. Weiss, R.L. Eoff, K. Singh, S.G. Sarafianos, Mechanism of nucleic acid unwinding by SARS-CoV helicase., *PLoS One.* 7 (2012) e36521. <https://doi.org/10.1371/journal.pone.0036521>.
- [89] F.S. Dawood, A.D. Iuliano, C. Reed, M.I. Meltzer, D.K. Shay, P.Y. Cheng, D. Bandaranayake, R.F. Breiman, W.A. Brooks, P. Buchy, D.R. Feikin, K.B. Fowler, A. Gordon, N.T. Hien, P. Horby, Q.S. Huang, M.A. Katz, A. Krishnan, R. Lal, J.M. Montgomery, K. Mølbak, R. Pebody, A.M. Presanis, H. Razuri, A. Steens, Y.O. Tinoco, J. Wallinga, H. Yu, S. Vong, J. Bresee, M.A. Widdowson, Estimated global mortality associated with the first 12 months of 2009 pandemic influenza A H1N1 virus circulation: A modelling study, *Lancet Infect. Dis.* 12 (2012) 687–695. [https://doi.org/10.1016/S1473-3099\(12\)70121-4](https://doi.org/10.1016/S1473-3099(12)70121-4).
- [90] E.B. Lőrincz, M. Herczeg, J. Houser, M. Rievajová, Á. Kuki, L. Malinovská, L. Naesens, M. Wimmerová, A. Borbás, P. Herczegh, I. Bereczki, Amphiphilic Sialic Acid Derivatives as Potential Dual-Specific Inhibitors of Influenza Hemagglutinin and Neuraminidase, *Int. J. Mol. Sci.* 24 (2023) 17268. <https://doi.org/10.3390/ijms242417268>.
- [91] Z. Chen, Q. Cui, M. Caffrey, L. Rong, R. Du, Small molecule inhibitors of influenza virus entry, *Pharmaceuticals.* 14 (2021) 587. <https://doi.org/10.3390/ph14060587>.
- [92] R.F. Nuwarda, A.A. Alharbi, V. Kayser, An overview of influenza viruses and vaccines, *Vaccines.* 9 (2021) 1032. <https://doi.org/10.3390/vaccines9091032>.

- [93] E. De Clercq, Antiviral agents active against influenza A viruses, *Nat. Rev. Drug Discov.* 5 (2006) 1015–1025. <https://doi.org/10.1038/nrd2175>.
- [94] J. Beigel, M. Bray, Current and future antiviral therapy of severe seasonal and avian influenza, *Antiviral Res.* 78 (2008) 91–102. <https://doi.org/10.1016/j.antiviral.2008.01.003>.
- [95] F.G. Hayden, N. Sugaya, N. Hirotsu, N. Lee, M.D. de Jong, A.C. Hurt, T. Ishida, H. Sekino, K. Yamada, S. Portsmouth, K. Kawaguchi, T. Shishido, M. Arai, K. Tsuchiya, T. Uehara, A. Watanabe, Baloxavir Marboxil for Uncomplicated Influenza in Adults and Adolescents, *N. Engl. J. Med.* 379 (2018) 913–923. <https://doi.org/10.1056/nejmoa1716197>.
- [96] DRUGBANK, (n.d.). <https://go.drugbank.com/drugs/DB13609>.
- [97] R.U. Kadam, I.A. Wilson, Structural basis of influenza virus fusion inhibition by the antiviral drug Arbidol, *Proc. Natl. Acad. Sci. U. S. A.* 114 (2017) 206–214. <https://doi.org/10.1073/pnas.1617020114>.
- [98] QikProp software version 6.2, Schrödinger, LLC, New York, NY, 2019.pdf, (n.d.).
- [99] M. Hu, J. Li, S.Q. Yao, In situ “click” assembly of small molecule matrix metalloprotease inhibitors containing zinc-chelating groups, *Org. Lett.* 10 (2008) 5529–5531. <https://doi.org/10.1021/ol802286g>.
- [100] Z.-C. Dai, Y.-F. Chen, M. Zhang, S.-K. Li, T.-T. Yang, L. Shen, J.-X. Wang, S.-S. Qian, H.-L. Zhu, Y.-H. Ye, Synthesis and Antifungal Activity of 1,2,3-Triazole Phenylhydrazone Derivatives, *Org. Biomol. Chem.* 13 (2015) 477–486. <https://doi.org/10.1039/c0xx00000x>.
- [101] H. Kawai, T. Takeda, K. Fujiwara, T. Suzuki, Isolation and low-temperature X-ray analysis of intramolecular triarylmethane-triarylmethyl cation complex: Preference for a C-H-bridged unsymmetric structure exhibiting a facile 1,5-hydride shift and charge-transfer interaction, *J. Am. Chem. Soc.* 127 (2005) 12172–12173. <https://doi.org/10.1021/ja053161h>.
- [102] D.B. Kendre, R.B. Toche, M.N. Jachak, Synthesis of novel dipyrazolo[3,4-b:3,4-d]pyridines and study of their fluorescence behavior, *Tetrahedron.* 63 (2007) 11000–11004. <https://doi.org/10.1016/j.tet.2007.08.052>.

7. Project in collaboration with the Rega Institute for Medical Research: “Effect of combination therapy of pritelivir or amenamevir with acyclovir or foscarnet on HSV-2 drug resistance evolution.”

7.1 Introduction

Herpesviridae is a large family of enveloped double-stranded DNA viruses that includes nine human herpesviruses (HHV) divided into three subfamilies: *alphaherpesvirinae* [herpes simplex virus 1 (HSV-1) and 2 (HSV-2) and varicella-zoster virus (VZV)]; *betaherpesvirinae* [cytomegalovirus (CMV), HHV-6A, HHV-6B and HHV-7]; and *gammaherpesvirinae* [Epstein-Barr virus (EBV) and HHV-8] [1]. All herpesviruses are able to establish latent infections that can be reactivated by endogenous or exogenous stimuli, causing clinical symptoms [2]. Herpesvirus infection of the central nervous system (CNS) can also result in long-term neurologic consequences and have recently been related to the onset of neurodegenerative diseases such as Alzheimer’s disease [3]. HSV infections (i.e., HSV-1 and HSV-2) are responsible for a variety of clinical symptoms. They are both responsible for genital herpes, although HSV-1 mostly causes oral infections and is often acquired during childhood [4] while HSV-2 is mainly responsible for genital herpes. HSV infections are associated less frequently with keratitis, encephalitis, and meningitis, and systemic disease in neonates and immunocompromised patients [5,6].

HSV-2 is a prototypical *alphaherpesvirus* with a 154,000 bp genome, located into an icosahedral capsid that is surrounded by a lipid bilayer characterized by the presence of several glycoproteins and transmembrane proteins. Another relevant structure is the tegument, located between the capsid and the envelope, which contains proteins playing an important role in the early stages of viral replication [3].

HSV-2 replication (Figure 1) occurs through a lytic cycle that begins with the entry of the virus into the host cell, a complex process mediated by the interaction of different viral envelope glycoproteins with specific host membrane cell receptors [7]. Attachment to the host cell membrane begins with the interaction of gB and gC with cell surface heparan sulfate (HS) proteoglycans, which brings the virus closer to the cell [8,9]. The binding of gD to one of the specific cellular receptors and the consequent conformational change that occurs in the structure of gD trigger a cascade of events that promote the formation of the core fusion machinery with

gB and the gH/gL complex that allows the virus entry [10]. After fusion, the tegument proteins bind to cytoskeleton microtubules, allowing transport of the capsid to the nucleus where viral DNA is released, and transcription and replication takes place. The HSV lytic cycle can be divided into three phases, characterized by the expression of viral genes that are translated at different time-points of infection: phase α or immediate early (IE), phase β or early (E) and phase γ or late (L). During the IE phase, α proteins that are responsible for the initiation of infection are produced. The E phase produces β proteins, including enzymes involved in viral DNA replication. Finally, the L phase produces structural proteins (γ) of the virion and other proteins responsible for the assembly of the viral particles. Within the β group, several proteins play a crucial role during HSV-2 replication, including viral DNA polymerase complex, composed by the catalytic subunit (encoded by the UL30 gene) and its processivity factor (encoded by UL42 gene), and the helicase-primase complex, encoded by UL5, UL8 and UL52 genes. HSV also encodes for non-essential E proteins involved in nucleotide metabolism, such as the thymidine kinase (TK, encoded by the UL23 gene). Viral proteins are synthesized by host cell ribosomes and processed using cellular enzymes and pathways, but the virus also encodes enzymes like proteases. Viral capsids assembly and genome packaging takes place in the nucleus and is followed by egress. The virion is formed through a complex multi-step process that also involves the Golgi apparatus and ends with the release of enveloped viruses from the cell through an exocytic mechanism.

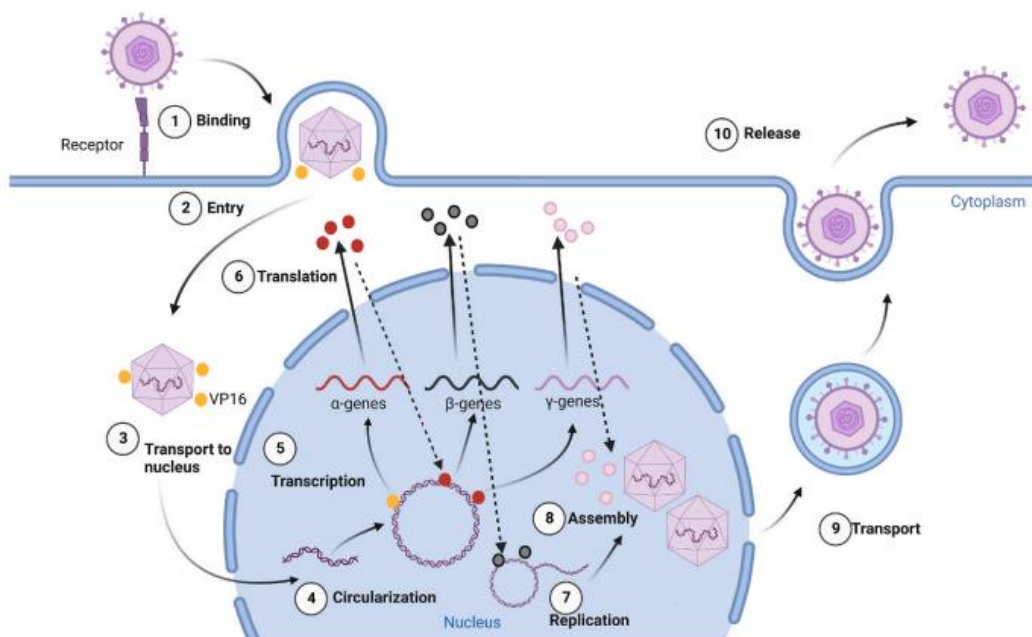


Figure 1. HSV life cycle [11]

All antiviral agents currently approved for the treatment of HSV-2 infections target viral DNA synthesis by inhibiting viral DNA polymerase (DP) [12] and include acyclovir (ACV) with its pro-drug valacyclovir (VACV), penciclovir (PCV) and its prodrug famciclovir (FCV), cidofovir (CDV) and foscarnet (PFA) (Figure 2). ACV, one of the first antiviral drugs used in the treatment of HSV infections, is a nucleoside analogue of 2'-deoxyguanosine that lacks the 3'-OH group and needs to be activated inside the cell through three subsequent phosphorylation reactions. The first phosphorylation step is performed by the virus-encoded TK. Since ACV is a poor substrate for cellular TK, this reaction occurs more efficiently in infected cells than in healthy ones [13,14]. Thereafter, two other phosphorylation steps are carried out by host cellular guanosine monophosphate kinase and nucleoside diphosphate kinase, to obtain the active triphosphate form of ACV [15,16]. Acyclovir triphosphate (ACV-TP) acts as a substrate for the viral DNA polymerase by competing with deoxyguanosine triphosphate (dGTP) for incorporation into the elongating DNA chain. Due to the absence of the 3'-OH group, ACV interrupts the elongation of the DNA chain, thereby blocking viral replication [17]. The high selectivity of ACV can be explained firstly by its affinity for viral TK; furthermore, ACV-TP is recognized and incorporated into the elongating DNA chain more efficiently by HSV DNA polymerase than by cellular polymerases [18]. Unfortunately, prolonged use of ACV has led to the development of resistant HSV strains, especially in immunocompromised patients. The onset of resistance appears to be mainly related to the acquisition of mutations in the viral TK, which in turn leads to reduced phosphorylation of the drug, but it can also occur due to an alteration of viral DNA polymerase, which therefore shows a lower binding capacity to ACV [19].

CDV is a nucleotide analogue that acts by blocking the viral DNA polymerase after being activated by cellular kinases through two consecutive phosphorylation steps. Intravenous administration is used to treat HCMV retinitis in patients with AIDS, but since its activity is not dependent on viral TK, it can also be used off-label to treat ACV- and/or PFA-resistant HSV infections. The use of CDV is complicated by the occurrence of side effects such as nephrotoxicity and impaired kidney function [20].

Foscarnet (phosphonoformic acid, PFA) is a pyrophosphate analogue that directly inhibits the DNA polymerase activity by blocking the pyrophosphate binding site. By interfering with the cleavage of pyrophosphate on the elongating DNA chain, PFA prevents the binding of new nucleotides and thus terminates replication. Since PFA does not require any phosphorylation by the viral TK, it can be used to treat ACV-resistant HSV infections with TK gene mutations. Unfortunately, the use of PFA is limited due to its poor bioavailability, requiring intravenous administration, as well as the frequent occurrence of nephrotoxicity and the development of

mutations in the viral DP that cause cross-resistance to PFA and ACV [21–23]. Both the emergence of drug-resistant viral strains, and drug toxicity issues, increase the need for new antiviral agents acting with different mechanisms of action from those currently in use.

In this context, a promising target for the development of antiviral agents is represented by the helicase-primase complex, which plays a crucial role in viral replication. It is involved in the unwinding of the double-stranded DNA and in the production of primers needed by the viral DNA polymerase to initiate DNA synthesis (Figure 2) [24]. Pritelivir (PTV) and amenamevir (AMV) are helicase-primase inhibitors currently under clinical evaluation for the treatment of HSV infections. PTV shows high activity against HSV-1 and HVS-2 [25,26], and a phase III trial evaluating its efficacy and safety for the treatment of ACV-resistant mucocutaneous HSV infections in immunocompromised subjects is currently ongoing (NCT03073967). AMV is highly active against HSV-1, HSV-2 and VZV, and is approved in Japan for the treatment of herpes zoster, caused by VZV [27]. AMV completed a phase III clinical trial assessing its efficacy and safety in patients with recurrent HSV infections (NCT01959295).

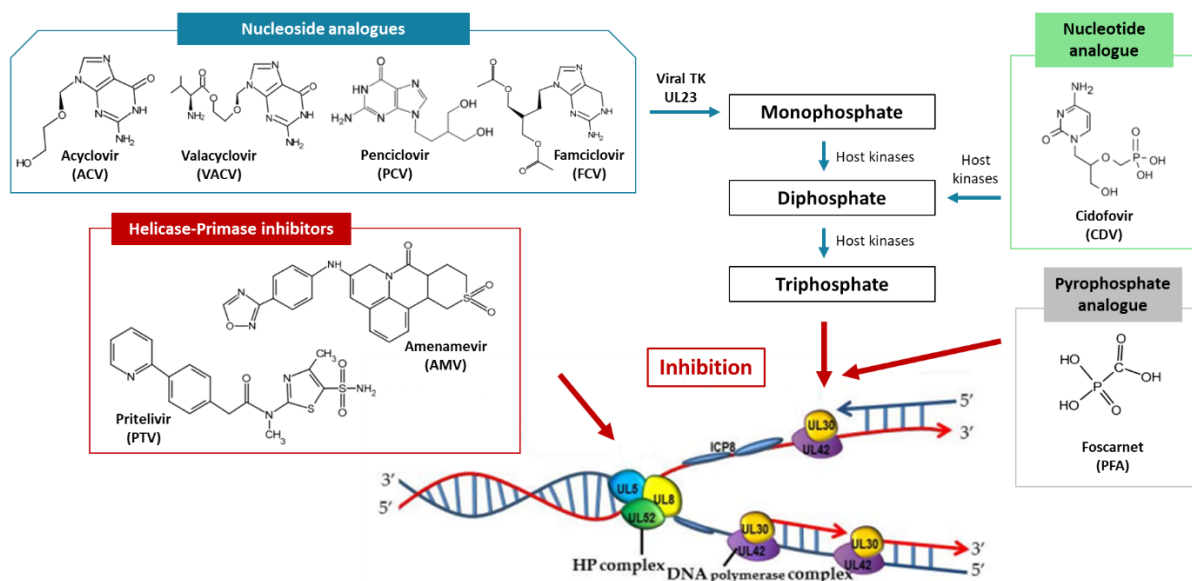


Figure 2. Treatment options for HSV-2 infections (created with BioRender.com). Nucleoside, nucleotide and pyrophosphate analogues are currently in use, while helicase-primase inhibitors are not yet approved

An interesting strategy to prevent the emergence of drug-resistant viral strains is to combine multiple drugs with different mechanisms of action. Several *in vitro* studies revealed a

synergistic and/or additive effect when a helicase-primase inhibitor (AMV or PTV) is administered in combination with ACV or other nucleoside derivatives [27–29]. Considering that Prof. Graciela Andrei's research group has recently found that the use of PTV in combination with ACV or PFA delays or prevents the acquisition of HSV-1 drug resistance *in vitro*, we decided to evaluate the effect of combination therapy of PTV and AMV with ACV or PFA on HSV-2 drug resistance evolution. In particular, our aim was to assess whether these drug combination therapies hinder acquisition of drug resistance in HSV-2 infections.

7.2 Experimental

7.2.1 Cells and viruses

Human embryonic lung (HEL) fibroblasts were cultured in Dulbecco's Modified Eagle's Medium (DMEM) supplemented with 8% foetal bovine serum (FBS), 0.1 mM non-essential amino acids, 10 mM HEPES, 1 mM sodium pyruvate and 2 mM L-glutamine, at 37 °C in a 5% CO₂ humidified atmosphere. The HSV-2 strain G was used and virus stocks were prepared in HEL fibroblasts (DMEM supplemented with 2% FBS). Viral clones were plaque-purified by limiting dilution on HEL fibroblasts and viral concentration (50% cell culture infectious dose, CCID₅₀) was defined using the Reed and Muench method [30].

7.2.2 Compounds

The following compounds were used: acyclovir (ACV), ganciclovir (GCV), foscarnet (PFA), adefovir (PMEA), cidofovir (CDV), amenamevir (AMV), pritelivir (PTV) and trifluridine (TFT).

7.2.3 Drug susceptibility assays

Susceptibilities of viral clones to a panel of antiviral drugs were determined using cytopathic effect (CPE) reduction assays [31]. HEL fibroblasts were inoculated with 100 CCID₅₀ of virus and serial dilutions of antivirals were added 2 hours post-infection. The CPE was scored 72 hours post-infection and EC₅₀ values (concentration inhibiting 50% of virus growth) were calculated for each compound.

7.2.4 Drug resistance selection

The HSV-2 G strain was sequentially passaged in HEL fibroblasts under increasing amounts of one (ACV, PFA, AMV or PTV) or two (ACV+PTV, ACV+AMV, PFA+PTV or PFA+AMV) drugs, starting from a concentration equal to one- to two-fold the EC₅₀. Viruses were harvested by freeze-thawing when full virus cytopathic effect (CPE) was observed and used to infect fresh cell cultures. Drug concentrations were increased by 2-fold in each passage when full CPE was observed within 10 days post-infection (up to passage 5). From passage 5 onwards, drug concentrations were not further increased. In case full CPE was not observed 10 days post-infection, the medium was replaced with drug-free medium every 5 days until full CPE was observed, and this was followed by a passage where drug concentrations were not increased. Following 2, 5 and 10 passages, the virus cultures were genetically characterized by next-generation sequencing (NGS) for the detection of drug resistance mutations.

7.2.5 Sanger sequencing

DNA was extracted from viral clones (QIAamp DNA blood kit, Qiagen) and the UL23 (thymidine kinase), UL30 (DNA polymerase), UL5 (helicase), UL8 (helicase-primase complex associated protein) and UL52 (primase) genes were amplified in overlapping amplicons by PCR (Platinum SuperFi PCR Mastermix, Invitrogen), using M13-labelled primers. PCR products were purified using the QIAquick PCR purification kit (Qiagen) and sequenced (BigDye Terminator v3.1 kit, ThermoFisher) on the ABI3730 sequencer (ThermoFisher). Sequences were aligned using the SeqScape v2.7 software (ThermoFisher) [32]. All sequences were mapped to the HSV-2 strain G genome (GenBank accession number OM370995).

7.2.6 Next-generation sequencing (NGS)

Full UL23, UL5, UL8 and UL52 genes and partial UL30 genes were amplified by PCR, using the Platinum Superfi PCR Mastermix (Invitrogen). PCR products were purified [QIAquick PCR purification kit (Qiagen)], quantified [Qubit dsDNA HS Assay Kit on the Qubit®2.0 fluorometer (Thermo Fischer Scientific)] and used to prepare DNA libraries with 1 ng of DNA employing the Nextera XT DNA Sample Preparation Kit and Nextera XT DNA Sample Preparation IndexKit (Illumina). After purification with Agencourt® AMPure® XPbeads, the resulting barcoded libraries were normalized to a 2 nM concentration and pooled. 5% PhiX Control v3

library (12.5 pM; Illumina) was added to the libraries after the normalization step. The Miseq v.2 system (Illumina) was used to sequence the library pool [33]. Results were analysed with CLC genomics workbench 12 (Qiagen). Reads were mapped to the HSV-2 strain G sequence (GenBank accession number OM370995), and the low-frequency variant detection tool was used to detect variants with a frequency >1%.

7.3 Results and discussion

7.3.1 PCR primer design & PCR optimization

In order to amplify the viral DNA to check for mutations, we started by designing the primers for UL5 and UL52 genes using the <http://primer3plus.com/cgi-bin/dev/primer3plus.cgi> website. UL23, UL30 and UL8 primers were already available at the laboratory (Table 1). Multiple primer pairs were designed, each amplifying 500-600 bp overlapping fragments to enable full coverage of the genes. For a good primer design, there are some parameters that should be respected to increase the chances of success in terms of specificity of binding at sensible annealing temperatures. In general, most primers require an annealing temperature between 50–65 °C. The annealing temperature is normally set at 2-5 °C below the melting temperature (T_m), defined as the temperature at which 50% of primers molecules will be disassociated from the parent strand at any time point. In optimal conditions, primers should contain about 18-22 bases and have a 50–60% GC content, thus resulting in an average T_m of about 60 °C. Runs of 3 or more of the same bases (particularly G and C) or consecutive G's should be avoided. In addition, primer pairs should have T_m 's within 2 °C from each other. To select the best primers, it is also necessary to screen for secondary structures (i.e. hairpin loops), self-dimerization or hetero-dimer formation, that could decrease the amplification efficiency.

Table 1. List of primers used for DNA amplification and Sanger sequencing. Primers used for gene amplification for next-generation sequencing are reported in bold.

Amplicon	Forward primer 5'-3'	Reverse primer 5'-3'
UL5-A	CCATCTGCCCGAGGAGAATC	CCCCCGAGAGCTTAACGTAC
UL5-B	AAAGAGTACGTGCGTGCAGA	GGTGTGGTACAGGGCGTTAA
UL5-C	CACCCGCAGCAACATTATCG	CCTCCTTGTGGGACGAGAAC
UL5-D	CACATGCAGTTTGTGGACCG	GGGCGCTGGAGAAAGTTGTA
UL5-E	GACAGCTTCGTGAAGACCA	CCCCATCAGCGTGTAGTTGT
UL5-F	AGCACCTACGTGGACAATGT	GCGAGGGAATGGAGGGTTAA

UL5-G	GACTACGGCATCAGCTCCAA	TGTTGTATCACCACGCCTCC
UL5-F2	AATGTCATCTTCCGGGGCTG	GTGATGTAGGCTGTACGCGA
UL52-A	GCGGCCCGAATCATCTCATA	CACGGTGAGAGCCATGATGA
UL52-B	CAACTCTGGACTTGGAGGCG	GTGGGCCAGGTAGATGTACG
UL52-C	CGCTGGAGAAGTTCATCGCC	AGCTTGAGGAGGCGCTTGA
UL52-D	GCAGAAAGGCTCCTAGTCCC	CTAAAGTGACCCAGGGCCTC
UL52-E	GATGTACGTGAACCGCAACG	CTTTACGTGGCTCCCTACGG
UL52-F	TTGTGCACGGCTCCCTGA	GATGCACGCGACTATTTGCC
UL52-G	GAGACCCTGACGGAGGTTCT	AATACATCGGTGGAGCGGAC
UL23-A	TAACAGCGTCAACAGCGTGCC	CCCGATATGAGGAGCCAGAACG
UL23-B	ACGCGGCGGTGGTAATGACA	CCAGGCAAACACGTTATACAGGTC
UL23-C	TGGCTATGCTGGCTGCGATTC	GAACAAACGACCCAACACCCG
UL30-A	CATCCCACCCCGAGCTGTTG	GACCCAGAAGCGTGATGACGG
UL30-B	ACCCACCGTCACCGTCTTC	CCAGGTTGTCCGCGCTGC
UL30-C	CCACCCGGTTTATCCTGGACAAC	ACCATCCCGTTCACCTTGATCTTG
UL30-D	TCTACAAGGTCCCCTCGACG	CCTCGTCGTCGTCCTTATCCTCG
UL30-E	GTTTCGGGGCCTCGACAAGG	CGAGCGGATCTGCTTTCGCA
UL30-F	ACCGGGACTACCTGGAGATCGAG	CTTGGCGATGAGCAGCAGCT
UL30-G	TGGGCGACAAGATGGCGAG	CCTTGATGGACGGGACCTGC
UL30-GH	GGTCGACCTGCTGTTTTACG	CGGTGATCTTGGCGTTATTT
UL30-H	GCAGGTCCCCTCCATCAAGG	CGTGGTCAGACGCAACGCAG
UL8-A	CTGACATCATTCTCGAGGCG	CGACGCCCTTTCGACCCTC
UL8-B	CTGTATGCGTGCGTTCTGG	ATCCCAGCACGGCAAAGTAT
UL8-C	ACCATCACGACGAGGACC	TGGAGCCCGGAGAAACAAAA
UL8-D	ACCATCCAATACTCGACCC	GATTCGTCTCAGCGCGTC
UL8-E	ATGACACCGACTTCCTGCAG	AGAAGAAAACCACAACCGGC

The best working conditions of each primer were found experimentally by performing a gradient PCR testing different annealing temperatures for each primer pair used to amplify the full UL23, UL30, UL5, UL8 and UL52 genes of the plaque-purified wild-type HSV-2 strain G. An annealing temperature of 62 °C was selected for all primer pairs and the UL5-F2 primer pair was used to replace both UL5-F and UL5-G.

7.3.2 Sanger sequencing analysis of wild-type HSV-2 strain G preceding antiviral pressure

Sanger sequencing of the plaque-purified wild-type HSV-2 strain G was performed without antiviral pressure to assess the homogeneity of viral population and to exclude the presence of minor variants. The selected viral clone was tested by Sanger sequencing to verify the wild-type genotype of UL23 (thymidine kinase), UL30 (DNA polymerase), UL5 (helicase), and UL52

(primase) genes. The presence of mutations in the UL8 protein was investigated solely by NGS. No mutations were detected in the UL5, UL23 and UL52 genes, while four known natural genetic polymorphisms linked to inter-strain variability (T801P, G904A, E905A and A906G) [23] were found for UL30, thus confirming that the selected viral clone had a wild-type genotype.

7.3.3 Next-generation sequencing (NGS) analysis of wild-type HSV-2 strain G preceding antiviral pressure

NGS performed on plaque-purified wild-type HSV-2 strain G revealed pre-existing minor variants in the UL30 [V657A (1.37%), R659L (1.73%), G660P (1.73%), E661P (1.73%), G662E (1.96%), E663A (2.40%)], UL52 [del T nt 1360 (1.64%), V456G (1.68%), D710V (2.11%)] and UL8 [del GC nts 136-137 (2.50%), E110G (2.27%), del T nt 1058 (3.93%), E433A (1.68%), del A nt 1463 (1.07%)] genes, all at a frequency below 5% (Table 2). No mutations were found for UL23 and UL5 genes. With the exception of the UL8 T deletion at nt 1058, detected at passage 10 under PTV pressure (5.16%), none of these pre-existing minor variants increased in frequency as a result of antiviral pressure during the resistance selection procedure, so they will not be considered in the following sections.

Table 2. Nucleotide (nt) and/or amino acid changes identified by next-generation sequencing (NGS) in the plaque-purified wild-type HSV-2 strain G.

Gene	Mutation	Frequency (%)
Thymidine kinase (UL23)	---	---
DNA polymerase (UL30)	V657A	1.37 ± 0.18
	R659L	1.73 ± 0.32
	G660P	1.73 ± 0.32
	E661P	1.73 ± 0.32
	G662E	1.96 ± 0.31
	E663A	2.40 ± 0.44
Helicase (UL5)	---	---
Helicase-primase complex associated protein (UL8)	del GC nts 136-137	2.50 ± 0.02
	E110G	2.27 ± 0.22
	del T nt 1058	3.93 ± 0.12
	E433A	1.68 ± 0.08
	del A nt 1463	1.07 ± 0.08
Primase (UL52)	Del T nt 1360	1.64 ± 0.33
	V456G	1.68 ± 0.35
	D710V	2.11 ± 0.24

7.3.4 Drug susceptibility assays

The susceptibility of the plaque-purified wild-type HSV-2 strain G to a panel of antiviral drugs was determined using the CPE reduction assays. Acyclovir (ACV), ganciclovir (GCV), trifluridine (TFT), cidofovir (CDV), adefovir (PMEA), foscarnet (PFA), pritelivir (PTV) and amenamevir (AMV) were used and EC₅₀ values were calculated for each compound (Table 3). Based on these EC₅₀ values, the starting concentrations (µg/mL) of the different drugs for the resistance selection procedure were established.

Table 3. Drug susceptibility of the plaque purified wild-type HSV-2 strain G to a panel of antiviral drugs.

Compound	EC₅₀ (µg/mL)
ACV	0.025
GCV	0.003
TFT	0.779
CDV	0.741
PMEA	15.784
PFA	34.950
PTV	0.038
AMV	0.025

7.3.5 Drug resistance selection

The HSV-2 G strain was passaged repeatedly in HEL fibroblasts under increasing amounts of one or two antiviral drugs. Eight different conditions were tested for the resistance selection procedure: 4 under monotherapy pressure (ACV, PFA, PTV or AMV) and 4 under combination therapy pressure (ACV+PTV, ACV+AMV, PFA+PTV or PFA+AMV), starting from a concentration equal to one- to two-fold the EC₅₀. Since CPE was not observed for ACV+AMV, PFA+PTV and PFA+AMV combinations, the resistance selection was initiated from lower concentration of both drugs corresponding to the EC₅₀ for all the combinations. The selection procedure initiated from lower drug concentrations will be referred to as “L” and the higher as “H”. The initial and final concentrations (in µg/mL) of the antivirals used during resistance selection as well as the total days in culture at passage 2, 5 and 10 are reported in Table 4.

Table 4. Initial and final concentrations (in $\mu\text{g/mL}$) of the antivirals used during resistance selection.

Condition	Initial concentration [$\mu\text{g/mL}$]	Passage 2		Passage 5		Passage 10	
		Final conc. [$\mu\text{g/mL}$]	Total days in culture	Final conc. [$\mu\text{g/mL}$]	Total days in culture	Final conc. [$\mu\text{g/mL}$]	Total days in culture
ACV	0.05	0.05	17	0.4	28	0.4	37
PFA	50	50	16	200	37	200	56
PTV	0.05	0.1	11	0.4	39	0.4	64
AMV	0.05	0.1	21	0.2	44	0.2	58
ACV+PTV ^H	0.05 + 0.05	0.05 + 0.05	26	0.2 + 0.2	52	N.P.	--
ACV+PTV ^L	0.025 + 0.025	0.05 + 0.05	20	0.2 + 0.2	43	N.P.	--
ACV+AMV ^L	0.025 + 0.025	0.05 + 0.05	30	N.P.	--	N.P.	--
PFA+PTV ^L	25 + 0.025	50 + 0.05	21	N.P.	--	N.P.	--
PFA+AMV ^L	25 + 0.025	N.P.	--	N.P.	--	N.P.	--

N.P.: not performed (experiments ongoing)

7.3.6 Next-generation sequencing (NGS) analysis of HSV-2 cultures following antiviral pressure

Following two, five or ten passages under antiviral pressure, virus cultures were genetically characterized by NGS to assess the emergence of resistance mutations. Some of these investigations are still ongoing.

Mutations emerged under monotherapy pressure. As reported in Table 5 and Figure 3, ACV pressure induced several resistance mutations in the TK gene: with the exception of the S182N (7.19%), only detected following 10 passages under antiviral pressure, all the other mutations (R221H, 50.35%; G insertion at nt 433, 14.31%; C insertion at nt 551, 19.92%) were already present at passage 5 and did not further increase in frequency at passage 10 (57.18%, 13.06% and 11.44% respectively). In the DP gene, the known genetic polymorphism D676G (33.58%) as well as two unknown substitutions (E672D, 36.04% and K674E, 31.21%) were detected at passage 5 under ACV pressure.

Following 10 passages under PFA pressure, the predominant mutations were the V719M (99.92%), which was already detected at passages 2 (61.14%) and 5 (99.98%), and the E930A (99.35%), that emerged at passage 5 (96.69%) but was not found at passage 2. Both mutations have not been previously described in literature, although the homologous V714M change in HSV-1 has been reported to confer drug resistance [23].

Virus cultured under PTV pressure developed two novel mutations in the helicase and primase: the V661I (81.70%), detected in UL5 gene at passage 5, which decreased in frequency at passage 10 (3.95%); and the A906T (98.73%) in the UL52 gene, solely detected with high frequency at passage 10.

In the AMV viral culture, two newly acquired substitutions were already detected at passage 2 in the UL5 (E399D, 3.82%) and UL52 (H913N, 9.01%) genes, which became predominant following 5 (85.29% and 97.52%) and 10 (99.95% and 99.93%) passages under antiviral pressure.

Mutations emerged under combination therapy pressure. Viruses cultured under ACV+PTV^H or ACV+PTV^L pressure developed a single mutation in the TK gene that was detected within two passages under combinatory pressure, while TK mutations emerged only at passage 5 under ACV monotherapy pressure (Figure 3 and Table 5). In the ACV+PTV^H viral culture the resistance mutation R223H was detected (34.68% and 96.43% at passage 2 and 5, respectively) and in the ACV+PTV^L culture, the G insertion at nt 433 was found (83.36% and 83.89% at passage 2 and 5, respectively). No mutations were detected in the DP, UL5 and UL52 genes of both ACV+PTV^H and ACV+PTV^L viral cultures up to passage 5. However, additional passaging under ACV+PTV combinatory pressure are still ongoing and the NGS sequencing will also be performed at passage 10.

After 2 passages under ACV+AMV pressure, apart from the C insertion at nt 551 (75.46%) in the TK gene (also detected under ACV monotherapy pressure), no other mutations were detected in the DP, UL5 and UL52 genes. The virus cultures PFA+PTV^L and PFA+AMV^L remained free of mutations at passage 2. However, additional passaging and NGS sequencing still has to be performed at passages 5 and 10 for both drug combinations as well as for ACV+AMV viral cultures.

Table 5. Frequency of nucleotide and/or amino acid changes emerging following 2, 5 or 10 passages under antiviral pressure.

Condition	Gene	Mutation	Frequency		
			Passage 2	Passage 5	Passage 10
ACV	TK	<i>G ins nt 433</i>	-	14.31 ± 0.32	13.06 ± 0.03
		<i>S182N</i>	-	-	7.19 ± 0.08
		<i>C ins nt 551</i>	-	19.92 ± 0.91	11.44 ± 0.34
		<i>R221H</i>	-	50.34 ± 0.52	57.18 ± 0.43
	DP	E672D	-	36.04 ± 0.63	34.27 ± 0.05

		K674E	-	31.21 ± 0.18	29.84 ± 0.09
		D676G	-	33.58 ± 0.77	32.07 ± 0.11
PFA	DP	V719M	61.14 ± 0.22	99.98 ± 0.01	99.92 ± 0.07
		E930A	-	96.69 ± 0.12	99.35 ± 0.01
PTV	UL5	V661I	-	81.70 ± 0.31	3.95 ± 0.28
	UL52	A906T	-	-	98.73 ± 0.18
	UL8	del T nt 1058	N.P.	N.P.	5.16 ± 1.03
AMV	UL5	E399D	3.82 ± 0.30	85.29 ± 0.17	99.95 ± 0.01
	UL52	H913N	9.01	97.52 ± 0.06	99.93 ± 0.02
	UL8	-	N.P.	N.P.	-
ACV+PTV^H	TK	<i>R223H</i>	34.68 ± 1.58	96.43 ± 0.28	N.P.
	DP	-	-	-	N.P.
	UL5	-	-	-	N.P.
	UL52	-	-	-	N.P.
	UL8	-	N.P.	N.P.	N.P.
ACV+PTV^L	TK	<i>G ins nt 433</i>	83.36 ± 0.02	83.89 ± 0.32	N.P.
	DP	-	-	-	N.P.
	UL5	-	-	-	N.P.
	UL52	-	-	-	N.P.
	UL8	-	N.P.	N.P.	N.P.
ACV+AMV^L	TK	<i>C ins nt 551</i>	75.46 ± 0.57	N.P.	N.P.
	DP	-	-	N.P.	N.P.
	UL5	-	-	N.P.	N.P.
	UL52	-	-	N.P.	N.P.
	UL8	-	N.P.	N.P.	N.P.
PFA+PTV^L	DP	-	-	N.P.	N.P.
	UL5	-	-	N.P.	N.P.
	UL52	-	-	N.P.	N.P.
	UL8	-	N.P.	N.P.	N.P.
PFA+AMV^L	DP	-	-	N.P.	N.P.
	UL5	-	-	N.P.	N.P.
	UL52	-	-	N.P.	N.P.
	UL8	-	N.P.	N.P.	N.P.

'L': refers to the lower initial drug concentration and 'H' to the highest one. The same antiviral concentrations were used from passage 5 onwards. Mutations for which the frequency did not exceed 5% at passages 2, 5 and/or 10 are not included. **Bold**: novel amino acid change with an unknown effect on drug susceptibility. *Italics*: known drug-resistance mutation [34,35]. **Green**: known genetic polymorphism. N.P.: not performed.

The chronological appearance of mutations detected under monotherapy and combination therapy pressure is depicted in Figure 3.

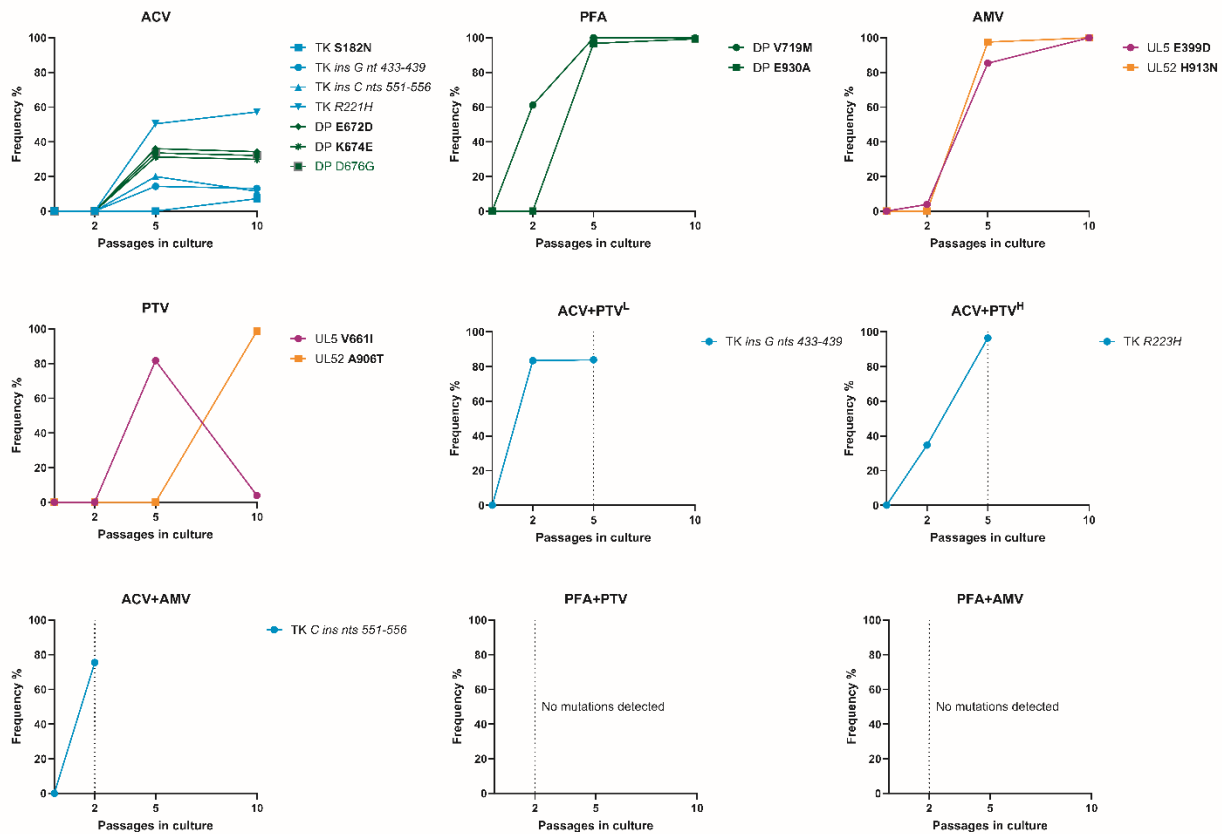


Figure 3. Chronological appearance of resistance mutations under monotherapy and combination therapy pressure. The frequency (%) of mutations was defined following passage 2, 5, and 10 using Next-generation Sequencing. ACV+PTV^L and ACV+PTV^H were cultured for five passages, while ACV+AMV, PFA+PTV and PFA+AMV were cultured for two passages (until dotted line). Changes detected in the viral thymidine kinase (TK) are marked in blue, in the DNA polymerase (DP) in green, in the helicase (UL5) in purple, in the primase (UL52) in orange. Changes detected in the viral helicase-primase complex associated protein (UL8) are not shown. **Bold:** novel amino acid change with unknown effect on drug susceptibility. *Italics:* known drug-resistance mutations [34,35]. **Green:** known genetic polymorphism.

Several novel mutations with unknown effect on drug susceptibility emerged in the viral DNA polymerase (E672D, K674E, V719M, E930A), helicase (E399D, V661D) and primase (A906T and H913N) during the resistance selection procedure. Though the fact that they emerged and increased in frequency under antiviral pressure suggests that they confer drug resistance, further investigations are needed to confirm this. Viral clones will be isolated from the virus cultures selected under monotherapy and combination therapy pressure by limiting dilution to obtain

mutant strains harboring novel mutations. Finally, the drug susceptibility profiles of these selected viral clones will be evaluated using the CPE reduction assays to investigate if the previously undescribed mutations detected during the current study could be linked to drug resistance.

7.4 Conclusions

In the present study, we investigated the effect of combination therapy of a helicase-primase inhibitor (AMV or PTV) with the nucleoside derivative ACV or the pyrophosphate analogue PFA, both targeting viral DNA polymerase, on HSV-2 inhibition and drug-resistance emergence. Indeed, combining multiple drugs with different mechanisms of action is considered a promising strategy to prevent the emergence of drug-resistant viral strains and reduce the occurrence of side effects related to each drug.

In our investigation, wild-type HSV-2 strain G was passaged repeatedly under increasing amount of one (ACV, PFA, PTV or AMV) or two drugs (ACV+PTV, ACV+AMV, PFA+PTV or PFA+AMV). NGS of the UL23 (thymidine kinase, TK), UL30 (DNA polymerase, DP), UL5 (helicase), UL8 (helicase-primase complex associated protein) and UL52 (primase) genes were used to genetically characterize the viral cultures emerged following two, five or ten passages under antiviral pressure.

Based on the results obtained, all the antivirals induced genetic substitutions within 10 passages when used in a monotherapy regimen. These changes included known ACV-resistance TK mutations (G ins at nt 433, S182N, C ins at nt 551 and R221H) as well as novel substitutions in the DP (ACV-induced E672D and K674E; PFA-induced V719M and E930A), UL5 (PTV-induced V661I and AMV-induced E399D) and UL52 (PTV-induced A906T and AMV-induced H913N) genes. Drug susceptibility testing of these novel mutants is necessary to confirm if these changes are involved in the development of drug-resistance. The combination pressure of ACV and PTV resulted in the acquisition of ACV resistance due to the appearance of mutations in viral TK but prevented the emergence of PTV resistance. The same behaviour was observed under ACV and AMV combinatory pressure, though the resistance selection for this drug combination was only continued for two passages. The absence of mutations in both the PFA+PTV and PFA+AMV viral cultures suggests that these combinations may be successful in preventing the emergence of drug resistance, although further passages are needed to confirm

this hypothesis. Viral clones bearing the newly identified mutations will be isolated, genotyped and phenotypically characterized to check for drug-resistance acquisition. Furthermore, synergistic effects of these drug combinations will be evaluated by virus yield inhibition assays.

Overall, these findings highlight the potential therapeutic use of combination therapies of DNA polymerase inhibitors with helicase-primase complex inhibitors as a valuable strategy to prevent the emergence of drug-resistant viral strains, representing a promising starting point for further investigations in the antiviral field.

7.5 References

- [1] C. Gilbert, J. Bestman-Smith, G. Boivin, Resistance of herpesviruses to antiviral drugs: Clinical impacts and molecular mechanisms, *Drug Resist. Updat.* 5 (2002) 88–114. [https://doi.org/10.1016/S1368-7646\(02\)00021-3](https://doi.org/10.1016/S1368-7646(02)00021-3).
- [2] C.P.P. De Mello, D.C. Bloom, I.C.N.P. Paixão, Herpes simplex virus type-1: Replication, latency, reactivation and its antiviral targets, *Antivir. Ther.* 21 (2016) 277–286. <https://doi.org/10.3851/IMP3018>.
- [3] K. Szczubiałka, K. Pyrc, M. Nowakowska, In search for effective and definitive treatment of herpes simplex virus type 1 (HSV-1) infections, *RSC Adv.* 6 (2016) 1058–1075. <https://doi.org/10.1039/c5ra22896d>.
- [4] R. Gupta, T. Warren, A. Wald, Genital herpes, *Lancet.* 370 (2007) 2127–2137. [https://doi.org/10.1016/S0140-6736\(07\)61908-4](https://doi.org/10.1016/S0140-6736(07)61908-4).
- [5] J. Wu, H. Power, M. Miranda-Saksena, P. Valtchev, A. Schindeler, A.L. Cunningham, F. Dehghani, Identifying HSV-1 Inhibitors from Natural Compounds via Virtual Screening Targeting Surface Glycoprotein D, *Pharmaceuticals.* 15 (2022) 361. <https://doi.org/10.3390/ph15030361>.
- [6] R. Whitley, J. Baines, Clinical management of herpes simplex virus infections: Past, present, and future., *F1000Research.* 7 (2018). <https://doi.org/10.12688/F1000RESEARCH.16157.1>.
- [7] S.A. Connolly, J.O. Jackson, T.S. Jardetzky, R. Longnecker, Fusing structure and function: a structural view of the herpesvirus entry machinery, *Nat. Rev. Microbiol.* 9 (2011) 369–

381. <https://doi.org/10.1038/nrmicro2548>.
- [8] P.G. Spear, Herpes simplex virus: Receptors and ligands for cell entry, *Cell. Microbiol.* 6 (2004) 401–410. <https://doi.org/10.1111/j.1462-5822.2004.00389.x>.
- [9] E.E. Heldwein, C. Krummenacher, Entry of herpesviruses into mammalian cells, *Cell. Mol. Life Sci.* 65 (2008) 1653–1668. <https://doi.org/10.1007/s00018-008-7570-z>.
- [10] S.A. Connolly, T.S. Jardetzky, R. Longnecker, The structural basis of herpesvirus entry, *Nat. Rev. Microbiol.* 19 (2021) 110–121. <https://doi.org/10.1038/s41579-020-00448-w>.
- [11] G. Cantero-González, N. Alvarenga, M.M. Florentín-Pavía, P. Gonzalez-Maldonado, P.H. Sotelo, Antiviral activity of two *Acanthospermum* species against herpes simplex virus 1, *J. Ethnopharmacol.* 303 (2023) 115958. <https://doi.org/10.1016/j.jep.2022.115958>.
- [12] T.E. Antoine, P.J. Park, D. Shukla, Glycoprotein targeted therapeutics: A new era of anti-herpes simplex virus-1 therapeutics, *Rev. Med. Virol.* 23 (2013) 194–208. <https://doi.org/10.1002/rmv.1740>.
- [13] R.J. Whitley, D.W. Kimberlin, B. Roizman, STATE-OF-THE-ART CLINICAL ARTICLE: Herpes Simplex Viruses, *Clin. Infect. Dis.* 26 (1998) 541–555.
- [14] J.E. Reardon, T. Spector, Acyclovir: Mechanism of Antiviral Action and Potentiation by Ribonucleotide Reductase Inhibitors, *Adv. Pharmacol.* 22 (1991) 1–27.
- [15] W.H. Miller, R.L. Miller, Phosphorylation of acyclovir (acycloguanosine) monophosphate by GMP kinase., *J. Biol. Chem.* 255 (1980) 7204–7207. [https://doi.org/10.1016/s0021-9258\(20\)79686-9](https://doi.org/10.1016/s0021-9258(20)79686-9).
- [16] W.H. Miller, R.L. Miller, Phosphorylation of acyclovir diphosphate by cellular enzymes, *Biochem. Pharmacol.* 31 (1982) 3879–3884. [https://doi.org/10.1016/0006-2952\(82\)90305-7](https://doi.org/10.1016/0006-2952(82)90305-7).
- [17] J.E. Reardon, T. Spector, Herpes simplex virus type 1 DNA polymerase, *J. Biol. Chem.* 264 (1989) 7405–7411. [https://doi.org/10.1016/s0021-9258\(18\)83248-3](https://doi.org/10.1016/s0021-9258(18)83248-3).
- [18] D.H. King, P.D.C. Madera, History, pharmacokinetics, and pharmacology of acyclovir, *J. Am. Acad. Dermatol.* 18 (1988) 176–179.
- [19] A.J. Wagstaff, D. Faulds, K.L. Goa, Aciclovir: a reappraisal of its Antiviral Activity, Pharmacokinetic Properties and Therapeutic Efficacy, *Drugs.* 47 (1994) 153–205.

<https://doi.org/https://doi.org/10.2165/00003495-199447010-00009>.

- [20] T. Kopp, A. Geusau, A. Rieger, G. Stingl, Successful treatment of an aciclovir-resistant herpes simplex type 2 infection with cidofovir in an AIDS patient, *Br. J. Dermatol.* 147 (2002) 134–138. <https://doi.org/10.1046/j.1365-2133.2002.04747.x>.
- [21] J. Piret, G. Boivin, Antiviral Drugs Against Herpesviruses, in: *Antivir. Drug Discov. Dev. Adv. Exp. Med. Biol.*, 2021: pp. 1–30. https://doi.org/https://doi.org/10.1007/978-981-16-0267-2_1.
- [22] J. Piret, G. Boivin, Resistance of herpes simplex viruses to nucleoside analogues: Mechanisms, prevalence, and management, *Antimicrob. Agents Chemother.* 55 (2011) 459–472. <https://doi.org/10.1128/AAC.00615-10>.
- [23] G. Andrei, R. Snoeck, Herpes simplex virus drug-resistance: New mutations and insights, *Curr. Opin. Infect. Dis.* 26 (2013) 551–560. <https://doi.org/10.1097/QCO.000000000000015>.
- [24] Y. Sato, T. Suenaga, M. Kobayashi, N. Miyazaki, T. Suzuki, K. Ishioka, T. Suzutani, Characteristics of Helicase-Primase Inhibitor Amenamevir-Resistant Herpes Simplex Virus, *Antimicrob. Agents Chemother.* 65 (2021). <https://doi.org/https://doi.org/10.1128/AAC.00494-21>.
- [25] G. Kleymann, R. Fischer, U.A.K. Betz, M. Hendrix, W. Bender, U. Schneider, G. Handke, P. Eckenberg, G. Hewlett, V. Pevzner, J. Baumeister, O. Weber, K. Henninger, J. Keldenich, A. Jensen, J. Kolb, U. Bach, A. Popp, J. Mäben, I. Frappa, D. Haebich, O. Lockhoff, H. Rübsamen-Waigmann, New helicase-primase inhibitors as drug candidates for the treatment of herpes simplex disease, *Nat. Med.* 8 (2002) 392–398. <https://doi.org/10.1038/nm0402-392>.
- [26] A. Wald, L. Corey, B. Timmler, A. Magaret, T. Warren, S. Tyring, C. Johnston, J. Kriesel, K. Fife, L. Galitz, S. Stoelben, M.-L. Huang, S. Selke, H.-P. Stobernack, H. Ruebsamen-Schaeff, A. Birkmann, Helicase–Primase Inhibitor Pritelivir for HSV-2 Infection, *N. Engl. J. Med.* 370 (2014) 201–210. <https://doi.org/10.1056/nejmoa1301150>.
- [27] K. Chono, K. Katsumata, H. Suzuki, K. Shiraki, Synergistic activity of amenamevir (ASP2151) with nucleoside analogs against herpes simplex virus types 1 and 2 and varicella-zoster virus, *Antiviral Res.* 97 (2013) 154–160.

<https://doi.org/10.1016/j.antiviral.2012.12.006>.

- [28] Z.W. Greeley, N.J. Giannasca, M.J. Porter, B.J. Margulies, Acyclovir, cidofovir, and amenamevir have additive antiviral effects on herpes simplex virus TYPE 1, *Antiviral Res.* 176 (2020) 104754. <https://doi.org/10.1016/j.antiviral.2020.104754>.
- [29] D.C. Quenelle, A. Birkmann, T. Goldner, T. Pfaff, H. Zimmermann, S. Bonsmann, D.J. Collins, T.L. Rice, M.N. Prichard, Efficacy of pritelivir and acyclovir in the treatment of herpes simplex virus infections in a mouse model of herpes simplex encephalitis, *Antiviral Res.* 149 (2018) 1–6. <https://doi.org/10.1016/j.antiviral.2017.11.002>.
- [30] L.J. Reed, H. Muench, A simple method of estimating fifty per cent endpoints., *Am. J. Epidemiol.* 27 (1938) 493–497.
- [31] G. Andrei, P. Fiten, M. Froeyen, E. De Clercq, G. Opdenakker, R. Snoeck, DNA polymerase mutations in drug-resistant herpes simplex virus mutants determine in vivo neurovirulence and drug-enzyme interactions, *Antivir. Ther.* 12 (2007) 719–732. <https://doi.org/10.1177/135965350701200502>.
- [32] H.H. Schalkwijk, S. Gillemot, M. Reynders, D. Selleslag, G. Andrei, R. Snoeck, Heterogeneity and viral replication fitness of HSV-1 clinical isolates with mutations in the thymidine kinase and DNA polymerase, *J. Antimicrob. Chemother.* 77 (2022) 3153–3162. <https://doi.org/10.1093/jac/dkac297>.
- [33] G. Andrei, E. Van Loon, E. Lerut, J. Victoor, B. Meijers, B. Bammens, B. Sprangers, S. Gillemot, P. Fiten, G. Opdenakker, K. Lagrou, D. Kuypers, R. Snoeck, M. Naesens, Persistent primary cytomegalovirus infection in a kidney transplant recipient: Multi-drug resistant and compartmentalized infection leading to graft loss, *Antiviral Res.* 168 (2019) 203–209. <https://doi.org/10.1016/j.antiviral.2019.06.004>.
- [34] A. Sauerbrei, K. Bohn-Wippert, M. Kaspar, A. Krumbholz, M. Karrasch, R. Zell, Database on natural polymorphisms and resistance-related non-synonymous mutations in thymidine kinase and DNA polymerase genes of herpes simplex virus types 1 and 2, *J. Antimicrob. Chemother.* 71 (2016) 6–16. <https://doi.org/10.1093/jac/dkv285>.
- [35] M. Collot, C. Rouard, C. Brunet, H. Agut, D. Boutolleau, S. Burrel, High conservation of herpes simplex virus UL5/UL52 helicase-primase complex in the era of new antiviral therapies, *Antiviral Res.* 128 (2016) 1–6. <https://doi.org/10.1016/j.antiviral.2016.01.015>.

8. Project in collaboration with Net4Science: “HSV-1 Glycoprotein D and its surface receptors: evaluation of protein-protein interaction and targeting by triazole-based compounds through *in silico* approaches.”

8.1 Introduction

HSV infections are widely spread around the world, thus representing a considerable public health issue. Currently, antiviral drugs available for the treatment of herpesvirus act by terminating viral DNA synthesis through the inhibition of the viral DNA polymerase [1]. However, these drugs are not effective in the complete eradication of the infection, but only in reducing the frequency and duration of the episodes. In addition, both the emergence of drug-resistant viral strains, in particular for immune-compromised patients, and drug toxicity issues, increase the need for new antiviral agents acting with different mechanisms of action from those currently in use [2]. An interesting strategy for the treatment of viral infections is to prevent viral attachment and entry into the host cell, a complex process mediated by the interaction of different viral envelope glycoproteins with specific host surface receptors [3]. The HSV-1 envelope contains 11 glycoproteins involved in the early stages of viral attachment and penetration [4]. Among them, gB, gC, gD, gH, and gL are considered essential for cell entry. Attachment to the host membrane begins with the interaction of gB and gC with cell surface heparan sulfate (HS) proteoglycans, which brings the virus closer to the cell [5,6]. The binding of gD to one of the specific cellular receptors and the consequent conformational change that occurs in the structure of gD trigger a cascade of events that promote the formation of the core fusion machinery with gB and the gH/gL complex that allows virus entry [7]. HSV-1 gD can bind three classes of receptors, depending on the cell type:

1. Herpesvirus entry mediator (HVEM), a member of the tumour necrosis factor receptor superfamily (TNFR) expressed on activate lymphocytes and in other human tissues including kidney, lung, and liver.
2. Nectin-1 and 2, immunoglobulin (Ig)-like cell adhesion molecules (CAMs) expressed on the surface of neuronal and epithelial cells [8].
3. 3-O-sulfated heparan sulfate (3-OS HS), whose biological role has not yet been well clarified [9].

Due to the crucial role that gD plays in host cell fusion, we decided to explore the interactions between gD and its cellular receptors by means of computational methods, taking advantage of the HSV-1 gD experimentally solved structures in complex to HVEM and Nectin-1. Considering that protein–protein interactions (PPI) represent attractive targets for drug design, a structure-based virtual screening (SBVS) was performed taking into account the key residues useful for gD to anchor human receptors. The complexes resulting from protein–protein docking experiments were submitted to molecular dynamic simulations (MDs). GBPM and free energy calculation analyses revealed the most stable complexes and their pivotal points of interaction. Considering that both 1,2,3-triazole based compounds [10,11] and naphthyridine derivatives have been reported in the literature for their promising antiviral activity [12,13], we decided to perform a structure-based virtual screening (SBVS) of a small set of 12 [1,2,3]triazolo[4,5-*h*][1,6]naphthyridines of our synthesis (**1–12**, Table 1) [14] to evaluate their ability to target gD binding interface with HVEM and Nectin-1. Moreover, with the aim of exploring the influence of electron-withdrawing and/or electron-donating substituents at N-3 and C-8 positions of the triazolo-naphthyridine core on gD-ligand interaction, a focused library of 63 triazolo[4,5-*h*][1,6]naphthyridines (**19–81**, Table 1) was also designed to evaluate their binding properties into gD pockets and to explore their structure-activity relationships (SARs). Furthermore, since triazolopyridine systems have been extensively studied as interesting scaffolds exhibiting antiviral activities [15,16], we also investigated the binding affinity of [1,2,3]triazolo[4,5-*b*]pyridines (**13–18** and **82–85**, Table 1), synthetic precursors of the aforementioned triazolo-naphthyridines, versus gD interface with HVEM and Nectin-1. The workflow is reported in Figure 1.

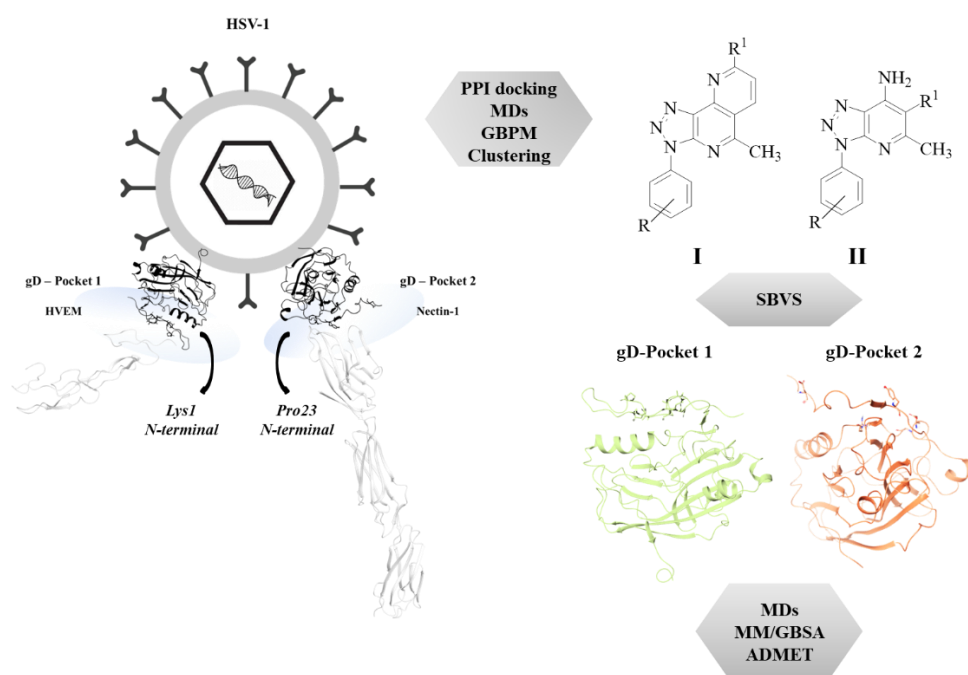
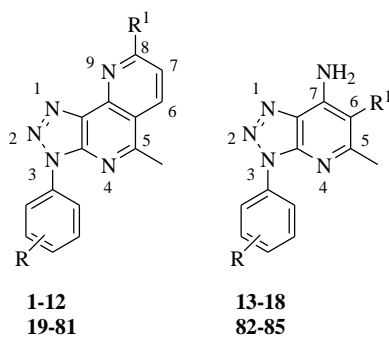


Figure 1. Graphical workflow of the applied *in silico* approaches on HSV-1 gD Pockets

Table 1. Synthetic (**1–12**) and designed (**19–81**) triazolo[4,5-*h*][1,6]naphthyridines and synthetic (**13–18**) and designed (**82–85**) triazolo[4,5-*b*]pyridines.



Cpd	R	R ¹	Cpd	R	R ¹
1	H	Me	9	3,4,5-(OMe) ₃	Me
2	H	Ph	10	3,4,5-(OMe) ₃	Ph
3	H	2-OMe-Ph	11	3,4,5-(OMe) ₃	2-OMe-Ph
4	H	4-OMe-Ph	12	3,4,5-(OMe) ₃	4-OMe-Ph
5	4-OMe	Me	13	H	COOEt
6	4-OMe	Ph	14	H	CH ₂ OH
7	4-OMe	2-OMe-Ph	15	4-OMe	COOEt
8	4-OMe	4-OMe-Ph	16	4-OMe	CH ₂ OH
17	3,4,5-(OMe) ₃	COOEt	52	4-Cl	4-OMe-Ph
18	3,4,5-(OMe) ₃	CH ₂ OH	53	4-Cl	CH ₃
19	H	2-F-Ph	54	4-Cl	Ph
20	H	2-Br-Ph	55	4-Cl	2-OMe-Ph
21	H	2-Cl-Ph	56	4-Cl	2-F-Ph
22	H	2-NO ₂ -Ph	57	4-Cl	2-Br-Ph

23	H	2-NH ₂ -Ph	58	4-Cl	2-Cl-Ph
24	H	2-CF ₃ -Ph	59	4-Cl	2-NO ₂ -Ph
25	H	2,3-(OMe) ₂ -Ph	60	4-Cl	2-NH ₂ -Ph
26	H	2,4-(OMe) ₂ -Ph	61	4-Cl	2-CF ₃ -Ph
27	H	2,5-(OMe) ₂ -Ph	62	4-Cl	2,3-(OMe) ₂ -Ph
28	H	2-OMe-5-Cl-Ph	63	4-Cl	2,4-(OMe) ₂ -Ph
29	H	2-OMe-5-Br-Ph	64	4-Cl	2,5-(OMe) ₂ -Ph
30	4-OMe	2-F-Ph	65	4-Cl	2-OMe-5-Cl-Ph
31	4-OMe	2-Br-Ph	66	4-Cl	2-OMe-5-Br-Ph
32	4-OMe	2-Cl-Ph	67	4-F	4-OMe-Ph
33	4-OMe	2-NO ₂ -Ph	68	4-F	CH ₃
34	4-OMe	2-NH ₂ -Ph	69	4-F	Ph
35	4-OMe	2-CF ₃ -Ph	70	4-F	2-OMe-Ph
36	4-OMe	2,3-(OMe) ₂ -Ph	71	4-F	2-F-Ph
37	4-OMe	2,4-(OMe) ₂ -Ph	72	4-F	2-Br-Ph
38	4-OMe	2,5-(OMe) ₂ -Ph	73	4-F	2-Cl-Ph
39	4-OMe	2-OMe-5-Cl-Ph	74	4-F	2-NO ₂ -Ph
40	4-OMe	2-OMe-5-Br-Ph	75	4-F	2-NH ₂ -Ph
41	3,4,5-(OMe) ₃	2-F-Ph	76	4-F	2-CF ₃ -Ph
42	3,4,5-(OMe) ₃	2-Br-Ph	77	4-F	2,3-(OMe) ₂ -Ph
43	3,4,5-(OMe) ₃	2-Cl-Ph	78	4-F	2,4-(OMe) ₂ -Ph
44	3,4,5-(OMe) ₃	2-NO ₂ -Ph	79	4-F	2,5-(OMe) ₂ -Ph
45	3,4,5-(OMe) ₃	2-NH ₂ -Ph	80	4-F	2-OMe-5-Cl-Ph
46	3,4,5-(OMe) ₃	2-CF ₃ -Ph	81	4-F	2-OMe-5-Br-Ph
47	3,4,5-(OMe) ₃	2,3-(OMe) ₂ -Ph	82	4-Cl	COOEt
48	3,4,5-(OMe) ₃	2,4-(OMe) ₂ -Ph	83	4-Cl	CH ₂ OH
49	3,4,5-(OMe) ₃	2,5-(OMe) ₂ -Ph	84	4-F	COOEt
50	3,4,5-(OMe) ₃	2-OMe-5-Cl-Ph	85	4-F	CH ₂ OH
51	3,4,5-(OMe) ₃	2-OMe-5-Br-Ph			

8.2 Experimental

8.2.1 Protein–protein preparation of gD–HVEM and gD–Nectin-1 and docking simulations

All computational studies were carried out using Schrödinger Suite 2018-1 [17]. The X-ray crystallographic structures of gD in complex with HVEM (PDB code: 1JMA) [18] and with Nectin-1 (PDB code: 3U82) [19] were used. Both gD structures were prepared and optimized using the Maestro Protein Preparation Wizard tool [20] with OPLS_2005 [21] as force field at pH 7.4. The structures were also optimized by the addition of missing loops using Prime software [22,23] and the determination of the protonation state of the ionizable amino acid residues by means of the Epik program [24]. Knowledge-based protein–protein docking of gD with HVEM and Nectin-1 was performed with HADDOCK 2.4 (High Ambiguity-Driven biomolecular DOCKing) webserver [25]. For each complex, the sampling parameters were as follows: 1000 structures for rigid-body docking, 200 structures for the final refinement, and a cut-off equal to 5.0 to define neighboring flexible regions. For the complex gD–HVEM from 1JMA model, gD amino acids Ala7, Ser8, Leu9, Lys10, Met11, Ala12, Asp13, Pro14, Asn15,

Val24, Leu25, Asp26, Gln27, Leu28, Thr29, Asp30, Pro31, Pro32 and HVEM amino acids Pro17, Lys18, Cys19, Ser20, Pro21, Gly22, Tyr23, Arg24, Val25, Lys26, Gly30, Glu31, Leu32 Thr33, Gly34, Thr35, Val36, Cys37, Glu38, Pro39, Ser74, Arg75, and Thr76 were considered as active residues, whereas passive residues were automatically identified as residues surrounding the active ones before submitting the docking job. For the complex gD-Nectin-1 from 3U82 model, gD amino acids Pro23, Leu25, Gln27, Arg36, Val37, Tyr38, His39, Gln132, Val214, Asp215, Ser216, Ile217, Gly218, Met219, Leu220, Pro221, Arg222, Phe223, Thr230, Val231, Tyr234 and Nectin-1 amino acids Ser59, Lys61, Thr63, Gln64, Thr66, Gln68, Lys75, Gln76, Asn77, Ile80, Tyr81, Asn82, Met85, Gly86, Val87, Ser88, Leu90, Glu125, Ala127, Thr128, Phe129, Pro130, Thr131, Gly132, and Asn133 were considered as active residues, whereas passive residues were again automatically identified. For each complex, the docked structures were loaded on Maestro interface of the Schrödinger software in PDB format for visual inspection and for the following *in silico* analysis.

8.2.2 MDs, GBPM, and MM/GBSA calculations of gD-HVEM and gD-Nectin-1 complexes

The best docked poses of each complex were submitted to 100 ns of MDs using Desmond ver. 4.2 [22]. To perform simulations in an aqueous biological environment, an appropriate system was built using OPLS_2005 as force field and an orthorhombic box with TIP4P water model extending of 10 Å outside the complex in all sides. The systems were maintained at a salt concentration of 0.15 M by adding appropriate Cl⁻ counter ions to neutralize them to maintain the physiological condition. After optimization of the solvated models, we relaxed the systems with the Martyna–Tobias–Klein isobaric–isothermal ensemble (MTK_NPT). Finally, 100 ns unconstrained MDs were carried out using the following conditions: the NPT ensemble, a constant temperature of 300 K, a pressure of 1 bar, and a recording interval equal to 100 ps both for energy and for trajectory collecting 1000 frames for each simulation.

For both complexes, all frames were considered for GBPM analysis [26]. As previously reported [27], in order to evidence hydrophobic and hydrogen bond donors and acceptors spots, we used DRY, N1, and O GRID probes, respectively. For each complex, gD was seen as guest and HVEM and Nectin-1 as hosts. The selected residues at the interface covered a maximum distance of 3 Å from the most relevant interaction energy points (GBPM features) of the computed molecular interaction fields (MIFs). After selecting an energy cutoff 30% above the global minimum, the pivotal hotspots were resulted by the summa of the related GBPM features interaction energy.

One thousand snapshots from 100 ns of MDs were applied for the Molecular Mechanics/Generalized Born Surface Area (MM/GBSA) free energy calculations [28] based on the following equation:

$$\Delta G_{\text{bind}} = G_{\text{comp}} - G_{\text{pro}} - G_{\text{lig}} = \Delta E_{\text{ele}} + \Delta E_{\text{vdw}} + \Delta E_{\text{int}} + \Delta E_{\text{GB}} + \Delta E_{\text{surf}}$$

where G_{comp} , G_{pro} and G_{lig} denote the free energy of the complex, protein, and the ligand; by splitting the energy contribution, it referred to ΔE_{ele} , ΔE_{vdw} and ΔE_{int} as the gas-phase interaction energy between protein and ligand, thus including the electrostatic energy term, the Van der Waals energy term, and the bond, angle, and dihedral terms, respectively. On the other hand, ΔE_{GB} and ΔE_{surf} indicate the polar and nonpolar desolvation free energy, respectively. The implicit solvation was calculated using the GB model [29], and the non-polar solvation energy was calculated using the solvent accessible surface area algorithm. The ΔG_{bind} reported in this study omitted the entropy contribution due to its relatively high computational demand and the lack of information of the conformational entropy that could lead to the introduction of additional error into the results [30].

8.2.3 Structure-based virtual screening of [1,2,3]triazolo[4,5-*h*][1,6]naphthyridines, and [1,2,3]triazolo[4,5-*b*]pyridines on gD-pocket 1 and gD-pocket 2

The MDs trajectories were clustered based on the RMSD matrix of backbone atoms, and we obtained three representative structures for each complex. After removing the HVEM and Nectin-1 structures, we used a total of six gD conformations for the SBVS. The target binding sites were defined by a regular grid of about 20 Å centered on the residues responsible for binding with the cell receptor [3,19,31,32]. The residues that defined the gD binding site at the interface with HVEM, called for clarity “gD-Pocket 1”, were as follows: Ala7, Ser8, Leu9, Lys10, Met11, Ala12, Asp13, Pro14, Asn15, Val24, Leu25, Asp26, Gln27, Leu28, Thr29, Asp30, Pro31, and Pro32. The gD binding site at the interface with Nectin-1, called “gD-Pocket 2”, was characterized by the following residues: Pro23, Leu25, Gln27, Arg36, Val37, Tyr38, His39, Gln132, Val214, Asp215, Ser216, Ile217, Gly218, Met219, Leu220, Pro221, Arg222, Phe223, Thr230, Val231, and Tyr234.

The selected ligands were taken from an *in-house* small library of [1,2,3]triazolo[4,5-*h*][1,6]naphthyridines (**1–12**) including also their synthetic precursor [1,2,3]triazolo[4,5-*b*]pyridines (**13–18**) [14]. Moreover, a focused library of 63 triazolo[4,5-*h*][1,6]naphthyridines

(**19–81**) was also designed, along with the corresponding [1,2,3]triazolo[4,5-*b*]pyridines (**82–85**). The 2D structures, reported in Table 1, were drawn using the ChemDraw Ultra 7.0 software and converted into 3D form using the import structures panel from Schrödinger maestro interface. All compounds were optimized via the Ligprep module [33], considering their ionization state at pH 7.4, and energy minimized using OPLS_2005 as force field [21].

The docking simulations of our focused library were computed using the Glide [34] ligand flexible algorithm at the standard-precision (SP) level, generating 10 possible poses for each site. The best docked poses for gD-Pocket 1 and gD-Pocket 2 were submitted to 500 ns of MDs in order to define the structural and energy profile of the best ligands in complex with both gD-Pockets. The simulations were carried out under the above-mentioned conditions. All simulations were performed by Desmond package [22] and “Simulation Interactions Diagram” panel was used as a post-MD analysis tool for exploring protein–ligand interactions. MM/GBSA free energy calculations of the best generated complexes were conducted along 100 frames of 500 ns of MDs. ADME descriptors and pharmacokinetic properties of the promising compounds were predicted by means of SwissADME tool [35].

8.3 Results and Discussion

In order to investigate the binding affinity of gD for its surface receptors and to gain useful structural insights regarding the pivotal interactions occurring at the gD interface, we performed a knowledge-based protein-protein docking employing HADDOCK 2.4 webserver [25]. Due to the involvement of gD both in cell adhesion function and viral entry mechanism depending on its cellular receptors, we considered the X-ray structure of gD both in complex to HVEM (PDB code: 1JMA) and Nectin-1 (PDB code: 3U82), respectively at 2.65 and 3.16 Å resolution. The complexes were prepared using Protein Preparation Wizard and uploaded in PDB format to the HADDOCK server. All the generated complexes were clustered according to their HADDOCK score, calculated as a weighted sum of a variety of energy terms (including Van der Waals, electrostatic, desolvation, and restraint violation energies) and buried surface area (BSA); the Z-score value was also calculated to select the best cluster with respect to all obtained clusters: the most negative Z-score is indicative of the top ranked cluster.

For the gD-HVEM and gD-Nectin-1 complexes, we obtained 188 structures gathered in 9 clusters, and 198 structures in 2 clusters, respectively. For both complexes, the docking results of each cluster were reported in Table 2.

Table 2. Number of generated clusters, HADDOCK scores, cluster size, Z-score, and BSA values of gD-HVEM and gD-Nectin-1 complexes.

Complex	Cluster	HADDOCK Score	Cluster Size	Z-Score	BSA
gD-HVEM	1	-124.3 ± 5.6	96	-2.1	2144.2 ± 59.6
	2	-89.1 ± 1.9	24	-0.2	1939.7 ± 69.3
	3	-97.5 ± 7.7	17	-0.7	1925.6 ± 72.1
	4	-93.7 ± 2.1	15	-0.5	1965.3 ± 124.9
	5	-54.1 ± 3.3	10	1.6	1401.2 ± 37.0
	6	-82.2 ± 4.4	9	0.1	1543.9 ± 50.6
	7	-76.3 ± 3.7	7	0.5	1864.7 ± 63.3
	8	-70.1 ± 7.6	6	0.8	1652.0 ± 72.3
	9	-75.7 ± 20.7	4	0.5	1701.5 ± 193.4
gD-Nectin-1	1	-146.0 ± 2.2	178	-1.0	2107.6 ± 20.8
	2	-101.4 ± 3.0	20	1.0	1887 ± 108.6

The best clusters (the lowest in energy) were analysed in terms of interactions using Maestro graphical user interface (Figure 2) and were aligned to the experimental structures through the Protein Structure Alignment tool.

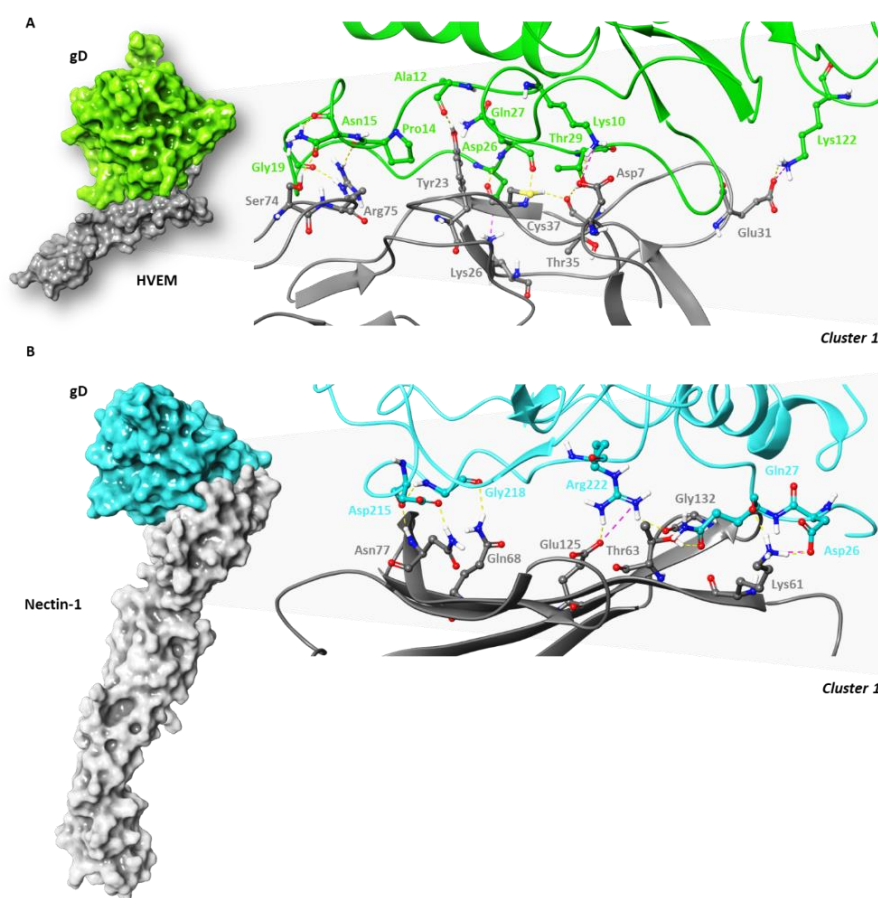


Figure 2. Surface representation of (A) gD-HVEM and (B) gD-Nectin-1 complexes and focus on the interface with key interactions labelled and displayed in carbon sticks

By overlapping, it resulted that for gD-HVEM and gD-Nectin-1 complexes, the RMSD value between the best docked pose and the X-ray structure was 1.54 and 0.80 Å, respectively. All the residues involved in the PPIs are summarized in Table 3.

Table 3. Residues involved in the interaction of gD with HVEM and Nectin-1.

	gD-HVEM		gD-Nectin-1	
	gD	HVEM	gD	Nectin-1
Hydrogen bonds	Lys10	Asp7	Asp26	Lys61
	Ala12	Tyr23	Gln27	Lys61
	Pro14	Arg75	Gln27	Thr63
	Asn15	Ser74	Gln132	Gln64
	Gly19	Arg75	Asp215	Asn77
	Gln27	Cys37	Asp215	Asn77
	Thr29	Thr35	Gly218	Gln68
	Lys122	Glu31	Arg222	Gly132
Salt bridges			Arg222	Glu125
	Lys10	Asp7	Asp26	Lys61
	Asp26	Lys26	Arg222	Glu125
	Lys122	Glu31		

The best obtained docked structures for each complex were refined using Protein Preparation Wizard and energy minimized with OPLS_2005 force field [21]. In order to explore any potential conformational changes of the gD interface, we submitted 100 ns of MDs for both complexes. The stability of MDs trajectories was monitored by the RMSD trend of the protein's backbone atoms from its initial conformation. The average RMSD values of gD-HVEM and gD-Nectin-1 complexes were 3.05 Å and 2.50 Å, respectively. By monitoring the distances between the interface's residues for gD-HVEM, we observed that several interactions previously detailed in Table 3 were maintained during MDs run, except for Asn15, Gly19, and Lys122 of gD, which were subjected to greater fluctuations, thus preventing the contacts with HVEM residues. Instead, Ala7 gained contacts with Ser20 during the whole MDs (Figure 3).

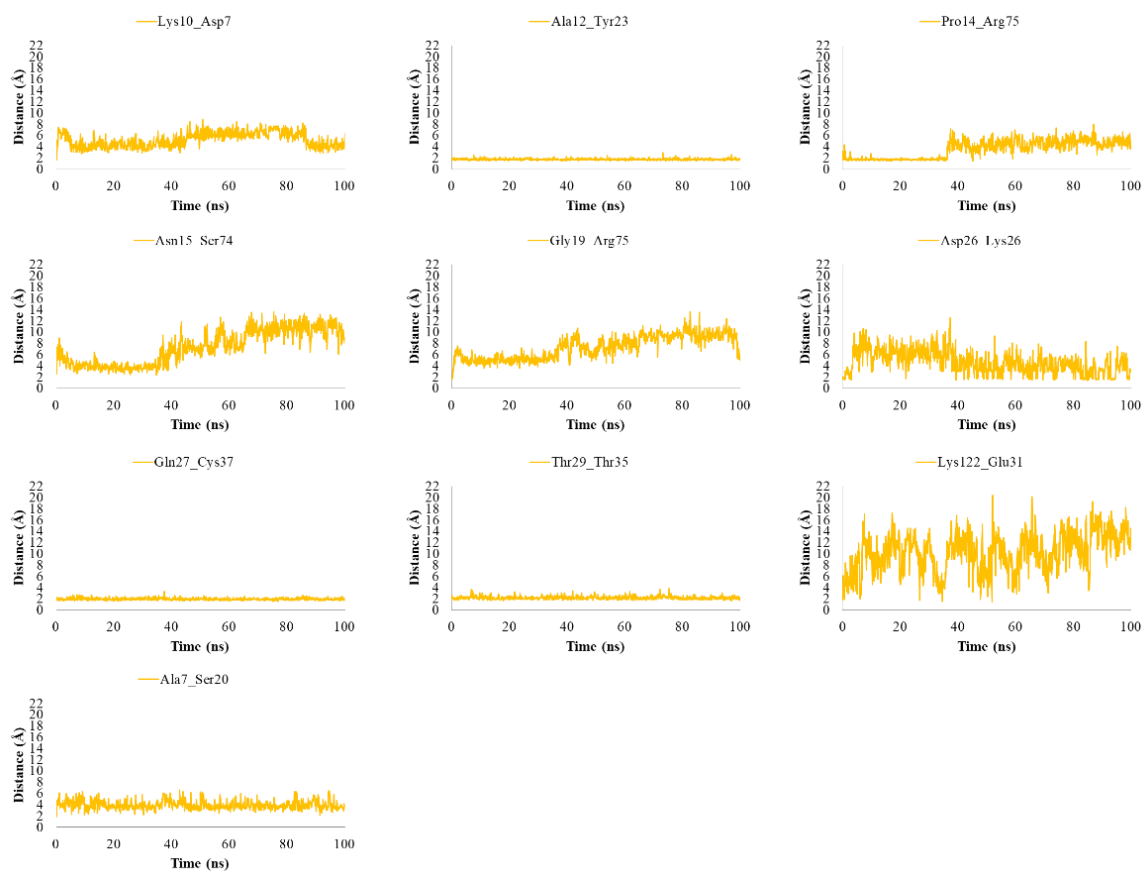


Figure 3. Plots of the distances between the residues of gD involved in the interaction at the interface with HVEM after 100 ns of MDs

Regarding gD in complex to Nectin-1, the interactions engaged by Gln27 and Gln132 of gD at the interface with Nectin-1 were lost, but it was found that Tyr38 was located in proximity to Gly86 of Nectin-1 during MDs (Figure 4).

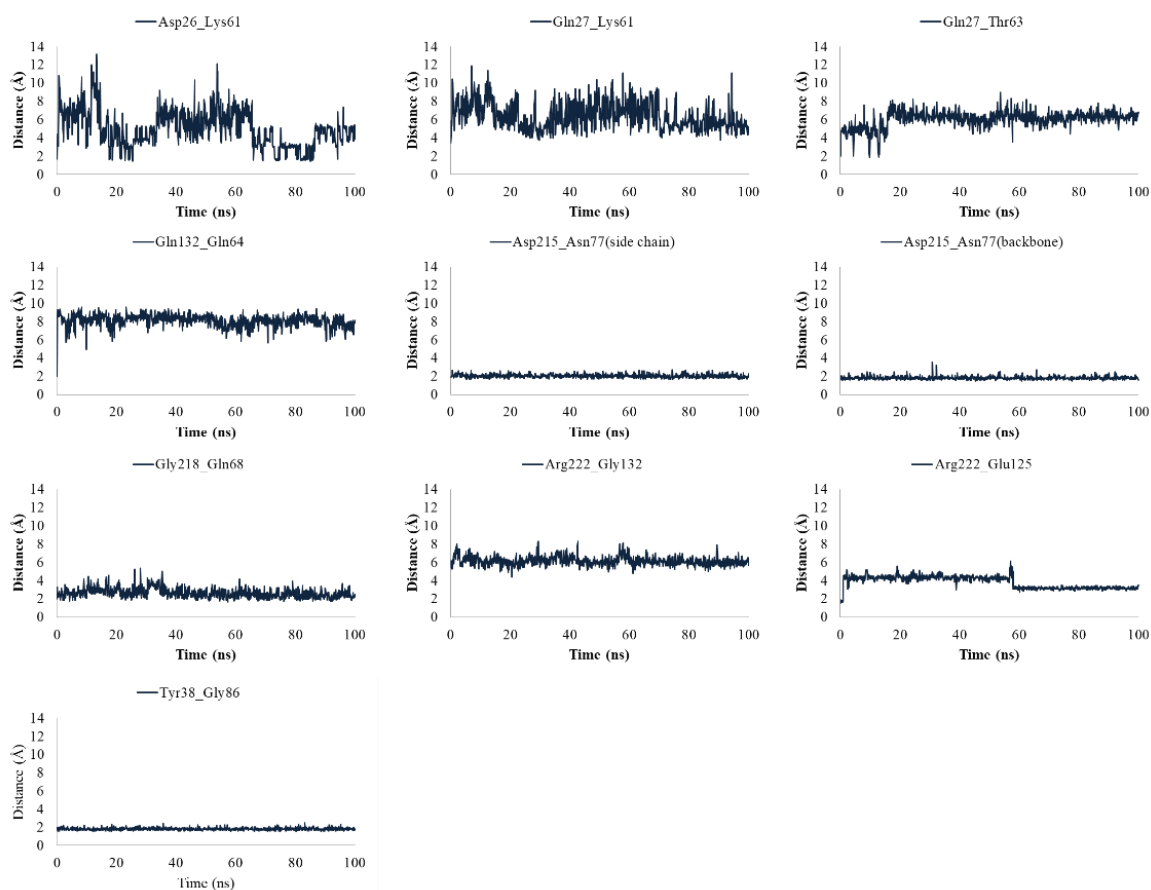


Figure 4. Plots of the distances between the residues of gD involved in the interaction at the interface with Nectin-1 after 100 ns of MDs

To better characterize the gD interface, a deeper analysis using GBPM was performed on all frames of MDs for each system. This method helps to map the key hotspots responsible for PPI by combining GRID molecular interaction fields (MIFs) according to the GRAB tool algorithm [26]. We considered gD as guest and HVEM and Nectin-1 as hosts. Three GRID probes, such as DRY, N1, and O, were chosen to mimic the hydrophobic, H-bond donor, and acceptor areas, respectively. Taking into account an energy threshold above the 30% from the global energy minimum GRID points, we summarized the pivotal residues up to 3Å from GBPM points. The contribution of each residue was derived by the summa of its GBPM points energy in the matching frames. After calculating the average score based on the total number of frames, the key hotspots were split into quartiles: quartile 1 (Q1) includes the residues with the major contribution to PPI until quartile 4 (Q4), which contains residues with the weakest interactions, during the entire trajectories. By results, gD N-terminus residues at position 10, 12, 13, 14, 15, 26, 27, 29, 33, and 35 were found pivotal for gD-HVEM binding, whereas nine residues, at

position 26, 27, 38, 215, 218, 219, 220, 221, and 222 were relevant for the connection with Nectin-1.

For both protein–protein complexes, 100 frames extracted by MDs were adopted to calculate the relative binding free energy (ΔG_{bind}) using Molecular Mechanics/Generalized Born Surface Area (MM/GBSA) methodology. The results of the calculated ΔG_{bind} trend for gD-HVEM and gD-Nectin-1 are depicted in Figure 5. Even showing a similar energy profile, the average values of -134.36 and -138.26 kcal/mol were turned out for HVEM and Nectin-1 in complex to gD, respectively, thus resulting in a more stabilizing effect of gD towards Nectin-1.

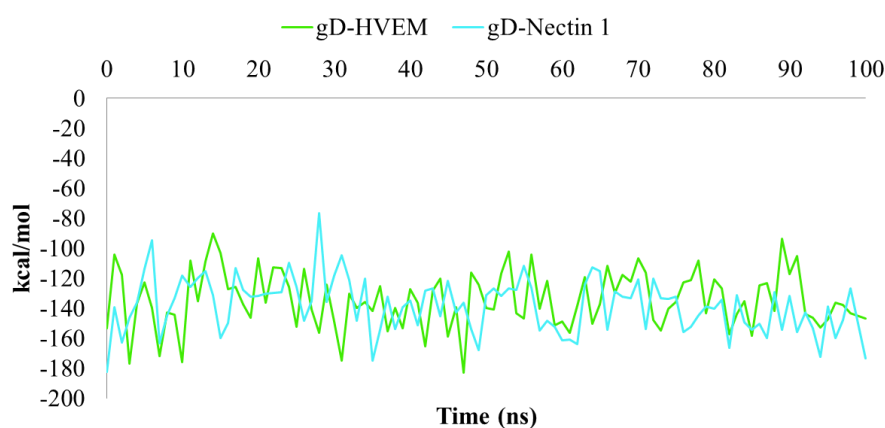


Figure 5. Plot of MM/GBSA trend for HVEM and Nectin-1 in complex to gD during 100 ns of MDs

After investigating the PPIs' structural details, we focused on the key residues of gD liable for the interaction with the analysed human receptors to find potential ligands able to prevent the connection with them. According to the literature, several gD N-terminus residues at positions 7–15 and 26–29 are responsible for the bind with HVEM [31], whereas two residues, such as Asp26 and Tyr38, also belonging to gD N-terminus, are relevant for the connection with Nectin-1 [19]. Apart from the shared Asp26 and Gln27 residues, both human receptors interact with different portions of gD. It was underlined that HVEM and Nectin-1 show non-reciprocal competition for binding to gD. Indeed, the interaction between HVEM and gD induces a conformational change in gD that results in the formation of the N-terminal hairpin structure that masks the binding site of Nectin-1 [36]. Similarly, the interaction with Nectin-1 induces a new conformation of the gD N-terminus that prevents the HVEM binding [37]. Considering

therefore that gD is not able to bind both receptors at the same time, we evaluated the possible conformational changes of gD during MDs. MDs trajectories were clustered based on RMSD matrix using the average hierarchical clustering linkage method, obtaining three representative structures of gD. Taking into account that the pivotal interactions of gD with HVEM and Nectin-1 involve distinct residues, we used all three representative structures generated from each complex as starting point for SBVS. Thus, we performed molecular docking simulations of our derivatives on each binding site, separately, using the docking program Glide in SP mode. We calculated the average G-score value for each cluster, aiming to focus on the compounds able to better recognize both Pocket 1 and 2. From the docking results, it clearly emerged that the tricyclic [1,2,3]triazolo[4,5-*h*][1,6]naphthyridine moiety showed a lower ability to recognize both the binding pockets compared to the bicyclic triazolo[4,5-*b*]pyridine derivatives. Furthermore, regardless of the electronic nature of the substituents at the N-3 phenyl ring of the triazolo-naphthyridine core, no significant differences could be observed. Concerning triazolo[4,5-*b*]pyridine derivatives, the presence of the 3,4,5-trimethoxyphenyl ring at N-3 reduced the theoretical binding affinity to gD. Conversely, better results were obtained with *p*-phenyl substituted derivatives bearing the hydroxymethyl group at C-6 (**14**, **16**, **83**, **85**, Figure 6).

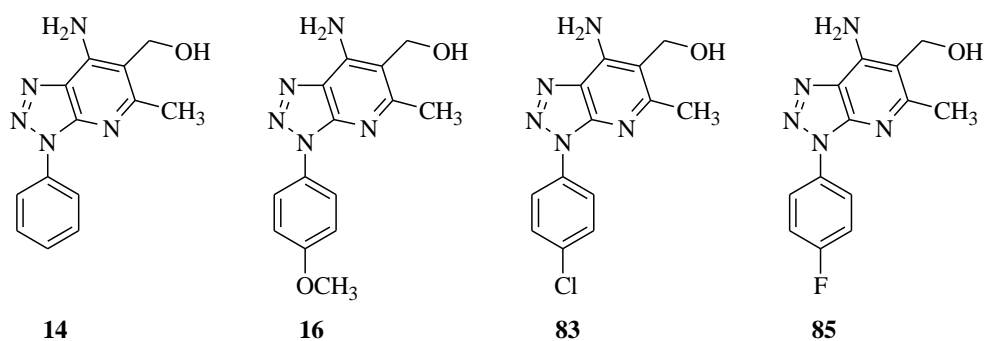


Figure 6. *p*-Phenyl substituted triazolo[4,5-*b*]pyridine derivatives **14**, **16**, **83** and **85**

Overall, among the 85 investigated compounds, we focused on the binding mode of the compounds able to recognize all the representative structures of both pockets with average G-score values lower than -5.00 kcal/mol. Accordingly, four triazole-pyridine derivatives, **14**, **16**, **83**, and **85** showed a favoured energetic profile in complex with all gD conformations. In detail, considering the most populated cluster resulted for gD-Pocket 1, the hydroxyl group of **14**

(Figure 7A), **16** (Figure 7B), **83** (Figure 7C), and **85** (Figure 7D) was anchored to Leu25. Moreover, **16** and **83** formed an additional H-bond between the amino group and Leu25.

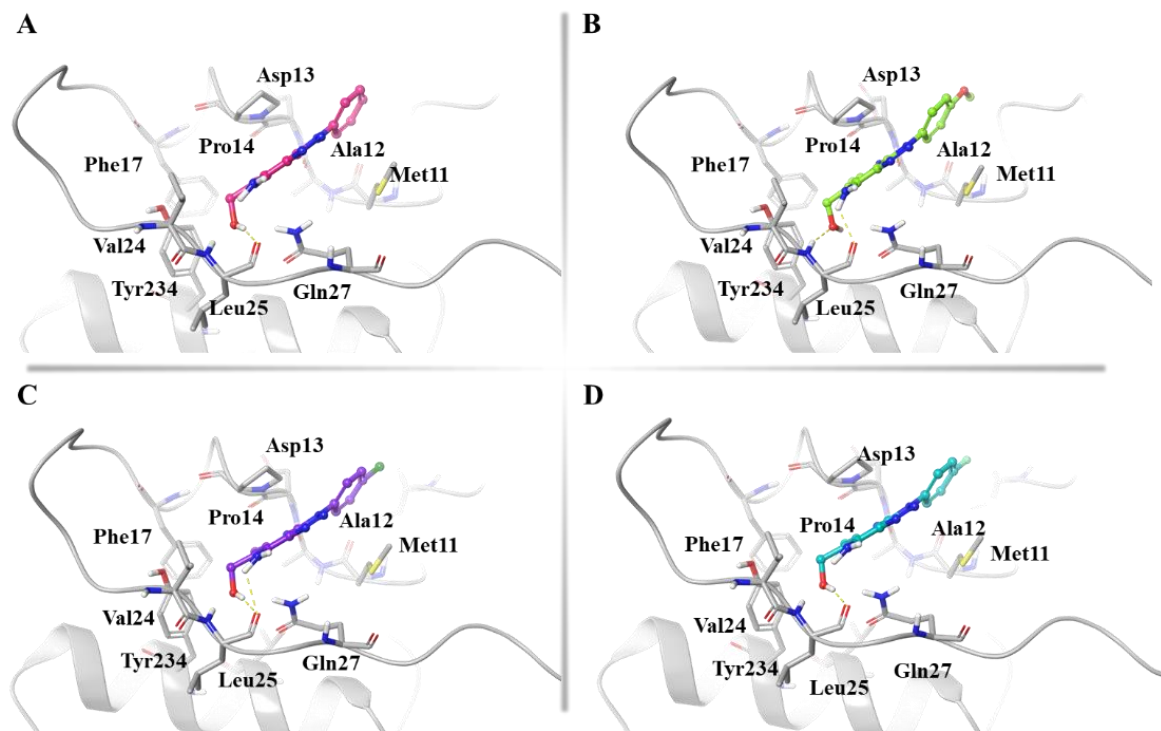


Figure 7. 3D representation of (A) **14**, (B) **16**, (C) **83**, and (D) **85** in complex to the most populated cluster of gD-Pocket 1. gD-Pocket 1 is illustrated in gray, with the residues involved in pivotal contacts shown as carbon sticks. **14**, **16**, **83**, and **85** are depicted as pink, green, violet, and cyan carbon sticks, and H-bonds are indicated as yellow dashed lines.

In gD-Pocket 2, derivatives **14**, **16**, **83**, and **85** engaged several H-bonds with Leu28, Asp30, Asn227, and a π - π stacking interaction with Phe223, probably due to the absence of the N-terminal extension (Figure 8).

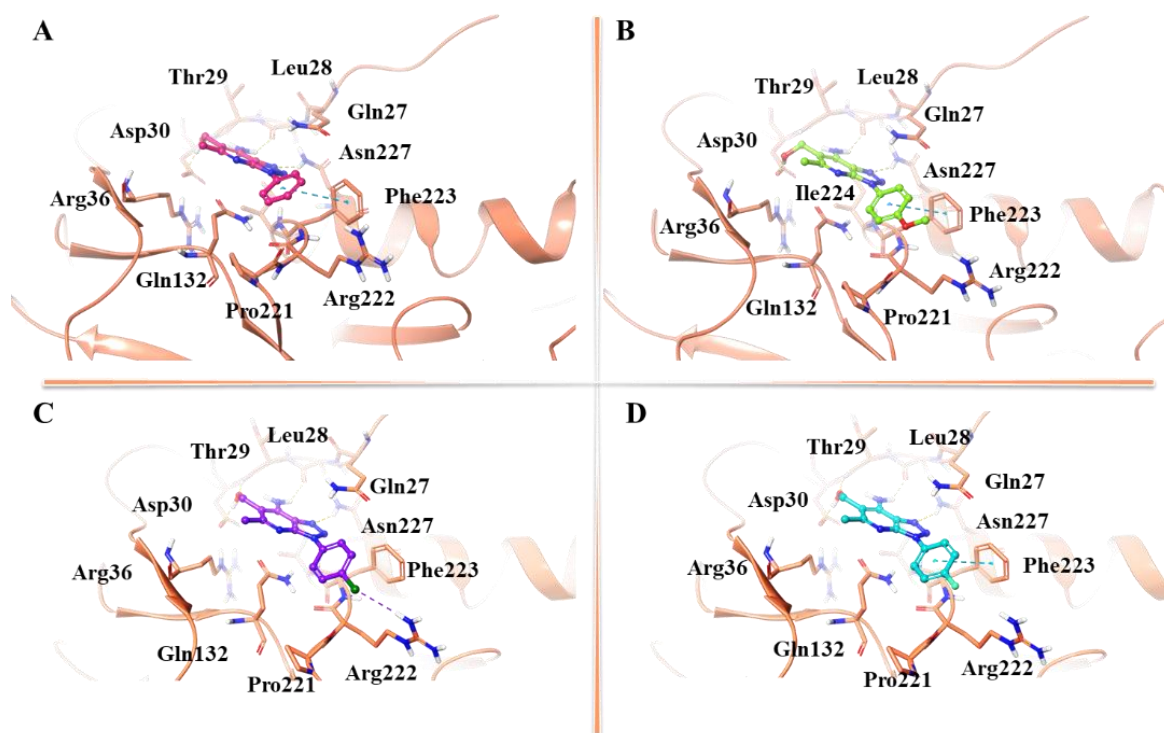


Figure 8. 3D representation of (A) **14**, (B) **16**, (C) **83**, and (D) **85** in complex to the most populated cluster of gD-Pocket 2. gD-Pocket 2 is illustrated in salmon, with the residues involved in pivotal contacts shown as carbon sticks. Compounds **14**, **16**, **83**, and **85** are depicted as pink, green, violet, and cyan carbon sticks, whereas H-bonds and π - π interactions are indicated as yellow and cyan dashed lines, respectively.

The best docked poses of **14**, **16**, **83**, and **85** in complex with the most representative cluster of gD-Pocket 1 and gD-Pocket 2 were submitted to 500 ns of MDs using Desmond [22]. The results of MDs were investigated in terms of stability and conformational flexibility in the presence of the selected compounds. The stability of the complexes was evaluated by calculating the RMSD of the protein's backbone atoms from its initial to final conformation over the whole simulation. By RMSD analysis, we observed that the most promising compounds maintained overall stability throughout MDs in both Pockets, as shown in Figure 9. In particular, for Pocket 1, the average RMSD values of 2.27, 3.09, 2.58, and 2.59 Å (Figure 9A) were computed for **14**, **16**, **83**, and **85**, respectively. On the other hand, for Pocket 2, we observed average RMSD values in the range of 2.17–2.51 Å (Figure 9B).

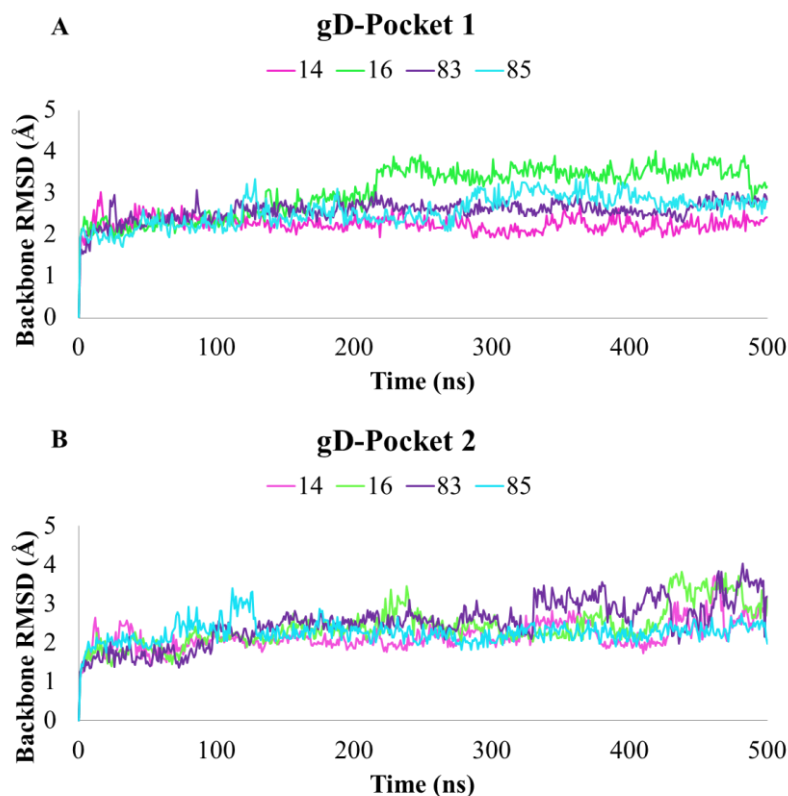


Figure 9. RMSD plots of **14**, **16**, **83**, and **85** compounds in complex with (A) gD-Pocket 1 and (B) gD-Pocket 2, calculated on protein's backbone atoms during 500 ns of MDs

Furthermore, for each system, the binding free energy ΔG_{bind} was calculated using MM/GBSA methodology, extracting 100 snapshots from 500 ns of MDs. MM/GBSA analysis showed that the average calculated ΔG_{bind} of **14**, **16**, **83**, and **85** complexed with gD-Pocket 1 were -38.88 , -36.52 , -40.22 , and -31.14 kcal/mol, respectively, during the entire trajectories. The average ΔG_{bind} of **14**, **16**, **83**, and **85** in complex to gD-Pocket 2 were -31.78 , -29.71 , -36.28 , and -34.63 kcal/mol, respectively. ADME parameters of the most promising compounds were predicted using the SwissADME server, and the obtained data are reported in Table 4. All the investigated compounds are achiral, fit Lipinski's rule of five, and were not found to be pan assay interference compounds (PAINS), thus resulting suitable for further HSV-1 *in vitro* investigation.

Table 4. Predicted ADME parameters: Molecular Weight (MW); Number of H-bond Acceptors and Donors; Octanol/Water Partition Coefficient (logP); Topological Polar Surface Area in Å² (TPSA); and Water Solubility (LogS).

Cpd	MW	H-Bond Acceptors	H-Bond Donors	LogP	TPSA	LogS
14	255.28	4	2	1.05	89.85	-2.77
16	285.30	5	2	1.06	99.08	-2.82
83	289.72	4	2	1.71	89.85	-3.35
85	273.27	5	2	1.61	89.85	-2.91

8.4 Conclusions

In the present computational investigation, the pivotal interactions occurring at the interface of gD and its human surface receptors were carefully explored. Since the availability of X-ray structures of gD in complex with HVEM and Nectin-1, this study aimed at highlighting the key residues involved in the binding interface during MDs. MM/GBSA analysis revealed a greater binding affinity of gD towards Nectin-1 with respect to HVEM, given that the rearrangement of N-terminal hairpin is not necessary for gD-Nectin-1 interaction, which instead ensured a more rigid gD-binding pocket. By analysing HSV-1 PPIs, through the GBPM method, gD N-terminus residues at position 10, 12, 13, 14, 15, 26, 27, 29, 33, and 35 were found pivotal for gD-HVEM binding, whereas nine residues, at position 26, 27, 38, 215, 218, 219, 220, 221, and 222 were relevant for the connection with Nectin-1. Afterwards, an SBVS targeting different conformations of HSV-1 gD binding interfaces was applied. *In silico* approaches are a consolidated strategy to speed up the drug discovery process, as demonstrated during the pandemic emergency, increasing our understanding of how biological systems work and translating this knowledge into new molecules with interesting therapeutic potential. In this context, the inhibition of HSV-1 through targeting viral gD protein represents a good way to act with virus adsorption and membrane fusion. Herein we identified four triazole-pyridines as potential HSV-1 gD inhibitors, with a favourable pharmacokinetic profile and a good theoretical affinity towards all conformations of HSV-1 gD. Although some of these compounds have been shown to be ineffective in inhibiting viral replication on cell cultures fully infected with HSV-1, the co-treatment assay is currently ongoing to assess the ability of selected compounds to interfere with viral entry into the host cell. Nevertheless, surface plasmon resonance technique could provide further information into the mechanism of action at a molecular level and could

move forward novel antiviral compounds. Our study suggests a promising basis for the design of a new generation of anti-HSV-1 drugs targeting gD-receptor interfaces.

8.5 References

- [1] L.A. Sadowski, R. Upadhyay, Z.W. Greeley, B.J. Margulies, Current drugs to treat infections with herpes simplex viruses-1 and -2, *Viruses*. 13 (2021) 1228. <https://doi.org/10.3390/v13071228>.
- [2] Y.C. Jiang, H. Feng, Y.C. Lin, X.R. Guo, New strategies against drug resistance to herpes simplex virus, *Int. J. Oral Sci.* 8 (2016) 1–6. <https://doi.org/10.1038/ijos.2016.3>.
- [3] S.A. Connolly, J.O. Jackson, T.S. Jardetzky, R. Longnecker, Fusing structure and function: a structural view of the herpesvirus entry machinery, *Nat. Rev. Microbiol.* 9 (2011) 369–381. <https://doi.org/10.1038/nrmicro2548>.
- [4] C.P.P. De Mello, D.C. Bloom, I.C.N.P. Paixão, Herpes simplex virus type-1: Replication, latency, reactivation and its antiviral targets, *Antivir. Ther.* 21 (2016) 277–286. <https://doi.org/10.3851/IMP3018>.
- [5] P.G. Spear, Herpes simplex virus: Receptors and ligands for cell entry, *Cell. Microbiol.* 6 (2004) 401–410. <https://doi.org/10.1111/j.1462-5822.2004.00389.x>.
- [6] E.E. Heldwein, C. Krummenacher, Entry of herpesviruses into mammalian cells, *Cell. Mol. Life Sci.* 65 (2008) 1653–1668. <https://doi.org/10.1007/s00018-008-7570-z>.
- [7] S.A. Connolly, T.S. Jardetzky, R. Longnecker, The structural basis of herpesvirus entry, *Nat. Rev. Microbiol.* 19 (2021) 110–121. <https://doi.org/10.1038/s41579-020-00448-w>.
- [8] P. Petermann, K. Thier, E. Rahn, F.J. Rixon, W. Bloch, S. Özcelik, C. Krummenacher, M.J. Barron, M.J. Dixon, S. Scheu, K. Pfeffer, D. Knebel-Mörsdorf, Entry Mechanisms of Herpes Simplex Virus 1 into Murine Epidermis: Involvement of Nectin-1 and Herpesvirus Entry Mediator as Cellular Receptors, *J. Virol.* 89 (2015) 262–274. <https://doi.org/10.1128/jvi.02917-14>.
- [9] V. Tiwari, C.D. O'Donnell, M.J. Oh, T. Valyi-Nagy, D. Shukla, A role for 3-O-sulfotransferase isoform-4 in assisting HSV-1 entry and spread, *Biochem. Biophys. Res. Commun.* 338 (2005) 930–937. <https://doi.org/10.1016/j.bbrc.2005.10.056>.

- [10] I. Seck, F. Nguemo, Triazole, imidazole, and thiazole-based compounds as potential agents against coronavirus, *Results Chem.* 3 (2021) 100132. <https://doi.org/10.1016/j.rechem.2021.100132>.
- [11] R. Bivacqua, M. Barreca, V. Spanò, M.V. Raimondi, I. Romeo, S. Alcaro, G. Andrei, P. Barraja, A. Montalbano, Insight into non-nucleoside triazole-based systems as viral polymerases inhibitors, *Eur. J. Med. Chem.* 249 (2023) 115136. <https://doi.org/10.1016/j.ejmech.2023.115136>.
- [12] L. Zhuang, J.S. Wai, M.W. Embrey, T.E. Fisher, M.S. Egbertson, L.S. Payne, J.P. Guare, J.P. Vacca, D.J. Hazuda, P.J. Felock, A.L. Wolfe, K.A. Stillmock, M. V. Witmer, G. Moyer, W.A. Schleif, L.J. Gabryelski, Y.M. Leonard, J.J. Lynch, S.R. Michelson, S.D. Young, Design and synthesis of 8-hydroxy-[1,6]naphthyridines as novel inhibitors of HIV-1 integrase in vitro and in infected cells, *J. Med. Chem.* 46 (2003) 453–456. <https://doi.org/10.1021/jm025553u>.
- [13] G. Falardeau, H. Lachance, A. St-Pierre, C.G. Yannopoulos, M. Drouin, J. Bédard, L. Chan, Design and synthesis of a potent macrocyclic 1,6-naphthyridine anti-human cytomegalovirus (HCMV) inhibitors, *Bioorganic Med. Chem. Lett.* 15 (2005) 1693–1695. <https://doi.org/10.1016/j.bmcl.2005.01.050>.
- [14] I. Frasson, V. Spanò, S. Di Martino, M. Nadai, F. Doria, B. Parrino, A. Carbone, S.M. Cascioferro, P. Diana, G. Cirrincione, M. Freccero, P. Barraja, S.N. Richter, A. Montalbano, Synthesis and photocytotoxic activity of [1,2,3]triazolo[4,5-h][1,6]naphthyridines and [1,3]oxazolo[5,4-h][1,6]naphthyridines, *Eur. J. Med. Chem.* 162 (2019) 176–193. <https://doi.org/10.1016/j.ejmech.2018.10.071>.
- [15] K. Karypidou, S.R. Ribone, M.A. Quevedo, L. Persoons, C. Pannecouque, C. Helsen, F. Claessens, W. Dehaen, Synthesis, biological evaluation and molecular modeling of a novel series of fused 1,2,3-triazoles as potential anti-coronavirus agents, *Bioorganic Med. Chem. Lett.* 28 (2018) 3472–3476. <https://doi.org/10.1016/j.bmcl.2018.09.019>.
- [16] A. Hartwich, N. Zdzienicka, D. Schols, G. Andrei, R. Snoeck, I.E. Głowacka, Design, synthesis and antiviral evaluation of novel acyclic phosphonate nucleotide analogs with triazolo[4,5-b]pyridine, imidazo[4,5-b]pyridine and imidazo[4,5-b]pyridin-2(3H)-one systems, *Nucleosides, Nucleotides and Nucleic Acids.* 39 (2020) 542–591. <https://doi.org/10.1080/15257770.2019.1669046>.

- [17] Schrödinger Release 2018-1: Maestro; Schrödinger LLC: New York, NY, USA, 2018, (n.d.).
- [18] A. Carfi, S.H. Willis, J.C. Whitbeck, C. Krummenacher, G.H. Cohen, R.J. Eisenberg, D.C. Wiley, Herpes simplex virus glycoprotein D bound to the human receptor HveA, *Mol. Cell.* 8 (2001) 169–179. [https://doi.org/10.1016/S1097-2765\(01\)00298-2](https://doi.org/10.1016/S1097-2765(01)00298-2).
- [19] N. Zhang, J. Yan, G. Lu, Z. Guo, Z. Fan, J. Wang, Y. Shi, J. Qi, G.F. Gao, Binding of herpes simplex virus glycoprotein D to nectin-1 exploits host cell adhesion, *Nat. Commun.* 2 (2011) 577. <https://doi.org/10.1038/ncomms1571>.
- [20] Schrödinger Release 2018-1: Protein Preparation Wizard; Epik, 2019; Schrödinger LLC: New York, NY, USA, 2018, (n.d.).
- [21] W.L. Jorgensen, D.S. Maxwell, J. Tirado-Rives, Development and testing of the OPLS all-atom force field on conformational energetics and properties of organic liquids, *J. Am. Chem. Soc.* 118 (1996) 11225–11236. <https://doi.org/10.1021/ja9621760>.
- [22] Schrödinger Release 2018-1: Desmond Molecular Dynamics System; D.E. Shaw Research, Maestro-Desmond Interoperability Tools; Schrödinger LLC: New York, NY, USA, 2018, (n.d.).
- [23] M.P. Jacobson, D.L. Pincus, C.S. Rapp, T.J.F. Day, B. Honig, D.E. Shaw, R.A. Friesner, A Hierarchical Approach to All-Atom Protein Loop Prediction, *Proteins Struct. Funct. Bioinforma.* 55 (2004) 351–367. <https://doi.org/10.1002/prot.10613>.
- [24] J.R. Greenwood, D. Calkins, A.P. Sullivan, J.C. Shelley, Towards the comprehensive, rapid, and accurate prediction of the favorable tautomeric states of drug-like molecules in aqueous solution, *J. Comput. Aided. Mol. Des.* 24 (2010) 591–604. <https://doi.org/10.1007/s10822-010-9349-1>.
- [25] G.C.P. Van Zundert, J.P.G.L.M. Rodrigues, M. Trellet, C. Schmitz, P.L. Kastiris, E. Karaca, A.S.J. Melquiond, M. Van Dijk, S.J. De Vries, A.M.J.J. Bonvin, The HADDOCK2.2 Web Server: User-Friendly Integrative Modeling of Biomolecular Complexes, *J. Mol. Biol.* 428 (2016) 720–725. <https://doi.org/10.1016/j.jmb.2015.09.014>.
- [26] F. Ortuso, T. Langer, S. Alcaro, GBPM: GRID-based pharmacophore model: Concept and application studies to protein-protein recognition, *Bioinformatics.* 22 (2006) 1449–1455. <https://doi.org/10.1093/bioinformatics/btl115>.

- [27] F. Ortuso, D. Mercatelli, P.H. Guzzi, F.M. Giorgi, Structural genetics of circulating variants affecting the SARS-CoV-2 spike/human ACE2 complex, *J. Biomol. Struct. Dyn.* 40 (2022) 6545–6555. <https://doi.org/10.1080/07391102.2021.1886175>.
- [28] T. Hou, J. Wang, Y. Li, W. Wang, Assessing the performance of the molecular mechanics/Poisson Boltzmann surface area and molecular mechanics/generalized Born surface area methods. II. The accuracy of ranking poses generated from docking., *J. Comput. Chem.* 32 (2011) 866–877. <https://doi.org/10.1002/jcc.21666>.
- [29] H. Kopitz, D.A. Cashman, S. Pfeiffer-Marek, H. Gohlke, Influence of the solvent representation on vibrational entropy calculations: Generalized born versus distance-dependent dielectric model, *J. Comput. Chem.* 33 (2012) 1004–1013. <https://doi.org/10.1002/jcc.22933>.
- [30] S. Genheden, O. Kuhn, P. Mikulskis, D. Hoffmann, U. Ryde, The normal-mode entropy in the MM/GBSA method: Effect of system truncation, buffer region, and dielectric constant, *J. Chem. Inf. Model.* 52 (2012) 2079–2088. <https://doi.org/10.1021/ci3001919>.
- [31] R.J. Eisenberg, D. Atanasiu, T.M. Cairns, J.R. Gallagher, C. Krummenacher, G.H. Cohen, Herpes virus fusion and entry: A story with many characters, *Viruses.* 4 (2012) 800–832. <https://doi.org/10.3390/v4050800>.
- [32] C. Krummenacher, V.M. Supekar, J.C. Whitbeck, E. Lazear, S.A. Connolly, R.J. Eisenberg, G.H. Cohen, D.C. Wiley, A. Carfi, Structure of unliganded HSV gD reveals a mechanism for receptor-mediated activation of virus entry, *EMBO J.* 24 (2005) 4144–4153. <https://doi.org/10.1038/sj.emboj.7600875>.
- [33] Schrödinger Release 2018-1: LigPrep; Schrödinger LLC: New York, NY, USA, 2018, (n.d.).
- [34] R.A. Friesner, R.B. Murphy, M.P. Repasky, L.L. Frye, J.R. Greenwood, T.A. Halgren, P.C. Sanschagrin, D.T. Mainz, Extra precision glide: Docking and scoring incorporating a model of hydrophobic enclosure for protein-ligand complexes, *J. Med. Chem.* 49 (2006) 6177–6196. <https://doi.org/10.1021/jm051256o>.
- [35] A. Daina, O. Michielin, V. Zoete, SwissADME: A free web tool to evaluate pharmacokinetics, drug-likeness and medicinal chemistry friendliness of small molecules, *Sci. Rep.* 7 (2017) 42717. <https://doi.org/10.1038/srep42717>.

- [36] E. Lazear, J.C. Whitbeck, Y. Zuo, A. Carfi, G.H. Cohen, R.J. Eisenberg, C. Krummenacher, Induction of conformational changes at the N-terminus of herpes simplex virus glycoprotein D upon binding to HVEM and nectin-1, *Virology*. 448 (2014) 185–195. <https://doi.org/10.1016/j.virol.2013.10.019>.
- [37] J. Wu, H. Power, M. Miranda-Saksena, P. Valtchev, A. Schindeler, A.L. Cunningham, F. Dehghani, Identifying HSV-1 Inhibitors from Natural Compounds via Virtual Screening Targeting Surface Glycoprotein D, *Pharmaceuticals*. 15 (2022) 361. <https://doi.org/10.3390/ph15030361>.